IOWA STATE UNIVERSITY
Digital Repository

1983

Design considerations for steel containments

Gary Alan Fils
Iowa State University

Follow this and additional works at: https://lib.dr.iastate.edu/rtd

Part of the Civil Engineering Commons, and the Structural Engineering Commons

Design considerations for steel containments

by

Gary Alan Fils

A Thesis Submitted to the

Graduate Faculty in Partial Fulfillment of the

Requirements for the Degree of

MASTER OF SCIENCE

Department: Civil Engineering
Major: Structural Engineering

Approved:

_____
In Charge of Major Work

_____
For the Major Department

_____
For the Graduate College

Iowa State University
Ames, Iowa

1983

TABLE OF CONTENTS

1. INTRODUCTION

1.1 Background

In the past decade, there has been heightened public concern about the safety of nuclear power. Especially since the Three Mile Island incident of 1979, this concern has tended to shift research emphasis away from the implementation of design innovations to increased certainty of current design practices. A positive result of this has been increased understanding and analytical formulation of plant design behavior. Indeed, it is becoming more feasible to quantify the reliability and, conversely, the risk of nuclear power and present an objective choice to the American public.

The basic question that the public wants answered is: "How safe is it?". A part of the answer is the explanation of the design philosophy and construction methods used to bring a nuclear plant into existence. An aspect of this design philosophy is that public safety is maintained by providing multiple levels of defense against accidents. Each level of defense is designed by postulating an extreme and severe series of events beyond any expected to occur. One of the last levels of defense and the subject of this document is the containment vessel which encloses the nuclear reactor. The purpose of the containment vessel is to contain and control the deposition of radioactive particles and gases released from an event with a low probability of occurrence.

1.2. Objective and Scope

Specifically, the type of containment vessels considered herein are those constructed with steel. The object of this work is to review the current aspects of structural design for steel containment vessels. This objective is accomplished by familiarizing the reader with the nature of the problem and introducing the current methods utilized for its solution. The scope of this work has been limited to a manageable volume by the following.

- Sources of and characteristics of design basis loads are discussed. However, explicit load descriptions are not defined.

- Modeling and analysis techniques are described generally as to acceptable and practical options and when they are applicable.

- Analyses for specific loads are introduced but are limited to summaries wherein the reader is directed to specific references for detailed analytical treatment of the problem.

- Penetrations and attached equipment (i.e., containment appurtenances) are not specifically treated.

- Considerations necessary for assessment of analysis results are presented for: formulation of load combinations; selection of allowable service limits; and determination of buckling capacity, based on current pratice as delineated by the ASME Code.

This work is provided as an aid, not so much for individuals already researching and developing steel containment designs, but for those entering the field. It is intended, however, to provide an overview of the problem of steel containment design that will benefit experienced as well as novice engineers.

2. RELIABILITY OF STEEL CONTAINMENTS

2.1. Probability Risk Assessment Procedures

Concern for public safety has prompted the need to be able to quantitatively assess the risk associated with the operation of nuclear power plants. The Reactor Safety Study, WASH-1400 [104], established a general approach to this problem which subsequent studies have used and expanded upon. These studies, referred to as probability risk assessments (PRA), are aimed primarily at determining the probability of (and magnitude of) the occurrence of radiological material being released to the environment. WASH-1400 showed that the various amounts of radiological material released could be well represented by a set of different "release categories" in which quantities of various radioactive isotopes are defined. The annual probability of occurrence of each release category depends on the severity and likelihood of the event damaging the reactor vessel and primary system piping, the overall mode of failure characterized by various internal paths and, ultimately, integrity failure of the primary containment boundary. Finally, release categories along with population, environmental, and property parameters form the basis of a consequence analysis. The consequence analysis results in a site-specific prediction of potential damage levels with corresponding probabilities of annual occurrence. To be meaningful, input analysis and final results of a PRA are qualified by a statement of uncertainty, i.e., confidence in the conclusions.

2.1.1. Event trees

WASH-1400 and other studies have used event trees (Fig. 2.1) as a principal means of providing a systematic determination of release category occurrence probabilities and the quantity of radiological material defined in each category. Event trees provide a logical method of identifying the various possible outcomes resulting from an event. The first event in an event tree is referred to as the initiating event and represents the 'hazard' leading to potential radioactive releases. The succeeding events are successes or failures of individual systems or components which make up a potential sequence of events inside the plant.

A particular sequence from the initiating event to a final outcome is termed an accident sequence. Based on knowledge of plant design and engineering principles, illogical or physically meaningless (zero probability) sequences and completely successful sequences of events are eliminated from the basic tree yielding the reduced tree, as shown in Fig. 2.1(b). The probability of occurrence of the remaining accident sequences are then calculated. If individual events are independent of each other, this calculation is simply the product of the event probabilities identified on a particular accident sequence (Fig. 2.1). Then, assuming that the accident sequences are mutually exclusive, the occurrence probability of a specific release category is the sum of probabilities of the accident sequences that result in that particular category.

One must be careful in assuming that the success or failure of each component in an accident sequence is an independent occurrence. In complex systems, it is often the case that the success or failure of a

component may depend on the outcome of more than one preceding event. Conversely, multiple failures may result from a single component failure. Such dependences, referred to as common mode failures, may exist in and between the accident sequences of the event tree. The probability associated with common mode failure becomes a dependent probability and is no longer tractable by simple methods assuming independence but must be solved using multivariate probabilistic methods. A conservative approach used in WASH-1400 to facilitate the assumption of branch independence was to give no consideration to partial component success. Often, however, even this is not sufficient and more complex methods must be used if serious errors are to be avoided.

2.1.2. Hazard analysis

The hazard, or initiating event, will produce conditions which various systems and components (including the steel containment) are designed to resist in order to protect the public and maintain the plant. The first step in a hazard analysis is to identify the hazards in the plant. Various hazards include breaks in the primary system piping, earthquakes and equipment malfunctions. If some type of hazard were to occur, its intensity may vary across a spectrum of values. Thus, hazard intensity is a random variable denoted Q. The results of the hazard analysis are statistical distributions reflecting both the annual occurrence frequency and intensity variability of a particular hazard. Intensity will be measured in appropriate units such as pressure, acceleration or temperature.

Various ways in which this information can be presented are the annual probability density, and annual cumulative and exceedence distributions shown in Figs. 2.2(a), (b) and (c), respectively. Fig. 2.2(c) is referred to as the hazard curve. The hazard curve function yields the probability of hazard intensities Q that are greater than or equal to a specified value of intensity q_s, i.e.,

$$P[Q \geqslant q_s] = 1 - F_Q(q_s) \qquad (2.1)$$

The curves of Fig. 2.2 should be thought of as mean or 'best fit' curves reflecting hazard variability. Because there is considerable uncertainty with regard to analytical models and, in some instances, statistical data bases, bounding curves which provide a confidence region around the best fit curves are necessary. These bounding curves are referred to as probability of nonexceedence curves that will not be exceeded a prescribed percentage of the time. A family of hazard curves that reflect analysis uncertainties is shown in Fig. 2.3. Throughout all parts of the PRA analysis it is essential that model uncertainties be quantified and propagated to the final outcome. This important detail of PRA is not dealt with in this study.

2.1.3 Resistance analysis

The ability of a particular component or system to resist the hazard will also be a random variable due to the inherent variability of component properties and workmanship. Random variables representing component

or system resistances are denoted R. Thus, each component will have a statistical distribution reflecting the probability that a certain level of resistance will be achieved. Resistance information in the form of probability density and cumulative distributions are shown in Figs. 2.4(a) and (b), respectively. The cumulative distribution function curve is referred to as the fragility curve (Fig. 2.4(b)) and gives the probability that a component resistance capacity is less than or equal to a specified level r_s, i.e.,

$$P[R < r_s] = F_R(r_s) \tag{2.2}$$

Again, uncertainty is not reflected in Fig. 2.4 but is necessary for a meaningful PRA.

Usually, the resistance distributions are expressed in terms of the same units used to measure the hazard, unless suitable transformations are available. The implication of this is that the components in the event tree are subject to a common hazard environment. The details of the resistance distributions of Fig. 2.4 will greatly depend on the definition of failure used for each system or component of the accident sequence. For example, if one steel containment is said to have failed when primary membrane strain is at material yield and another is said to have failed when primary membrane strain has reached one-half yield, the resistance probability density distribution of the former will lie considerably to the right of the latter. The definition of failure depends

entirely on the nature and function of the component in question and is left to the judgment of the analyst.

Recalling that each accident sequence is composed of a series of components (including the primary containment), a resistance distribution of _each_ of these components is required to complete the PRA. For event tree components that are mechanical systems, these resistance distributions are generally obtained through the use of fault tree analysis. Fault tree analysis is a method that uses a logic that is essentially the reverse of that used in event tree analysis. Fault trees are generally not practically suited to analysis of structural components and will not be explained further here [104].

For structures, e.g., steel containments, Monte Carlo and multivariate probabilistic methods are generally employed to evaluate resistance distribution. These methods are particularly useful because they make it possible to include more than one mode of failure in a structure and the degree of correlation which exists between these failure modes. For a steel containment various failure modes include, among others, the containment shell, penetrations, anchor bolts, welds and seals [109]. The individual failure modes may be likened to the individual accident sequences in the event tree; both represent various paths to failure. The main difference is that accident sequences are often assumed to be mutually exclusive while failure modes may show considerable correlation effects.

The statistical distributions of each component in an accident sequence can be used to formulate an overall or joint resistance distribution for that accident sequence. In the simplified example shown in Fig. 2.1(b), all internal systems and structures of the plant, except the primary containment, are represented as a single component in the tree. Thus, the longest accident sequence is made up of only two branches. However, this is sufficient to illustrate the construction of an accident sequence resistance distribution. For example, with respect to the accident sequence in Fig. 2.1(b) which results in a Release Category 1, its cumulative distribution of resistance becomes [5]

$$F_R(r) = F_{ss}(r) \ F_{mc_2}(r) \tag{2.3}$$

and the probability density function is

$$f_R(r) = \frac{d \ F_R(r)}{dr} \tag{2.4}$$

It should be recognized that Eqs. 2.3 and 2.4 are based on the assumption that the branches of the accident sequence are statistically independent and subject to a common hazard environment.

2.1.4. Calculation of occurrence frequencies

Given the information described in Secs. 2.1.1 to 2.1.3, it is possible to calculate annual frequencies of the various sequences in the event tree. Recall that the hazard curve describes the initiating event. Following this, the probability of failure calculated for each component failure branch may be found using the fragility curve function $F_R(r)$ where the subscript R is used in the general sense to represent a

single component resistance. The probability of success, i.e., the
reliability of each component success branch, is found using the
function

$$P[R > r] = 1 - F_R(r) \qquad (2.5)$$

which is the probability that component resistance capacity is greater
than a specified value of r. The probability (or frequency) of failure
or success is considered 'conditional' when it is calculated for a speci-
fied value of r. The conditional frequency of a component failure or
success is found using Eqs. 2.2 or 2.5, respectively. With the above,
the annual frequency of an accident sequence is found by calculating the
product of the frequency of occurrence of a particular size of hazard and
the conditional frequency of success or failure of each branch along the
accident sequence, and then summing such products over all sizes of that
hazard [102,104].

It will be supposed that a resistance distribution function $F_R(r)$
has been developed for an entire accident sequence as was discussed in
Sec. 2.1.3. Such a resistance distribution will reflect the
probabilities of failure or success of each component along the accident
sequence. Now, the hazard is a random variable, Q, of some intensity and
the sequence resistance is a random variable, R, of some capacity. Then
the annual frequency of an accident sequence (of a given radiological
release category) is analogous to a probability of failure P_f
occurring when the sequence resistance is less than the hazard intensity,
i.e.,

$$P_f = P[R < Q] \tag{2.6}$$

The probability of a sequence failure for a specified level of hazard intensity q_s is

$$P_f \big|_{q_s} = F_R(q_s) \tag{2.7}$$

The probability that the hazard intensity Q is within a small interval dq at the specified level q_s is

$$P\left(q_s - \frac{dq}{2} < q < q_s + \frac{dq}{2}\right) = f_Q(q_s)\ dq \tag{2.8}$$

Then the probability of such a hazard occurring and leading to failure or occurrence along the accident sequence is the product

$$f_Q(q_s)\ dq \cdot F_R(q_s) \tag{2.9}$$

When integrated over all conceivable levels of hazard intensity this becomes

$$\int_0^\infty f_Q(q)\ F_R(q)dq \tag{2.10}$$

This is the annual frequency of the sequence or the annual probability of failure P_f resulting in the given level of radiological release. The resistance and hazard distributions used in Eq. 2.10 are shown in Fig. 2.5. Equivalently, the probability of failure can be formulated on the basis of hazard intensity exceeding sequence resistance

$$P_f = P[Q > R] \tag{2.11}$$

which when integrated over all possible values of q yields [50]

$$P_f = \int_0^\infty [1 - F_Q(q)] \, f_R(q) dq \qquad (2.12)$$

The resistance and hazard distributions used in Eq. 2.12 are shown in Fig. 2.6.

2.1.5. PRA example

Using the simplified event tree of Fig. 2.1(b), example calculations follow to illustrate the determination of release category frequencies. Suppose in this example that the hazard is a break in the primary system piping (i.e., a loss-of-coolant accident). In this discussion, loads caused by this hazard will be limited to "statically equivalent" internal pressure (psi). Further, suppose that a statistical study of this phenomenon indicates that the probability density of hazard intensity, Q, is exponentially distributed as

$$f_Q(q) = 0.3e^{-0.3q} \qquad (2.13)$$

The probability density would graph as shown in Fig. 2.7(a) and the resulting hazard curve as Fig. 2.7(b) where

$$F_Q(q) = 1 - e^{-0.3q} \qquad (2.14)$$

Again, all calculations utilize best fit curves and uncertainties in the modeling are not quantified and propagated herein.

Next, resistance of the containment and internal safety systems to the internal pressure conditions must be evaluated. Working with data on property variability and appropriate definitions of failure, distributions of resistance vs. statically equivalent internal pressures (psi)

must be derived. For the steel containment, this means applying Monte Carlo or other multivariate methods in conjunction with various structural analysis techniques [108,109]. Suppose that these evaluations yield lognormal resistance distributions that reflect the randomness of structural properties such as yield point, modulus of elasticity and analysis error.

If the random variable of resistance R is lognormally distributed then the transformation lnR is normally distributed. The mean μ and variance σ^2 of the normally distributed, transformed variables can be found from [50]

$$\mu_{lnR} = \ln \mu_R - 1/2 \ln (V_R^2 + 1) \qquad (2.15)$$

and

$$\sigma^2_{lnR} = \ln (V_R^2 + 1) \qquad (2.16)$$

where V_R is the coefficient of variation, i.e.,

$$V_R = \sigma_R / \mu_R \qquad (2.17)$$

Statistics of the event tree branch that represents the various internal safety systems are taken as

$$\mu_{R_{SS}} = 20 \text{ psi}$$

$$V_{R_{SS}} = 0.3 \qquad (2.18)$$

where random variables of internal safety system resistance are denoted

R_{SS}. Then, using Eqs. 2.16 and 2.15

$$\sigma_{\ln R_{SS}} = 0.2936 \qquad (2.19)$$

$$\mu_{\ln R_{SS}} = 2.9526$$

By transforming the resistance variables R_{SS} to normally distributed variables $\ln R_{SS}$ and then standardizing them by [50]

$$Z = \frac{\ln r - \mu_{\ln R}}{\sigma_{\ln R}} \qquad (2.20)$$

tables may be used for

$$F_R(r) = \Phi(z) \qquad (2.21)$$

where $\Phi(.)$ is the cumulative distribution of the standard normal distribution. For the internal safety systems, the fragility curve based on Eq. 2.21 will graph as shown in Fig. 2.8.

Similarly, for the steel containment with a lognormally distributed resistance, the following parameters will be used

$$\mu_{R_{mc_2}} = 25 \text{ psi} \qquad (2.22)$$

$$V_{R_{mc_2}} = 0.25$$

where the random variables of metal containment resistance are denoted by the subscript mc_2. The transformed statistical parameters become

$$\sigma_{\ln Rmc_2} = 0.2462 \qquad (2.23)$$

$$\mu_{\ln Rmc_2} = 3.1886$$

and by Eq. 2.21 the fragility curve will graph as Fig. 2.9. Note that the internal physical conditions under which F_{Rmc_1} (located in the upper

branch) is evaluated may be quite different than those associated with F_{Rmc_2} because of variations in succeeding events. This may cause a different mode of failure to predominate resulting in two different fragility curves for the containment. A complete PRA would require the determination of both fragility curves, if different.

After the fragility curve of each branch in the event tree is determined, the overall or joint resistance distribution of each accident sequence can be found. If the safety systems and containment are statistically independent and subject to a common hazard environment, then Eqs. 2.3 and 2.4 may be used. Restricting our attention to Release Category 1 in Fig. 2.1(b), Eq. 2.3 gives

$$F_R(r) = F_{R_{SS}}(r) \, F_{R_{mc_2}}(r)$$

then, using Eq. 2.21 the fragility curve is obtained and graphed in Fig. 2.10.

The probability of failure for this accident sequence may be found using Eqs. 2.10 or 2.12. Since incremental data in terms of $F_R(r)$ are available, it is convenient to use Eq. 2.10 shown again as

$$P_f = \int_0^\infty F_R(q) \, f_Q(q) dq \tag{2.10}$$

or, numerically

$$P_f = \sum_i f_Q(q_i) \, F_R(q_i) \, \Delta q \tag{2.24}$$

With $\Delta q = 2.5$ psi, numerical integration yields

$$P_f = 1.1 \times 10^{-3} \tag{2.25}$$

That is, in this example, the annual frequency of occurrence of Release Category 1 due to a pipe break is 1.1×10^{-3}. Of course, this value is purely for this example and is not intended to reflect conditions at any particular nuclear facility. Numerical methods may also be applied to Eq. 2.12 to obtain the same results.

If other accident sequences were identified to result in a Release Category 1, then the overall frequency of Category 1 would be the sum of all such accident sequence frequencies (assuming the sequences are mutually exclusive). The overall release category frequencies are then used in a consequence analysis to complete the PRA. To facilitate this, a graph of annual frequency of occurrence vs. various release categories is used, as hypothetically illustrated in Fig. 2.11. This figure should also be qualified by bounding curves that reflect the uncertainty in the PRA. A consequence analysis basically amounts to a reinterpretation of radiological releases into terms of the damage done to the public and environment. Consequence analyses are site-specific and depend on such things as population density and local geography. Figure 2.12 shows a hypothetical damage or 'risk' curve where release categories have been redefined into terms of the associated damage expected. Schematically, the complete PRA process is described by Fig. 2.13.

2.2. Containment Reliability and ASME Service Limits

ASME Boiler and Pressure Vessel Code, Section III, Division 1, Subsection NE [4] applies to the design of the containment system which is

defined as the steel containment vessel and the penetrations and appurtenances attached thereto. Specific load combinations for steel containments are not defined in the ASME Code, unlike many structural codes. Rather, the ASME Code defines six conditions for load combinations: Design; Service Levels A, B, C and D; and Testing wherein different types of loads may be identified. However, the USNRC provides some direction in its Standard Review Plan, Sec. 3.8.2 [114] in which a listing of loads and load combinations for analysis are specifically given. The Service Levels A, B, C and D are categories in which load combinations associated with the function and life of the containment are descriptively defined. These four conditions are hereafter referred to as Load Categories A through D.

Steel containments designed according to Subsection NE are based on working stress concepts. Even in the cases where local inelastic behavior is permitted, the allowable behavior is given in terms of allowable stresses [90]. The design allowable stresses increase from Load Categories A through D. Although it is not spelled out, the implication is that the probability of encountering loads defined in the respective categories lessens from Category A to Category D, thus justifying the increase of stress limits. Still, the existing ASME Code criteria are strictly deterministic and provides factors of safety with expectantly sufficient margins, but with unquantified uncertainty. The philosophy associated with the ASME Code Load Categories sets the direction, however, for true safety or 'reliability' analyses.

In the risk assessment conducted in WASH-1400, analysis of reactor core melt-down was given the most attention because the associated consequences are the greatest. Similarly, because of the important function prescribed to the primary steel containment, a thorough containment reliability assessment is also warranted. From this, a more accurate measure of safety margins can be found; or at least a better understanding of uncertainty attached to safety margins gained. If reliability assessments of containments for a variety of hazards could be confidently done, then the knowledge gained could one day be reflected in the ASME Code. Such a Code, whose design stresses consistently considered the probability of occurrence of the various loads, would reflect a more uniform degree of safe design. Currently, the ASME Code does not permit design allowable stresses to be increased <u>consistently</u> with each consecutively less likely Load Category.

To illustrate this, consider the definitions of the various Load Categories. Category A includes all loads to which the containment vessel is exposed during normal plant operation plus the loads caused by a loss-of-coolant accident (LOCA) for which the containment function is required. Category B includes the applicable loads of Category A plus the additional loads resulting from natural phenomena for which the plant must remain operational. For steel containments enclosed in secondary concrete containments, this natural phenomenon is typically an earthquake referred to as the operating basis earthquake (OBE). The ASME Code [4, NE-3221] requires that both of these Categories be designed for the same allowable design stress levels. For primary membrane stress in the

containment, stress is restricted to approximately half of the yield stress. Since the probability of occurrence of Category B is obviously less than Category A, it is not consistent to impose the same limitations on allowable design stresses [88].

Category C includes the applicable loads of Category A plus the additional loads resulting from natural phenomena for which safe shutdown of the plant is required. Again, for steel containments this is typically an earthquake referred to as the safe shutdown earthquake (SSE). Generally, the SSE has a peak ground acceleration that is about twice that encountered for the OBE [95]. Again, it is obvious that the probability of occurrence of Category C is less than either Categories A or B. The ASME Code also recognizes this and allows primary membrane stress in the containment to rise up to near the yield stress.

Category D includes the relevant loads in Categories A, B and C plus additional dynamic loads which produce a localized effect on the containment vessel. Jet impingement and the dynamic pipe reactions resulting from a LOCA are examples of this. This is the only ASME Category that specifically allows for inelastic behavior in the continuous membrane of the containment shell. (See Appendix F of ASME Code for more details.) Therefore, the ductile capacity of the containment vessel as a whole in resisting LOCA pressures or severe earthquakes is not formally recognized by the Code.

From the previous discussion, it is seen that the per year encounter probability decreases for the loads in Categories A to D. Some preliminary work to actually quantify this decrease has already been done

with respect to ASME Code Section III as exemplified in Table 2.1; however, this table was not created for steel containment vessels [93]. The desired case would be service limits defined for each Category such that when combined with the probability of the hazardous event, acceptable and near uniform margins of safety would exist. Hence, hazards or loads that are almost certain to occur during the containment design life should be designed for such that there is very low probability of failure. Similarly, the containment can rationally be proportioned so that defined failure is more likely given extreme hazard intensities which are not likely to occur. As mentioned before, this type of reasoning is somewhat reflected in the current ASME Code.

The conservative stand of the ASME Code can be appreciated when one considers the important function delegated to the containment vessel and the large number of unknowns attached to various aspects of the loading and ultimate strength. Probabilistic methods for structural design are only good when the input data is well-described and correctly manipulated. Thus, the uncertainty in data bases and analytical models presents a very significant obstacle to probabilistic based code criteria. For example, buckling of the containment vessel is still not well-understood analytically and requires the use of knock-down factors to account for theoretical vs. experimental discrepancies. Therefore, while it would be reasonable to permit Category B stress limits to be larger than Category A, statements such as safely designing for inelastic behavior in continuous regions of the containment shell are much easier said than done. Such consideration of containment ductile capacity depends upon

available methods of reliably predicting it. Additionally, the nature of the unlikely severe hazards where inelastic behavior could be allowed must be well-described. As a result, the idea of a code fully based on probabilistic concepts is sound but not completely practical at this time.

Currently, studies are being conducted to make reliability approaches to design and analysis practical [27,108,109]. It is because of the current interest and activity in this area that reliability concepts have been introduced in this document. The remainder of this study, however, is written in terms of current design practice which is deterministic. Reliability concepts do not replace traditional deterministic designs. Rather, the tools of traditional structural analysis are supplemented by statistical theory to enhance the safety and economy of structural design.
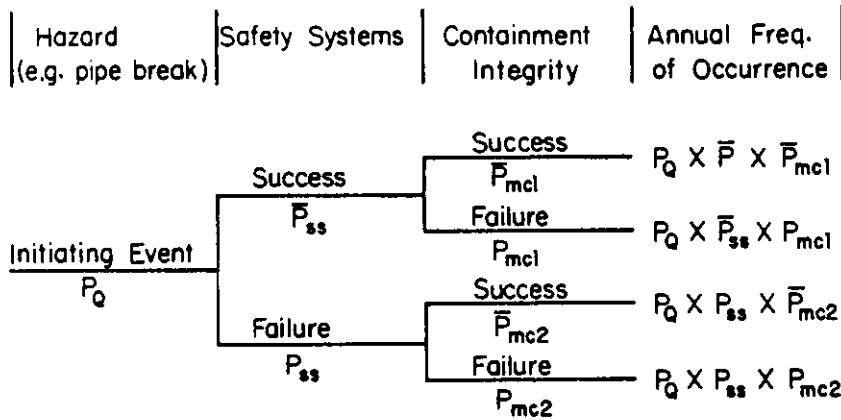
Hazard (e.g. pipe break)	Safety Systems	Containment Integrity	Annual Freq. of Occurrence

Initiating Event P_Q

Success $\bar{P}_{ss}$ — Success $\bar{P}_{mc1}$ — $P_Q \times \bar{P} \times \bar{P}_{mc1}$

Failure P_{mc1} — $P_Q \times \bar{P}_{ss} \times P_{mc1}$

Failure P_{ss} — Success $\bar{P}_{mc2}$ — $P_Q \times P_{ss} \times \bar{P}_{mc2}$

Failure P_{mc2} — $P_Q \times P_{ss} \times P_{mc2}$

Fig. 2.1a. Basic event tree

	Resulting Release Categories

Initiating Event P_Q

Success $\bar{P}_{ss}$ — Failure P_{mc1} — $P_Q \times \bar{P}_{ss} \times P_{mc1}$ — 4

Failure P_{ss} — Success $\bar{P}_{mc2}$ — $P_Q \times P_{ss} \times \bar{P}_{mc2}$ — 2

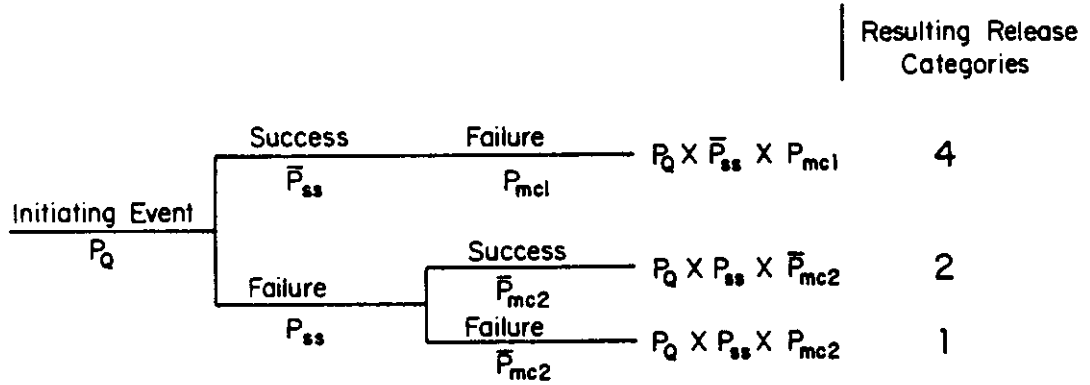Failure $\bar{P}_{mc2}$ — $P_Q \times P_{ss} \times P_{mc2}$ — 1
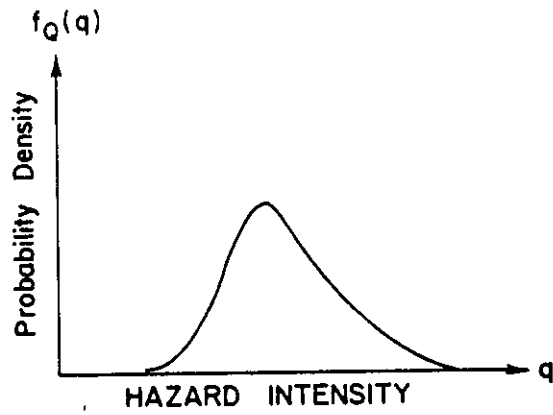
Fig. 2.1b. Reduced event tree

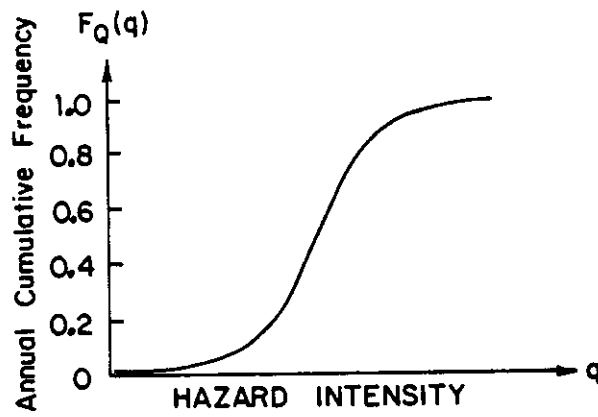Fig. 2.2a. Hazard probability density distribution

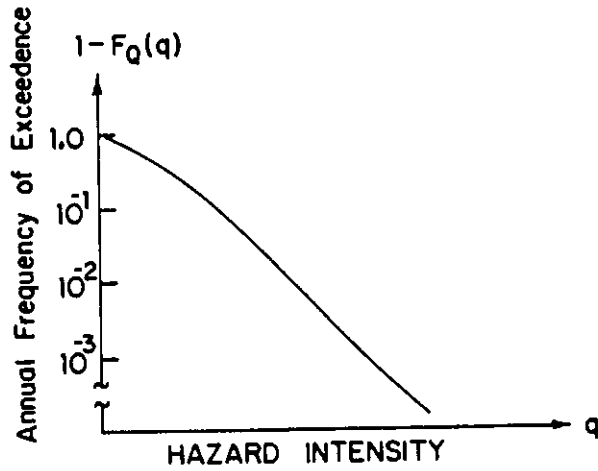

Fig. 2.2b. Hazard cumulative distribution
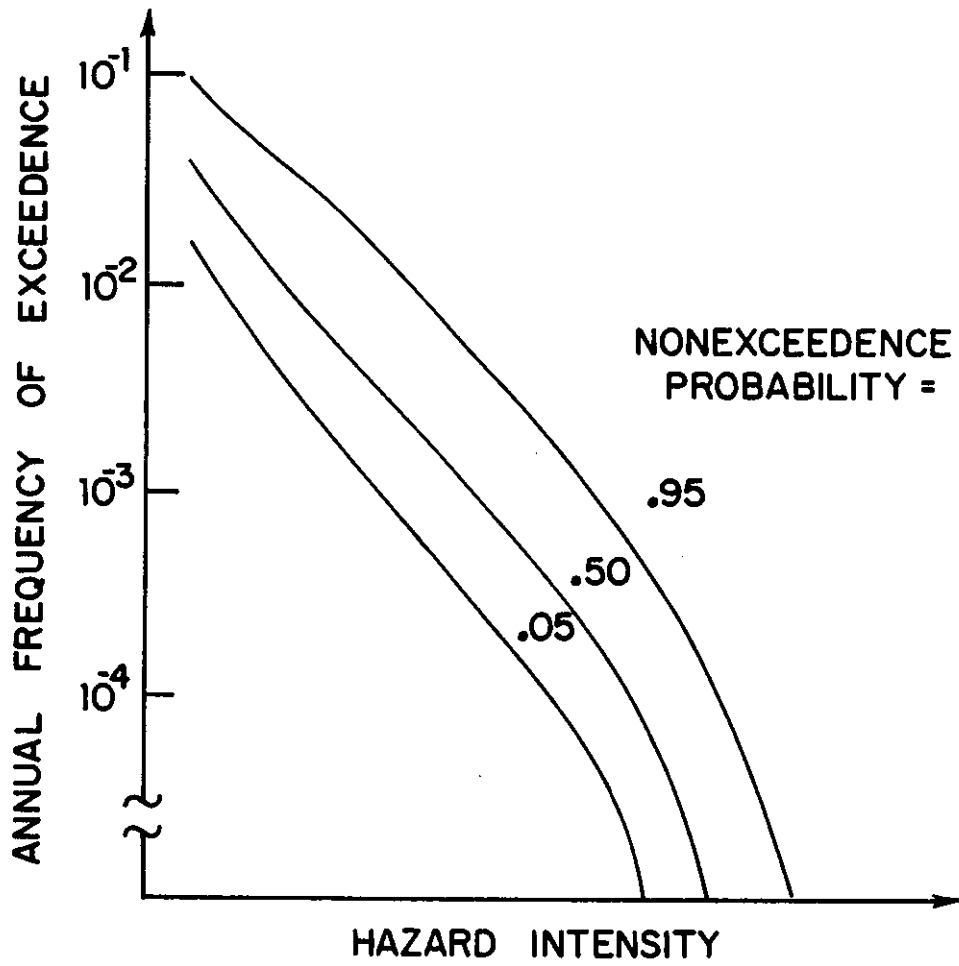

Fig. 2.2c. Hazard curve

Fig. 2.3. Hazard curves reflecting uncertainty [102]
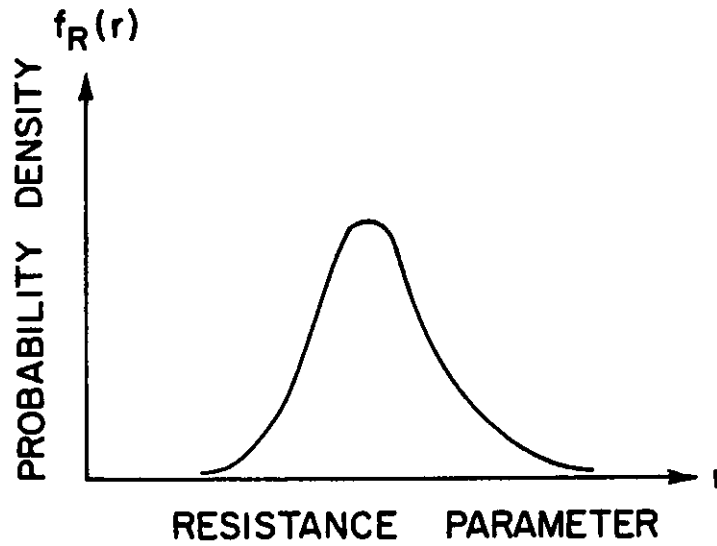
Fig. 2.4a.   Resistance probability density distribution
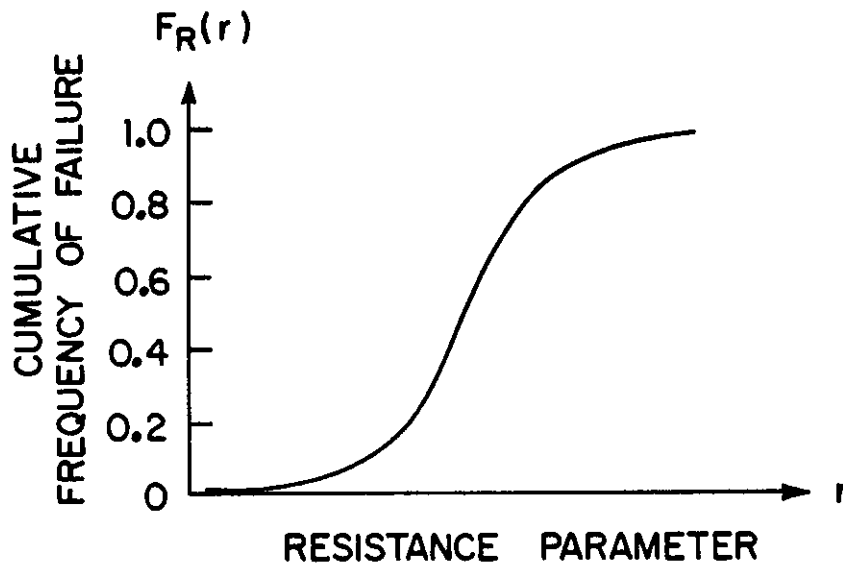
Fig. 2.4b.   Fragility curve

RESISTANCE

$F_R(q)$

Cumulative Freq. of Failure

1.0
0.8
0.6
0.4
0.2

q_s

q

$P\left[R \leq q_s\right]$

HAZARD

$F_Q(q)$

Probability Density

$q_s - dq/2$ $q_s + dq/2$

q_s

q

$P\left[q_s - dq/2 < q_s \leq q_s + dq/2\right]$

Fig. 2.5. Resistance and hazard distributions used in Eq. 2.10

RESISTANCE

$f_R(q)$

Probability Density

$q_s - dq/2$ $q_s + dq/2$

q_s

q

$P\left[q_s - dq/2 < q_s < q_s + dq/2\right]$

HAZARD

$1 - F_Q(q)$

Annual Freq. of Exceedence

1
10^{-1}
10^{-2}
10^{-3}
10^{-4}

q_s

q

$P\left[Q \geq q_s\right]$
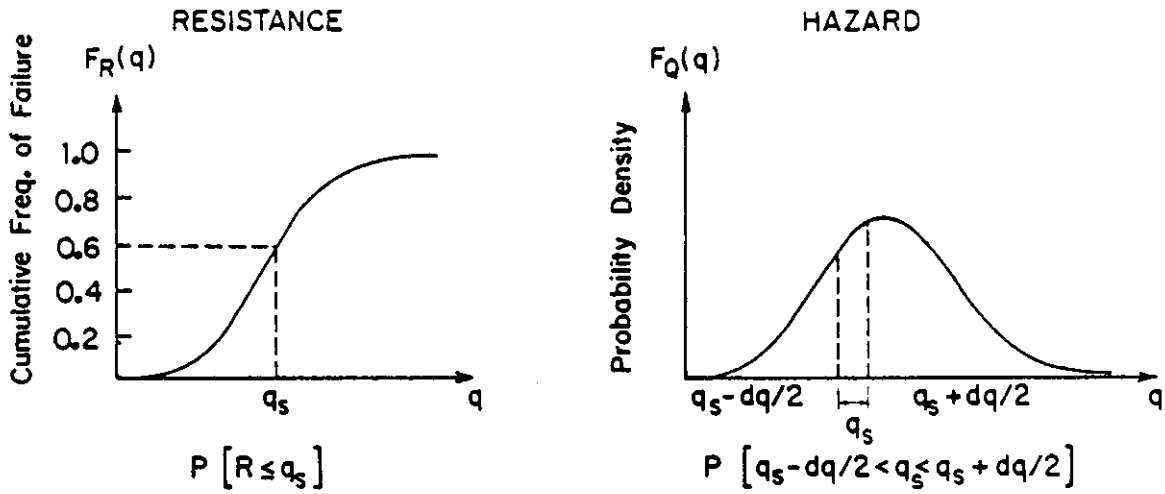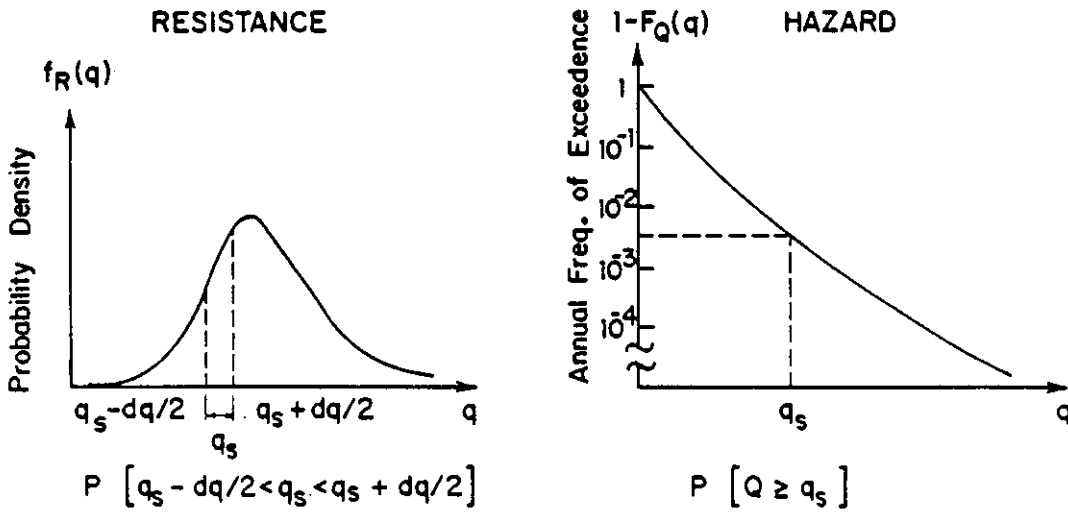
Fig. 2.6. Resistance and hazard distributions used in Eq. 2.12
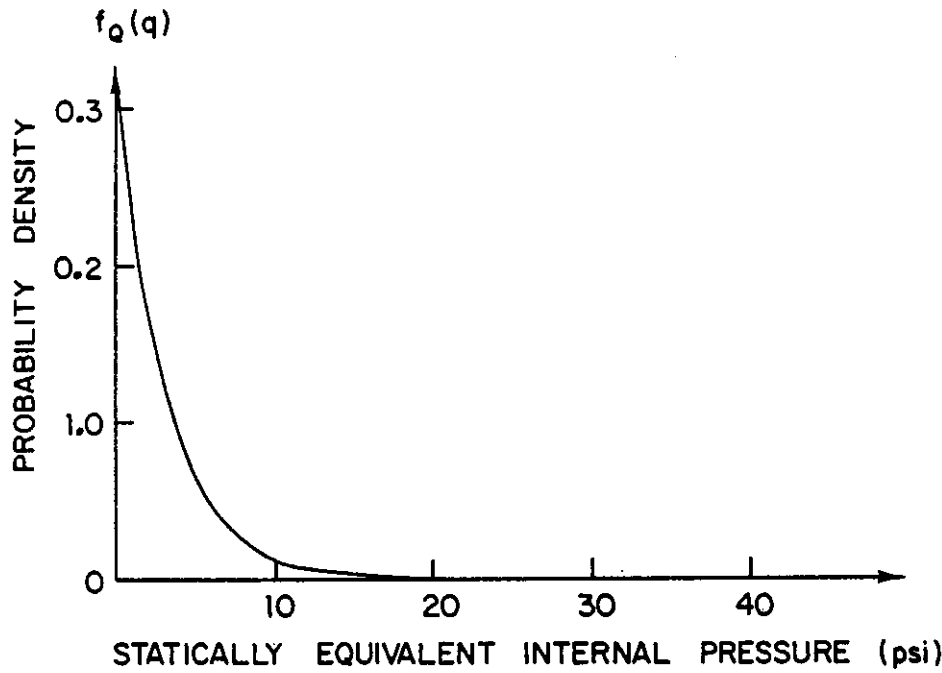
Fig. 2.7a. Hypothetical pipe break probability density distribution
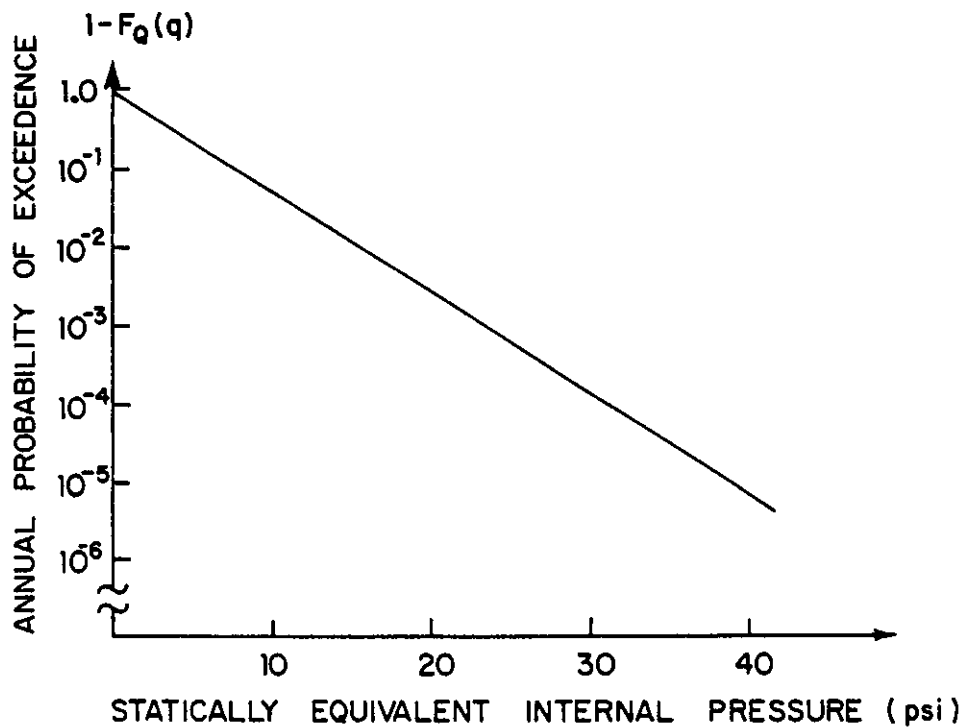
Fig. 2.7b. Hypothetical pipe break hazard curve
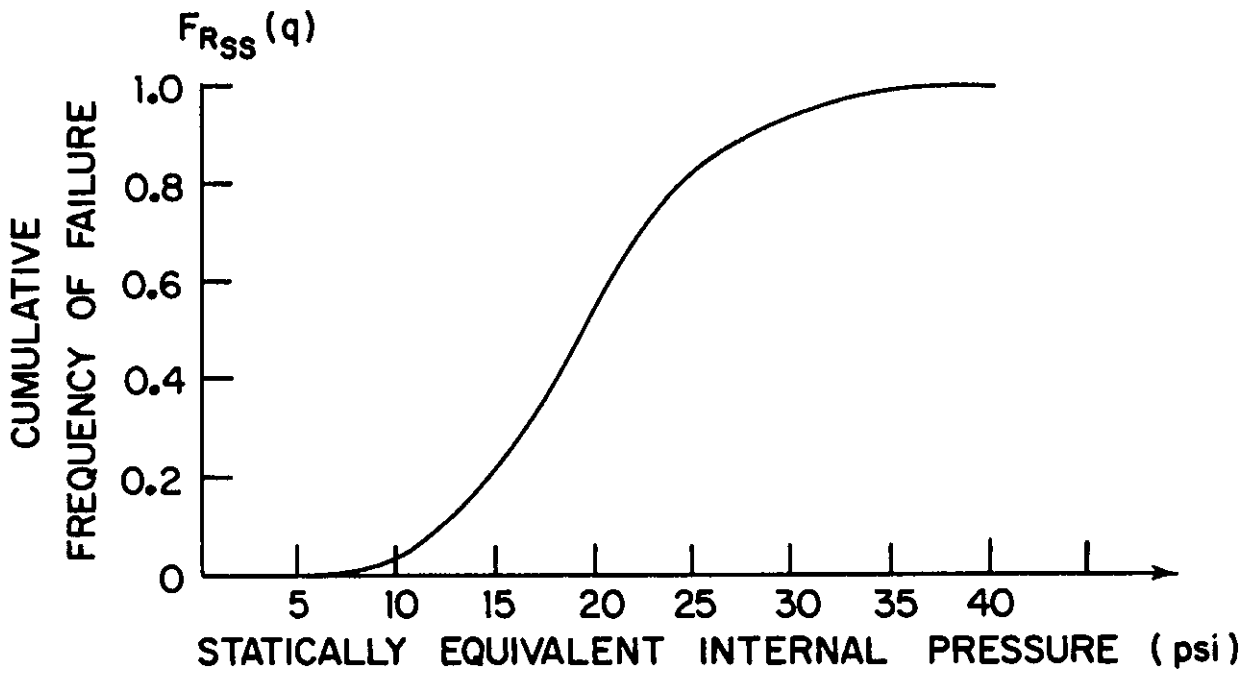
Fig. 2.8. Hypothetical fragility curve of plant safety systems
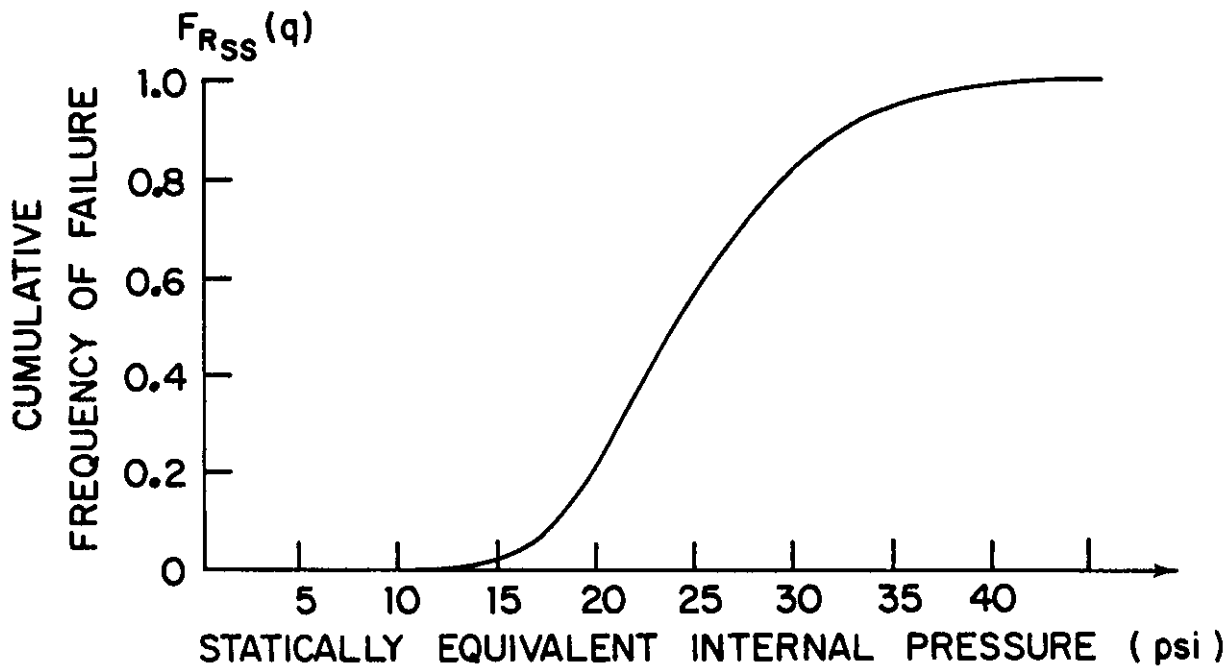
Fig. 2.9. Hypothetical fragility curve of steel containment integrity
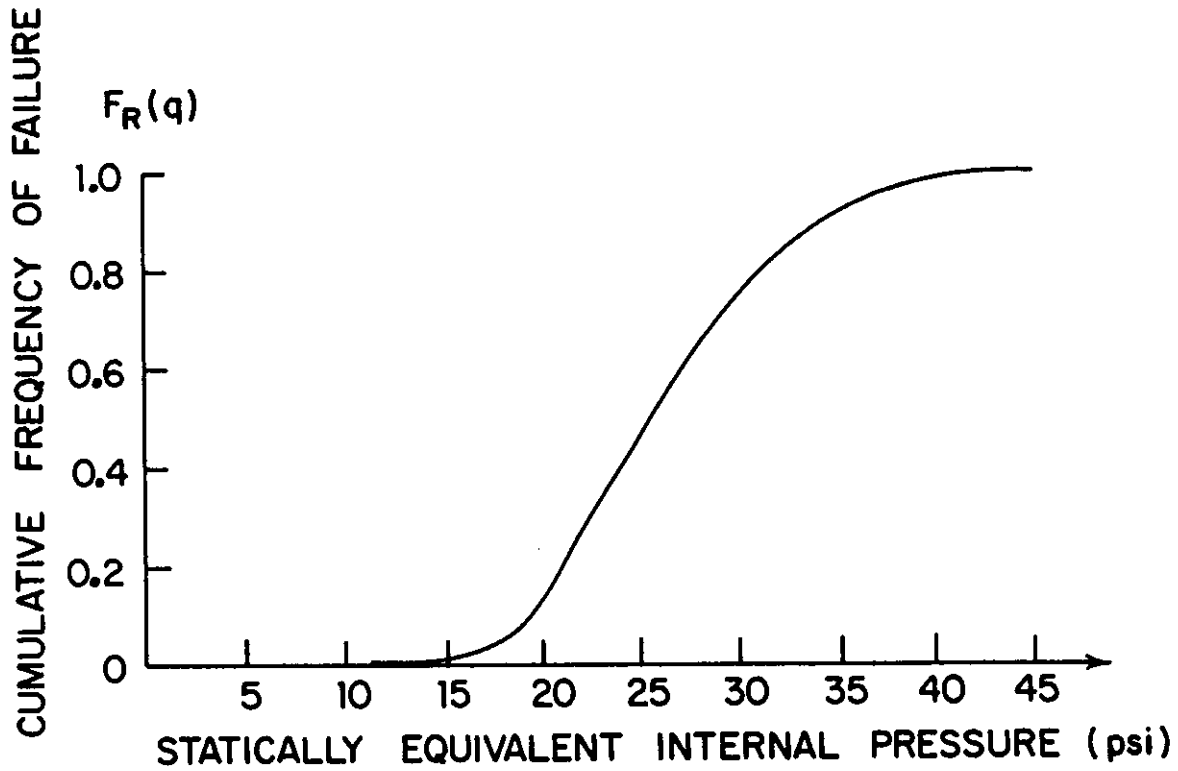
Fig. 2.10. Fragility curve reflecting joint resistance of
systems and components of Figs. 2.8 and 2.9
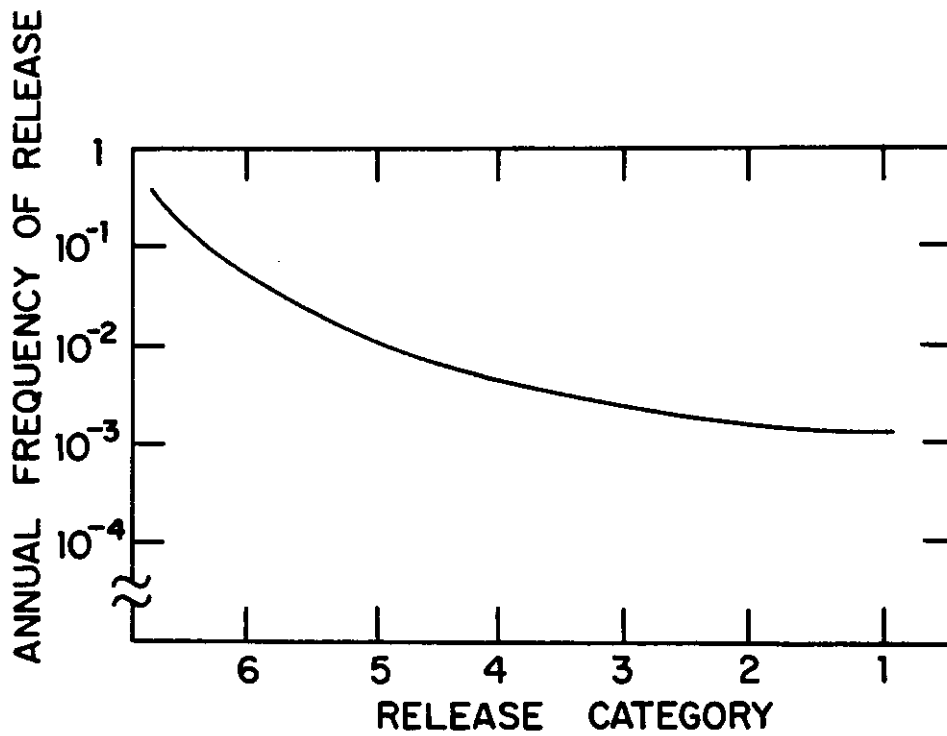
Fig. 2.11. Exemplary graph of annual radiological
release frequencies [102]
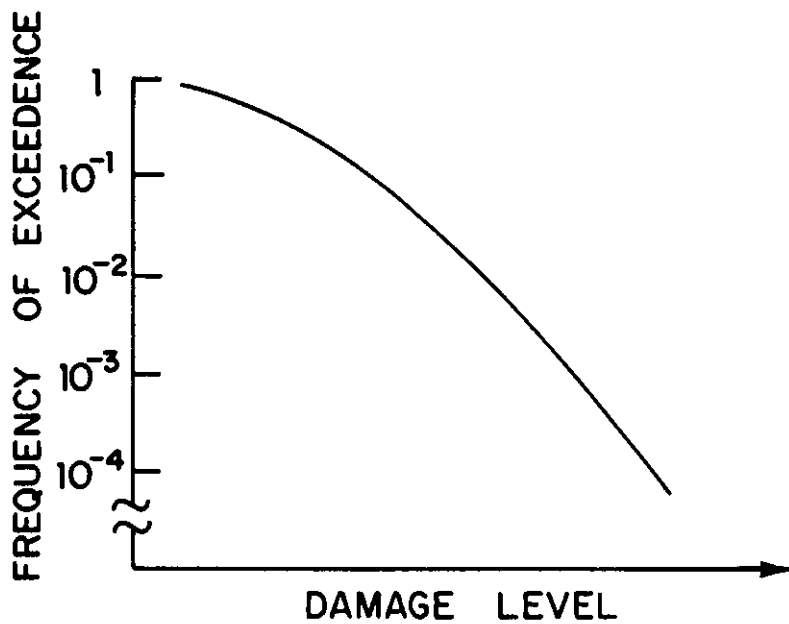
Fig. 2.12. Exemplary risk curve [102]

Hazard analysis

Frequency of exceedence

P_s

Hazard parameter

Cumulative frequency of failure

P_s

Resistance parameter

Component-fragility evaluation

Event trees
Fault trees
Containment analysis

Systems analysis

Probability density

Release category

1 3 2

Frequency

Release frequency

Weather data
Atmospheric dispersion
Population
Evacuation
Health effects
Property damage

Consequence analysis

Frequency of exceedence

P_i

Damage

Risk

31

Fig. 2.13. Overview of risk analysis [102]

Table 2.1. Correlation of event encounter probabilities
            and the ASME Code [93]

Per year event encounter probability	ASME Sec. III Service Levels
$1.0 \geqslant P\ (A_1, A_2, \ldots A_n,\ \text{simult.})^a > 10^{-1}$	A
$10^{-1} \geqslant P\ (B_1, B_2, \ldots B_n,\ \text{simult.}) > 10^{-2}$	B
$10^{-2} \geqslant P\ (C_1, C_2, \ldots C_n,\ \text{simult.}) > 10^{-3}$	C
$10^{-3} \geqslant P\ (D_1, D_2, \ldots D_n,\ \text{simult.}) > 10^{-4}$	D

[a]The subscripted letters, e.g., A_2, B_1, D_n, etc., represent the various loads that are defined for the respective Service Level Categories.

3. LOAD DESCRIPTIONS

3.1. Normal Operation

Primary containment structures are designed to provide a low leakage barrier against radiological release in conjunction with unlikely loading events. These loads, subsequently defined in Secs. 3.2 and 3.3, are of a much greater order of magnitude than the loads which the containment experiences during normal operation. Normal operating loads are all loads and combinations thereof that result from the plant start-up, operation, and normal shutdowns for repair and refueling. They are primarily of interest with respect to their additional contribution to the design basis peak responses of the containment.

Plant start-ups will result in a number of transient load peaks as the system approaches an operating equilibrium state. Several of these transient load peaks are imposed upon the containment vessel. However, the magnitudes of start-up loads on the containment are generally insignificant compared to the design capacity of the containment provided for unlikely loading events, hereafter referred to as internal and external events. Upon start-up, a pressure and temperature differential will develop across the containment shell. Also, since the containment is penetrated by main steam pipes, dynamic pipe reactions may be applied at the vessel penetrations. Even though the time-dependent magnitude of loads associated with plant start-up and shutdown is probably not as great as that resulting from internal or external design events, USNRC criteria lists its consideration [114].

In general, normal operating load levels result from the constant, or else transient and continuous, effects of the following:

D - Dead load of steel containment plus that of:

    (1) Equipment or piping within penetrations and on various appurtenances.

    (2) Hydrostatic head of the suppression pool water in BWR containments.

L - Live load of supported equipment (e.g., polar crane in some containment configurations).

T - Temperature.

P - Pressure.

R - Pipe reactions.

The magnitude of dead load is constant and relatively straightforward to determine. Live loads, as defined for steel containments, will generally be intermittent loads caused by moving equipment and do not include loads caused by natural or hazardous environments, such as wind or pressure, as is the case for conventional buildings. Such live loads may be calculated as the weight of the equipment increased by an appropriate dynamic load factor [11] to account for their motion. Equipment that vibrates must also consider potential resonance frequencies of the equipment and supporting containment.

The temperature of the containment shell, when taken as steady-state, is nearly uniform through the shell thickness due to: (1) relative thinness of shell; (2) high conductivity of steel; and (3) temperature variation per time interval is small. The temperature of a particular region

inside the containment will basically result from heat radiated and convected from the reactor and primary system piping. Thus, regional temperatures will depend, among other things, on the proximity of the containment shell to the reactor and the internal volume of the containment. Typical shell temperatures at normal operating conditions are around 75° to 150°F [3,49,80,92].

Pressure differential across the containment boundary under operating conditions is a result of external vs. internal atmospheric changes related to the natural environment or internal operating temperatures. Changes in one or the other will result in pressure differentials across the containment shell whose net effect is either an externally or internally applied pressure. With respect to operating conditions, only the external pressure needs to be considered since the steel containment, modeled as a thin shell, is more susceptible to external rather than internal pressure associated with operating conditions. Typically, the containment will be designed for a uniform external pressure of a few pounds per square inch or less [2,3,120]. The magnitude of external pressure is limited by the provision of redundant vacuum relief safety valves to alleviate significant external pressures.

Pipe reactions at steady state are basically a function of the pipe size and line pressure. The nature of the loads imposed on the supporting structure will also depend on the type of attachments used. Pipe reactions of the primary system piping may be bearing on the concrete secondary containment (outside), or the concrete sacrificial shield wall (inside), the primary steel containment. Therefore, actual pipe

reactions on steel containments will depend on if and how the pipes which penetrate the containment bear on the primary containment.

After normal operating loads are determined, they are carried forward and appropriately combined with design basis internal and external events. Dead and live loads must always be combined with loads resulting from internal and external events. Internal or external events may result in conditions in which the magnitude and time-space characteristics of temperature, pressure, and pipe reactions radically exceed those found during normal operating conditions. The actual variation will depend on the sequence of hazardous events. Generally, the worst is assumed to occur and thus temperature, pressure, and pipe loads resulting from internal and external events are applied concurrently to the containment. Therefore, it is unlikely that transients of normal operation can produce stress states in excess of those resulting from design basis events. Hence, such transients were not discussed in detail except to say that they do occur. Calculation of pressure, temperature, and pipe reaction load levels at continuous plant operating conditions are needed in any case to provide initial conditions for calculation of the more critical states occurring during design basis events.

3.2. Internal Events

This section addresses the loads associated with the loss-of-coolant accident (LOCA) in the pressurized water reactor (PWR) and the boiling water reactor (BWR) containments and with safety-relief valve (SRV) actuation in the BWR containments. A LOCA is defined as the rupture of

the primary system piping resulting in the release of high energy, radio-active fluids from the primary reactor system and reactor core into the containment vessel. The most critical LOCA for which the containment is designed is a circumferential or "double-ended" rupture with free discharge of the hot pressurized water flowing from both ends of the ruptured pipe. This limiting situation is also referred to as a design basis accident (DBA). If a LOCA occurred, the steel containment vessel provides a barrier against the release of the radioactive materials to the environment. Loads experienced by the containment in fulfillment of this function depend greatly on the type of containment in question.

Boiling water reactor vessels have several pipes connecting the reactor vessel atmosphere to a suppression pool of water. A safety-relief valve (SRV) is placed in each one of these pipes. When the BWR vessel becomes over-pressurized, one or more of the SRVs open and release steam and air to the suppression pool. In some respects, SRV actuations could be considered as normal operating loads. However, because of their somewhat unpredictable, intermittent occurrence and because their loading effects on the containment wetwell are similar to those caused by LOCA; SRV actuation is included here.

Both LOCA and SRV actuation produce a number of different types of loading on the containment vessel. The following deconvolves and identi-fies separate loads produced by these two events. In some cases (e.g., chugging in BWRs) the effect on the containment is similar from either event.

3.2.1. Pressure

Internal events of Sec. 3.2 can result in liquid and/or gas pressure loadings on the containment vessel. In this section, pressures are those due to internal vs. external gas pressure differentials. Upon initial occurrence of the internal event the internal pressures are swiftly increased. At this time, the pressure increases will often be nonaxisymmetric. Therefore, the space and time variation of these pressures must be adequately known. Sometime after the internal event occurs a more stable state of equilibrium is approached and the pressures become essentially uniformly distributed and steady. The actual magnitude and time of this quasi-steady state depend greatly on the type of containment. This long-term response is characterized by the energy input to the containment atmosphere being balanced by minimum heat removal capability of safety systems such as sprays and emergency-core-cooling systems (ECCS).

3.2.1.1. BWR containments

In the United States, containments housing BWRs operate on the principle of condensing the steam released during a LOCA in a large pool of water to prevent large initial containment pressures. This arrangement is necessary because dry containments for BWRs could not be designed to be economically competitive with PWRs. An economically comparable dry containment for a BWR could not handle the higher LOCA pressures resulting from the higher energy content per kilowatt of output in the BWR primary system [119]. At this time there are three basic types of pressure suppression containments known as Mark I (Fig. 3.1), Mark II (Fig. 3.2) and Mark III (Fig. 3.3). In all three there are two distinct volumes of containment.

The first is referred to as the drywell. In this volume, the reactor vessel and the primary system piping (Fig. 3.4) are housed. The recirculation loop of the primary system piping contains the highest energy fluid. Design and sizing of Mark I and Mark II for pressure are generally based on an instantaneous double-ended break in the recirculation loop. Mark III containments are usually designed for a double-end break in the main steam pipe. However, drywell response for Mark III containments is analyzed for a break in the recirculation loop, also [115]. If a rupture occurs in the primary system piping, the high enthalpy water flows out of both ends of the broken pipe, flashing partly to steam. The drywell receives this released fluid and immediately channels it to the wetwell through a system of vents.

The wetwell encloses a large pool of water called the suppression pool. The amount of water in this pool varies from 2500 to 5000 tons [115]. The vents from the drywell are submerged in the suppression pool of the wetwell. The hot steam and water initially received in the drywell is intended to discharge into this suppression pool. There, much of the energy of the escaping fluid is absorbed to mitigate damage to the plant and public. The suppression pool condenses the steam and cools the hot water in this process. Noncondensibles, mainly air entrained in the fluid discharged into the suppression pool, bubble to the surface and collect in the wetwell air space. In addition, steam from the heated suppression pool, and initial steam that was not completely condensed, may also collect in the wetwell air space.

3.2.1.1.1. Short-term pressure response   BWR pressure suppression containment designs experience a short-term and long-term response to the pressures in the drywell and wetwell volumes of the containment. The peak short-term response occurs within the first seconds to minutes following a LOCA. The magnitude and time of this peak pressure depends on the containment design housing the BWR. Primarily, this amounts to consideration of:

1) Maximum break size conceivable for the primary system piping.

2) Total vent area available for the drywell to discharge the steam-water-air mixture to the wetwell.

3) Air space volumes in the drywell and wetwell and the size of the suppression pool (i.e., heat sink capacity).

The blowdown from the ruptured pipe subsides and ends within the first few minutes [115,119]. Before and concurrent with the end of blowdown, the emergency-core-cooling system (ECCS) flow enters the reactor vessel and then flows from the assumed pipe break and condenses the steam in the dry well. This leads to a substantial pressure reduction in the drywell and, subsequently, in the wetwell; and the end of the short-term phase.

The short-term pressure peak is the design controlling peak for both the drywell and the wetwell for each of the Mark I, II and III containment designs with one exception. For the Mark III containment, the wetwell design is determined by the long-term peak pressure [115]. The Mark I wetwell and drywell is typically designed for a short-term pressure peak of 60 to 65 psig. Pressure loading for the Mark II wetwell and drywell is also based on short-term pressure response with a pressure

peak of 45 to 50 psig. For both the Mark I and Mark II designs, the short-term pressure peak occurs in a time period of about 10 to 100 seconds [115]. The Mark III containment drywell is designed for a short-term pressure response with a peak of 25 to 30 psig. This peak occurs within a few seconds after the pipe rupture [115,119].

The transient nature of short-term pressure requires consideration of dynamic effects on the containment shell. Further, the initial pressurization of the dyrwell and wetwell may be significantly nonaxisymmetric, depending on the location and nature of the pipe rupture. Therefore, time-space variation should be known for short-term pressure response. Typical pressure time histories of BWR drywells and wetwells are shown in Figs. 3.5 and 3.6 from which the order of short-term responses can be seen. Also, the drywell should be studied for local pressure peaks caused by internal compartment routing of the steam.

3.2.1.1.2. Long-term pressure response   ECCS water is provided to cool the reactor core and to assure that the decay heat from the fuel will not eventually cause primary containment failure and, consequently, release of radioactive material. This water floods the reactor pressure vessel and then flows from the assumed pipe break. Initially, this spilling water condenses the steam in the drywell leading to a substantial pressure reduction. Vacuum breakers from the wetwell to the drywell are provided to alleviate the pressure differential potentially produced between these two volumes. Steam condensation and vacuum breaker activation results in wetwell and drywell pressures of about

5 psig at this point [115]. However, it is possible, depending on ECCS and vacuum breaker performance, for the Mark III drywell to be subject to an external pressure at this time (Fig. 3.6) of several psi.

The process of the foregoing paragraph marks the beginning of the long-term pressure response. Thereafter, the wetwell pressure continues to rise as the ECCS transfers core decay heat from the reactor pressure vessel to the suppression pool. The peak long-term pressure in the wetwell occurs when the heat input rate from the reactor pressure vessel is balanced by the mimimum capability of the heat removal systems. This occurs several hours after the LOCA. Due to the large wetwell volume in the Mark III containment designs, the design pressure for the wetwell is determined by the long-term pressure peak. Typically, Mark III wetwells are designed for a pressure of about 15 psig [115,119]. The relatively small wetwell volumes of the Mark I and Mark II designs result in short-term pressures exceeding the long-term pressures. The time-space variation of long-term pressure is not important because it is nearly uniformly distributed and varies slowly over time.

3.2.1.1.3. Safety relief valve actuation

Safety relief valves (SRVs) are provided to vent off steam from the BWR vessel when it becomes over-pressurized. SRVs are located in pipes that go from the reactor pressure vessel directly into the suppression pool. Therefore, only the wetwell is directly pressurized when a SRV is actuated. However, pressurization of the drywell is also possible if the vacuum breakers open. Since a LOCA results in depressurization of the reactor vessel the SRVs should be closed during a LOCA.

SRV gas pressures in the wetwell result from: the air initially inside the connecting pipe that is injected into the wetwell; pool swell (Sec. 3.2.3); incomplete condensation of steam discharged from the reactor pressure vessel; and the heating of the suppression pool. The most severe situation of SRV actuation occurs when main steamline isolation values are closed with the reactor at full power [115]. The BWR is thus isolated and quickly overpressurizes resulting in multiple-sequential relief valve actuation. Such an event is an extreme accident and the resulting hydrodynamic loads (Sec. 3.2.3.2) can be more severe than gas pressure loads associated with multiple SRV actuation. This is also often the case in single SRV actuations. However, the pressures produced in the wetwell airspace must also be quantified and added to the hydrodynamic response.

3.2.1.2. PWR containments   A pressurized water reactor (PWR) system is shown in Fig. 3.7. In this system, pressure is applied to the primary coolant system (i.e., primary system piping) by a pressurizer, allowing no net vaporization of the coolant. Nuclear fission of the fuel transfers energy to the primary coolant (i.e., water), thus increasing its temperature. The heated water of the primary loop is then circulated to steam generators where much of its energy is transferred to water in a secondary loop which is vaporized and used to power turbines. The pressurized water in the primary coolant system is directly in contact with the nuclear fuel, i.e., the primary loop and reactor vessel form a closed

system. For a PWR a design basis LOCA is initiated when a design basis break occurs in the primary coolant system.

The coolant water in the primary loop of a PWR is kept at about 2500 psia which is about twice the pressures found in BWRs [124]. Primary coolant water leaving the PWR is at about 600°F which is near the saturation point of the coolant for the system pressure [124]. If a rupture occurs, the saturated water undergoes rapid flashing and expansion in the reduced pressure environment of the containment. The steam and nonflashing water are released to the interior of the facility and must be contained. Therefore, containments for PWRs are sized to provide an adequate volume that will safely accommodate pressures resulting from the reactor coolant energy released during a LOCA. The containment vessel must be large enough to resist the resulting pressures and keep the containment below dangerous stress levels.

In a dry containment, the LOCA energy is released directly into the containment atmosphere, quickly pressurizing its entire volume. An alternative, introduced by the Westinghouse Electric Corporation, is the ice condenser containment for the PWR which provides pressure suppression capability similar in principle to the BWR pressure suppression containments. Instead of allowing the released energy to flow directly into the entire volume of the containment, the high energy fluid is initially trapped and routed within subcompartments in the lower part of the containment vessel. The high energy fluid is then made to flow through a compartment filled with a latticework of ice. Here, much of the fluid

energy is absorbed before reaching the main volume of the containment, resulting in much lower pressures.

3.2.1.2.1. Dry containments

Steel dry containments are typically free-standing cylinders with spherical, elliptical, or torispherical domes (Fig. 3.8). Also, some spherical dry containments have been constructed (Fig. 3.9). Primarily, the internal pressure rise is a function of the free volume in the containment vessel. And, the internal pressure rise is directly related to the size (i.e., megawatt rating) of the PWR. The minimum volume required to enclose the primary coolant loop, steam generators, and their supporting concrete structures is generally about 1.6 to 2.0 million cubic feet [120]. Typically, though, dry containments range in volume size from 2 to 3 million cubic feet depending on the megawatt rating of the PWR and the containment strength. Many economic considerations go into the amount of strength vs. increased volume that can practically be provided.

In the lower central region of the containment, the reactor vessel, primary loop, and steam generator are supported and partially enclosed by thick concrete structures (Figs. 3.8 and 3.9). These concrete structures also serve as internal missile protection for the containment vessel and they reduce pressure transients on the containment vessel shell [41]. Consequently, LOCA pressure loading in a dry containment will essentially be uniform; however, it will vary over time.

Dry containments have few features designed to specifically suppress the 'initial' energy released by a LOCA. For a given containment volume,

the time of initial peak pressure (assuming full power operation) depends primarily on the break size and hence the duration of the blowdown. Usually, the severe conditions imposed for design purposes result in peak pressures occurring in about 10 seconds as shown in Fig. 3.10 [14,49,115,120]. Pressure peaks of 45 to 65 psig have been designed for depending on a number of parameters, some of which were briefly introduced in the foregoing paragraphs.

Within about a minute after the LOCA occurs, various safety systems are operating to mitigate the accident. ECCS provides water to cool the reactor vessel and control its fuel decay heat. Sprays shower water into the heated atmosphere of the containment vessel. Also, the heat conducting solid structures act as heat sinks to absorb energy. These and other safeguards all help to arrest and reverse the initial pressure rise. Their ability to successfully accomplish this and maintain a downward trend in pressure depends on their design capacity and successful operation. That is, their heat removal capability must balance the energy input to the containment atmosphere. If they cannot, then long-term pressure will continue to slowly rise beyond normal design strength of the containment.

The implication of continued rise in the long-term pressure leads to a load state referred to as overpressure. As the name implies, this load consists of quasi-static internal pressures that exceed the design capacity of the containment. The containment material would eventually

yield and behave inelastically until the ultimate strength of the
containment occurs and, eventually, integrity failure. Such a situation
cannot occur unless the various internal safety systems fail. In this
case, melt-down of the reactor core could also be a potential danger.
The severe consequences of the above have made its prevention mandatory.
Determination of ultimate containment capacity and its respective level
of overpressure [109] is of interest in "what if" scenarios in which the
time factor anticipated before failure could be of aid in deciding what
public safety measures are best and/or feasible.

3.2.1.2.2. Ice condenser containments   Free-standing steel
containment vessels housing ice condenser systems have thus far been
upright cylinders with capping domes (Fig. 3.11). The pressure suppres-
sion capability provided by the ice has permitted reduced containment
volume and design pressure. Containment volumes for PWR pressure
suppression containments are generally on the order of about half the
volume required in a dry containment housing an equivalent sized PWR.
For example, the Sequoyah containment requires a free volume of 1.2
million cubic feet for a LOCA design pressure of 12 psig. An equivalent
dry containment would require about 2.3 million cubic feet for a LOCA
design pressure of 47 psig [53]. In this example, about 1200 tons of ice
is housed in an annulus around the inside of most of the containment
perimeter to make these significant reductions possible [53].

Here again, the use of the pressure suppression principle introduces
two distinct phases that characterize the response of a free-standing
steel containment vessel to a LOCA. Therefore, it is convenient to

describe short-term and long-term characteristics of the pressure loading.

Similar to the drywell/wetwell arrangement in BWR containments, the ice condenser containment is divided into two distinct volumes connected by a passage designed to be a heat sink (i.e., the ice-filled compartment). Analogous to the BWR suppression pool, the high energy fluid released by a LOCA is intended to traverse and be dissipated in the ice filled compartments as it flows from the lower to the upper volume due to the differential pressure. The lower volume boundary is defined by various structural concrete walls and slabs that house and support the reactor vessel, primary loop and steam generators. Within the lower volume, there are various subcompartments incident to equipment housing and support purposes. The base of the ice-filled compartments rings the outside of the lower volume (Fig. 3.11) and is accessible to all regions of the lower volume. The upper volume is simply the open air space of the containment vessel into which the flow from the ice-filled compartment is released.

If a design basis rupture occurs in the primary coolant system, steam and nonflashing water enters the lower volume, pushing the air therein through the ice condenser. The constraint of the lower volume causes almost instantaneous peak pressures in the lower subcompartments. As the high energy fluid flows into the ice condenser, initial pressure peaks in the ice-filled compartments follow, occurring in about 0.1 second after the rupture (Fig. 3.12). These pressures quickly reach their initial peaks and are reduced as condensation of the steam is

initiated in the ice. Condensation of steam within the ice condenser allows a continual flow of steam from the lower volume, thus substantially reducing the time that the containment is at an elevated pressure [53]. Since the free-standing steel containment vessel forms the outer shell of the ice condenser compartments, it will be subject to dynamic non-axisymmetric pressures of the initial air and steam flows. Figure 3.13 shows examples of the time-space variation of the pressure load around the containment shell. Typical peaks are on the order of 10 psig [53,115].

The pressure in the upper volume rises steadily from the beginning of the LOCA primarily due to the initial displacement of air from the lower volume. Within about 10 seconds after the start of blowdown, the upper volume reaches a peak pressure approximately equal to the lower volume (i.e., about 10 psig) [53,115]. However, the critical phase occurs within the first second(s) after blowdown where the lower volume and ice condenser are being dynamically pressurized. From here on dynamic time-space variation is not significant and the short-term response is over.

After the first 10 seconds, almost the entire containment vessel has reached a uniform pressure of around 10 psig, maintained at this point by the ice condenser. Upon completion of blowdown (on the order of a minute after rupture occurs) the containment spray system has started and the ECCS has begun flooding the reactor vessel to keep the core cool. The spray system cools the containment atmosphere and the remaining ice in the ice condenser is now exposed primarily to only residual core heat.

These safety features bring about a slow and steady decline of the containment pressure (Fig. 3.14). After about 10 minutes, return air fans are started to reduce the internal pressure even further as the upper volume air is returned to the lower volume.

Calculations for a DBA include enough ice after blowdown to absorb fuel decay and residual core heat for about one hour. After ice meltout, steam from the reactor coolant system is removed by the containment spray system. As a consequence, the containment pressure rises again reaching a peak of around 15 psig in about 1.5 hours after the accident [53] (Fig. 3.14). At this time, the minimum heat removal capability of the sprays balances the energy input from the reactor vessel. It is this second peak pressure which establishes the design pressure for the overall containment vessel, assuming non-axisymmetric dynamic short-term pressures are not controlling. Because of the uniform, slowly varying nature of the long-term pressures, long-term containment response can be based on the peak pressure without regard to time-space variation.

3.2.2. Temperature

Significant thermal stress in the steel containment vessel primarily results from a LOCA. The LOCA releases saturated steam and/or superheated steam into the steel containment. This high energy steam then transfers some of its energy in the form of heat to the steel shell thus inducing a state of stress in the shell. The quality and temperature of the high energy steam in contact with the shell will vary with both space and time. To evaluate the above, considerations will have to be given to

the type of reactor (e.g., BWR or PWR) and containment vessel; the postu-
lated break location in the primary piping system; and channeling effects
of internal structures. This discussion is restricted ot heat trans-
ferred by the released steam. Heat transfer via an impinging jet of high
energy fluid partially or solely composed of water is not covered.

3.2.2.1. Heat transfer   The transfer of heat from the steam to
the steel shell is a complicated process. To give the analyst some in-
sight into the mechanism behind the time-space variation of the steel
shell temperature, some of the basic concepts of heat transfer will be
presented.

Steam released by a rupture in the primary piping system comes in
contact with the cooler steel shell of the primary containment and con-
denses to liquid. The condensation of the steam will take place in the
form of dropwise condensation and/or filmwise condensation. Experience
with steel surfaces has shown that filmwise condensation is most likely
and it is recommended that calculations be made assuming this process is
taking place [33]. The process of condensation represents a phase change
that liberates energy. This energy, referred to as latent energy, is in
the form of heat which is transferred to the cooler steel shell by con-
duction and convection through the film of water.

The theory for film condensation is based on saturated steam coming
in contact with the containment surface. However, if superheated steam
is known to be contacting the steel shell, a different and more compli-
cated approach is appropriate. In BWR facilities, a small break in the

steam line can result in throttling of the reactor system high pressure steam to the low pressure drywell; in turn, this can result in super-heating of the steam [115]. Dealing with superheated steam is beyond the scope of this manual. In most circumstances, experiments have suggested that the effect of superheat may be ignored and that calculations may be based on saturated steam with little error [38]. Therefore, in accordance with theory, the film surface temperature will be taken as equal to the temperature of the adjacent saturated steam.

The rate of heat transfer is referred to as the surface or film coefficient h and is measured in units of energy/(time·area·temp.). The value of h is very important in determining whether the initial temperature rise through the thickness of the steel shell is predominantly in the form of a gradient or if it may be characterized as uniform.

The surface coefficient h depends on the temperature, thickness and flow characteristics (e.g., laminar or turbulent) of the water film and the purity of the saturated steam driving the process. The surface coefficient is also directly dependent on the film density ρ, dynamic viscosity μ and thermal conductivity k which are all in turn dependent on the film temperature. Film thickness and flow characteristics depend upon the dimensions and geometry of the steel shell and the film temperature where the temperature effects are often incorporated in terms of the differential temperature Δt across the film thickness, ($\Delta t = t_s - t_v$ where t_v is the film surface temperature, i.e., temperature of the adjacent saturated steam, and t_s is the steel shell surface

temperature). The film properties, μ, ρ and k, are evaluated at the average temperature t_m of the film, i.e., $t_m = (t_s + t_v)/2$.

The interdependence of the parameters with respect to temperature complicates the problem because the steel shell surface temperature rises over time after the steam contacts it. Thus, the surface coefficient is constantly changing as the containment vessel heats up. Also, the quality of the steam is very important. Air entrained in the saturated steam will significantly reduce the values of h [38].

Methods for calculating values of h are based on theory modified by empirical factors to fit experimental data. An often used equation for turbulent flowing film on veritical surfaces developed by Nusselt in 1916 and modified by Kirkbride in 1934 is [38,42]

$$h = 0.0076 \left[\frac{k^3 \rho^2 g}{\mu^2} \right]^{1/3} (N_{Re})^{0.4} \tag{3.1}$$

where N_{Re} is Reynolds Number which will always be greater than 1800 for turbulent films. Reynolds Number may be expressed as

$$N_{Re} = \frac{4\Gamma}{\mu}$$

where Γ is the mass flow rate of the film in mass/(length·time). Solutions derived from Eq. 3.1 and similar equations must be regarded as estimates because of their empirical nature and the constantly changing temperature dependent properties of the film. Technically, temperature dependence can be accounted for by up-dating all parameters for each time-step in a computer code designed to solve the heat transfer problems

over time and space. However, such sophistication may not be justifiable if the distribution and nature of the steam is not equally well-described. Correct determination of h is very important in determining the nature of the temperature rise in the steel shell. Unfortunately, the designation of h is largely an art based on experience.

Once h is known on the inside and outside surfaces of the containment the problem may be solved. Since the h for the steam condensate will be several orders of magnitude larger than the h for air, the exterior surface of the steel plate may be idealized as an adiabatic surface [38]. Assuming the initial plate temperature to be uniform through its thickness and the nature of the steam driving the process to be constant, the classical solution of the temperature distribution in a plate with respect to time is [38,42]

$$\frac{\Theta}{\Theta_i} = \sum_{n=1}^{\infty} 2 \frac{\sin p_n}{\sin p_n \cos p_n + p_n} e^{(-p_n^2 \alpha \tau / s^2)} \cos(p_n \frac{x}{s}) \qquad (3.2)$$

where

Θ = difference between temperature of saturated steam and temperature of plate at time τ at point x.

Θ_i = difference between temperature of saturated steam and initial uniform temperature of the plate.

τ = time.

x = distance from adiabatic surface toward exposed surface.

s = plate thickness.

α = thermal diffusity of plate = k/cp

k   = thermal conductivity of plate.

c   = specific heat of plate.

p   = density of plate.

p_n = roots of the transcendental equation: $p_n \tan p_n = \dfrac{k}{hs}$

For a steel containment shell initially at 60°F subjected to satu-
rated steam of 250°F, Figs. 3.15 and 3.16 show the temperature distribu-
tions at various times for two very different values of h used in Eq.
3.2. It is obvious that whether or not gradient effects should be con-
sidered during a LOCA is very dependent on the surface coefficient, i.e.,
the rate of heat transfer. Approximate values of h in $Btu/(ft^2)(hr)(°F)$
for condensing steam are given in Ref. 42. They show the wide orders of
magnitude involved, varying from h=200 to 20,000.

3.2.2.2. Thermal stress   In general, thermal stresses arise
because thermal displacements (expansion or contraction) which would
otherwise freely occur are fully or partially constrained. More specif-
ically, there are two important mechanisms that can be identified to give
a clearer picture of the causes of these stresses. In the following
explanation, both uniform and gradient variation of temperature through
element thicknesses are capable of producing a state of stress by means
of these mechanisms.

The first mechanism by which thermal stresses are generated is when
a system of mutually connected elements impose restraint upon one another

either from nonuniform thermal action due to their combined response or because the connected elements have different coefficients of expansion [74]. This latter concern may be present if the containment vessel has a cladding. The ASME Code [4] classifies this as a local stress which is mainly considered only for fatigue effects (NE-3213.13). The former effect is usually the more severe. Typical examples of this occur where ring and stringer stiffeners or other appurtenances are attached to the containment vessel. Stresses will then occur if the combined thermal displacements of these mutually connected elements are forcibly altered from what they would be individually. The ASME Code classifies this as a general sitaution subject to secondary stress criteria (NE-3213.13).

The second mechanism by which thermal stresses are generated is when there are non-uniformities in the temperature field over a region of a single element or due to the geometeric properties of the individual element [74]. These stresses arise to preserve internal equilibrium of the element. The containment vessel may be considered as a single element in which both of these conditions are present.

Most notably, during a LOCA, the circumferential and meridional variation of the escaping high energy steam produces non-uniform heating of the steel vessel. Thus the containment will be subjected to circumferential, meridional, and radial temperature variations. The degree of radial temperature variation is largely dependent on the surface coefficient formed inside the containment as discussed in Sec. 3.2.2.1. In any case there will be regional variations in the

temperature field associated with the circumferential and meridional directions that must be considered.

In addition, during shell temperature changes involving no radial variation, there will be stresses produced at restraints imposed by boundary conditions [98]. For example, such stresses will occur in upright cylindrical containment vessels at the base and cylinder-dome intersections. If a radial gradient is known to be formed then the stresess it induces must also be considered. In this case, the geometric properties of the element (e.g., containment vessel) give rise to stresses independent of the boundary conditions [98].

Stresses arising from the second mechanism are classified as secondary stresses in the ASME Code Section NE-3213.13. This same section in the Code also warns that an elastic analysis may be invalid if thermal stress exceeds twice the material yield strength. Another consideration is the change of the steel material properites due to the rising temperature. These effects are minimal though for the design conditions experienced inside a steel containment vessel; except in the case of jet impingement.

3.2.2.3. Through thickness gradient considerations   After a careful study of the postulated temperature and quality of LOCA released steam, it will be possible to estimate the severity of initial thermal gradients generated in the containment shell based on expected values of the heat transfer coefficient h. If shell gradients are not severe, it may be possible to do quasi-steady state analyses assuming shell temperatures are uniform through the thickness. In such cases, the stresses are

primarily assumed to be caused by the restraint of mutually connected elements (e.g., ring stiffeners on the vessel) and regional variations in the temperature field. However, gradients through elements such as stringer stiffeners that have significant radial dimensions will need to be considered.

The quality of the steam will depend greatly on the volume of air in the containment; the proximity of the pipe break to the containment shell; and the channeling effects of internal components. Therefore, scenarios in and between differnt types of previously described containments will yield very different potential heat transfer coefficients. The temperature of the released steam near the containment interior surface will be subject to similar variability. Typically, this steam will range in temperature from 250°F to 350°F [2,14,,49,80]. Since pressurized water or steam in the primary system piping is near 600°F [49,124], a break which is very near the containment shell may result in local heating with temperatures exceeding the 250-350°F range. Values of h in this situation (which may be bordering on jet impingement classification) will also be relatively large, potentially causing significant local gradient effects.

Gradient temperature states would primarily be associated with the short-term response in the containment after LOCA. They are particularly more likely to occur in the relatively small drywell volumes of BWR containments or the lower volume of the ice-condenser containments. In the large receiving volumes of PWR dry containments, such gradients are less likely to occur due to air-entrainment of the steam and the mitigation of

its temperature. The long-term response may exhibit the peak temperature conditions occurring about the same time as the long-term peak pressures. This is true for the wetwells in the Mark I, II and III designs for BWRs [115]. However, because of the relatively long periods of time involved and the relative thinness of the containment, these peak temperatures will be practically uniform through the thickness.

Figure 3.17 shows a postulated temperature-time history at a specific location in a PWR dry containment. This example is from Ref. 14 and reflects a small value of about $h=140$ Btu/$(ft^2)(hr)(°F)$. This is as could be expected in the large internal volumes of PWR dry containments. It may also be seen that while it only took about 10 seconds for the containment atmosphere to reach its maximum (about 290°F) at this location, it took about one minute for the inner surface of the containment shell to reach about 85 percent of that value. Unfortunately, the temperature-time history on the outer surface of the shell is not given. However, the small value of h and slow rise time on the inner surface indicates that it would closely follow that shown for the inner surface. Consequently, gradient effects through the containment shell would be neglected in this case.

3.2.3. Hydrodynamic Pressure

Hydrodynamic pressure is usually a concern in only BWR suppression containments wherein a pool of water is used to absorb LOCA and SRV energy. Occurrence of either of these events results in the discharge of a high energy air-steam-water mixture into the suppression pool of the wetwell. The reader is referred to Sec. 3.2.1.1 for more information on

what occurs during a LOCA or SRV. The important subject here is that the discharge from a SRV actuation or a LOCA produces a hydrodynamic condition in the suppression pool. Consequently, the hydrostatic pressures on the submerged containment shell are increased by the pressure transients in the water pool. Vibrations of the containment shell are also produced. As a result, incident pressures of the event can be amplified by the shell wall motion.

It is useful to think of the above as two pressure fields that superimposed on one another. The initial pressure field propagated in the pool is referred to as an incident or "rigid wall" pressure [9]. During application of the incident pressure, the containment shell deforms while interacting with the water in the wetwell. This produces another pressure field whose contribution is proportional to the radial displacements. This phenomenon is referred to as fluid-structure interaction and can result in significant increases of the maximum pressure [62]. The feedback effect of this second pressure field, generated at the structure-water interface, on the source pressures originating at the vent exits is generally neglected [62].

If the containment shell is extremely stiff and can be approximated as rigid, then the problem is simplified and one does not need to consider the effect of fluid-structure interaction. In this case, the containment is subjected to incident pressures caused by the hydrostatic head, pressure pulses from the SRV or LOCA discharges, and the effect of gas pressure increase in the wetwell airspace. When the containment is a flexible shell, fluid-structure interaction must be included.

Although SRV actuation and LOCA both produce air-steam-water discharges that disturb the suppression pool, the initiation and resulting hydrodynamic characteristics are significantly different enough to merit separate discussion for each. Further, the events involved in different "stages" of an air-steam-water discharge from either SRV or LOCA occurrence are very sensitive to small parameter changes. Some very important parameters are: mass flow rate and composition of the high energy fluid, initial vent submergence depth, and initial drywell/wetwell temperatures and pressure differentials [15,115]. Therefore, it is very difficult to accurately quantify either of these events (SRV or LOCA) even for a specific type of containment due to uncertainties of the particular parameters. The following is limited to basically a narrative description of the different stages of the hydrodynamic loading.

3.2.3.1. LOCA pool dynamics   For BWR containments following a postulated LOCA, high quality steam is released in the drywell and flows through the vent system where it is condensed at steam-water interfaces near the vent exits in the suppression pool. This disturbance of the suppression pool results in the hydrodynamic loads. The blowdown from a severe LOCA generally subsides within a minute or two [115,119]. This period is initially characterized by high to medium steam mass flow rates during which condensation in the suppression pool is steady and stable. Later, as the blowdown subsides and the ECCS is in operation, low steam mass flow rates result in unstable condensation in the suppression pool. Consequently, it is possible to consider a LOCA as a relatively long

duration event in which certain phases are occurring rapidly and distinctly enough to be considered as separate dynamic loadings [63].

The initial phase of the transient consists of clearing the air from the drywell and vent exits. (Some of this air, however, will be discharged as a mixture with the LOCA steam and water.) This rapid compression of air into the vents causes causes a subsequent acceleration of the water slug in the submerged portion of each vent. Vent clearing is followed by the formation of an air-steam bubble at the vent exits [115]. The highly compressed air immediately begins to expand to the lower wetwell pressure, displacing the water still more and continuing the propagation of the initial pressure disturbance throughout the suppression pool [63]. Any steam accompanying this phase is condensed; however, the continued addition and expansion of the drywell air causes the water displacement to continue [115]. Thus, the initially undisturbed volume of water is displaced in an upward direction by the introduction of the air and steam.

This initial phase is referred to as pool swell and lasts up to a second or two [10,63,115]. The pressure propagated during this phase is similar, in effect, to an increase in the hydrostatic pressure on the containment shell [115], although it is more realistic to model it as a triangular pulse load [63]. As the air bubbles break through the surface, the driving force for pool swell is dissipated. Accompanying this, there may be air-water froth impingements on the wetwell containment shell to consider [115].

After the pool swell phase has subsided, there is a relatively long period of high to medium steam flow through the vent system where it is condensed at the vent exits. At these conditions of high to medium steam flow, the steam-water condensation interface oscillates due to bubble growth and collapse. The condensation oscillations produce harmonic oscillations of the steam-water interface synchronized with the vent pipe pressure [34,75]. This results in a relatively steady pressure oscillation of varying amplitude and period on the suppression pool boundary. This phase is referred to as condensation oscillation.

It is difficult to predict whether or not the vents will all be equally sharing in the depressurization of the drywell. This will depend greatly on the location of the break and the manner in which it blows down into the drywell. Therefore, axisymmetric and nonaxisymmetric scenarios will need to be considered. This is also true with the vent-clearing/pool-swell phase in which nonaxisymmetric conditions could be even more likely. Near the end of the blowdown and shortly thereafter the condensation oscillation phase, the conditions within the drywell are expected to be nearly uniform and similar phenomena may be expected at all vent exits. Since the condensation oscillation phase is the result of high to medium steam flux, its duration depends on size and duration of the blowdown and the size of the drywell which acts as a high pressure reservoir after the blowdown subsides. Typically, this phase will last on the order of a minute [63,115].

As the differential pressure between the drywell and wetwell begins to equalize, the condensation of the steam near the vent exits becomes unstable. This may occur throughout small break accidents [34]. However, for large breaks, this marks the end of the condensation oscillation phase. Both cases are the result of low steam mass flow rates for which condensation is unstable and occurs randomly. The pressure pulses that result are sharp peaked and are of short duration. This type of dynamic pressure is referred to as chugging.

Chugging pressure oscillations exhibit a wide variety of amplitudes and periods and their time and space variations are random [75]. Due to the nearly uniform conditions in the drywell, these pressure pulses will be propagated somewhat simultaneously from all vent exits, in and out of phase. It follows, then, that the containment shell will be subjected to impulsive incident pressures applied in a relatively random fashion in terms of location, intensity and time. Statistical studies have been used to describe chugging pressure oscillations for specific plant containments. Since the incident pressures and added water inertia are frequency dependent, trial-and-error impulsive forcing signals applied at the steam-water interface of the vent exits have been used to conservatively envelope critical containment shell responses [8].

3.2.3.2. SRV pool dynamics   Safety relief valves (SRV) are located in pipes going directly from the reactor vessel to the water pool. SRVs are designed to open and vent off steam when the reactor vessel becomes overpressurized. Therefore, the driving force behind a

SRV discharge is much greater than that associated with a LOCA. For example, typical BWRs have been designed to operate with saturated steam at about 550°F and 1000 psig [124]. This compares to drywell LOCA pressures generally less than 65 psig. Another significant difference is that the SRV discharges directly into the wetwell, bypassing the drywell, thus occurring more quickly and intensely.

Prior to SRV actuation the connecting pipe is filled with water up to the same level as the wetwell suppression pool. Between this water level and the SRV is a column of air. When required, the SRV opens and releases high pressure steam from the reactor vessel. The rapid pressure buildup in the discharge pipe quickly compresses the column of air and subsequently accelerates the water slug in the submerged portion of the pipe. The water slug is forced out. As the compressed air exits, it immediately expands to the low wetwell pressure. This also occurs in the vents that connect the drywell to the wetwell during a LOCA. However, SRV actuation accomplishes this process much more forcefully and quickly. Also, the division between air discharge and steam discharge is more distinct in SRV actuation since less mixing of the two can occur.

With the ejection of the water slug and expanding air in the suppression pool, the water level quickly rises and a pressure disturbance is propagated throughout the pool. Further, as the air bubbles rise to the surface, they are observed to expand and contract [19,115] producing oscillatory loads on the containment shell. The phenomenon is also observed in plants equipped with quenchers at the ends of the discharge

pipes. Quenchers are designed to disperse the air into a cloud of smaller air bubbles [8,115]. The pressure time-history has often been represented as Raleigh Bubbles as shown in Fig. 3.18 [19,34,63,72,77]. Full-scale SRV actuation tests done in a Mark II BWR at Caorso, Italy demonstrated that many variations of the pressure-time history may occur depending on the number of valves opened, water level, and other parameters [77]. However, the description recommended in Ref. 72 and shown in Fig. 3.18 has been shown to yield conservative responses and is appropriate in lieu of measured pressured time-histories [9,77].

Following the Raleigh Bubbles which are produced by the air-clearing phase, pure steam is injected into the water pool [115]. Condensation oscillations, similar to those found during a LOCA, occur during this time. Because steam condensation at the steam-water interface is relatively stable, the amplitudes of these pressure oscillations are relatively small. However, if the pool temperature increases to a certain level, referred to as the threshold temperature, then steam condensation becomes unstable [115]. In this event, high sharp-peaked pressure pulses are produced similar to those produced during the chugging phase of a LOCA. Consequently, the containment shell also experiences severe, non-axisymmetric pressure pulses. Current practice for BWR plants is to restrict the allowable operating temperature of the water pool such that the threshold temperature is not reached [115]. In this way, the SRV discharge loading is simplified to vent clearing, Raleigh Bubbles and condensation oscillations.

There are a number of SRVs provided for a single BWR. The number which may open depends on the circumstances inside the reactor and its power level. Therefore, the containment wetwell must be able to withstand any number of valves discharging at a given moment. Several different combinations of SRV actuations are usually chosen to represent conservative design conditions. This will result in both axisymmetric and nonaxisymmetric dynamic pressure loadings.

3.2.4. Impulsive loads

Described here are loads that can occur with a LOCA and which have primarily a lcoalized effect on the containment vessel. The loads specifically considered are: 1) jet impingement; 2) the restraint reactions caused by broken, whipping pipes; and 3) postulated blast pressures caused by the accumulation of combustible gases in the containment atmosphere. Describing these loads as impulsive implies that the response time history of the containment is of secondary importance and that the analyst is mainly concerned with the peak response capacity required to withstand these dynamic loads. For example, blast pressures are considered as short-duration loads whose impulse is signficant as a damage factor rather than the details of the pressure-time response history. The reverse is generally true for long-duration loads. If significant levels of rapidly applied loads and associated pipe reactions are determined to be of moderate duration, then both initial impulse and the subsequent load level are evaluated. Such loads are generally force, but not energy, limited [92].

When a pipe ruptures it emits a jet of saturated steam or hot water or a mixture of the two. If this hits the containment vessel, the resulting hydraulic and temperature loading is referred to as jet impingement. The initial effect is an impulse that is generated by the jet momentum transfer as it is stopped by the containment shell. The hydraulic force of this jet will depend on the line pressure, distance from break to the containment shell, the angle of jet dispersion, the shape of the shell, and the angle of incidence between the jet path and shell surface [20]. According to Ref. 92 the steel shell temperature may be assumed to be at the ambient plant temperature during the initial impulse phase.

At the rupture, the hydraulic force is the product of the line pressure and break area at the instant of rupture. Thereafter it begins to increase as the fluid is accelerated out the break [12]. After a short time, flow chokes at the break and hydraulic force decreases rapidly to a quasi-steady state. This point approximately defines the end of the impulse phase. The quasi-steady state decreases gradually as the fluid inventory in the system is exhausted. The static response of the containment during this latter phase should also be evaluated. During the quasi-steady state phase, the containment shell temperature should be taken as equal to that of the impinging jet [92] which may be on the order of 500°F to 600°F [49,124].

The essence of the pipe support reactions is the same as jet impingement force except in the opposite direction. The type of stresses produced in the containment will depend on the characteristics of the

supports attached or passing through the containment. In some instances, devices or structures are specifically provided to carry or mitigate pipe reactions. This is also the case for jet impingement. Sub-compartments and shields, referred to as jet deflectors, are provided to deflect or redirect potential LOCA jets to minimize damage to essential components. The analyst should assess these features before doing extensive analyses for jet impingement and pipe reactions on the containment shell [3,110].

During a LOCA it is postulated that certain metals chemically reacting with steam and water, and the radiolitic decomposition of the water in the reactor core, and that spilled in the containment, may result in the production of hydrogen and oxygen [115]. A very flammable mixture of these gases may accumulate if enough hydrogen is produced and allowed to concentrate in the containment atmosphere. If such an accumulation were ignited, its effects could range from burning to explosion, depending on the concentration and its confinement. In the worst case of an explosion, the blast magnitude and length are represented as an impulse applied to the containment.

Accumulation of significant hydrogen concentrations can occur more rapidly in pressure suppression containments (e.g., BWR containments) because of their relatively small containment volumes. The large open volumes of PWR dry containments make significant accumulations less likely. In any case, the severe consequences that could result from hydrogen detonation have made its prevention mandatory. Safety systems are required to prevent the accumulation of hydrogen gas in all containments as per Appendix A of Ref. 94. Various methods include:

inerting the hydrogen with nitrogen gas; recombining hydrogen with
oxygen to form water; and mixing the containment atmosphere to reduce the
concentration levels [115]. Therefore, USNRC Regulations and current
Code criteria do not require the containment to be specifically designed
to resist hydrogen detonation blast pressures.

3.2.5. Impact loads

Impact loads occur when objects strike the steel containment causing
relatively large impulsive forces to be exerted between the bodies [51].
The mechanics of the impact depends on the geometrical, inertial, and
stiffness properties of the missile and target. These parameters will
determine whether the impact results in primarily localized damage to the
containment or if overall containment response must also be considered
[92]. In general, it will usually be necessary to prove that overall
response is insignficant before concentrating on only local effects.

With respect to overall containment response, the formulation of the
impact force will depend on the type of impact. Specifically, if signif-
icant local deformation of the missile and/or containment occur during
impact then this is classed as a "soft missile impact" [92]. In this
case, deformation characteristics of the missile or target are used to
develop a force-time history applied to the containment. The overall
response to the forcing function is analyzed as for an impulse load.
Conversely, the second type of impact is referred to as "hard missile
impact" and is based on a hard missile impacting a hard target [92]. In
this situation, local deformations and the energy absorbed by them are

considered negligible. This conservative approach must sometimes be used when local deformation of the missile or containment cannot be accurately determined. Impact solutions for overall containment response are then based on energy and momentum balance tehcniques. The containment will withstand the impact if its (strain) energy absorption capability exceeds the energy transmitted to the containment by the missile.

After it has been determined that the overall response of the containment is safe, the integrity of the region of local impact should be checked. In general, when local impact effects are being investigated, the dynamic characteristics of the entire vessel do not need to be considered. The opposite is true for overall response in which the dynamic characteristics of the containment are very important. To check localized effects, missile parameters such as material type, size, and velocity are typically used in empirical formulae [92].

For steel containments, the following have been identified as among potential missiles [110]:

    valve bonnets

    valve stems

    retaining bolts

    control rod drive assemblies (in PWR containments)

    ends of broken pipes

A rupture in the pressurized piping system inside the reactor containment building may be accompanied by one or more of the above missiles propelled by the force of pressurized water. Such missiles are classified as plant generated missiles. Plant generated missiles will primarily

strike the interior of a steel primary containment because it is typically surrounded by a concrete secondary containment which protects its exterior. This is obviously the case for PWR containments and usually the case for BWR containments. Missiles generated by tornados or in the form of a crashing aircraft represent extreme environmental missiles which will always impact on exterior structures, such as the concrete secondary containment, before the steel primary containment. Consideration of such effects, which may be extreme, is beyond the scope of this study.

During a LOCA, the broken pipes can also be propelled by the escaping pressurized fluid. This phenomenon is referred to as pipe whip and can also result in impact loads on the steel containment. Pipes may also transmit impactive forces to structural elements that are supporting the pipe. The nature of this force will depend on the characteristics of pipe-to-structure attachments. Normally, however, pipe reactions will be of significant duration so as to be best considered as dynamic forces in which the force-time history is an important consideration, i.e., impulsive loading.

Missiles and pipe whip represent the primary sources of impact on the steel containment. The occurrence of these events is small, though, because safety features are provided to specifically prevent and mitigate them. Safety walls and shields are provided where missile sources are most likely and hold down devices are provided for piping to prevent pipe whip. If such safety features are specifically designed for all conceivable sources then NRC licensing may not require extensive impact analyses [3,110].

3.3. External Events

The steel containment vessel used to house a BWR or PWR is itself also housed in a large concrete building, usually referred to as the secondary containment. The secondary containment provides a protective shield for the primary steel containment, particularly against such natural environmental loads as snow and wind. As a result, there are relatively few loads externally applied to the containment.

One of the most important external loads on the containment is that caused by earthquakes. All containment vessels are required to be designed to resist seismic loading [95]. Depending on the particular site, seismic loads in excess of the minimum presribed in Ref. 95 will often need to be designed for. An earthquake excites the foundation of the containment and thus sets the containment shell mass into motion. The resulting relative displacements of the containment shell induce stresses. Since it is currently implied in the ASME Code [4], and given as criteria in Ref. 114, that seismic load be combined with LOCA load, a significant percent of containment resistance may need to be allotted to seismic effects. It is desirable to describe the seismic load as accurately as possible without bringing too much additional conservatism into the already conservative load combinations.

The only other important external load considered in Sec. 3.3 is external pressure. It occurs because of basically the same reasons as discussed in Sec. 3.1. The only major difference is that Sec. 3.1 discussed external presure in conjunction with normal plant conditions,

whereas abnormal plant conditions (i.e., internal or external events) are considered here.

3.3.1. Seismic

The designs for all nuclear power plants are required to incorporate potential effects of earthquakes [95]. Earthquakes are usually explained as a vibrating wave system which emanates in all directions from a rupture in the earth rust. Generally, the rupture or sequence of ruptures occur at fault lines in the earth crust. The resulting wave system is composed of a number of different types of identifiable waves which are responsible for producing respective types of ground motions. For nuclear facilities these ground motions are currently represented by translational acceleration-time histories in two orthogonal horizontal directions and the vertical direction [95], normally obtained or derived from recorded measurements. Typically, rotational ground motions are considered small enough to neglect [55].

The most important features of these three orthogonal components are: the frequency content of the motion; some measure of the earthquake size; and the duration of the strong motion [29,55]. Response spectra are the best available "overall" measure of earthquake severity. A response spectrum is a plot of the maximum elastic response (acceleration, velocity or displacement) of a family of single-degree-of-freedom oscillators with a given amount of damping which have been subjected to an input motion at their supports. The resulting curves can be plotted on arithmetic or logarithmic scale of acceleration vs. structural period

or frequency and on tripartite log paper with displacement, pseudo-velocity and pseudo-acceleration plotted vs. structural period or frequency (Figs. 3.19 and 3.20). Although they are limited to elastic structural response an do not completely account for the duration of the strong motion, they do reflect the frequency content of the motion and allow for inclusion of the effect of the earthquake size.

The earthquake size is usually given in terms of its peak ground acceleration at the site [29,30,44,55,86]. Alone, peak ground acceleration is a poor measure of the severity of an earthquake. However, it provides a convenient standard of measure by which the amplitude of the earthquake frequency content can be specified. Almost universally, this parameter is used to normalize input motions that form the statistical basis of design response spectra.

The peak ground accelerations in the two horizontal directions are normally taken as equal while the vertical component is commonly about two-thirds of the horizontal peak [95,106]. Appendix A of Ref. 95 requires that two sizes of earthquakes be considered at each site. The first, denoted as the "Operating Basis Earthquake" (OBE), is the earthquake which could reasonably be expected to affect the facility during its operating life. The plant is intended to safely continue operating throughout this event. When an earthquake occurs which exceeds the OBE, the plant is to be shut down and remain that way until inspected for damage. Thus, the second and larger earthquake considered is referred to as the "Safe Shutdown Earthquake" (SSE) and it represents the maximum level of ground motion considered possible for the site. The steel

containment vessel is required to maintain its integrity throughout this event, also. The minimum SSE allowed by Ref. 95 is 0.1 g peak ground acceleration. The minimum peak accelerations, horizontal and vertical, of the OBE are to be at least one-half the corresponding values of SSE in lieu of valid site justification [95]. In most instances, nuclear facilities have been designed for OBE equal to one-half of SSE.

Appendix A of Ref. 95 describes the geological and seismological characteristics that must be assessed to get an estimate of the maximum earthquake that could be generated. All significant faults must be identified and the seismological history evaluated. Important features that will determine the characteristics of the earthquake at the particular site include:

(1) Source characteristics, e.g., magnitude and extent of rupture of the earth crust.

(2) Transmission of seismic waves, i.e., characteristics of the transmitting medium and distance to the site.

(3) Regional and local geology, e.g., the site soil profile and properties therein and the effects of major geological structures.

This only gives the reader an idea of the extent of the difficulty and unknowns associated with prescribing OBE and SSE levels for nuclear sites. Further, basic data concerning the influence of such factors as magnitude, distance and local soil conditions on the characteristics of earthquake motions are still very scarce. Similarly, occurrence frequencies or return periods of earthquakes are still basically crude estimates

based on limited statistical data. This makes it very difficult to produce an earthquake hazard curve that reflects a high level of certainty for use in PRA studies.

As a consequence, design earthquakes for nuclear facilities are generally input into structural analyses in a deterministic fashion. The design earthquake itself is the culmination of a statistical study of the appropriate available data, i.e., measured earthquake motions that have occurred. Data bases made up of artificial earthquake acceleration-time histories are a possibility. However, the current state-of-the-art for design practice has not made this transition.

The appropriate data for statistical study should, as expected, be compatible with the conditions found at the particular site in question. Therefore, after the geological and seismological features of the site have been established, accelerograms recorded at sites with similar characteristics are collected to form a statistical sample. Because of the extensive work already done in categorizing accelerograms and the relative scarcity of data, this job is not a difficult as it sounds [44,55,85]. Each of the accelerograms of the statistical sample is normalized to be representative of the earthquake size being considered, e.g., the OBE or SSE level of shaking. Since geology formed the basis of admittance to the sample, normalization is generally done to account for differences in magnitude and distance between the SSE (for example) and the selected accelerograms. For simplicity and convenience, magnitude is usually expressed and normalized in terms of peak ground acceleration at the site.

Each of these normalized accelerograms is then used as the input motion for a response spectrum. These individual response spectra will have numerous peaks and valleys that reflect the frequency content of the individual accelerogram. Since there is considerable uncertainty about the frequency characteristics of a future earthquake, it has been conservative practice to base the final design response spectra on the mean plus one standard deviation of the statistical sample [55,76]. The resulting design response spectra are smoothed curves or straight lines between control points as explained in Ref. 106 and shown in Figs. 3.19 and 3.20.

The design response spectra of Figs. 3.19 and 3.20 are those specified in NRC Regulatory Guide 1.60 [106] and have been used in the design of the majority of current nuclear power plants [55]. These spectra were developed with no particular nuclear facility in mind and are considered as site-independent. They were developed from statistical studies of a number of past strong-motion earthquakes recorded on relatively firm or stiff sites and encompass a wide range of frequency characteristics for such ground conditions. Due to the nature of the selected accelerogram sites, the design response spectra of NRC Regulatory Guide 1.60 are not to be used when: (1) the site is relatively close to the epicenter of an expected earthquake, or (2) the site has physical characteristics that could significantly affect the spectral pattern of input motion such as being underlain by poor soil deposits [106]. When the site characteristics permit, the site-

independent design response spectra of Ref. 106 are generally used. They are normalized to a peak horizontal ground acceleration of 1.0 g. The design level of seismic excitation at a particular site will be some percent of 1.0 g. The numerical values of design displacements, velocities, or accelerations for the particular site are obtained as this same percentage of the 1.0 g values (i.e., response is linearly sealed).

Whether or not the design earthquake utilizes the site-independent design response spectra or response spectra derived for the particular site will depend on the site characteristics [30]. In any case, design response spectra currently provide the best characterization of the design earthquake severity for structural analysis. Also, with response spectra the engineer can do a modal analysis (Sec. 4.4.1) and graphically determine structural displacements which translate directly into stresses.

With respect to the use of design response spectra in analysis, it should be pointed out that they represent free-field motions at the site. Free-field motions are the soil-surface accelerations which have not been altered by the presence of the plant structures. Consequently, design response spectra are to be considered as being applied at the proposed finished grade level of the site. An alternate procedure acceptable to the USNRC is to apply the design response spectra at the foundation level of Category I structures in the free-field [112]. In addition, since response spectra are based on free-field motions, no interaction between the supporting soil (i.e., the source of input ground motions) and the

structure is represented. This phenomenon, denoted soil-structure interaction, can be significant at soft soil sites and is explained in more detail in Sec. 5.1.

Design response spectra are also used as a standard in the construction of artificial earthquake acceleration-time histories which are, in turn, used for in-structure dynamic analyses and soil-structure interaction analyses. These are both very important analyses for steel containments and are difficult to do correctly with response spectra described in this section. Artificial acceleration time-histories are usually generated either by adjusting existing accelerograms or through stochastic processes. The resulting free-field ground motions at the finished grade level are required to give response spectra that essentially envelop the design response spectra for each level of structural damping required.

In order to do a soil-structure analysis, the artificial earthquake often must be deconvolved to the base of the site soil profile. When the results obtained by deconvolution are applied at the base of the soil profile, the response spectra produced by the free-field ground motions must again envelop the design response spectra. This applies to site models with and without the proposed structures in place [112].

This points out the essential role that the design response spectra have in providing a standard of acceptance for the more involved

techniques. Further, the design response spectra are also directly used at times. They are particularly useful for proportioning a structure during preliminary design stages. And, for extremely stiff or rock sites, they provide an adequate input for all but in-structure analyses of the containment vessel.

3.3.2. External Pressure

External pressure discussed here results from abnormal events inside the containment. In this sense, such pressure is also a part of the internal events described in Section 3.2; however, it is included here since it is externally applied. This pressure, also referred to as a reverse pressure, can result from the following events:

1) Inadvertent actuation of containment sprays during normal plant operation.

2) Inadvertent operation of the ice condenser return airfans in PWR ice condenser containment.

3) During a LOCA in a BWR containment, ECCS spillage condensing the steam in the drywell.

4) After a LOCA or small steam line break in a Mark III BWR containment, the containment spray is started.

Therefore, PWR containments and both the drywell and wetwell of BWR containments must be designed for external pressures. Vacuum relief valves between the wetwell and drywell, and vacuum breakers between the containment interior atmosphere and the external environment are provided

to limit the magnitude of reverse pressures. Containment designs

generally allow for a uniformly distributed external presure on the order

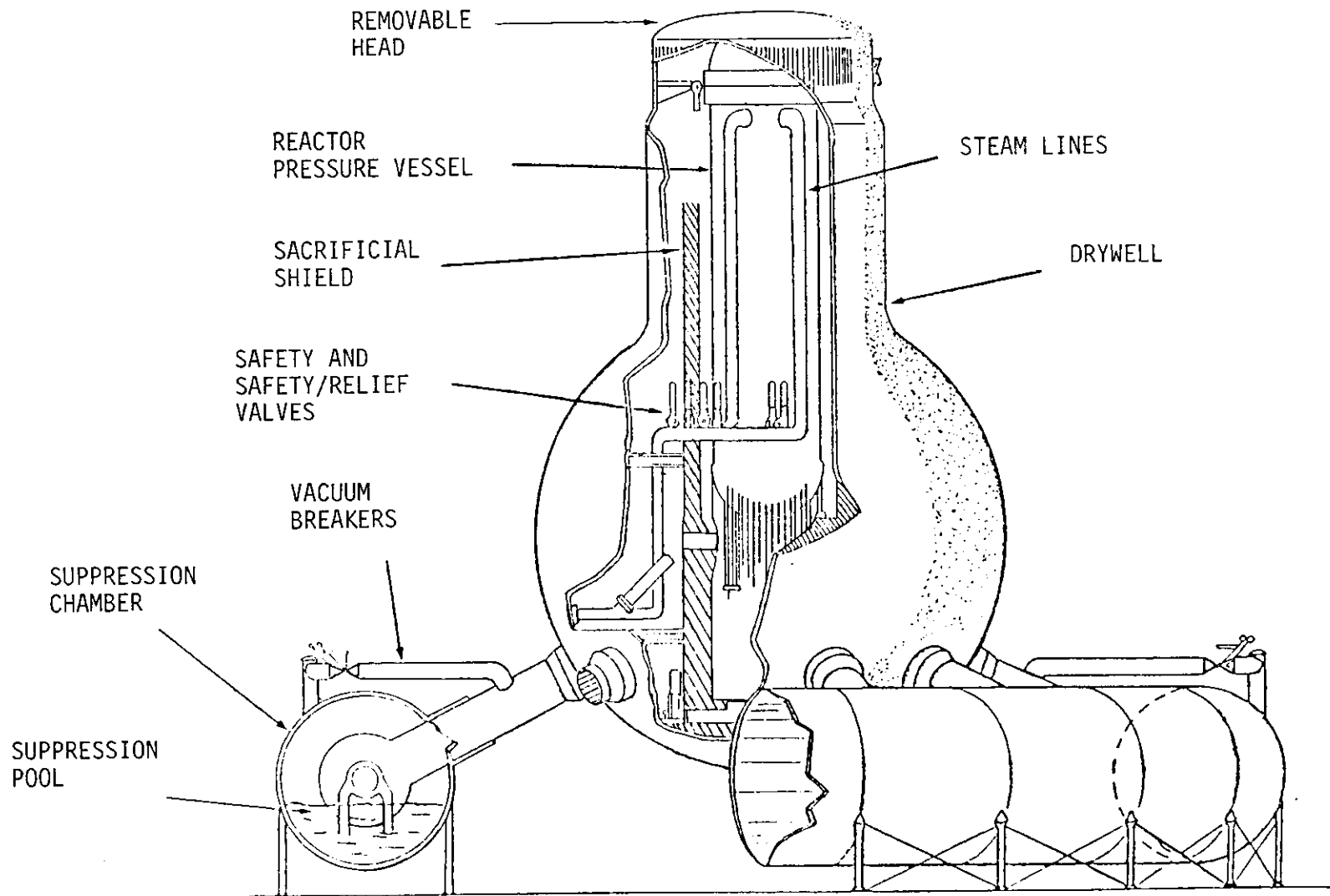of a few pounds per square inch or less [2,3,120].

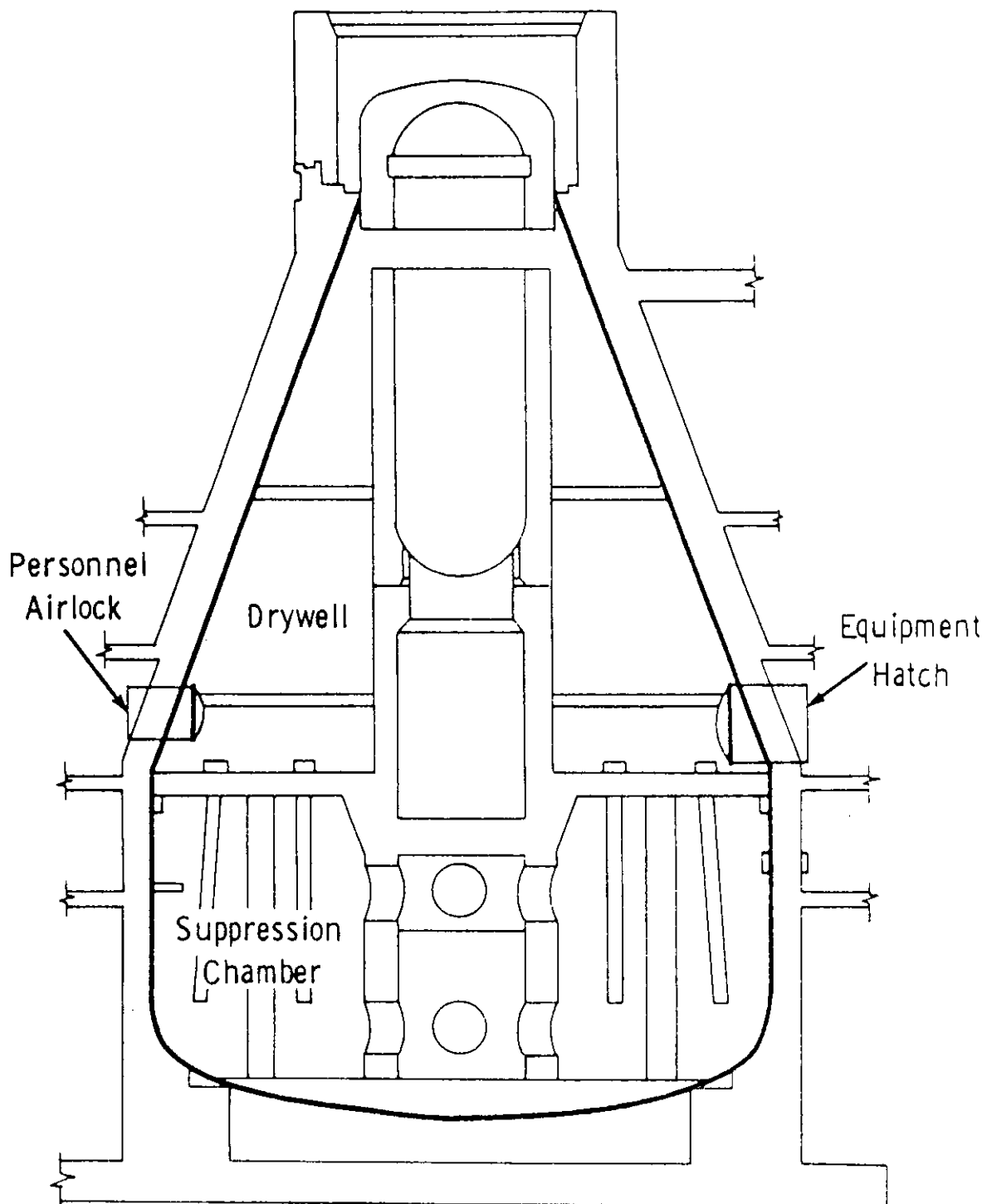Fig. 3.1. Mark I steel containment for boiling water reactor [91]

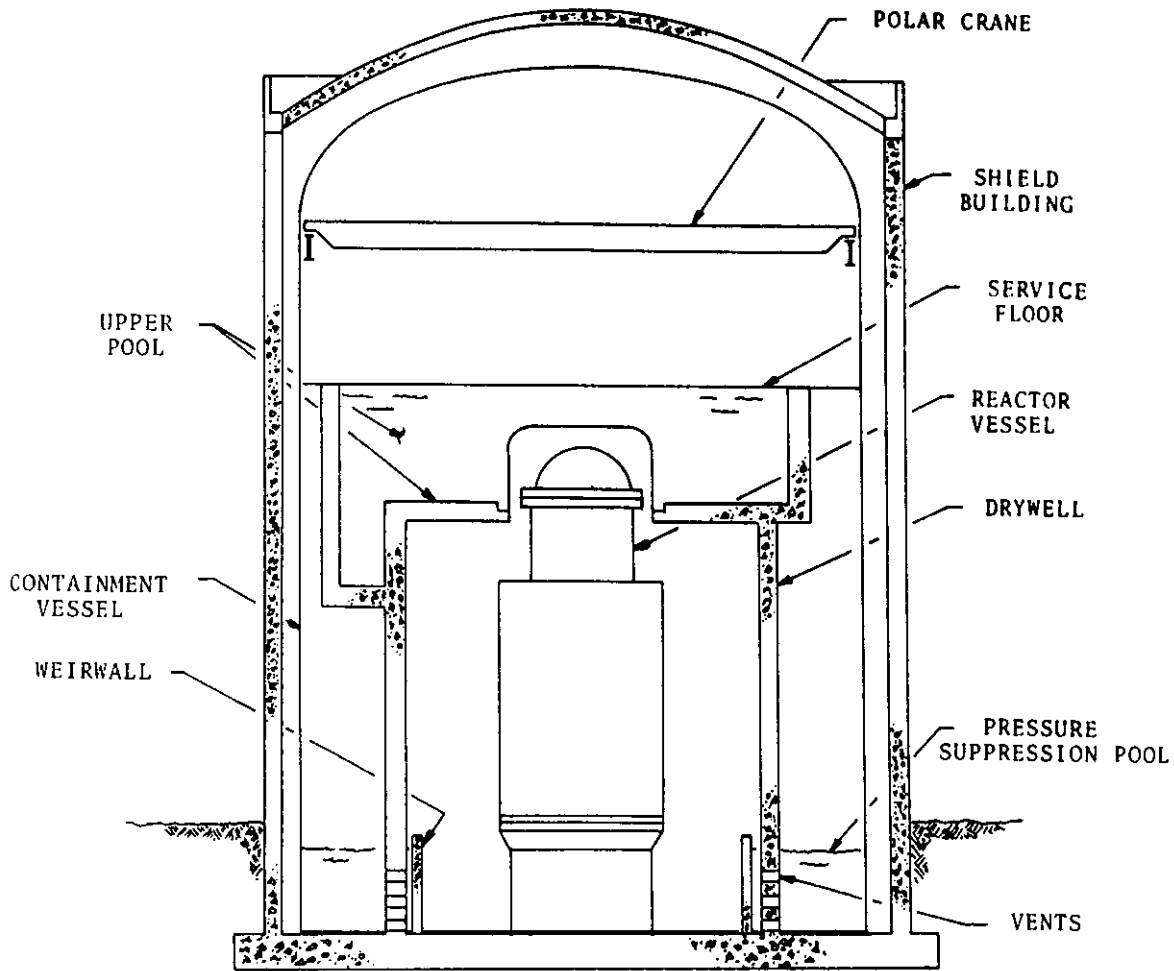Fig. 3.2. Mark II steel containment for boiling water reactor [21]

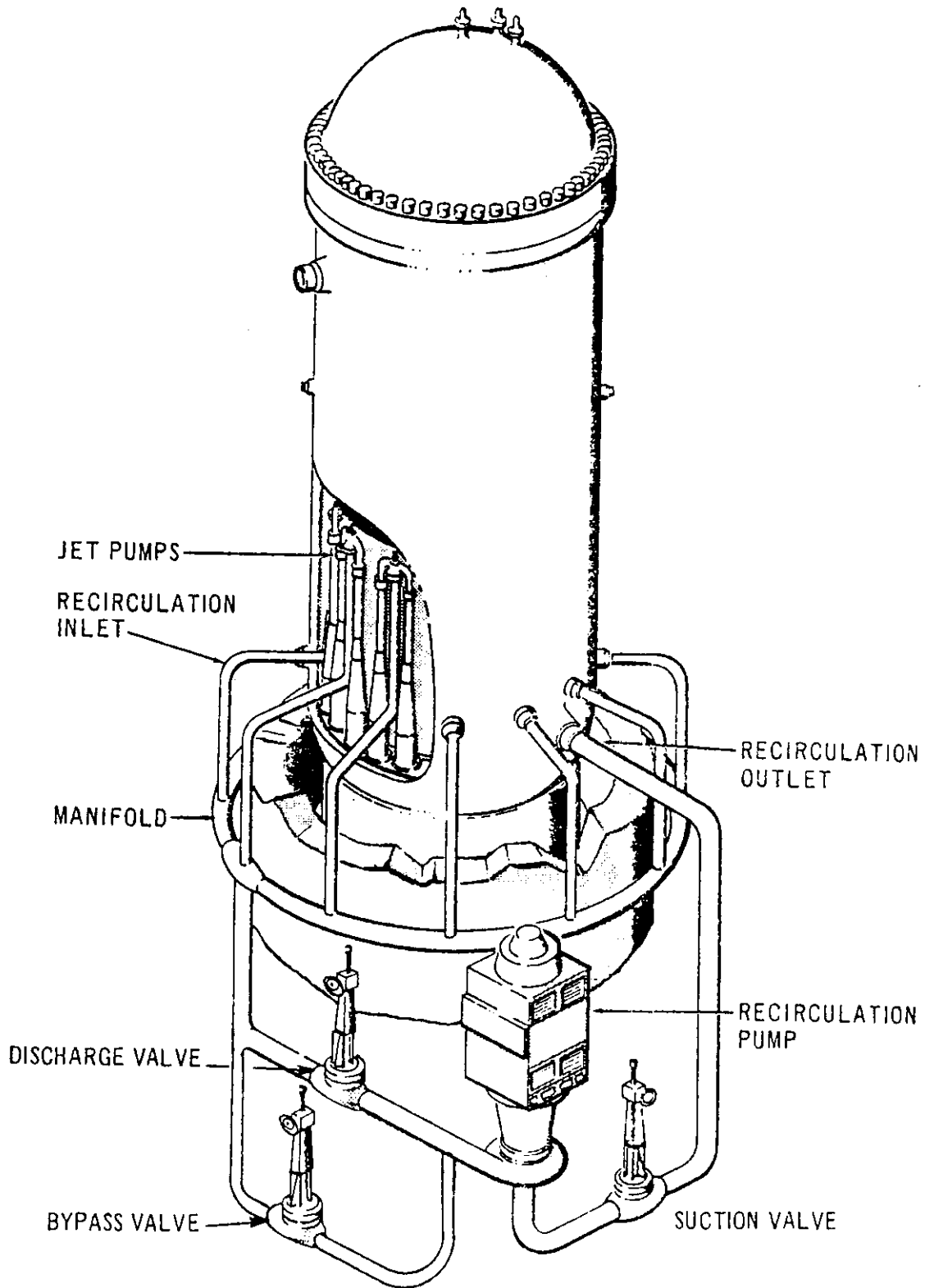Fig. 3.3. Mark III steel containment for boiling water reactor [34]

Fig. 3.4. Schematic of boiling water reactor [104]

Fig. 3.5. Typical pressure transients in Mark I or Mark II containments as result of loss-of-coolant accident [21]
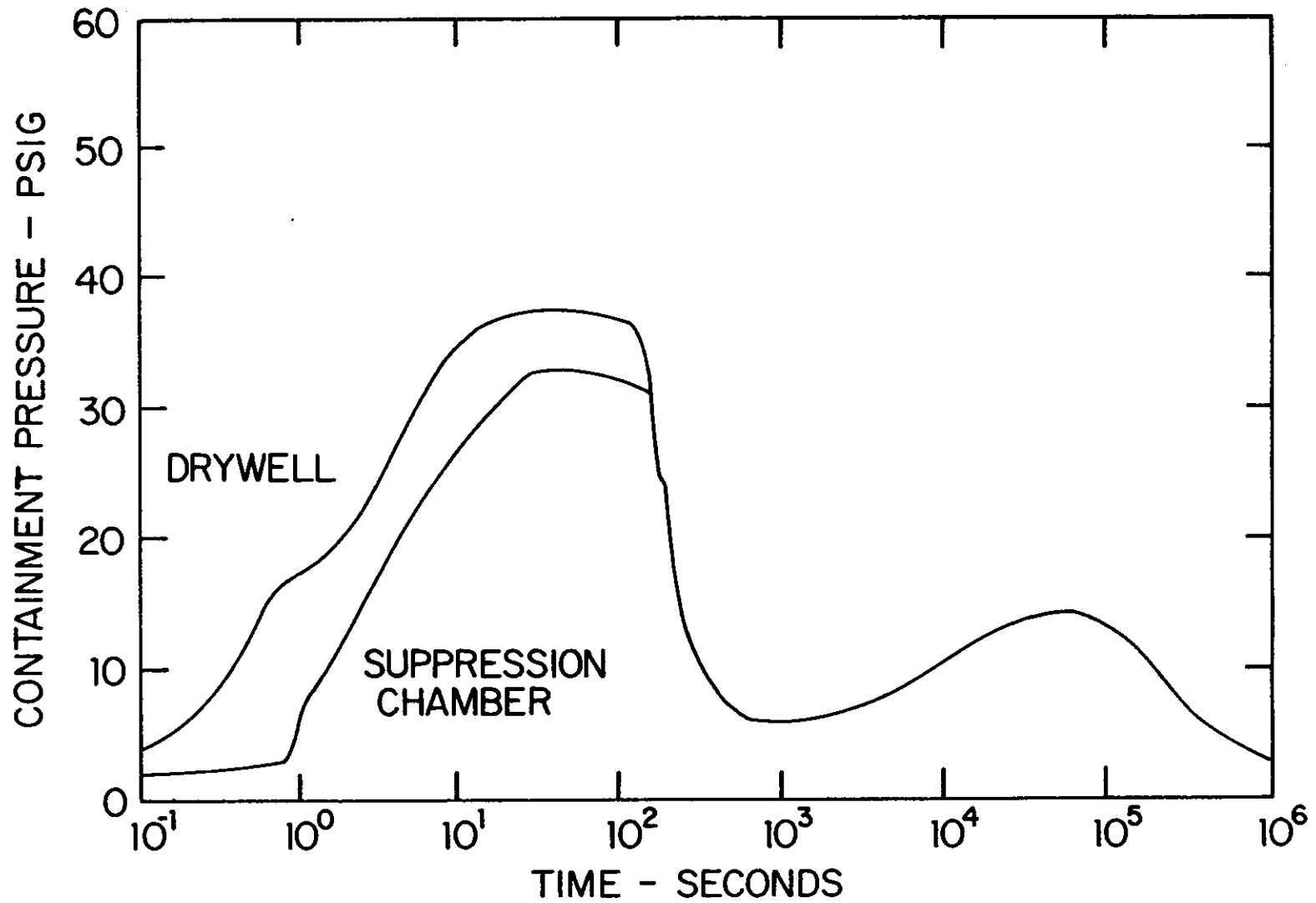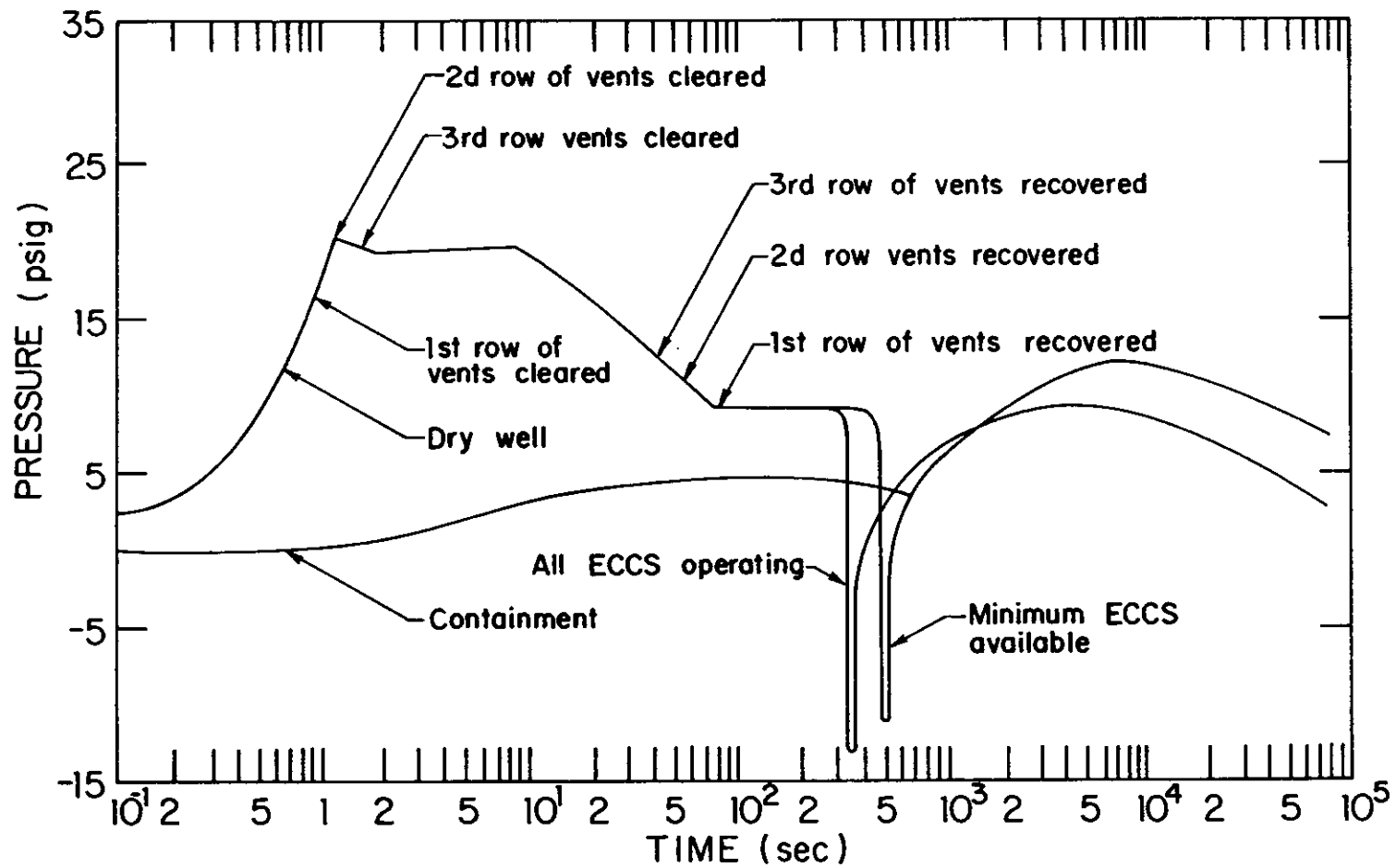
Fig. 3.6. Typical pressure transients in Mark III containment as result of loss-of-coolant accident [119]
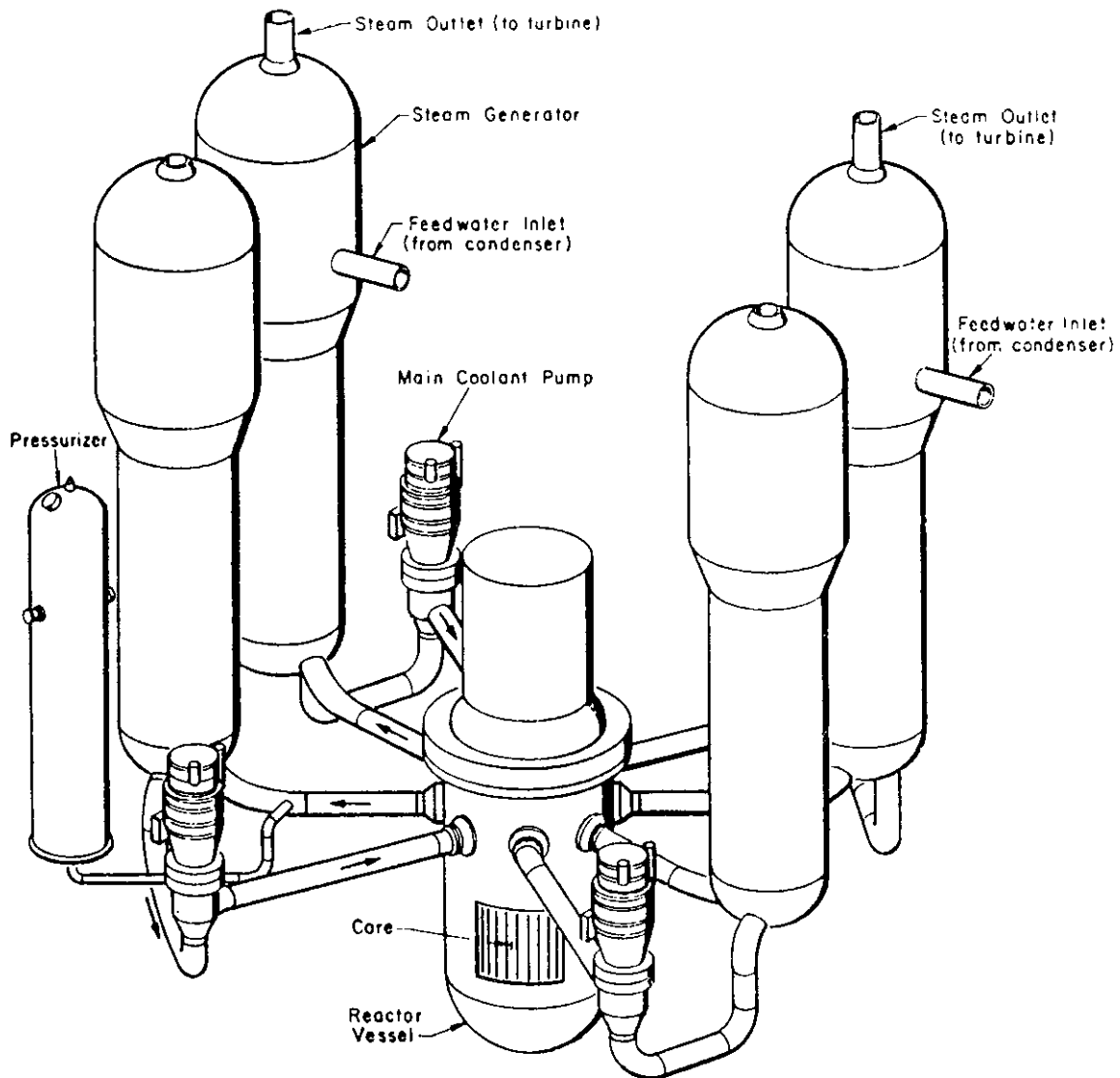
Fig. 3.7. Schematic of pressurized water reactor [104]
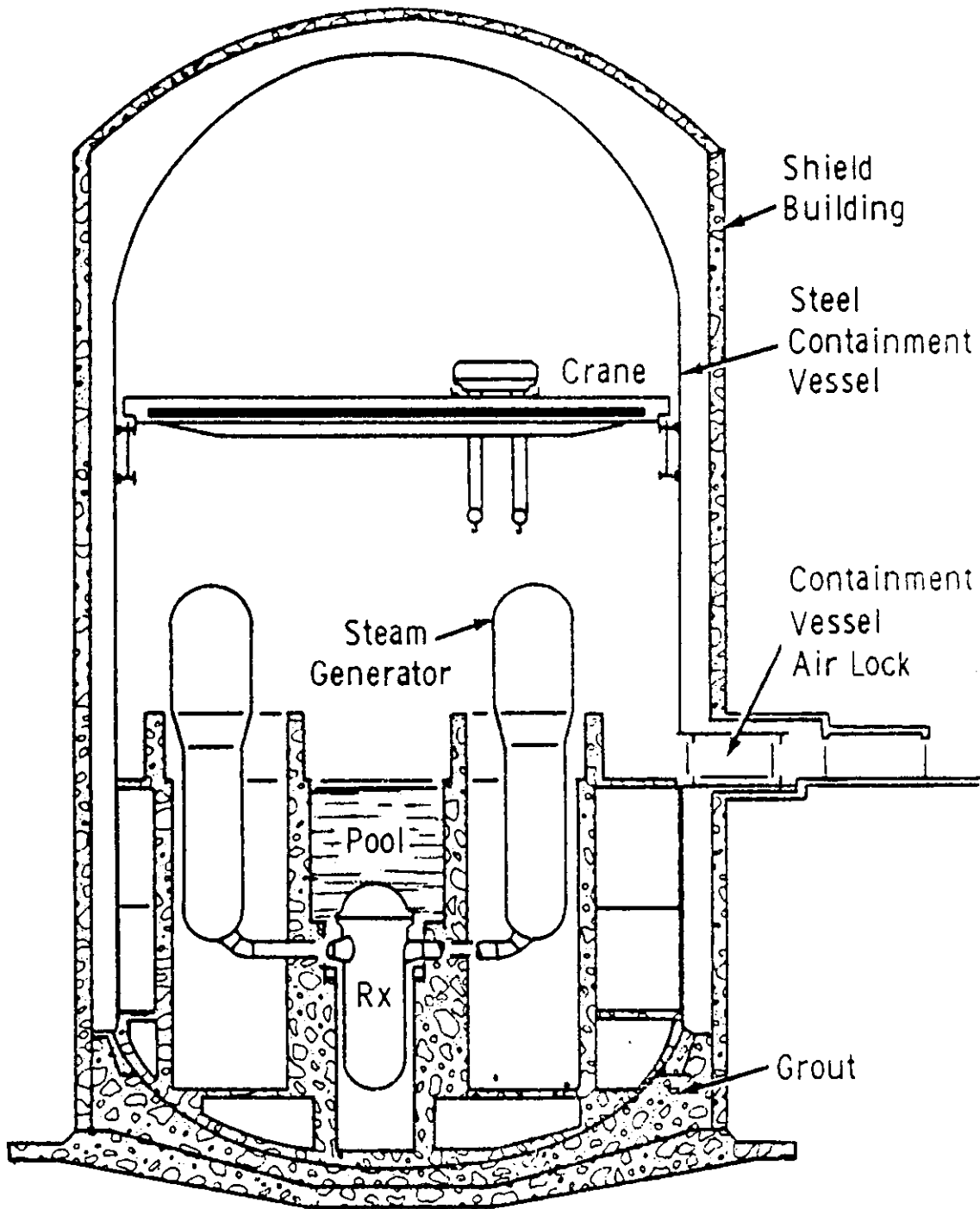
Fig. 3.8. Upright cylindrical dry containment for pressurized water reactor [21]

STEEL PRESSURE BOUNDARY
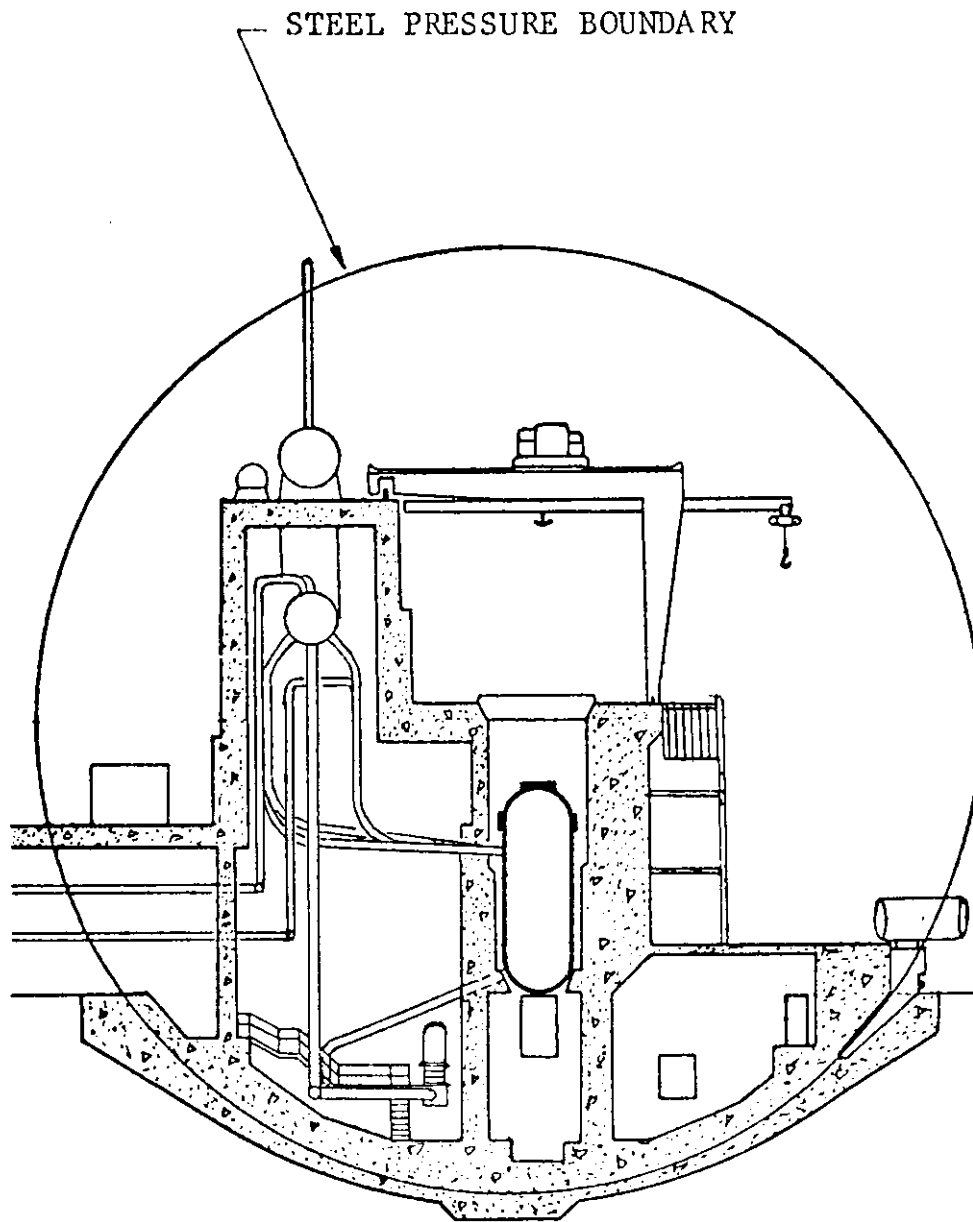
Fig. 3.9. Spherical dry containment for
pressurized water reactor [91]

The graph shows CONTAINMENT PRESSURE (psig) on the vertical axis (ranging from 10 to 60) versus TIME (SECONDS) on the horizontal axis (logarithmic scale from 1 to 10^3).

① ECCS assumed partially effective and one containment cooling system operating

② ECCS assumed fully effective and one containment cooling system operating
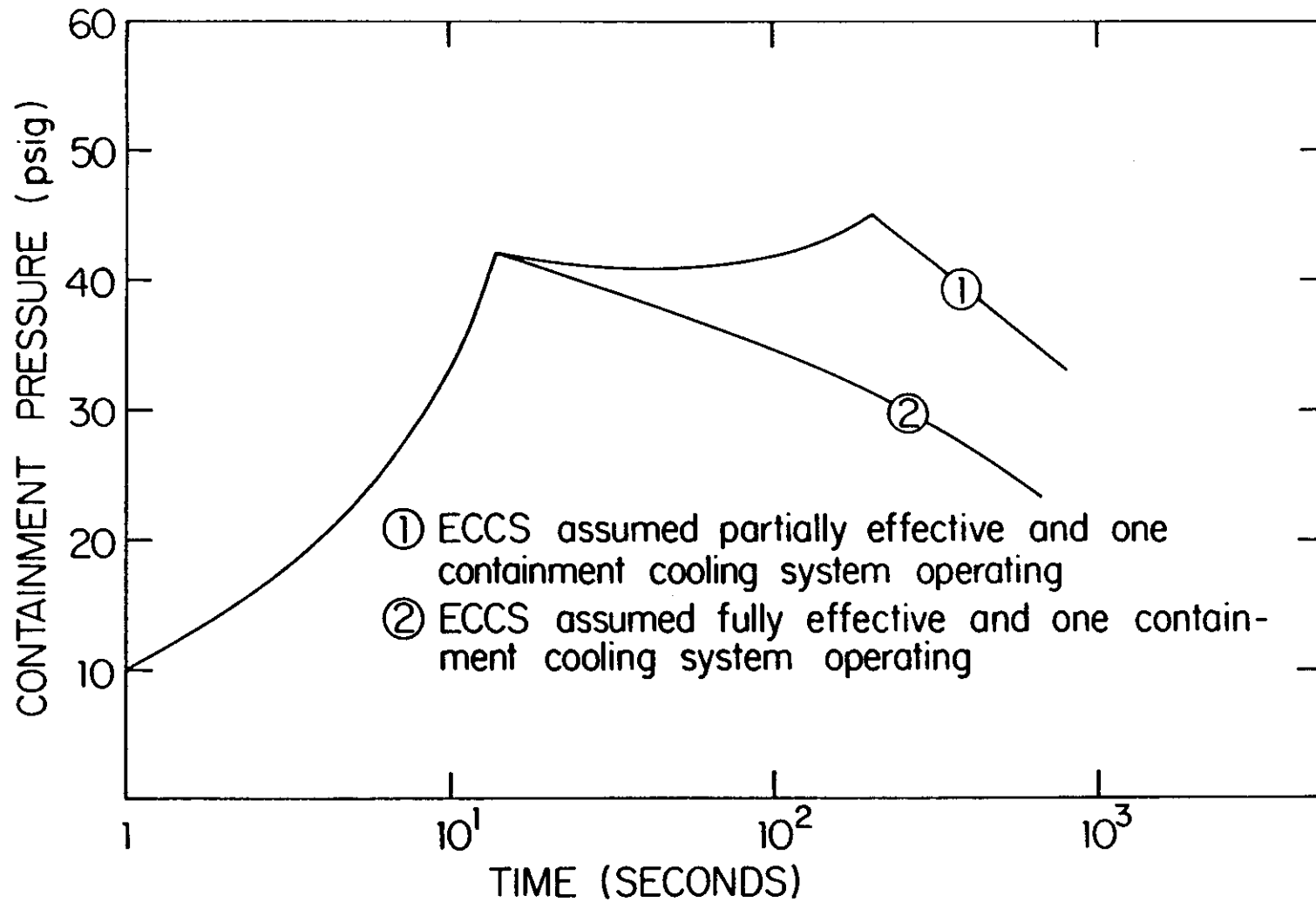
Fig. 3.10. Typical pressure transients in dry containments as result of loss-of-coolant accident [49]
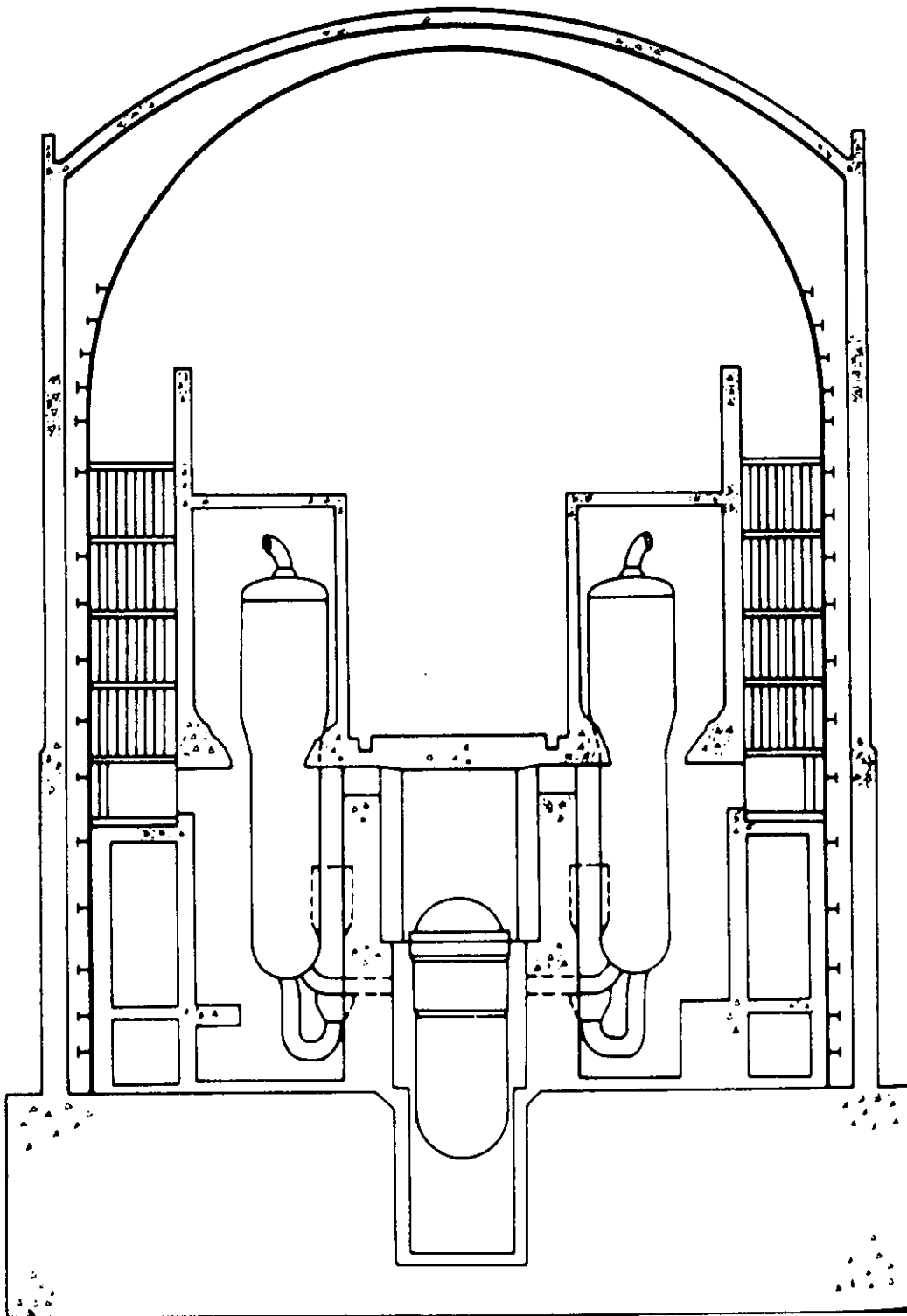
Fig. 3.11. Ice condenser containment for
pressurized water reactor [22]
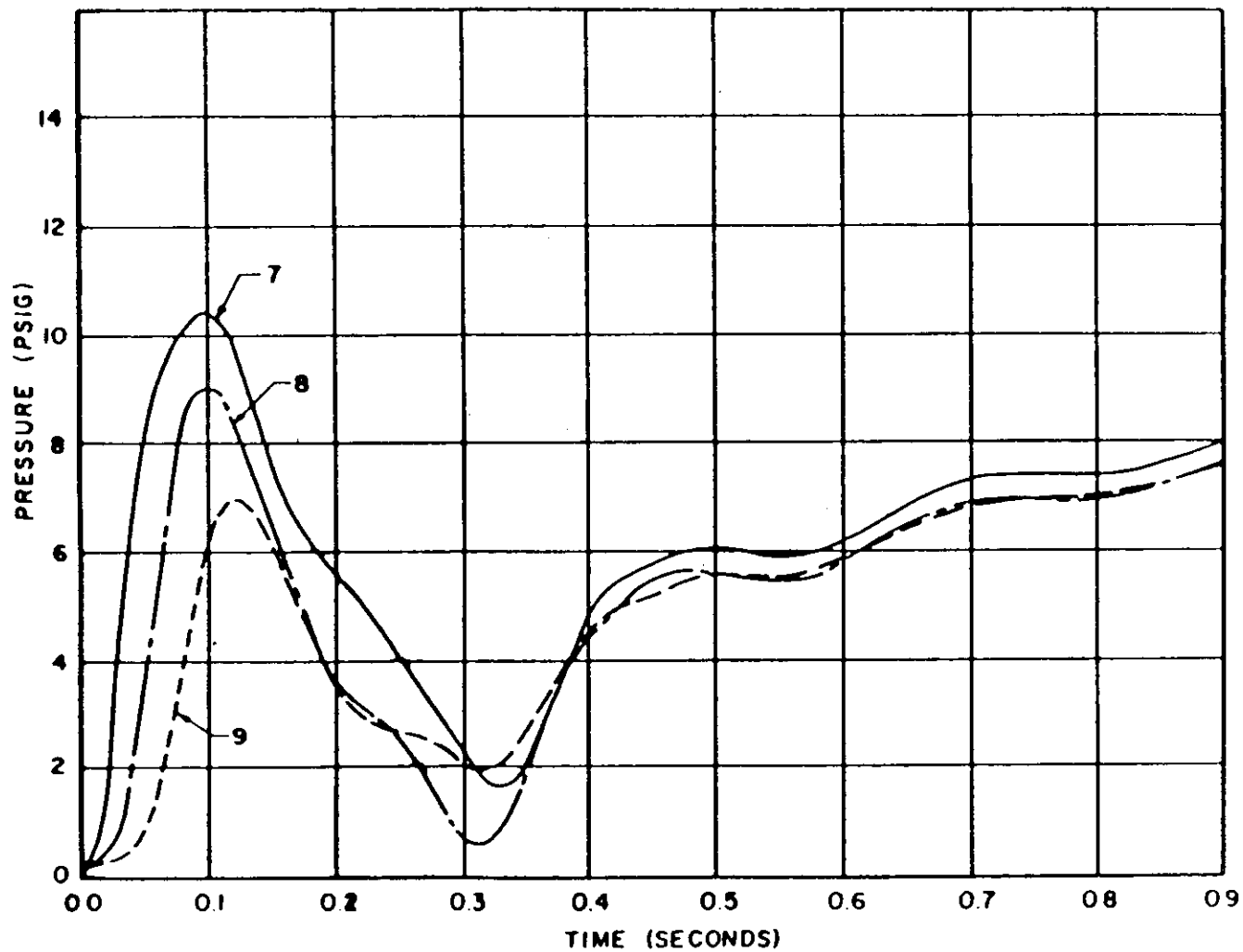
Fig. 3.12. Typical pressure transients in three ice condenser compartments as result of loss-of-coolant accident (Final Safety Analysis Report submitted to NRC by Duke Power Co., Charlotte, North Carolina)
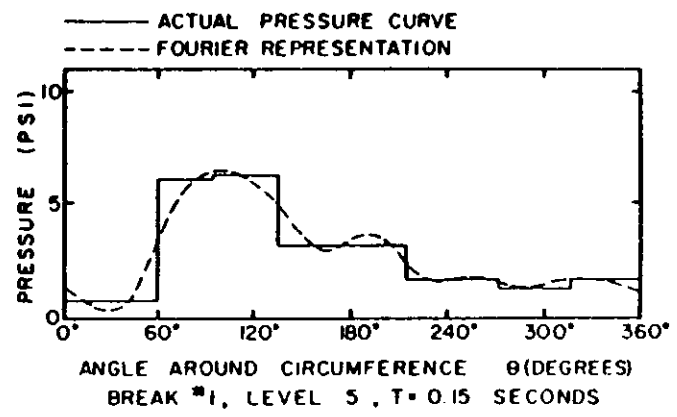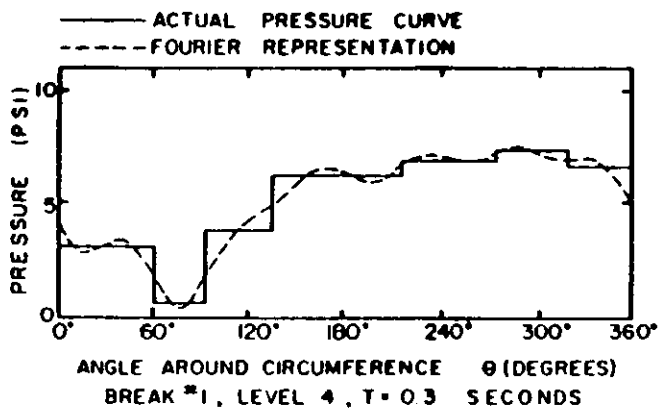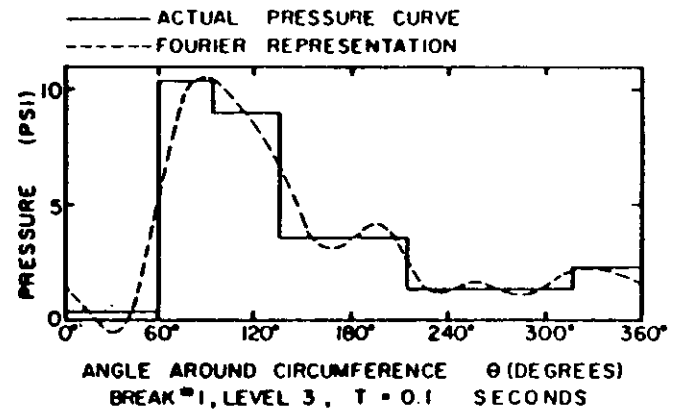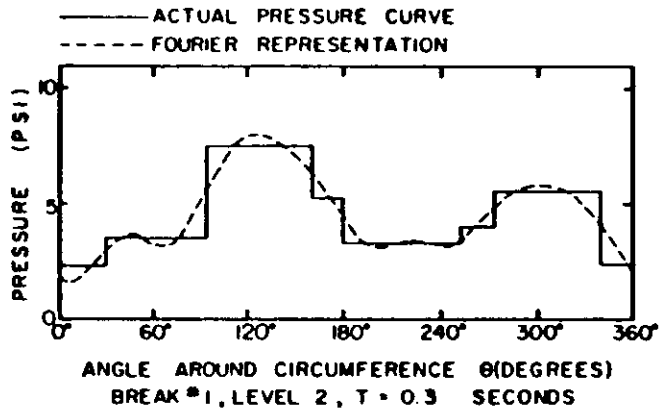
Fig. 3.13. Examples of the time-space variation of pressure transients as result
of loss-of-coolant accident in ice condenser containment (Final Safety
Analysis Report submitted to NRC by Duke Power Co., Charlotte, North
Carolina)
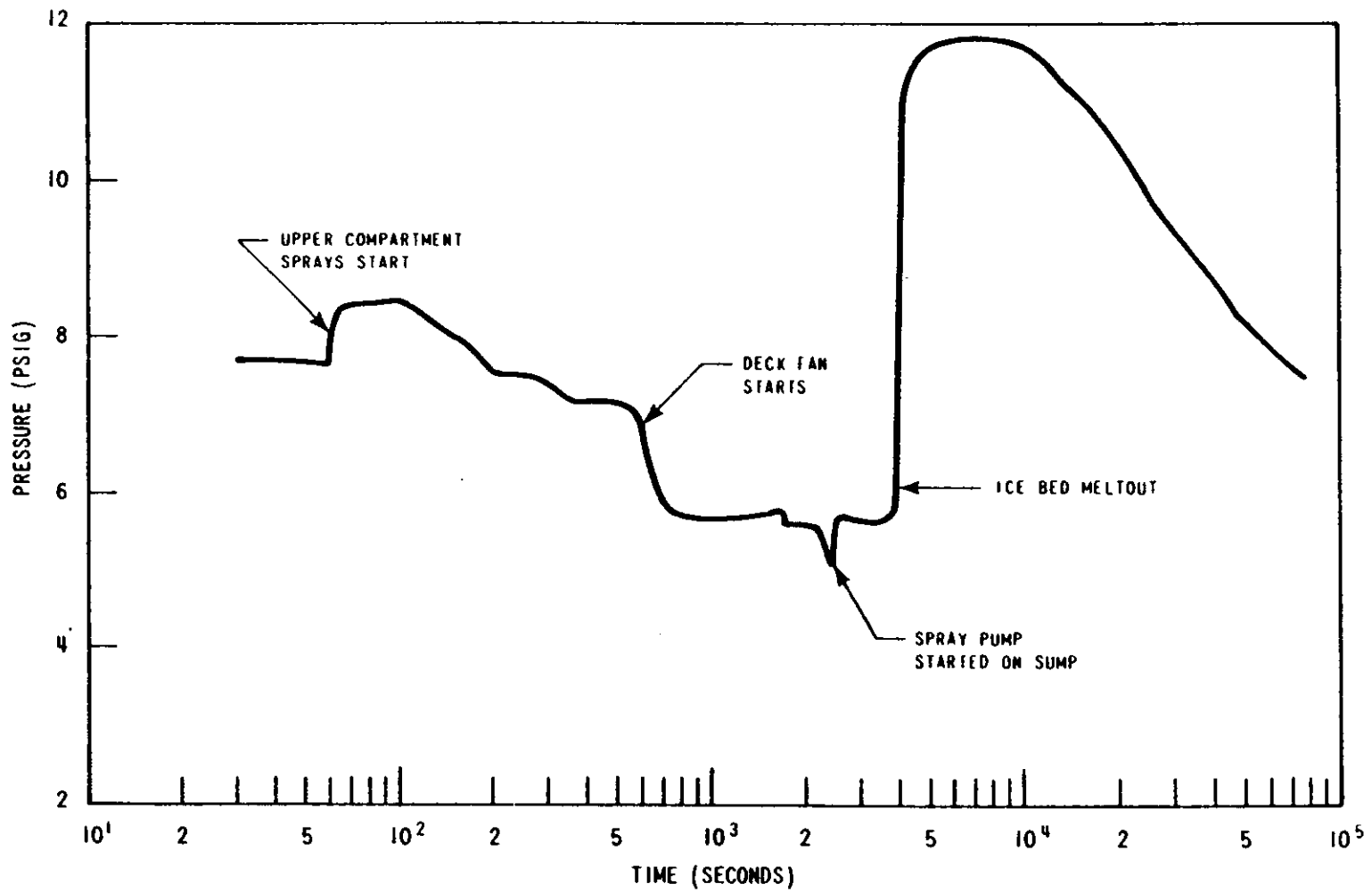
Fig. 3.14. Typical pressure-time history in free volume of a ice condenser
containment after a loss-of-coolant accident [110]
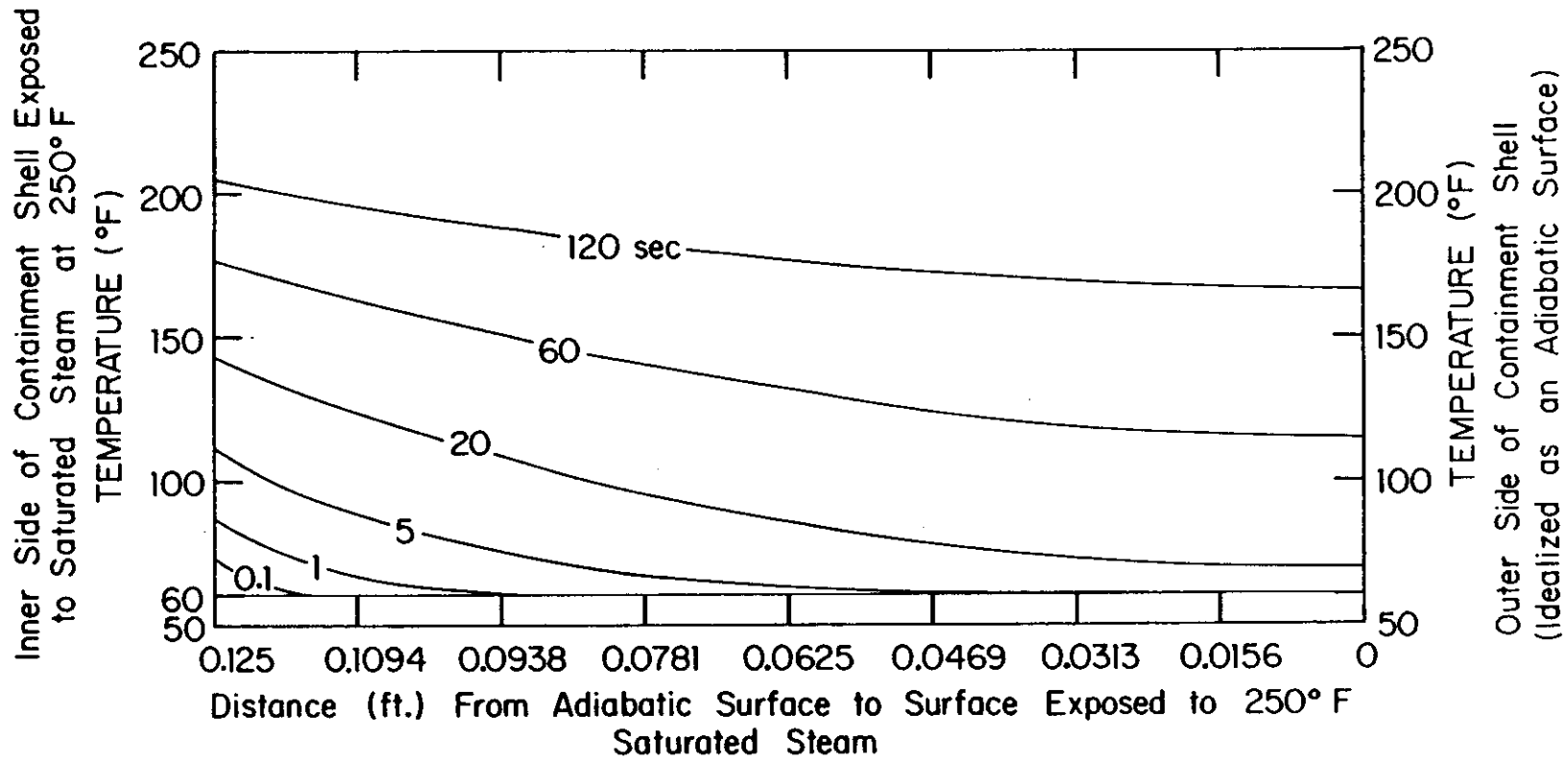
Fig. 3.15. Transient temperature distributions in 1½ inch steel plate, initially at 60°F then exposed to 250°F saturated steam and heat transfer coefficient h=300 Btu/(ft^2·ft·°F)
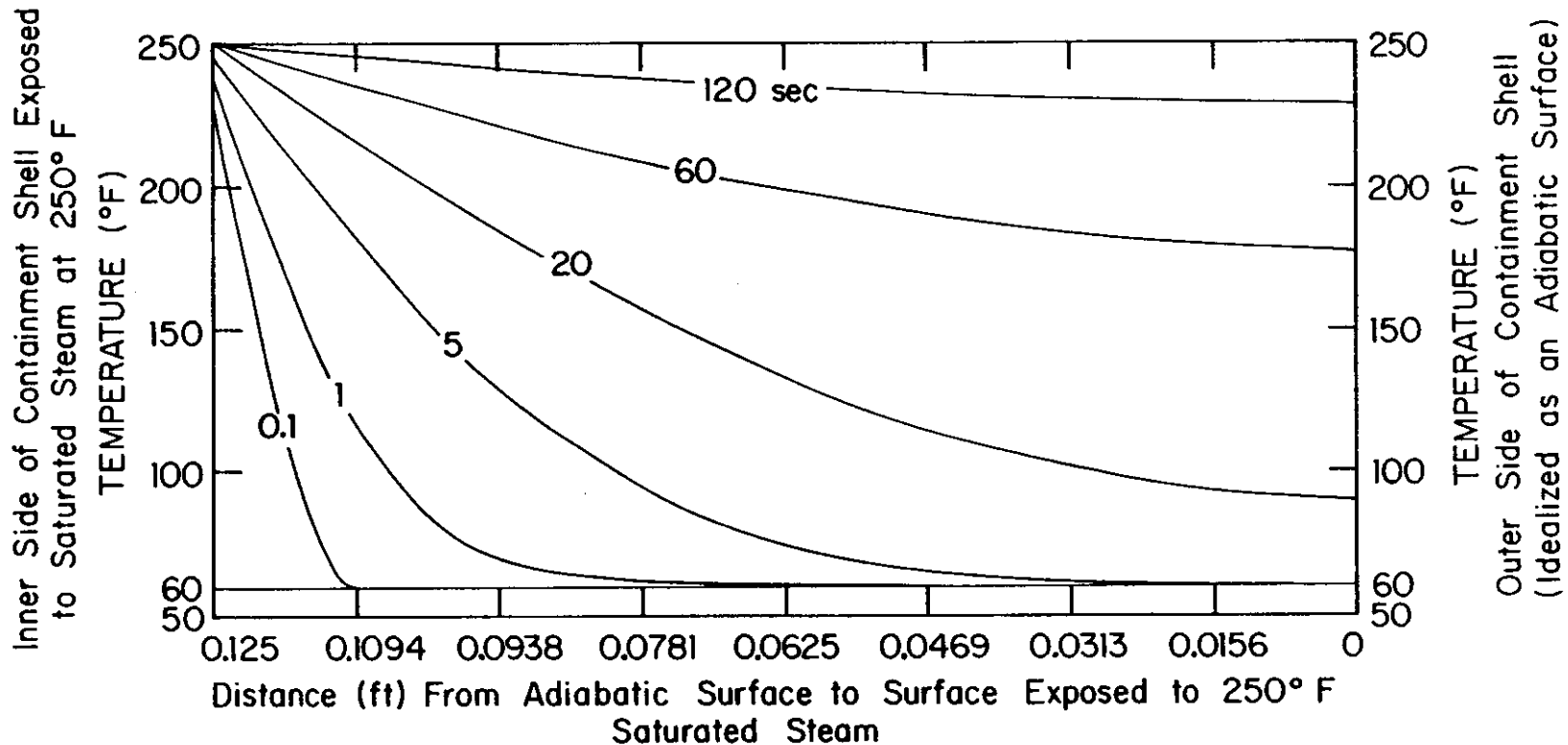
Fig. 3.16. Transient temperature distributions in 1½ inch steel plate, initially at 60°F then exposed to 250°F saturated steam and heat transfer coefficient h=20,000 Btu/(ft^2·ft·°F)
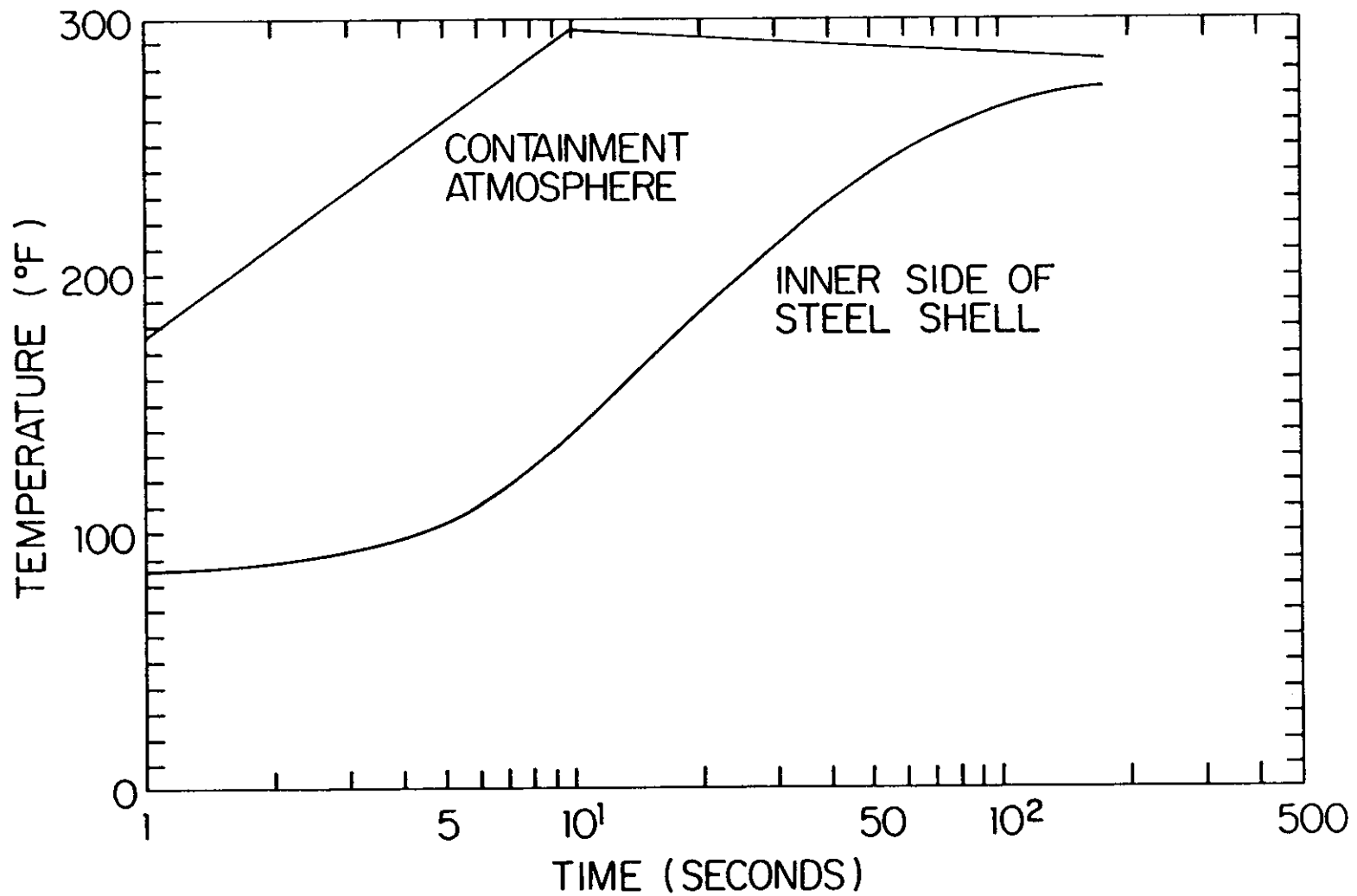
Fig. 3.17.   Example temperature-time histories of containment atmosphere and steel shell as result of loss-of-coolant accident in a dry containment of a pressurized water reactor [14]
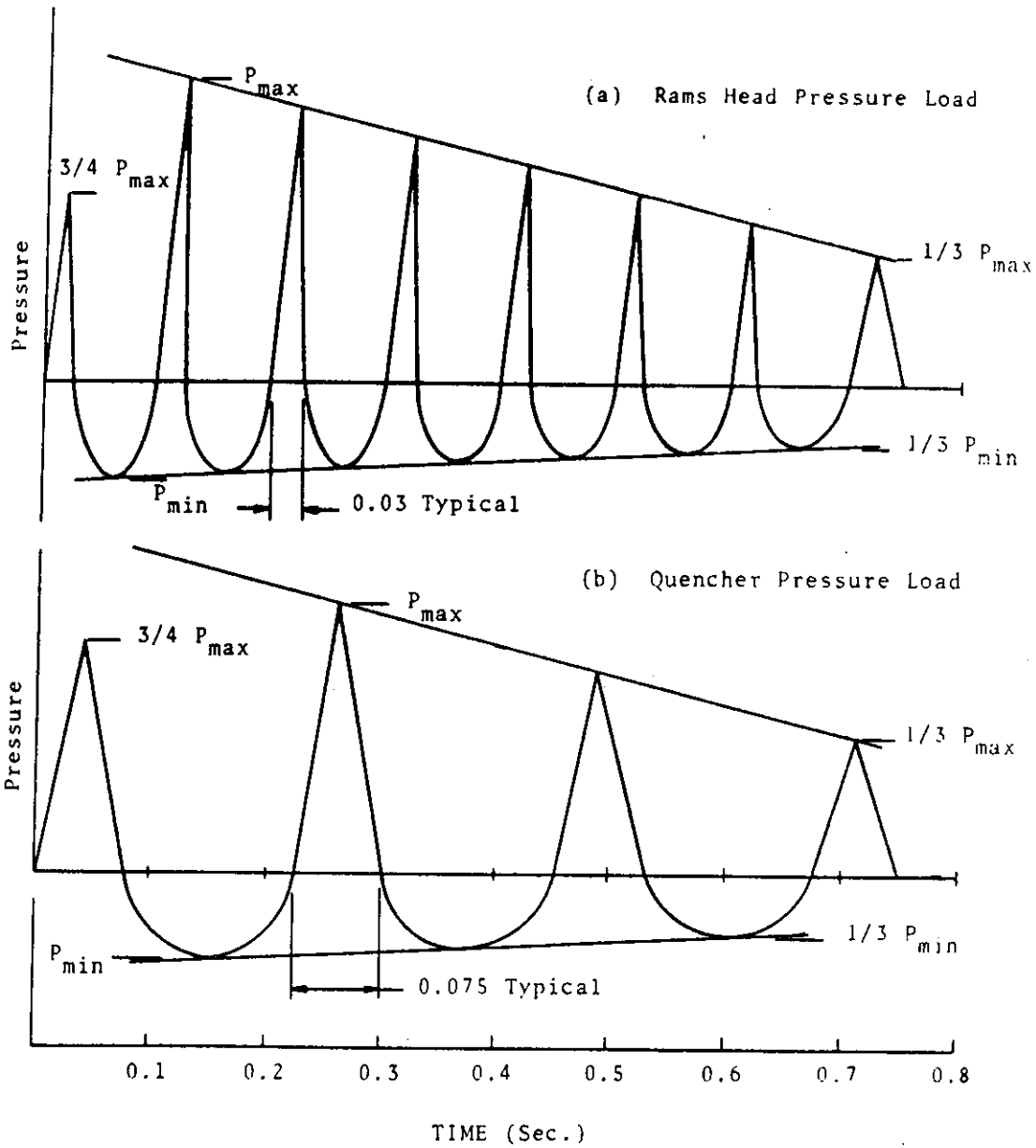
Fig. 3.18.   Normalized pressure forcing function for two
             safety relief valve discharge devices [34]
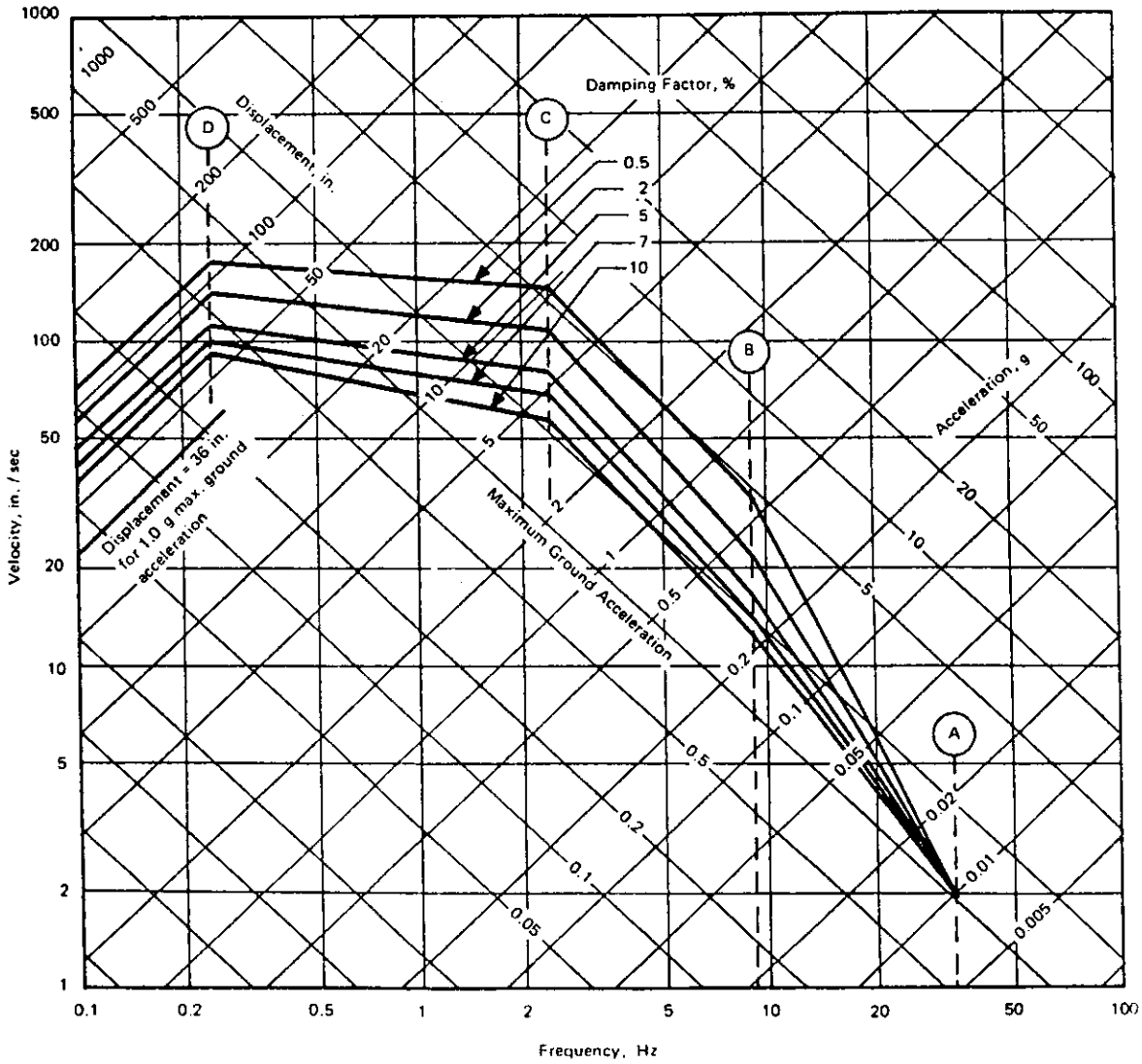
Fig. 3.19. Horizontal design response spectra -- scaled
to 1g horizontal ground acceleration [106]
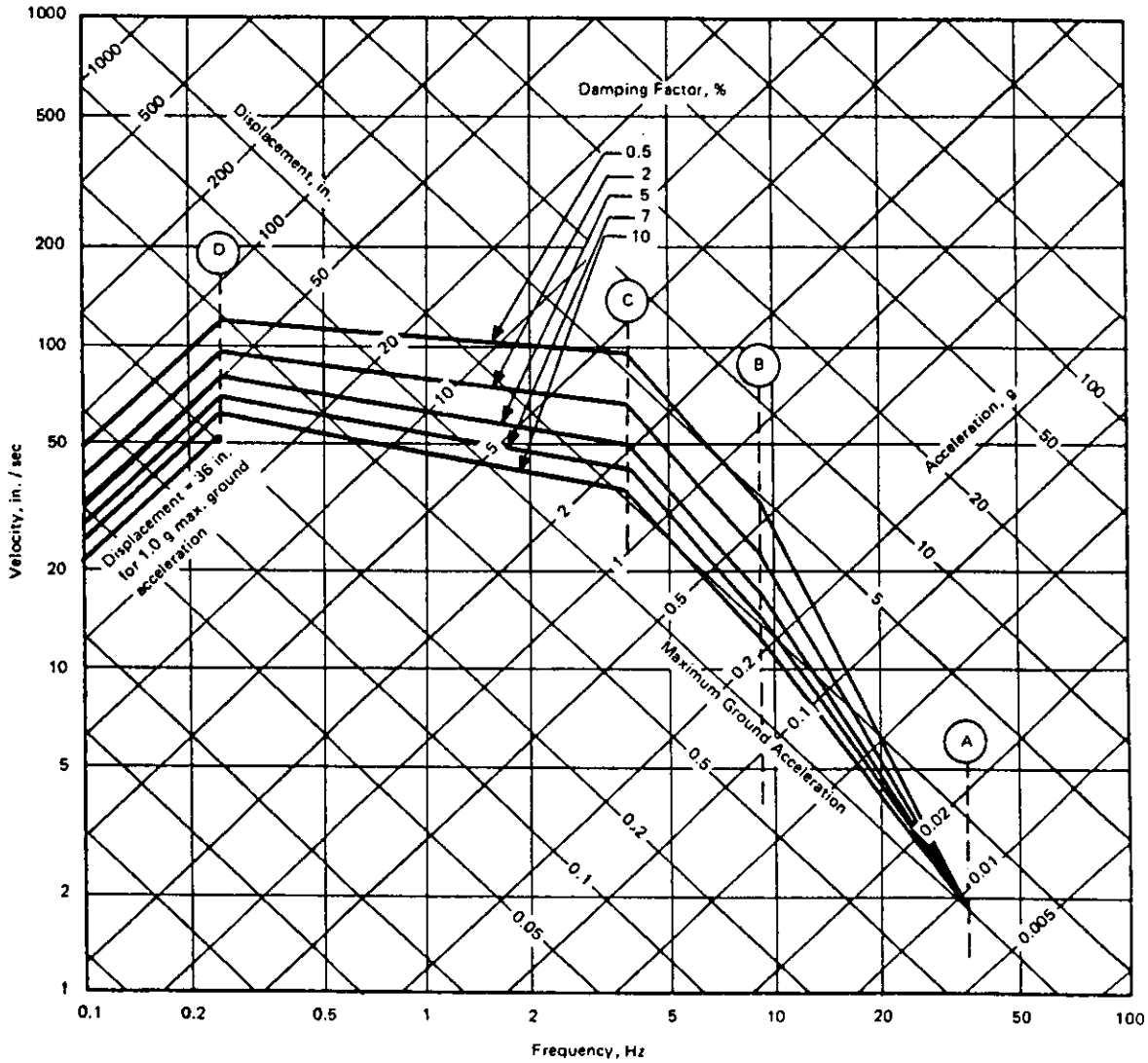
Fig. 3.20. Vertical design response spectra -- scaled
to 1g horizontal ground acceleration [106]

4. STRUCTURAL ANALYSIS

Steel containments are designed in accordance with owner design specifications with the mutual agreement of the NRC. This approach applies to the selection of loads, analysis techniques and interpretation of the results. The ASME Boiler and Pressure Vessel Code, Section III, Division 1, Subsection NE [4] provides a standard of acceptance for this approach but still allows for independent interpretation of some criteria. The uniqueness of each nuclear plant facility and its resulting specialized design nature make it difficult to generalize the design process as in conventional building codes. Therefore, decisions regarding loads and analysis for steel containments are made based on the collective judgment of the nuclear industry and NRC, guided by the ASME Code.

The design rules for free-standing steel containments are given in Article NE-3000 of the Code which is broken down into three areas: NE-3100 titled General Design, NE-3200 titled Design by Analysis and NE-3300 titled Design by Formula. NE-3300 is basically a carry-over from Section VIII where rules and formulas are given for designing specific vessel geometries. It is applicable when pressure is the only substantial load. This is rarely the case for steel containments and consequently they are virtually all designed by analysis. Design by formula of NE-3300 is practical only for preliminary sizing.

Structural analyses of the containment are done to determine the detailed states of stress in the vessel subject to various postulated

loading conditions. These analyses must account for both gross and local structural discontinuities. The state of stress is ultimately expressed in terms of the difference between the algebraically largest principal stress and the algebraically smallest principal stress at a given point (i.e., twice the maximum shear stress) and is referred to as the "stress intensity" in the ASME Code. NE-3200 classifies stress intensities with respect to: type (e.g., bending or membrane), origin (e.g., pressure or temperature) and location. Once classified, they are compared with different allowable stress levels that have been established. Basically, NE-3200 provides a standard for assessing the acceptability of the containment state of stress after the structural analysis has been completed.

4.1. General Analysis Considerations

Structural analysis is basically the process of relating loads to quantities such as displacements, strains and stresses in the structure. This relationship can be thought of as a transformation from one entity to another. The success of this operation depends on the validity of the assumptions used to formulate the transformation. The essence of the remaining discussion in Sec. 4 is to summarize the current state-of-the-art of the transformations.

4.1.1. Linear analysis

Current design practice for steel containments is, for the most part, based on linearly elastic analysis in the spirit of the ASME Code. Notable exceptions to this are buckling analyses and localized impulse or

impact loads where nonlinear analyses may be more appropriate. However, the majority of the analyses assume that the containment response is and remains linearly elastic. This assumption simplifies the computations in the transformation. But, just as important, it allows the analyst to use the principle of superposition to linearly combine the results of various loads and load combinations.

The principle of superposition is valid whenever structure deformations are proportional to the applied loads. This occurs when: 1) the stresses in the containment steel do not exceed elastic limits, i.e., the material obeys Hooke's Law, and 2) the shell displacements remain small compared with the dimensions of the containment shell. The second requirement means that containment displacements are so small that changes in the containment geometry and stiffness due to the loads do not significantly affect calculations based on the undeformed containment geometry.

When the above conditions are met, the containment can be referred to as a linearly elastic structure and the principle of superposition can be used. The displacements or the internal forces caused by a set of loads can be found by superposition. In the subsequent discussion, analysis modeling and solution procedures (i.e., the transformation) will presume linearly elastic analyses unless specifically stated otherwise.

4.1.2. Closed form solutions

A closed form solution is a mathematical expression that transforms loads to the desired unknown quantity at any point in the structure. As discussed in Sec. 3, most of the loads that constitute the design basis

for free-standing steel containments are very complex, varying with both time and space. Therefore, it is practically impossible to design a containment using only closed form solutions. For the most part, closed form techniques are relegated to preliminary sizing of portions of a containment shell.

In the preliminary design, the basic geometry and thickness of the containment shell are determined. Design basis pressures, potentially approximated as an "equivalent" static pressure, may be applied to the containment using Refs. 6, 82, 96 and 98. To this, the approximate effects of steady state temperatures can be added using Refs. 97 and 98. Continuous regions and gross discontinuities of clean shells can be readily checked with the above references.

The effects of stiffeners, attachments and penetrations are much more difficult to assess with closed form methods. There are, however, some references available to aid in examining such discontinuities. Analysis of the shell at circular penetrations can be checked using results in Ref. 35. Local membrane and/or bending stresses due to isolated concentrated static loads on the containment can be determined by methods described in Ref. 123.

Stresses in the shell due to seismic loading can be approximated using a cantilever beam analogy. This method (discussed in Sec. 4.2.2) is not a closed form procedure but its results are somewhat compatible with those from closed form techniques and so it is mentioned here.

Thus, it is possible to perform an analysis for the gross effects of design pressure, temperature and seismic loads using relatively simple

techniques and get preliminary component sizes of the containment. Further refinement to check containment integrity and economy is then necessary using well-described loads (Sec. 3) and more powerful analysis techniques.

4.1.3. Finite element/finite difference solutions

Because of attachments (e.g., stiffeners) and complex loadings it is not possible to complete the design of a containment using closed form methods. Therefore, the analyst resorts to numerical methods that give approximate, but more general, solutions. Numerical methods of structural analysis usually represent the structure as an assemblage of smaller units or "elements". Then the solutions obtained are approximate values of the unknown quantities (e.g., displacement or strain) at the points where the elements are connected together. This process of dividing the overall structure into an equivalent system of assembled elements is referred to as "discretization" and the element connection points are termed mesh or "node" points.

While closed form solutions attempt to directly characterize the response of the whole structure, numerical methods find solutions for each element, combine their effects and thus obtain the solution of the whole structure. As a consequence, it is possible to consider variations in containment loading and geometry at the local level and then add their effects to obtain the global response of the containment. It is often the case for containment vessels that numerical methods offer the only way that such considerations are tractable.

Numerical methods are usually based on energy principles, differential equations or a combination of the two. Two popular methods currently used to analyze containments are the finite difference method and finite element method. For analyzing containments, the finite difference method is based on numerically solving the shell differential equations. The displacement-based finite element method can be considered as an extension of the popular and well-known displacement method of analysis used for the analysis of beam and truss structures. In effect, the beam and truss elements are just finite elements with stiffness properties specifically formulated for their appropriate intended use.

There are numerous finite element types in the literature; which one(s) is(are) appropriate will depend entirely on the type of unknown physical quantities sought. That is, the analyst must provide elements that can behave like the real material in order to expect acceptable answers. As a general rule, the more closely the finite element can be mathematically formulated to deform like the real structural segment and the smaller the element used, the greater the analysis accuracy will be. In fact, these two criteria are the major source of misuse and error of the method.

Error associated with the element not displacing exactly as the real structure is a problem in a similar sense for the finite difference method. In the finite difference method, numerical solutions to the governing differential equations of load-displacement behavior are found at discrete points in the structure. In this process, the various derivatives that characterize structural deformations are approximated by

polynomial expressions. In general, if the differential equation correctly describes the physical process and as the number of mesh points approaches infinity, the results can be considered as "theoretically exact".

4.1.3.1. Three-dimensional discretization

Ideally, all structural models should be represented by three-dimensional models composed of three-dimensional finite elements (Fig. 4.1(c)). Alternately, for finite difference methods, three-dimensional differential equations and corresponding mesh networks should be used. At this point, discussion will refer to finite elements since, in essence, the same concepts apply to either method.

With three-dimensional elements, all attachments, penetrations, shell thickness variations, nonuniformities in the soil, and so forth that exist for the real containment can be represented. However, to do an adequate job of this would require thousands of elements [25]. The manhours required to input data and assess the computer output would be tremendous when one considers the number and type of loads to be analyzed. And, even if much of the effort associated with data input and output assessment were automated, the cost of an analysis computer run for one loading would be huge. Further, great potential exists for errors in the mesh and the handling of input and output data.

As a result, overall or "global" analyses of containments using three-dimensional elements are not practical. For containment vessels the practical use of three-dimensional elements is currently limited to

local analyses when it is necessary to know the three-dimensional state of stress to calculate the stress intensity at a point.

4.1.3.2. Two-dimensional discretization   Common two-dimensional finite elements are the triangle, rectangle and quadrilateral shapes. The displacement behavior and stiffness characteristics of these elements has been formulated for plane strain, plane stress and plate bending (Figs. 4.1(b) and (e)). Elements of this type are formulated with respect to two of their spatial dimensions. The third dimension is generally taken as very small and the following assumptions are used:

(1) plane strain - out of plane displacement is zero and loads are applied in the plane;

(2) plane stress - stress through the thickness of the material is zero and loads are applied in the plane;

(3) plate bending - stress through the thickness is zero and shear deformations are governed by either Kuchhoff or Mindlin theory [7]; membrane stress is not included.

These are flat elements which can be used to build a structure model in three dimensions if the three-dimensional loading and structural behavior is compatible with the abilities of the element used.

A flat shell element is obtained by superimposing a plate bending stiffness and a plane-stress membrane stiffness [7,32,37]. These flat shell elements can be used to model flat components of shells (e.g., folded plates) and are also used to approximately model general curved shells. Curved thin shell elements have also been formulated to more closely model a shell structure (Fig. 4.1(g)) [37]. This element is

really just a special case of the general three-dimensional shell ele-
ment, in which the thickness variable is taken as a constant [7]. Two-
dimensional shell elements can be used to represent the steel containment
as a three-dimensional model. However, such a model is similarly subject
to the limitations discussed in Sec. 4.1.3.1 and hence are not very prac-
tical for modeling entire containments. In fact, Ref. 25 pegged the cost
of analyzing a containment vessel for all required load combinations on
the order of $1,000,000.

Shell elements may be excellent, though, for local analyses on the
containment. The flat two-dimensional elements discussed may also be
used (depending on their capabilities) to approximate a portion of the
containment shell or for situations where the load and structural
response are planar. For example, flat shell elements can be useful for
performing local analyses of equipment hatch openings or steam and feed
water penetrations. Plane strain elements have been used to model a
slice through the site soil profile for seismic analyses.

Two-dimensional elements, by definition, represent material behavior
as a function of two independent variables; the third (e.g., thickness)
is considered as a constant. When a structure is essentially rotational-
ly symmetric about an axis, it may be possible to express a three-dimen-
sional model of it using only two independent variables. In this situ-
ation, a cylindrical coordinate system, r, z and Θ, may be applicable and
all structural properties are independent of the Θ coordinate [7,37].
The element then used is termed an axisymmetric finite element and is in
the form of a ring of constant cross section spun around the z axis (Fig.

4.1(d)). The cross section is typically the triangle, rectangle or quadrilateral. Even though the element appears to be three dimensional, only two independent variables, r and z, are available and so the discretization is referred to as two-dimensional. The circumferential coordinate is described by an angle Θ and the nodal points of the element are nodal circles.

For symmetric loading, the displacements v in the Θ direction are zero, i.e., the applied load and structural response are independent of the θ coordinate. However, containment loadings are often nonaxisymmetric resulting in displacements v in the circumferential direction of the containment. In this three-dimensional problem, if a Fourier series can be used to represent the load and the solution in the Θ direction, then only the two-dimensional discretization is needed [7,32,37]. In this case, both the loading and circumferential dependence of displacements are expressed in terms of $\cos\Theta$ and $\sin\Theta$ and related to the r and z variables by the Fourier series [7,37].

Axisymmetric elements will build a three-dimensional model but cannot directly account for components and structural properties that vary around the containment. It may be noted that this is not a limitation when the more expensive model composed of two-dimensional thin shell elements is used. Axisymmetric elements cannot, for example, directly include the effects of stringer stiffeners, penetrations, or attachments. Since steel containments are relatively thin structures, the thickness variable of two-dimensional axisymmetric elements is not vital. One-dimensional axisymmetric elements are more appropriate for the steel

containments and, therefore, further discussion of the use and limitations of axisymmetric elements is referenced to Secs. 4.1.3.3 and 4.2.1.

However, two-dimensional axisymmetric elements do have important applications in other aspects of containment analysis. For example, they are sometimes used at the cylinder/base intersection and to model thick concrete internal structures that are rotationally symmetric. Also, they are used to create three-dimensional models of the site soil profile for seismic soil-structure interaction analyses. This application is limited to uniform or uniformly layered soil deposits due to the rotational symmetry of the elements.

4.1.3.3. One-dimensional discretization

Elements of this type are currently the most popular for modeling the entire containment. The economy realized in their use is considered to outweigh any loss of accuracy associated with modeling inaccuracies. This also facilitates economical parametric studies of variations in material (e.g., soil) and load (e.g., frequency content) properties so that critical response can be bracketed. Therefore, given the computer hardware and software currently available, one-dimensional discretization is considered the most practical for overall analysis and two- and three-dimensional discretization is mostly reserved for local analysis [25,40,121]. Since one-dimensional discretization is generally used for containment modeling, further discussion is given in Sec. 4.2.

4.2. Containment Modeling

The integrity of the steel containment is required to remain intact during a LOCA and/or an earthquake. At this time, there are no reliable methods of proving that large inelastic deformations do not jeopardize containment integrity. As a a result, current practice is to design and analyze the containment as if it remains essentially elastic [55,65].

A rigorous analytical solution for idealized seismic response of a cylindrical containment based on linear shell theory and a fixed-free perfect cylinder has been provided [65]. The horizontal ground motion was described with first harmonic loadings applied along the circumferential direction. Assuming small deformations (less than the thickness of the shell), the formal solution contains only the first harmonic (n=1) circumferential mode. This implies that circular cross section remains undeformed and that the cylinder vibrates purely as a cantilever beam.

As a result of this finding and from comparisons with other model solutions, simple one-dimensional beam element containment models (Fig. 4.2) are considered adequate for some purposes in determining dynamic response from horizontal seismic motion. In particular, upright cylindrical containment vessels are theoretically verified. However, in practice many other containment geometries have been modeled with one-dimensional beam elements.

When a cylindrical shell is subjected to a vertical motion, an axisymmetric (n=0) mode of vibration will be excited. For any given number of axial waves (m=1,...j) of free vibration, the shell may have three

modes having three separate eigenvalues (i.e., natural frequencies).
These three modes are pure torsion and longitudinal motions and a primarily radial motion [67]. Beam elements cannot adequately model vertical modes of containment shell vibration, especially the containment dome. As a result, a model constructed with shell elements (e.g., one-dimensional axisymmetric finite elements) is needed to adequately describe vertical response.

Experiments have shown that a steel containment subjected to horizontal base motion actually exhibits higher-order circumferential modes, i.e., $n>1$ [65]. The higher circumferential modes are thought to be caused either by nonlinear vibrations or irregularities in the containment. If irregularities, such as penetrations and appurtenances, are deemed significant then a finite element model using two-dimensional shell element discretization would be required to incorporate these effects. This type of model could potentially exhibit the resulting higher shell modes. Currently, however, the extra cost for "questionable" increased precision is not considered justified. Rather, current practice for overall response to seismic load is to use one-dimensional discretization of axisymmetric ring or, in some instances, beam finite elements.

For design basis loads such as dynamic LOCA pressures and hydrodynamic pressures, the containment will almost certainly experience higher circumferential modes (i.e., $n=2,3,...$) along with numerous axial waves

(i.e., m=1,2,3,...). The beam element model is limited to essentially n=1 dynamic behavior and is not adequate for the above. For loads that induce response behavior with the above characteristics, the overall containment is generally represented by a three-dimensional model composed of one-dimensional axisymmetric curved shell or conical frustrum finite elements (Sec. 4.2.1) as shown in Fig. 4.3.

The axisymmetric shell model is obviously more versatile than the beam element model but it is also more expensive to use. Axisymmetric shell models can be used for all purposes identified for the beam element model (Sec. 4.2.2) plus other purposes for which the beam element model is not adequate, e.g.:

1) Vertical modes of containment shell vibration.

2) Circumferential modes of containment shell vibration where n>1.

3) Accurate assessment of stress states in the containment shell, particularly at axisymmetric gross discontinuities.

4) Evaluation of buckling stresses.

5) Generating response spectra for analysis of attachments that are affected by dynamic behavior of (1) and (2).

4.2.1. One-dimensional axisymmetric modeling

As mentioned in previous sections, one-dimensional axisymmetric discretization is the most popular and economically practical method of modeling containments for general design basis loads. This section will primarily focus on what type of axisymmetric elements are used and how their limitations are accounted for.

4.2.1.1. Finite element   One-dimensional finite elements include beam, truss and axisymmetric ring elements (Figs. 4.1(a) and (f)). The beam element is often used to model the containment for seismic analyses but will be discussed alone in Sec. 4.2.2. The element of interest here is the axisymmetric ring element. This element can be used to construct a three-dimensional model of the entire containment. The components and properties of the model are rotationally symmetric about a vertical axis in the center of the containment, like the two-dimensional axisymmetic discretization. In fact, the main difference between the one- and two-dimensional axisymmetric elements is that the thickness variable becomes a constant in the formulation of the one-dimensional axisymmetric element. Thus, for the containment, through thickness stress is neglected and only bending and membrane stress are considered.

One type of one-dimensional axisymmetric element often used is a conical frustrum. This is a straight or flat element with the capability to represent bending and membrane stress states. The containment model is built by connecting adjacent elements at their nodal circles. Curved regions such as the containment dome are approximated by a series of flat segments. Another element type that can be used in the curved regions is the axisymmetric shell element [32]. This element is curved so that it can more directly represent the containment dome.

Since model components are taken as rotationally symmetric about a vertical axis in the center of the containment, discrepancies in the real structure must either be approximately included or shown to have a negligible effect on overall containment behavior. Discrepancies that are

not directly included in an axisymmetric model include penetrations and, structural and non-structural attachments.

In axisymmetric modeling, it is often assumed that the effect of all containment penetrations has a negligible effect on the overall containment response and capacity [25,67,121]. Major penetrations that cannot be included in the overall response include the personal lock and equipment hatch. A local verification analysis is generally required for major penetrations, and small mechanical or electrical penetrations are reinforced in accordance with ASME Code replacement rules. The intent of these requirements is to make the penetrated vessel at least as strong against buckling and collapse as the unpenetrated shell. This has been borne out experimentally on smaller vessels and is part of the basis for assuming that penetrations do not affect overall behavior.

Ring stiffeners can be easily added to the model because they are rotationally symmetric. The web and flange may be modeled with thin shell plate elements [25]. Other programs may equivalently model the ring stiffener as a flat conical element with an equivalent thickness to compensate for the exclusion of the flange [40]. Stringer stiffeners also require some method of equivalent modeling when the axisymmetric elements are used. A procedure is to input the steel shell as an orthotropic material with properties in the meridional direction modified to uniformly reflect the effect of the stringer stiffeners. Properties in the circumferential direction are input as usual, based on shell geometry and material. Orthotropic approximation becomes more questionable as the stringer stiffener spacing increases.

Circumferential variations in shell thickness can conservatively be accounted for by basing the thickness of the element on the thin region of the vessel at the level in question. Meridional variations in shell thickness can be accounted for by using the average thickness of the containment shell segment represented by the axisymmetric element or by changing elements at thickness changes.

The dead load and corresponding mass of equipment on attachments and in penetrations of the containment shell are added at their respective meridional level by uniformly distributing it (i.e., dead load or mass) around the shell circumference. Mass may be concentrated at the nodal circles of the axisymmetric elements by simple lumping or by the consistent-mass method as explained in Sec. 4.3.2.

As a perspective, structural parameters of stiffness, loading, and mass that are rotationally symmetric are modeled and input in a straightforward manner. On the other hand, these parameters for attachments (structural and nonstructural) and penetrations have their "effects" distributed around the shell in an approximate manner, or else are neglected (if appropriate).

This axisymmetric model is for analysis of the overall response of the containment. Unless provisions are made for geometric and material nonlinearities, this model will probably not detect overall or local instabilities (Sec. 6.3). In lieu of provisions for nonlinearities, a linear analysis may be done and then the resulting stresses and displacements examined to see if a linear analysis was valid. If valid, and if

criteria for buckling stress are available, then a factor of safety against buckling can be determined.

If the containment is subjected to axisymmetric loads, then only a unit radian section of the vessel need be considered. However, in the usual case, the design basis loads are nonaxisymmetric and require that the response of the entire containment be considered. That is, non-axisymmetric loads will cause membrane and bending stress to vary meridionally and circumferentially in the containment. As mentioned in Sec. 4.1.3.2, the three-dimensional problem presented can still be handled with one-dimensional discretization if the load and solution can be expressed as a Fourier series in the Θ direction [7,32,37]. As a result, the Θ dependence of all displacements, stresses and strains can be expressed in terms of $\sin\Theta$ and $\cos\Theta$.

Local analyses at discontinuities such as attachments and penetrations must be done separately, usually using two- and three-dimensional elements. Gross discontinuities such as dome/cylinder and cylinder/base intersections are generally axisymmetric and can potentially be considered in the overall analysis. The local analysis model should be provided with boundary conditions that deform the same as the typical containment shell. Boundary conditions may consist of defining the boundary node degrees of freedom (such as free or fixed) and/or may consist of boundary node forces or forced displacements that have been determined from previous overall analyses. Local analyses are done to check stress intensity against material capacity and assess potential fatigue and fracture conditions (Sec. 6.2). In addition, they are done

at large penetrations to verify that their integrity (e.g., buckling strength or collapse resistance) matches or surpasses that of the unpenetrated shell (Sec. 6.3). This is important since penetrations are typically neglected in axisymmetric shell models.

4.2.1.2. Finite difference   The finite-difference method is a numerical method to solve the differential equation for displacement or stress resultant at chosen points on the structure, referred to as nodes or pivotal points. Programs are available, such as Kalin's KSHEL [58] and Bushnell's BOSOR4 [16], that are formulated for shells of revolution under axisymmetric and non-axisymmetric loadings (thermal or mechanical, varying with time). Using such programs, the steel containment can be represented as a number of one-dimensional segments of revolutions. Such discretizations have been shown to reliably determine deformations and stresses in axisymmetric shells subjected to arbitrary loading [25,40].

Basically, the one-dimensional finite difference analysis is subject to the same limitations described for the one-dimensional axisymmetric finite element method. Similar to the finite element method, the effect (if any) of penetrations and the stress states around them cannot always be included. Also, non-axisymmetric loading is modeled as a Fourier series. Ring and stringer stiffener effects are also included, though, sometimes by indirect equivalent methods [40]. The finite difference method may have an advantage over the finite element method in that less computational effort may be required for a comparable degree of accuracy [25]. The finite difference method does require special considerations at boundaries, although this does not tend to be a large difficulty when

analyzing shells of revolution. However, the availability and user familiarity with the finite element method has maintained its popularity.

4.2.2. Beam element modeling

The overall dynamic characteristics of a cylindrical portion of a containment, subject to horizontal base motion, are often adequately defined by treating the containment as a hollow cantilever beam [67]. That is, theoretically, all modes of vibration resulting from horizontal excitation of a perfect upright cylinder contain only the first harmonic (n=1) circumferential mode. For horizontal base motion, it is therefore often possible to model the containment with a one-dimensional discretization of beam elements. This model shall be referred to as the beam model and is shown in Fig. 4.2.

As explained earlier, the beam model is very limited in its ability to describe vertical containment response. For upright cylinders, the fundamental mode of the vertically excited axisymmetric mode (n=0) is mostly composed of longitudinal motion. Therefore, the beam model can yield a good measure of the fundamental frequency (m=1) for containments that are essentially upright cylinders. Higher shell modes and capping domes or spherical containment geometries cannot be accurately modeled for vertical base motion using beam elements [67].

As a conclusion, the beam model should be considered as adequate only for investigating containment response to horizontal base motion. In this role, the beam models are used to determine overall forces on the containment and foundation, check clearance tolerance and to generate in-

structure response spectra [67]. They are also especially useful for preliminary sizing analyses, verification of more complex analyses and as cost-effective tools for parameter studies.

Typically the containment building is composed of large internal support structures enclosed by the primary steel containment which, in turn, is also enclosed by a secondary concrete containment. The steel containment and other important structures (e.g., those mentioned above) should be modeled separately [46]. This discussion addresses the steel containment alone but in actual analysis the presence of the other structures on the common containment building base should be included, especially if a soil-interaction analysis (Sec. 5.1) is being conducted.

Adequate results for the above purposes can be obtained if sufficient discretization is provided. As a guideline, Ref. 92 suggests that the proper steel containment model should have twice as many mass points as the mode number of interest. Mass may be concentrated at the nodes by simple lumping or by the consistent-mass method (Sec. 4.3.2). The consistent-mass method is based on the interpolation functions for a uniform beam segment. For this case, these functions are cubic hermitian polynomials.

Lin and Hadjian [68] have shown that the effect of rotatory inertia in a containment may be rather insignificant in the first two modes but becomes increasingly more noticeable in the higher nodes. Since the first few modes are typically the most important ones for seismic analysis, the decision to include or neglect rotatory inertia in the containment becomes somewhat arbitrary. Generally speaking, a beam model built

from a large number of elements in which the consistent-mass method (rotatory inertia is thus inherently included) is used to concentrate the containment mass should give the best results. If the analyst is using the model to determine something relatively sensitive and important, such as in-structure response spectra, then it may be desirable to apply these so-called refinements.

If the beam model is to be used in a seismic analysis in which the effects of soil-structure interaction are to be included, then the rotatory inertia of the containment should always be accounted for. This is because the analysis model will have at least one rotatory dynamic degree of freedom at the containment base associated with rigid body rocking of the containment building. Therefore, if the rotatory inertia of the containment is not included in the mass matrix of the containment vessel, then its effect should be accounted for at the containment base rotatory dynamic degree of freedom. In this case, the rotatory inertia at the base is the summation of the base rotatory inertia and that of all the containment building masses about their own individual axes [46,100].

Since the containment is being treated as a hollow beam, the stiffness properties are based on the uniform, undeformed cross-section of the containment. The containment is divided into segments by passing an appropriate number of horizontal planes through the vessel at appropriate locations. Each axisymmetric segment is replaced by a beam element. The stiffness properties of the beam element are calculated from the segment cross-section just as is done in conventional frame analysis. The contribution of stringer stiffeners to the cross-section can be included

but the ring stiffeners are neglected. Because of the relatively high r/l ratio of the segments, it is important to include shear deformation effects in the stiffness matrix of each element [68,78]. Technically, this will also affect the formulation of the consistent-mass matrix but could be neglected [47].

For the segments that correspond to capping domes or spherical shells, the beam element between two adjacent nodes may be assumed to be uniform. The stiffness of a beam element may be approximated by basing the moment of inertia and cross-sectional area on the average cross section between the adjacent nodes [67]. More rigorous methods to accurately calculate these stiffnesses tend to defeat the purpose of the beam modeling method. However, when modeling spherical containments or spherical portions of containments (e.g., the Mark I bulb), the analyst should use segments that are small enough so that the average cross section is not too much different from that existing at the beam element nodes.

In parting, Ref. 67 showed that the Timoshenko beam equation predicts the structure frequencies (for upright cylinder type containments) with reasonable accuracy for a beam type mode (n=1) up to the third mode. They also demonstrated that bar theory predicts the fundamental frequency of the axisymmetric mode (n=0) with equally acceptable accuracy. The height of the Timoshenko beam and uniform bar was taken equal to the apex of the dome. It may also be noted that Timoshenko's beam equation includes the effects of shear deformation and rotatory inertia.

4.3. General Considerations for Dynamic Modeling

Ideally, the containment vessel should be modeled as the mass continuum it really is. In this case the problem would be formulated in terms of partial differential equations and the solution would define displacements and accelerations at any point on the shell. However, since closed form solutions are limited to only special cases for thin shells and are not practical for seismic and LOCA containment analyses, the analyst resorts to numerical methods using discrete elements. The following discussion applies to numerical modeling of the containment and supporting soil, in general, for dynamic analyses.

Soil modeling is particularly required in seismic analyses because, unless the containment building is founded on rock or rock-like material, soil-structure generally must be considered (Sec. 5.1). This interaction is coupled and unless special techniques are employed (Sec. 5.1.2.2) the soil-structure system must be analyzed as a whole [52]. Since the soil and containment properties are very different, this system may be referred to as a composite system or structure. The composite structure can include, for example, the primary steel and secondary concrete containments, their internal structures and the local foundation soil.

4.3.1. Discretization

In the use of discrete elements (Sec. 4.1.3), the mass continuum of the structure is considered concentrated in a series of discrete nodes or lumps. This greatly simplifies the dynamic problem because inertia forces can be developed only at the selected mass lumps. The solution

will initially define displacements and accelerations at only these selected nodes. This information may in turn be used to determine displacements, stresses and strains in the element between the nodes based on the displacement interpolation functions [7,29,32,37] used to define and formulate the element. Interpolation functions define the element shape between the specified nodal displacements.

The nodes are carefully selected so that they coincide with significant changes in geometry, concentration of mass (e.g., equipment hatch and personnel lock), and with points important for accurate stiffness characterizations (e.g., shell thickness transition points) [78]. Generally, node locations become more arbitrary in regions of the containment or soil that are characterized by uniform distribution of mass and stiffness. In this case, nodes should be uniformly spaced and numerous enough so that the discrete element displacement capabilities can represent the structure vibration shapes. For example, Ref. 67 suggests that for a containment model composed of axisymmetric ring elements and subjected to horizontal base motions, the ratio of containment radius to element length should be greater than 3. At gross and local discontinuities the structure responses (especially stresses) are more complex. If the goal of the analysis is to evaluate stress and strain at such locations, then the discretization must be relatively fine there.

The nature of displacements and accelerations at the selected nodes is, even in the confines of mass lumping, a three-dimensional phenomenon. That is, with respect to a three-dimensional orthogonal coordinate

system, each node can potentially have three translations and three rotations. These six displacement components are termed the number of dynamic degrees of freedom (DDOF). However, it may very well be that inertial forces corresponding to some of these components (e.g., rotation) have an insignificant effect on the problem and can be neglected.

4.3.2. Mass properties

The discrete mass elements used to build the model are connected together at their nodes just as is done in the displacement method of analysis. For example, axisymmetric finite elements are connected together at their nodal circles. As mentioned before, the solution process initially defines displacements and accelerations only for the DDOF at the selected nodes. Therefore, all excited inertial forces must be appropriately defined in terms of these nodes and associated DDOF. This means that the mass continuum is assumed to be concentrated at the nodes and the elements used to build the model are considered to be massless.

Each element represents a portion or segment of the actual structure and its mass. There are two methods commonly used to concentrate the element mass at the element nodes. The simpler method is referred to as "lumping". In simple lumping, this mass is considered to be equally shared by each node of the particular element. For the assembled elements, this amounts to lumping the mass of the contributory region adjacent to the node. That is, the total mass concentrated at a given node of the complete structure is the sum of the nodal contributions for all the elements attached to that node [29]. For rotatory inertia, an

upper bound can be estimated by assuming that the structure section adjacent to the node is rigid [68].

The resulting model should be examined to make sure that the total mass of the structure is conserved and that the center of gravity of the structure and individual components is preserved. With respect to conservation of mass, the mass of all appurtenances should be included in the model unless it can be decoupled from the containment model. Criteria for decoupling equipment and components from the containment can be found in Ref. 113. As an example, equipment supported on very flexible connections are candidates for decoupling. Whether the attached equipment is decoupled from the containment model or not, the attached equipment itself is generally analyzed as a decoupled system from the containment and the seismic input for the former is obtained by the analysis of the latter.

The second method is termed the consistent-mass method. This method is based on the interpolation functions used to formulate element stiffness. The reader is referred to Ref. 29 for details. Basically, however, an "element" matrix of mass influence coefficients is formed. From this the inertial force at a given DDOF of the element is the total effect of all DDOF accelerations of the element. That is, rather than just proportionally lumping some portion of the element to one of its nodes, the total mass of the element is allowed to appropriately participate in a DDOF acceleration of the element. After the mass coefficients of the elements are evaluated, the mass matrix of the complete structure is developed by the same assembly process used for developing the

structure stiffness matrix. Technically, this method is more accurate than simple lumping. However, it has been found that similar results are often obtained by either method [29].

4.3.3. Stiffness properties.

Stiffness properties of the containment for dynamic analysis are the same as those used for static analysis. For the numerical methods being discussed here, the element stiffness matrices are evaluated and then assembled, as usual, to form the stiffness matrix of the entire structure. Appropriate properties, such as thickness, area, and cross-sectional moment of inertia, are determined for the particular element type being used, based on the containment segment or portion being modeled.

The analyst should make sure that the stiffness matrix of the element being used contains terms that account for all significant strain energies of the deforming material. For example, containment deformation is caused by flexure, axial, shear and torsional stress; conventional building analysis often only considers deformation due to flexure. It has been stated that when using one-dimensional beam element discretization (Sec. 4.2.2), large containment radius to element length ratios cause shear deformation to be a significant factor [68]. So in this instance, for example, the analyst should make sure the element stiffness matrices include shear deformation effects.

For the most part, stiffness properties of the elements and structure are those from conventional static matrix analyses. However, a modification of the usual assembled structure stiffness matrix that is often done is as follows:

Typically, structures of the type discussed herein are assembled with 3 or 6 degrees of freedom (DOF) at each node depending on whether a two- or three-dimensional analysis is being done. Frequently, however, the significant inertial forces are considered associated with only certain selected DDOF. In this case, simple mass lumping to these selected DDOF is often done and the mass associated with the other DOF (e.g., rotational DOF) is assumed to effectively be zero. The remaining DOF are not explicitly involved in the dynamic analysis and are therefore "condensed" out [29]. That is, these nondynamic DOFs are removed from the numerical computations but their effect on the remaining DDOFs is preserved. This is generally done by a process known as kinematic condensation [7,29,32,37].

4.3.4. Damping properties

During the dynamic excitation of structures, some of the energy imparted to the styructure is internally dissipated. This effect, termed material damping, results in some attenuation of the structure dynamic response. Unlike mass and stiffness properties, there are currently no general expressions available to evaluate material damping. Rather, such damping values are determined experimentally and from previous experience.

Another form of energy loss occurs in composite systems wherein local foundation soil is included in the dynamic analysis. The seismic loading sets the containment building in motion and, in turn, the containment building imparts some of the energy to the soil through the propagation of waves [122]. This energy loss is referred to as radiation

or geometric damping. Material damping in the soil also takes place. It is important to account for both of these damping mechanisms when a soil-interaction analysis is done.

Generally, the force dissipated at the DDOF by damping is assumed to be proportional to the DDOF velocity. This mechanism of damping is referred to as viscous damping and is more of a mathematical convenience than a physical reality. Viscous damping is used to approximate actual mechanisms of damping because it simplifies the differential equations of motion. Usually, it is expressed as a percent or ratio of critical viscous damping.

There are various acceptable ways of incorporating damping values into seismic analyses. The manner in which damping is incorporated depends largely on the numerical method chosen to solve the equations of motion (Sec. 4.4). Often the solution for the equations of motion is found by superimposing the dynamic response of each significant mode of vibration that makes up the total dynamic response of a structure (Sec. 4.4.1). When this can be done, an experimentally substantiated damping value can be assigned to each mode. Typical modal damping values for steel containments are 2 to 4 percent of critical damping [107]. In principle, this can only be done for structures composed of a single material and in which damping does not significantly alter the undamped mode shapes.

The above concept results in damping assigned to each mode rather than associated with each DDOF of the structure. Sometimes, it is desired to implement numerical methods wherein the damping force

associated with each DDOF is needed. In this case, there are expressions available [29] to determine DDOF damping from the modal damping ratios. This is often done because it provides a proven basis for the DDOF damping values that are otherwise difficult, to impossible, to rationally determine [29,45]. Structure damping based on modal damping ratios is often referred to as "proportional" damping because it is formulated with respect to the mass and/or stiffness properties.

In soil-interaction analyses (i.e., a composite structure), the damping of the soil will be relatively high compared with that of the containment building [45]. The higher soil damping results in significant damping in some of the otherwise lightly damped modes of steel containment vibration. That is, the damping forces in the soil of a composite model cause coupling between soil-structure modes of vibration. The coupled damping of a composite structure can be derived by assuming modal damping ratios for each type of material, i.e., substructure. Then individual DDOF damping ratios can be derived (as explained in the previous paragraphs) for each substructure and assembled together to yield the coupled DDOF damping in the composite structure [29,79]. In such systems, the method of mode superposition is not applicable because individual modes of vibration do not exist due to inter-mode coupling.

When it is not possible to express the damping of a structural system so as to facilitate mode uncoupling, the response must be obtained by integrating the equations of motion simultaneously rather than individually. Other methods to solve the coupled equations of motion are also available such as the Fast Fourier Transform method [71] and the Foss

method [36]. This condition of coupled damping is often referred to as "nonproportional" damping.

The damping in most soil-structure interaction problems will generally be coupled and therefore cannot be assumed to satisfy the modal orthogonality condition. However, techniques to get around this have been developed for determining equivalent modal damping ratios for the soil-structure system [83,99]. The expressions derived in Refs. 83 and 99 yield weighted modal damping ratios that approximately account for the coupled soil-structure damping experienced in each mode (assuming classical normal modes exist). This work was done mainly so that the response spectrum method could still be used.

4.4. Dynamic Analysis Methods

This section outlines the dynamic analysis methods most frequently used to analyze steel containments. The goal here is to give some perspective on the various solution techniques available for the system equations of motion. The reader is referred to Refs. 7, 11 and 29 for more details. Which solution technique is most appropriate will, of course, depend on the nature and complexity of the problem. In some instances, correctness and economy are best realized by using more than one of the following techniques (Secs. 4.4.1 to 4.4.3) in the solution of a given problem.

Transient pressure and hydrodynamic loading are applied directly to the containment shell. The equations of motion for a multi-degree of freedom (MDOF) system with dynamic load applied at several points are:

$$[M]\{\ddot{D}(t)\} + [C]\{\dot{D}(t)\} + [K]\{D(t)\} = \{F(t)\} \qquad (4.1)$$

where:

    $[M]$ = Mass matrix representing the mass of the structure.

    $[C]$ = Damping matrix of structure.

    $[K]$ = Stiffness matrix of structure.

    $\{D(t)\}$ = A vector of coordinate displacements relative to the global coordinate system of the structure.

    $\{F(t)\}$ = A vector of applied joint loads that are a function of time.

Seismic loading is not directly applied to the containment shell. Rather, an earthquake excites the foundation of the containment which in turn sets the containment shell mass into motion, inducing inertial forces. In this case, damping and stiffness forces result from structure displacements relative to a global coordinate system which translates (or rotates) with the structure base. The inertial forces, however, result from absolute acceleration of mass. For a fixed base MDOF structure subjected to a translational base acceleration, the equations of motion can be written as

$$[M]\{\ddot{X}(t)\} + [C]\{\ddot{X}(t)\} + [K]\{X(t)\} = -[M]\ddot{u}_g(t)\{1\} \qquad (4.2)$$

where $[M]$, $[C]$ and $[K]$ are the same as in Eq. 4.1 and:

    $\{X(t)\}$ = A vector of physical (or geometric) coordinate displacements relative to the ground motion at the structure base.

$\ddot{u}_g(t)$ = Input ground motion at the structure base.

{1}   = A unit vector with ones corresponding to mass DDOF that

are excited by the input ground motion; zeros appear

elsewhere in the unit vector.

It may also be noted that $\{D(t)\} = \{X(t)\} + u_g(t)$ where $\{D(t)\}$ is

referred to as absolute displacement.

It is usual practice for seismic loading to assume that the entire

containment foundation is uniformly excited. Unless the containment is

founded on rock or rock-like material, soil-structure interaction must be

considered as described in Sec. 5.1.

4.4.1. Modal analysis

Modal analysis is a classical method used to solve the equations of

motion. This method is based on the premise that structural vibration is

the total or superimposed effect of a number of independent modes of

vitration that are characteristic of the structure. While this is often

approximately the true physical situation that exists no matter what

analysis technique is being used, a modal analysis depends on the "inde-

pendence" of the vibration modes.

Strictly, the assumption of mode independence does not generally

exist since material damping and nonlinearities cause coupling between

the modes. Coupling between modes can also be a significant problem in

composite structures wherein the various materials have significantly

different damping characteristics. This occurs in seismic analysis that

includes soil-structure interaction (SSI) because the soil and contain-

ment building have distinctively different damping properties [45]. However, for structures of like material with relatively little damping (i.e., modal damping of less than 20% of critical) the assumption of independent modes is adequate for engineering purposes [91].

Since the final result depends on the superposition of the individual modes, this method is limited to linear analyses. Approximate nonlinear analyses have been done using nonlinear response spectra, but such analyses can only be considered as crude estimates.

During the early stages of the method, damping is neglected and classical normal modes are sought. For Eqs. 4.1 or 4.2, the analyst proceeds to solve the eigenvalue problem

$$([K] - \omega^2[M])\{\phi\} = \{0\} \tag{4.3}$$

From standard procedures [7,11,29] the eigenvalues ω^2 and the eignevectors $\{\phi\}$ can be found. The eigenvalues and corresponding eigenvectors are the natural frequencies (squared) and mode shapes, respectively, of each mode of structure vibration. For a structure in which the number of DDOF is n, there will be n mode shapes and n natural frequencies.

The above is done in the mode shape coordinate basis wherein displacements are referred to as modal coordinates $\{\lambda\}$. To calculate stresses, the analyst is interested in physical or geometric coordinates $\{D\}$ expressed in terms of the usual finite element coordinate basis. The linear transformation matrix $[\Phi]$ is used to relate modal displacements $\{\lambda\}$ to the actual displacements $\{D\}$, i.e.,

$$\{D(t)\} = [\Phi]\{\lambda(t)\} \tag{4.4}$$

The matrix $[\Phi]$ is an $n \times n$ matrix which contains the mode shapes $\{\phi\}$ in its columns. The transformation of Eq. 4.4 is also applicable to velocity $\{\dot{\lambda}(t)\}$ and acceleration $\{\ddot{\lambda}(t)\}$.

Because of the orthoganality relationships:

$$\{\phi_i\}^T[M]\{\phi_j\} = 0 \quad i \neq j$$
$$\{\phi_i\}^T[K]\{\phi_j\} = 0 \quad i \neq j \tag{4.5}$$

the similarity transformations $[\Phi]^T[M][\Phi]$ and $[\Phi]^T[K][\Phi]$ result in diagonal matrices $[M_e]$ and $[K_e]$, respectively. At this point, it will be assumed that the damping matrix $[C]$ is also diagonalized under the same transformation that diagonalizes $[M]$ and $[K]$, i.e., proportional damping is assumed. With consideration of the above, substitution of Eq. 4.4 into Eq. 4.1 yields the n uncoupled equations

$$\{\ddot{\lambda}(t)\} + [2\beta_i\omega_i]\{\dot{\lambda}(t)\} + [\omega_i^2]\{\lambda(t)\} = [M_e]^{-1}\{F_e(t)\} \tag{4.6}$$

where:

β_i = percent of critical modal damping in the ith mode.

$\{F_e(t)\} = [\Phi]^T\{F(t)\}$, i.e., the transformed force vector.

In a similar manner, substitution of Eq. 4.4 into Eq. 4.2 yields the n uncoupled equations

$$\{\ddot{\lambda}(t)\} + [2\beta_i\omega_i]\{\dot{\lambda}(t)\} + [\omega_i^2]\{\lambda(t)\} = -\{\Gamma\}\ddot{u}_g(t) \tag{4.7}$$

where:

$\{\Gamma\} = [M_e]^{-1}[\Phi][M]\{1\}$, i.e., a vector of participation factors.

Equation 4.7 can be rewritten for a structure subjected to simultaneous horizontal H and vertical V components of ground acceleration by replacing the right side of Eq. 4.7 with:

$$-\{\Gamma^H\}\ddot{u}_{gH}(t) - \{\Gamma^V\}\ddot{u}_{gV}(t)$$

For each $\{\Gamma^\ell\}$ the unit vector $\{1\}$ will have ones at DDOF that match an excitation in the ℓ direction and zeros elsewhere.

If the damping matrix [C] is not proportional to [M] and/or [K] then $[2\beta_i\omega_i]$ must be replaced by $[\Phi]^T[C][\Phi]$ and Eqs. 4.6 and 4.7 are no longer completely uncoupled by the techniques discussed here. Then, other techniques such as numerical time integration must be used to solve the equations of motion. An alternative procedure would be to solve the complex eigenproblem which occurs when the damping matrix is of general form [29]. Then, the damped equations of motion can again be uncoupled. However, the computational effort required to do this may make numerical time integration the preferable choice.

With respect to seismic analysis, the discussion has been limited to a fixed base structure where the base is the source of excitation. In the more general case that includes soil-structure interaction (SSI), the base itself is excited and the source of excitation is associated with some other reference point, such as the bedrock. In this case, the transformation matrix [Φ] is no longer solely adequate for the overall SSI problem. It becomes necessary to formulate another transformation matrix [T], of which [Φ] is typically a part [52,99]. Even if proportional damping is assumed for [C], difficulties may be experienced in completely

uncoupling the SSI modified equations of motion. Approximate techniques, that also include the use of weighted modal damping, are discussed in Refs. 83, 99 and 100 to uncouple the equations of motion.

Given a transformation matrix that uncouples the equations of motion and assuming that modal values of β_i are found that reflect the effect of SSI (if appropriate), the individual uncoupled equations of motion in Eqs. 4.6 and 4.7 are of the form:

$$\ddot{\lambda}_i(t) + 2\beta_i \omega_i \dot{\lambda}(t) + \omega_i^2 \lambda(t) = Q_i(t) \tag{4.8}$$

where λ_i is the modal response in the ith mode and:

for Eq. 4.6; $Q_i(t) = \dfrac{\{\phi_i\}^T \{F(t)\}}{\{\phi_i\}^T [M]\{\phi_i\}}$

for Eq. 4.7; $Q_i(t) = \dfrac{\{\phi_i\}^T [M]\{1\}\ddot{u}_g(t)}{\{\phi_i\}^T [M]\{\phi_i\}} = -\Gamma_i \ddot{u}_g(t)$

Equation 4.8 is of the same form as the equation of motion for a single degree of freedom oscillator. The response of each modal coordinate λ_i will therefore be equivalent to the solution of a single DOF system subjected to the effective excitation $Q(t)$. After the modal response λ_i is determined for all n modes, the total dynamic response of the structure in geometric coordinates is found by applying the linear transformation such as in Eq. 4.4.

There are a number of methods available to compute the modal response $\lambda(t)$ of the single DOF equation of motion. Depending on the

complexity of {F(t)} or $\ddot{u}_g(t)$, these methods range from closed form solutions to numerical approximations.

For the case of seismic excitation, a popular and relatively inexpensive method is to use the response spectra defined by an earthquake. The reader is referred to Sec. 3 for information on what a response spectrum is and how it is developed. If soil-structure interaction (SSI) is anticipated, the use of response spectra becomes limited or is not appropriate. This is because response spectra are typically defined at the site surface in the free-field and do not include any SSI effects.

Assuming that response spectra are available and appropriate, the maximum displacement $\lambda_i max$ for each mode can be determined by multiplying the modal participation factor Γ_i for a given mode by the spectral displacement $S_d(\omega_i, \beta_i)$ obtained from the specified response spectra, i.e.,

$$\lambda_i max = S_d(\omega_i, \beta_i)\Gamma_i \tag{4.9}$$

where S_d is a function of the single DOF oscillator natural frequency and damping, graphically portrayed on the response spectra. For a fixed base structure, the maximum displacements relative to the structure base that occur in the ith mode are

$$\{X_i\}max = \{\phi_i\}\lambda_i max \tag{4.10}$$

These displacements {X} may then be used to determine the stresses in the structure due to the ith mode by the familiar expression

$$\{F\} = [K]\{X\} \tag{4.11}$$

When geometric displacements are found using the response spectrum approach, the time phasing between the various modes is not accounted for. Therefore, some judgment must be used in order to assess the overall response of the structural found when the n modes are superimposed. An upper bound can be found by adding the absolute values of all the maximum mode responses. However, because earthquakes are stochastic phenomena, a method referred to as the square-root-of-the-sum-of-the-squares (SRSS) is commonly used to predict the most probable overall response. For example, the design displacmeent of the jth node in $\{X\}$, i.e., X_j, in the ℓth direction, i.e., $X_{j\ell}$, can be approximated by [66]

$$X_{j\ell} = \left(\sum_{i=1}^{n} [(\phi_{j\ell})_i \Gamma_i {}^H S_{di} {}^H]^2 + \sum_{i=1}^{n} [(\phi_{j\ell})_i \Gamma_i {}^V S_{di} {}^V]^2 \right)^{1/2} \tag{4.12}$$

Equation 4.12 is only justified when the simultaneous horizontal H and vertical V seismic exitations can be considered mutually independent. The general form of the SRSS method given in Eq. 4.12 may not be adequate if the frequencies of the modes are not well separated. In that case, modified SRSS rules are available to treat the closely spaced modes. Rules and discussion for this situation may be found in Refs. 92 and 113.

There are other methods available to compute the modal response λ_i by which the complete time history of each mode is obtained. Since the modal analysis results in n uncoupled equations, it is possible to calcu-

late the modal response of each mode using the Duhamel integral. For example, for support motion with $\ddot{u}_g(t)$ rewritten as

$$\ddot{u}_g(t) = \ddot{u}_{g1} f(t) \tag{4.13}$$

where $\ddot{u}_{g1}$ is the peak ground acceleration, the Duhamel integral for a damped system with zero initial conditions can, for the ith mode, be expressed as

$$\lambda_i(t) = -\frac{\Gamma_i \ddot{u}_{g1}}{\omega_i} \int_0^t f(\tau)e^{-\beta_i\omega_i(t-\tau)}\sin\omega(t-\tau)d\tau \tag{4.14}$$

The undamped frequency has been used in Eq. 4.14 in place of the damped value. For earthquake motions, the irregular nature of the acceleration time history implies that Eq. 4.14 must be solved by numerical techniques, e.g., Runge-Kutta.

The modal response λ_i of each uncoupled equation of motion can also be found by the techniques subsequently mentioned in Secs. 4.4.2 and 4.4.3. There, it will also be seen that other techniques can be optimized by taking advantage of the fact that dynamic response is essentially the cumulative effect of the structure modes of vibration excited.

4.4.2. Time integration

Time integration is a method of stepping through the equations of motion in the time domain. Essentially the dynamic response is the result of a series of static equilibrium problems solved at discrete time intervals. At a given time step, the quasi-static analysis will include acceleration dependent inertial forces, velocity dependent damping forces

and displacement dependent element stiffness forces. The input motion (e.g., ground motion) or applied forces are a prescribed function of time. Assuming that the discrete model of the structure is adequate, the accuracy of this method basically depends on the characteristics of the numerical integration technique and the size of the time step used in conjunction with it.

At time zero, initial conditions of the structure are presumably known and some assumption is made as to how the time derivatives will vary over each time step. With this information, equilibrium conditions are considered either at the beginning (explicit integration) or near the end (implicit integration) of the time step. The time dependent results are then used in the next time step. Generally, an assumption is made as to how the acceleration will vary over the time step and then velocity and displacement are expressed with respect to their higher derivatives. There are several methods such as the central difference method, the Houbolt method, the Wilson-Θ method, and the Newmark-B method that have been successfully applied [7].

Either the coupled equations of motion (Eqs. 4.1 and 4.2) or the uncoupled equations (Eq. 4.8) may be solved. When the coupled equations are integrated, the technique is referred to as "direct", step-by-step numerical integration because no transformation of the equations into a different form is done before numerical integration is carried out. If this is done by implicit integration (e.g., Houbolt, Wilson-Θ or Newmark-B methods) then the assembled matrices of the structure must be used and the equilibrium condition of all the coupled equations of motion is

satisfied simultaneously for each time step. If explicit integration (e.g., central difference method) is used, it is possible to carry out the solution on the element level [7]. That is, it is not necessary to initially assemble the structure mass and stiffness matrix to solve the dynamic problem, resulting in computational savings. Subsequently, of course, the contributions of each element must be assembled to yield the dynamic response of the overall structure at each time step. Both implicit and explicit methods have advantages and disadvantages so that the method used will depend on the problem to be solved [7,29].

When the uncoupled equations of motion are integrated, the technique is referred to as just step-by-step integration. The procedure is the same as is done in direct integration except that it is no longer necessary to solve simultaneous equations. The time history of each uncoupled equation (i.e., mode) is computed and the total response is found by applying the appropriate coordinate transformation. The basic difference between mode superposition and a direct integration analysis, as described here, is that the principle of mode superposition requires a change of basis from the finite element (or geometric) coordinant basis to the basis of the eigenvectors (modal coordinates) before the time integration is performed. In either case, the same space is spanned and the same solution is obtained.

As a consequence of the above, it is possible to perform coordinate transformations that only succeed in partially uncoupling the equations of motion before time integration is applied. This will be the case, for example, when nonproportional damping of a structure occurs. Even though

the eigenproblem (Eq. 4.3) must be solved to perform the uncoupling, this approach may be computationally more efficient. This will be the case if a good approximate solution to the actual dynamic response can be found by considering only a moderate number of the vibration modes. Numerical integration need then be applied to this reduced set of equations.

The sufficiency of this reduced set of equations can be understood by recalling that dynamic response is related to the natural vibration characteristics of a given structure and the frequency content of the loading. The frequency content of the loading can be identified by a Fourier analysis and structural vibration characteristics are exhibited in the natural periods T_i of the structure vibration modes. In general, maximum dynamic responses are sensitive to the occurrence of congruous reinforcement between the structure mode frequencies and the frequency content of the loading (i.e., similar to resonance). Therefore, quantification of these two frequency characteristics is desirable in order to aid in specifying the optimum size of the time step Δt and to identify the significant modes of vibration expected.

The size of the time step used in the time integration must be small enough to give accurate results and maintain stability as the integration proceeds through time. For accuracy, the time step Δt should be small enough to accurately calculate the response of all modes which significantly contribute to the total structural response. When time integration is applied to uncoupled modal equations of motion, an optimum time step can be conveniently selected for each equation based on its corresponding period T_i.

Accuracy in direct integration is more difficult to control because very high frequencies (i.e., very small periods), which may be of little significance, are automatically included in the analysis. For example, a selection of $\Delta t = T_S/10$ where T_S is the smallest period of the modes considered significant, means that some of the higher modes are not integrated accurately. This introduces the question of stability in the integration. If the integration technique is to be stable, then modes that experience large $\Delta t/T$ values must not interfere with the accurate integration of the significant lower modes. Also, errors due to successive round-off errors in each time step must not grow as the integration proceeds through time. Of course, stability can be enforced by selecting very small Δt that will result in accurate integration of the high frequency responses. However, this can be expensive and undesirable when high frequencies are insignificant.

Some integration techniques (e.g., Houbolt, Wilson-Θ and Newmark-B) are unconditionally stable, meaning that the solution does not diverge for any time step Δt. Evidently, the time step Δt must still be small enough to obtain accuracy in the solution. A method (e.g., central difference method) is conditionally stable if $\Delta t/T$ must be smaller than a certain value Δt_{cr} in order to avoid interference from the high modes and round-off errors. Generally, choosing Δt to satisfy Δt_{cr} will result in a Δt that is small enough to obtain an accurate integration of practically all n equations [7].

4.4.3. Frequency domain solutions

Frequency domain analysis refers to solving Fourier transform equations of motion rather than the original ordinary differential equations. Frequency domain solutions are particularly attractive over solutions in the time domain when SSI analysis must be done. This is because this method is more amenable to the inclusion of soil and structure damping forces and the frequency dependence of some structure properties. In fact, the method subsequently described requires that some level of damping be considered. As a result, the nonproportional damping of a SSI analysis can be directly accounted for. Time domain methods can be formulated or modified to account for nonproportional damping but do not have the freedom found in a frequency domain method. Also, the frequency domain method can directly consider the frequency dependence of the foundation stiffness functions sometimes used to describe the soil in a SSI analysis (Sec. 5.1). This approach is also computationally competitive with the traditional time domain analyses.

The dynamic response problem is solved by transforming the system of ordinary differential equations (Eqs. 4.1 and 4.2) to a system of algebraic equations for each frequency using the Fourier Transform method. This involves expressing the applied loading $\{p(t)\}$ in terms of its harmonic components by the direct Fourier Transform of $\{p(t)\}$ to the frequency domain, i.e., [29]

$$\{c(\omega)\} = \int_{t=-\infty}^{\infty} \{p(t)\}e^{-i\omega t}dt \qquad (4.15)$$

where the function $c(\omega)$ is the loading expressed as the summation of its harmonic components (i.e., frequency content). Then the response $\{r(\omega)\}$ of the structure to a harmonic component ω_i of the loading is found by multiplying $\{c(\omega)\}$ by the transfer function $H(\omega)$

$$\{r(\omega_i)\} = H(\omega_i)\{c(\omega_i)\} \tag{4.16}$$

where $H(\omega_i) = (-\omega_i^2[M] + i\omega_i[C] + [K])^{-1}$. The desired solution in the time domain is found by obtaining the inverse transform of the response in the frequency domain

$$\{x(t)\} = \frac{1}{2\pi} \int_{\omega=-\infty}^{\infty} \{r(\omega)\}e^{i\omega t}d\omega \tag{4.17}$$

where the integration sums the response components over the entire frequency range to give the total response of the structure.

The derivations above consider loading and structural response as continuous functions, e.g., the node displacements found in Eq. 4.17 are obtained by summing the response components over the entire frequency range by means of the integration. In practice, Eq. 4.15 and 4.17 will be accomplished by a numerical analysis procedure. Discrete Fourier transforms are most economically accomplished by use of the Fast Fourier Transform (FFT) algorithm [29]. The number of frequencies that must be considered in the numerical process depends on the frequency content of the input motion. It may be desirable, and often necessary, to truncate high frequencies and interpolate between frequency components in order to keep the computation to a practical size. To this end, the concepts of modal analysis are useful in identifying appropriate frequency ranges to

scan in the analysis. The appropriate frequencies ranges are where significant frequency content of the loading (Eq. 4.15) matches modal frequencies of the containment (Eq. 4.3).

(a) Framework member

(b) Plane stress

(c) Solid elements

(d) Axisymmetric solid

(e) Flat plate bending

(f) Axisymmetric thin shell

(g) Curved thin shells
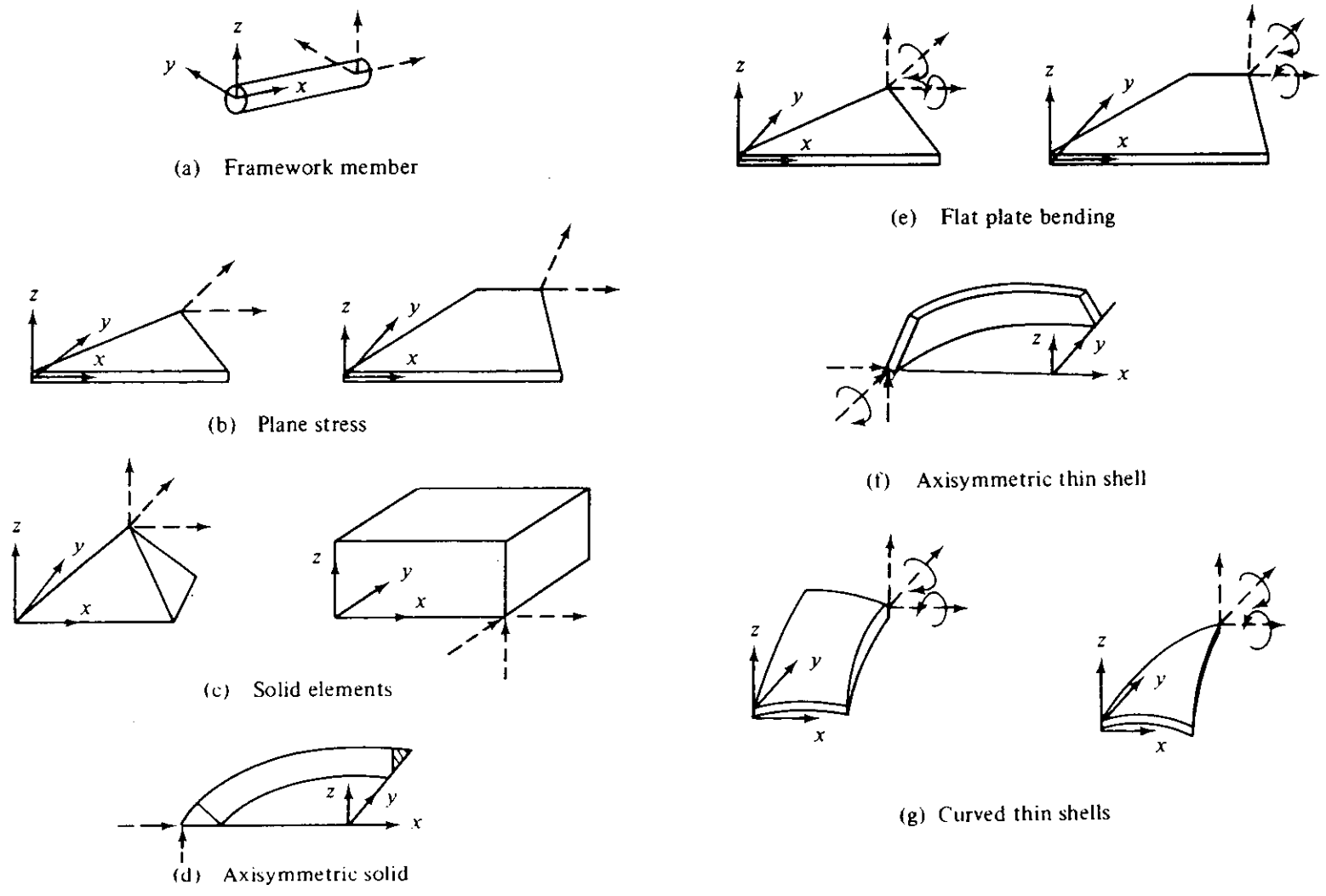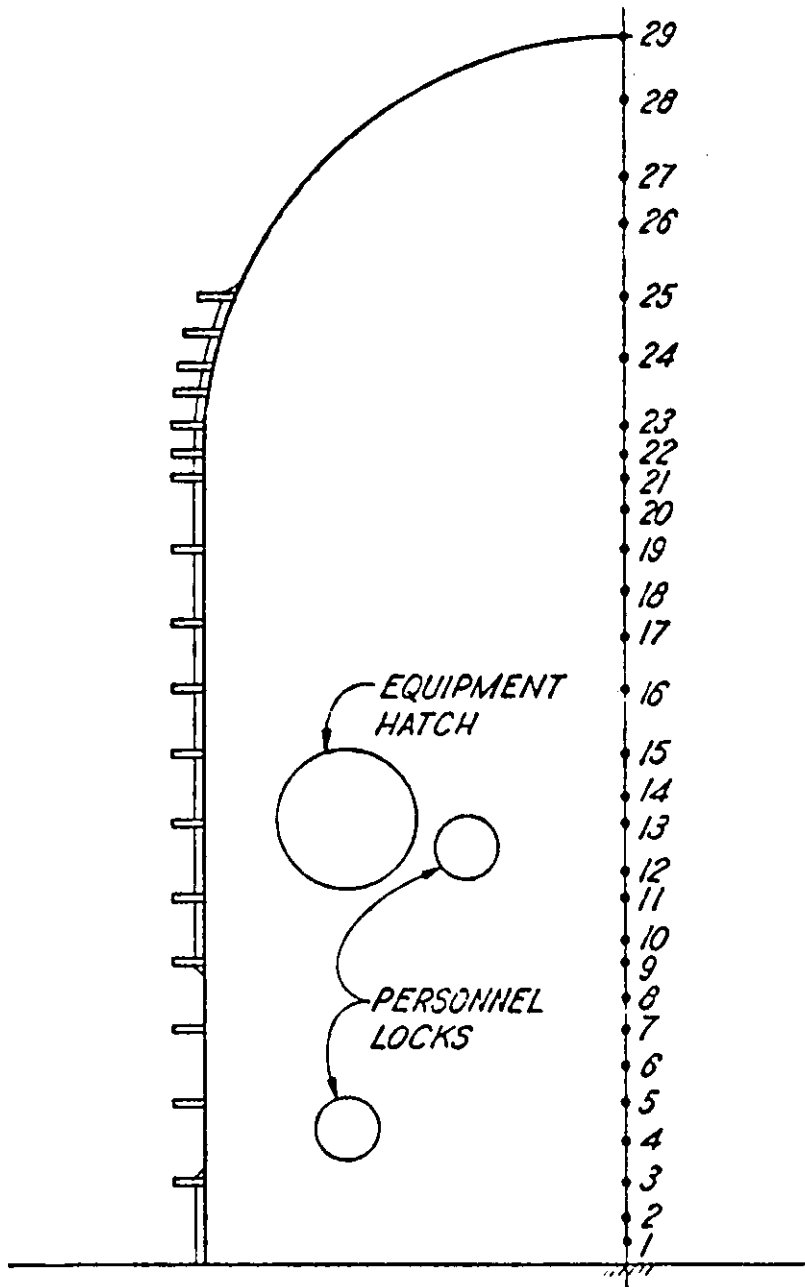
Fig. 4.1. Types of finite elements [37]

Fig. 4.2. Beam element model of steel containment for
dynamic analysis (Final Safety Analysis Re-
port submitted to NRC by Tennessee Valley
Authority, Knoxville, Tenn.)
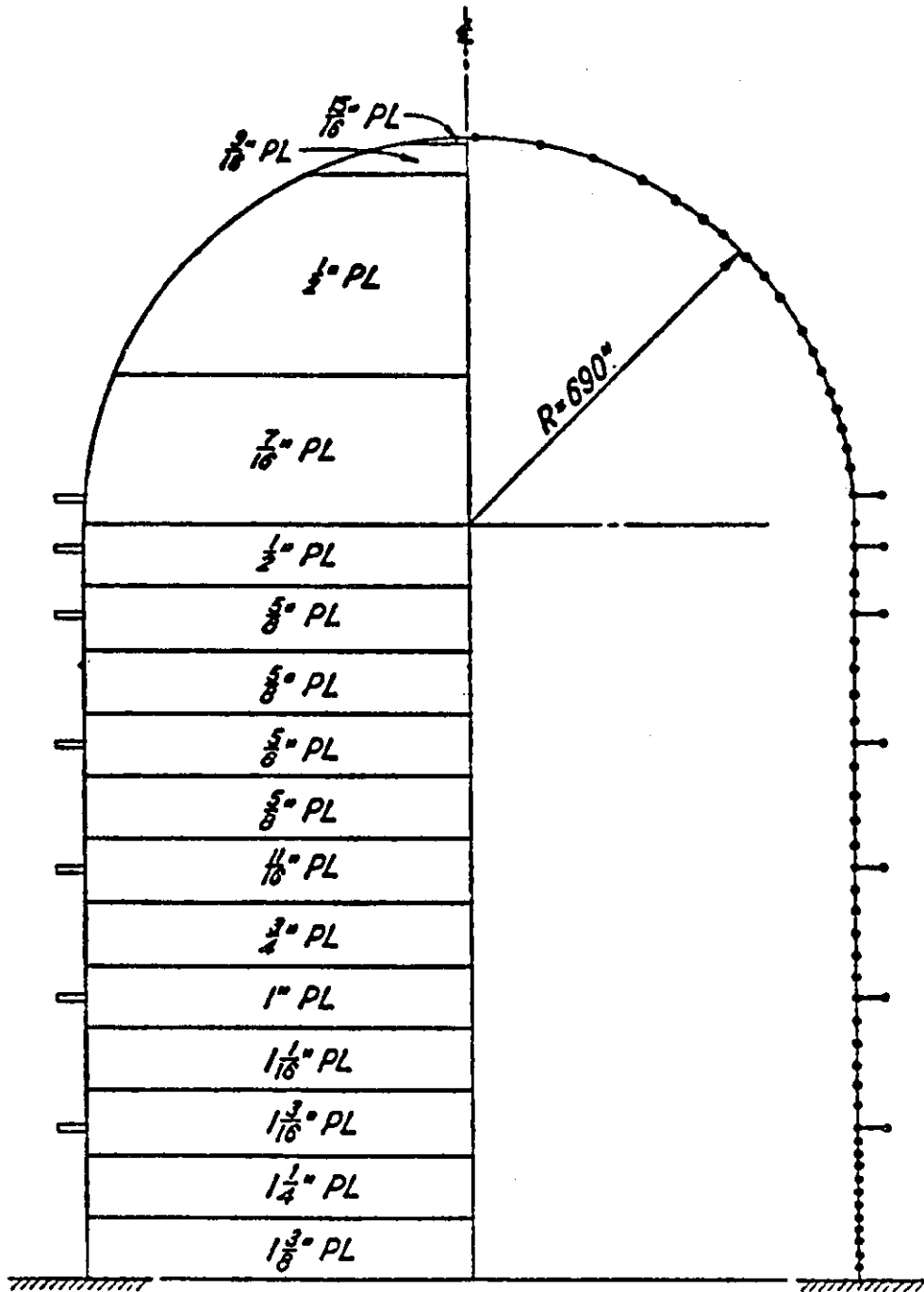
Fig. 4.3. One-dimensional axisymmetric ring element model
of steel containment (Final Safety Analysis Re-
port submitted to NRC by Tennessee Valley Author-
ity, Knoxville, Tenn.)

5. ANALYSIS CONSIDERATIONS FOR SPECIFIC CONTAINMENT LOADS

This section considers some specific load case analyses that are used to form load combinations (Sec. 6.1). The individual loads of this section are, in general, those on which the design of the steel containment is based. Specific modeling and analysis considerations are provided for each type of load as a supplement to Sec. 4.

5.1. Seismic

The seismic problem is to determine the time-varying containment shell stresses generated to equilibrate the inertial forces caused by the accelerations of the containment shell mass. The containment shell mass is set into motion by the seismically excited foundation on which it rests. The accelerations found at the foundation can exhibit the effects of soil deformability (i.e., soil-structure interaction) and of the nearby structures that modify the seismic input to the containment foundation (i.e., structure-structure interaction). An overall or general analysis is performed that can, if necessary, include the above interaction effects. Using the insights and results gained from the overall analysis, the detailed response of individual components and attachments can be found.

5.1.1. General considerations

As discussed in Sec. 4.2, the overall analysis of the containment is typically done using either a beam model or one-dimensional axisymmetric shell model, depending on the purpose of the analysis. And, as noted in

Sec. 4.4, if the containment is supported on rock or rock-like soil, the seismic motions are defined (Sec. 3.3.1) and input at the base of the structure model. On the other hand, if the supporting soil is considered compliant then the seismic motions are defined and input at the base of a model that includes soil stiffness and damping. The soil is generally considered compliant, i.e., significantly deformable, if the shear wave velocity of the soil is less than about 3500 feet per second [113]. The dynamic response of either case above will be found by applying one of the solution methods of Sec. 4.4 to Eq. 4.2.

When the supporting soil is compliant, it will be found that during an earthquake, the motions measured at a point away from the structure are different from the motions measured on the foundation due to the reciprocal influence of the containment building with the soil [45]. The effect of this interaction between the soil and containment is referred to as soil-structure interaction (SSI). SSI is found to be important when the containment is supported on or significantly embedded in compliant soil. Embedment effects should be considered during seismic excitations if the depth-to-diameter ratio is greater than about 0.5 [48]. Embedment effects may occur even if the containment is founded on rock but is surrounded by compliant soil. It is Nuclear Regulatory Commission (NRC) policy that the above SSI effects be included in seismic analysis [113].

The specific effects of SSI are: 1) significant changes in the accelerations applied to the base of the containment, and 2) significant changes in the natural frequencies of the structure. These changes are

important not only from the standpoint of containment shell design but also for the design of equipment attached to the containment shell. The seismic analysis methods outlined later in this section will be for the general case that may include SSI. When the containment is supported by competent rock with negligible embedment, the base can be assumed fixed and response spectra of USNRC Regulatory Guide 1.60 [106] can be directly used to perform a seismic analysis using the modal analysis technique of Sec. 4.4.1. This, however, is a special case which the general methods (i.e., Secs. 5.1.2.1 and 5.1.2.2) simplify to when SSI is negligible.

As discussed later, seismic analyses that include SSI are typically not very amenable to the modal analysis technique, nor can response spectra in the usual sense as defined in Sec. 3.3.1 be directly used as solutions. Rather, time integration and frequency domain analysis techniques are usually used to obtain solutions and design response spectra are used as a basis to define alternate input forms (e.g., acceleration-time histories) to be used as input in the above two techniques. The fact that soil will be included in the model used for SSI analysis means that decisions must be made regarding how the soil should be idealized and included in the containment model described in Sec. 4.2. Much of the subsequent discussion will reflect these decisions and their inclusion in dynamic analysis techniques of Sec. 4.4.

A general seismic analysis that can include SSI should [52,84]:

1) Consider the transmission mechanism and spatial variation of the seismic waves that produce the ground motions.

2) Account for the variation of soil characteristics with depth.

3) Consider the nonlinear behavior and damping characteristics of a soil.

4) Account for the three-dimensional nature of the problem.

5) Consider the effects of adjacent structures on each other (i.e., structure-structure interaction).

The potentially irregular nature of the soil deposits underlying a nuclear plant site and the complex pattern of the seismic wave system are shown schematically in Fig. 5.1(a). Ground motions at any depth of the site which are not altered by the presence of the site structures are referred to as free-field motions. Usually, the analyst is given design or "control" ground motions which are defined as free-field motions located at the surface of the structure site (Fig. 5.2). Essential characteristics of the control motion (e.g., peak ground acceleration and frequency content) are usually described by response spectra. These response specra provide a standard to which the adequacy of acceleration-time histories or other input forms can be compared.

To conduct a seismic analysis it is necesary to describe the spatial variations and transmission mechanism of the seismic waves in the underlying soil. Currently, the transmission mechanism (i.e., composition of seismic wave system) is assumed to consist of plane shear (SH) and dilatation (P) waves propagating vertically [52,111,118]. The SH-waves and P-waves represent the horizontal and vertical ground motions, respectively. Usually, each type of ground motion input is considered separately then the results are added together as a final analysis step. The

spatial variation of SH- and P-waves is assumed to be adequately described by one-dimensional wave propagation theory [52,60,84,118].

With respect to spatial variation of the ground motions, one dimensional wave propagation theory indicates that ground motion accelerations vary with depth and composition of the soil medium. Generally, the accelerations decrease with depth beneath the surface [111]. The NRC limits the amount of acceleration attenuation that can be considered in actual design [112]. It will also be found that some frequencies may be suppressed at various levels due to the composition of the soil medium [30]. If response spectra were generated from the ground motions at various points of interest, then the idealized problem may be pictured as Fig. 5.2. These response spectra of Fig. 5.2 illustrate the variability of earthquake aceleration and frequency content with soil depth, and also that associated with SSI.

When evaluating ground motions at various locations or depths (a process referred to as "deconvolution") it should be recognized that some levels of acceleration may not feasibly exist for a given soil type. The same applies to frequency content. For example, specifying high frequency content in the control motion in accordance with the often-used response spectra of Ref. 106 may not be reasonable at a soft soil site. In that case, analyses based on site dependent response spectra are more appropriate (Sec. 3.3.1).

The potentially irregular orientation of the underlying soil deposits is generally approximated by assuming uniform layering of the various soil strata types identified at the side. The nonlinear strain dependent

properties of the soil are approximated by equivalent linear values compatible with the expected strains developed in the soil profile during seismic excitation [52,111]. Technically, the heterogenous and nonlinear properties of the soil could be modeled by finite elements with iterative updating of nonlinear properties. However, the uncertainties of the soil sampling and testing results and the computational cost to include such information in the analysis have discouraged such refinements.

By using equivalent linear soil properties (e.g., soil shear moduli and damping) it is possible and common procedure to do linear seismic analyses. Since the priniple of superposition is thus assumed valid it is possible to perform the analysis in phases or parts and superimpose the results. From the preceding discussion the heterogeneous, nonlinear problem of Fig. 5.1(a) is in practice approximated by a linear analysis of the schematic idealization shown in Fig. 5.1(b).

Three-dimensional behavior arises in seismic analysis from basically two sources: 1) out-of-plane structural response to planar excitation, i.e., translational and torsional coupling, and 2) three-dimensional radiation of energy from the excited foundation in the form of spherical waves. The first source most visibly arises from asymmetry of the containment and can potentially be included in a model of the containment. However, it is convenient and common to consider the containment to be rotationally symmetric. Usually, this results in little error [116]. However, if the containment is on a common foundation with auxiliary plant buildings and symmetry about two axes is not present, then torsional response should be included in the model.

The second source of three-dimensional behavior occurs in the supporting soil, of which the soil model should be able to account for three-dimensional transmission of energy. The direct (i.e., unmodified) use of plane-strain finite element soil models will not be satisfactory because the model transfers energy from the foundation as two-dimensional cylindrical waves instead of spherical waves. However, such models can be modified (as is explained in Sec. 5.1.2.1) to approximately include three-dimensional propagation of energy. Soil models built from two-dimensional axisymmetric finite elements can directly model the radiation of energy [24]. In addition, when applicable, soil models based on three-dimensional analytical solutions of the soil represented as an elastic half-space (Sec. 5.1.2.2.2) have been shown to yield solutions comparable with axisymmetric soil models [52,118]. It should be noted that all of the above models are symmetric and do not include a torsional mode of response to planar excitation.

Structure-structure interaction presents a problem that still has not been satisfactorily resolved. This three-dimensional phenomenon cannot adequately be represented by any of the models of the foregoing paragraph [89]. Three-dimensional finite elements could conceivably be used to build a three-dimensional model but this is currently economically impractical. Approximate methods have been introduced but their validity still needs verification [89].

5.1.2. Solution procedures

There are basically two methods to perform a seismic analysis that can include SSI effects. These methods, namely, the direct method and

multistep method, both encompass various types of model discretization and solution algorithms. The terminology "direct" and "multistep" is adopted from the literature used as references for this section, particularly the extensive information available in Refs. 52 and 111. The direct method, discussed in Sec. 5.1.2.1, represents the containment building and surrounding soil as one model to be analyzed together at the same time. The multistep method, discussed in Sec. 5.1.2.2, models the containment building and surrounding soil independently and the interaction is determined by principles of force equilibrium and displacement compatibility. The multistep methods include the conventional substructure method as presented in Refs. 7, 32 and 37 and a special case of the substructure method that is often referred to as the lumped spring method. It is therefore considered convenient to distinguish the two under the mutual designation of multistep methods.

5.1.2.1. Direct method   Direct methods consider the containment building and surrounding soil as one composite structure to be analyzed by numerical techniques. The composite structure is subjected to a seismic excitation and its overall dynamic response solved as a single analysis step. Current practice is to input the seismic motions at the base of the composite model. This seismic input is found by one-dimensional deconvolution of the free, surface control motion to a corresponding motion at the base (Fig. 5.2). The one-dimensional deconvolution iteratively computes the base acceleration by equivalent linear analysis [111]. The deconvolution procedure utilizes and generates the strain compatible shear moduli and damping values in the different soil layers

which are in turn used in the direct method. In this way, nonlinear soil behavior is approximated in the linear dynamic analyses.

The direct analysis itself could be accomplished by a number of different numerical solution techniques such as finite element or finite difference. Usually, though, the finite element method is employed. The composite structure is therefore discretized using either plane-strain or axisymmetric finite elements (Fig. 5.3). Since direct methods involve discretization of the composite structure such factors as: (1) the extent of embedment, (2) the depth of soil over rock, and (3) the layering of the soil strata, are relatively easy to include in the model. However, the three-dimensional aspects of the problem are not so easy to include. Asymmetry of the underlying soil and bedrock can only be approximated by using two orthogonal slices of plane-strain elements through the site in an attempt to capture the most significant effects of of the site asymmetry. Asymmetry in the distribution of the mass and stiffness in horizontal planes of the containment building cannot be adequately handled with plane-strain or axisymmetric shell finite element models. Multistep methods (Sec. 5.1.2.2) must be used to represent any coupling in the translational and torsional responses of the containment.

Since translational and torsional coupling is to be avoided, plane-strain soil models for the direct method are constrained to making use of symmetry around the center line of the containment building (assuming it exists). The containment building may be modeled with beam elements and lumped masses [118]. The embedded part of the containment may be

represented by finite elements without mass--all mass is associated with the lumped masses as shown in Fig. 5.3(b). Constraints will be needed to correctly couple the beam elements of the containment superstructure to the finite elements representing the embedded part of the containment. Approximate modeling of the containment with plane-strain elements is likely to be unsatisfactory [111], though it has been done in the past [61]. Plane-strain modeling of rectangular frame or shear wall buildings may be adequate.

Plane-strain models attempt to simulate the three-dimensional behavior of the soil by placing viscous dampers at all the side nodes of the soil (Fig. 5.4). Thus, energy radiating normal to the model is dissipated by the dampers [84]. Plane-strain models have been compared with three-dimension models (e.g., axisymmetric finite element and half-space models) and have been shown to give good evaluations of the response at the base of the containment building but not necessarily within the structure [84]. As a result, it may be desirable to use the plane-strain model of the soil in conjunction with a multistep method (Sec. 5.1.2.2) rather than the direct method [24,118].

In the ideal situation where the underlying soil and containment building are both axisymmetric, it may be possible to construct a realistic three-dimensional composite model with axisymmetric finite elements (Fig. 5.5). However, a nuclear plant facility generally has many different types of structures together and so axisymmetric situations are the exception rather than the rule. In any case, the axisymmetric solutions

provide a useful standard to which the validity of other approaches can be compared.

The input for the plane-strain model is typically input at the base of the model [26,52], all base nodes being excited in phase (i.e., identically) for either horizontal or vertical input. The axisymmetric model, however, requires that horizontal input be equivalently re-expressed as the first harmonic of a Fourier series. Vertical input is input in a straightforward manner like the plane-strain model.

Whether using the plane-strain or axisymmetric model, it is necessary to ensure that the lateral and bottom boundaries of the finite element model are sufficiently far removed from the containment building so that the full effects of radiation damping are correctly represented. As a guideline, the distance of the lateral boundaries from the edge of the containment should be about three times the base slab dimension [113]. The adequacy of the lateral boundaries can and should be checked by generating response spectra at the lateral boundary surface and comparing it to the free-field, surface control motion spectra--they should be the same as shown in Fig. 5.2. The distance of the bottom boundaries from the base of the containment should be about twice the largest base slab dimension (i.e., the criteria of a half-space) or to the interface between soil and rock, if that comes first.

The bottom boundary is typically considered rigid while various displacement constraints are used for the lateral boundaries. The simplest method for the lateral boundaries is to constrain the end nodes such that they can move only in the horizontal direction for the case of

horizontal input motion at the rigid base, and only in the vertical

direction for the case of veritcal input motion [52].

An alternative for the lateral boundaries is the use of transmitting

boundaries [84] (Fig. 5.3(a)). Such boundaries represent the lateral

soil extending to infinity and include spring action as well as radiation

and material damping. In principle, this type of boundary can be placed

at the very edge of the containment building if the soil properties do

not signficantly vary horizontally near the containment. Transmitting

boundaries greatly reduce the required soil mesh.,

5.1.2.2. Multistep methods   Mathematically, the analysis

approaches described here are equivalent to the direct method of analy-

sis. Solution differences that may arise can be due to differences in

the degree of idealization or because of inconsistencies in their use.

The multistep methods are required when significant coupling of the

translational and torsional response in a structure is expected. Multi-

step methods are based on the principle of superposition and are, there-

fore, restricted practically to linear analyses. As the title implies,

the SSI problem is done in several steps and assimilated together to get

the final result. In contrast, the direct method is a load-in and

stress-out approach. The multistep method is sometimes advantageous

because it may be easier to acertain analysis reliability as the solution

progresses and it may be computationally more efficient to solve a series

of small problems rather than one huge problem.

5.1.2.2.1. Basic superposition theorem   The following

breakdown of the SSI problem illustrates a procedure by which the overall

problem is divided into two parts. Assuming a linear analysis, this theorem applies to discretizations discussed for the direct method and for other methods of modeling that will be introduced. This theorem is particularly useful in implementations of the lumped spring method.

Consider first the general undamped equations of motion of a composite structure (i.e., structure-soil system) given by the matrix equation

$$[M]\{\ddot{X}\} + [K]\{X\} = -[M]\{1\}\ddot{u}_b \qquad (5.1)$$

where $[M]$ and $[K]$ are the system mass and stiffness matrices, $\{X\}$ is a vector of relative displacements between points in the soil or containment and the top of the bedrock, $\{1\}$ is the appropriate unit vector, and $\ddot{u}_b$ is the bedrock motion [60]. Kausel et al. [60], pointed out that the solution of Eq. 5.1 is equivalent to the solution of the two matrix equations [52]

$$[M_s]\{\ddot{X}_1\} + [K]\{X_1\} = - [M_s]\{1\}\ddot{u}_b \qquad (5.2)$$

$$[M]\{\ddot{X}_2\} + [K]\{X_2\} = -[M_c](\{\ddot{X}_1\} + \{1\}\ddot{u}_b) \qquad (5.3)$$

where $X = X_1 + X_2$, $[M_s]$ is the mass matrix excluding the mass of the structure and $[M_c]$ is the mass matrix excluding the mass of the soil which when added give the total mass matrix $[M]$ of the composite structure; X_1 is the relative motion between a point in the composite structure and the rock when the containment building has no mass and X_2 is the additional relative displacement resulting from the mass of the containment building. The SSI problem expressed by Eq. 5.1 is therefore the summation of the responses found in the solutions of Eqs. 5.2 and 5.3.

In effect, the presence of the structure modifies the free-field ground motions in an identifiable manner in each equation (i.e., Eqs. 5.2 and 5.3). Initially, it may be noted that the mass and stiffness of the soil and the stiffness of the containment building are considered in both Eqs. 5.2 and 5.3. However, in Eq. 5.2 the mass of the containment and its foundation are excluded. As a result, the containment and foundation motions of Eq. 5.2 reflect only geometrical aspects of motion caused by seismic soil motions. In the literature [52,60,111], this effect is referred to as "kinematic" interaction.

Physically, kinematic motions reflect the disruption of the seismic waves that occurs as these waves encounter the containment foundation. This is because the stiffer foundation cannot conform to the seismically induced soil deformations that would normally occur in the free-field. For an embedded rigid foundation, kinematic effects are rigid body translations and rotations of the foundation and superstructure. If there is no embedment and the foundation is excited by vertical propagating SH- or P-waves, then the motions of the foundation and soil are identical. That is, the foundation motions are the free-field motions (assuming a massless structure).

If the structure is embedded, then the solution of Eq. 5.2 will exhibit the kinematic effects of embedment. The force- and acceleration-time history of each node of the containment found from Eq. 5.2 is stored for use in Eq. 5.3 and to obtain the final solution. That is, the accelerations $\ddot{X}_1$ of Eq. 5.2 are added to the base rock accelerations $\ddot{u}_b$ to form the input motions for Eq. 5.3. The force-time history

of Eq. 5.2 is to be added to that resulting from Eq. 5.3 to obtain the final solution.

In Eq. 5.3 the mass of the containment building and foundation is accounted for. The solution of Eq. 5.3 simply reflects the reciprocal force-displacement relationship between the supporting soil and seismically excited containment structure. This effect is sometimes referred to as "inertial" interaction in this theorem. The inertial force at each node in the containment is the product of the node mass and acceleration where, as alluded above, the acceleration is the sum of the Eq. 5.2 acceleration $\ddot{X}_1$ and the base rock acceleration $\ddot{u}_b$.

The final solution is found by adding the force- and acceleration-time histories of Eq. 5.2 and 5.3. It may be noted that if the first step (i.e., Eq. 5.2) is done including the mass of the containment structure, then a direct SSI method has been done and the need for the second step (i.e., Eq. 5.3) is eliminated. In addition, the direct method and general substructuring method automatically account for the artificially separated kinematic and inertial interaction effects as the SSI solution progresses. However, the breakdown described here is very useful in understanding and correctly performing the lumped spring method described subsequently.

5.1.2.2.2. Lumped spring modeling   This approach is a specialization of the two step approach described above and it is based on the assumption of a rigid foundation. Normally, containment building foundations are stiff enough to be idealized as rigid [24,52]. However, this may not be the case if the containment is supported by a mat

foundation that also supports adjacent plant structures. In the lumped spring method, it is useful to recognize that the supporting soil can be modeled with finite elements, or equivalently, with a (far-coupled) matrix of stiffness functions modeling the supporting soil and defined at the soil-structure interface [60]. These stiffness functions can be thought of as resulting from a kinematic condensation of all the degrees of freedom in the soil.

With the assumption that the foundation is rigid, it is possible to replace the soil-structure interface node stiffness functions with over-all translational, rotational and torsional stiffness fucntions. Then, on an analysis model, the stiffness functions give parameter values for the soil springs and dashpots that model the subgrade soil as shown in Fig. 5.6. The stiffness functions are frequency dependent and so a solution in the frequency domain (Sec. 4.4.3) is implied.

The assumption of a rigid foundation also means that the kinematic interaction of Eq. 5.2 is defined completely by the rigid body rotations and translations of the massless containment building. Since the rigid containment building is massless in Eq. 5.2, it is equivalent to replace the whole containment building with only its rigid foundation base, as shown in step 1 of Fig. 5.7, and then solve Eq. 5.2.

The above assumptions are very useful because they make the problem compatible with the assumptions used to derive closed form solutions for the soil stiffness functions. This is explained in more detail later. The assumption of a rigid foundation also makes it possible to re-express

the superposition theorem of Sec. 5.1.2.2.1 as shown in Fig. 5.7 and written here as [60]:

1) Determine the motion of the massless rigid foundation when sub-
    jected to the base rock acceleration $\ddot{u}_b(t)$. This is the
    solution of Eq. 5.2 and will generally result in translations
    and rotations for embedded structures.

2) Determine the frequency-dependent stiffness and damping of the
    supporting soil.

3) Determine the dynamic response of the containment building sup-
    ported by frequency-dependent springs when subjected at the base
    of these springs to the motions obtained in step 1.

The only approximation in this procedure is that the foundation is rigid.
If this is true and all other parameters are consistently defined then
the solution found here is theoretically the same as that found by the
direct method.

                    Step 1 - Spring base motions:

For the case of no embedment and under the assumption of vertically
propagating seismic waves, the kinematic "interaction" effects are zero
[60]. In this case, the motion of the massless containment is identical
to the ground motion at the surface in the free-field [52]. Thus, the
spring base motion is simply the control point motion.

As the foundation becomes embedded in the soil, kinematic interac-
tion becomes increasingly more pronounced. Under the assumption of a
rigid foundation, the resulting rigid body translations and rotations are
a function of foundation geometry, subgrade soil properties and seismic

excitation [52]. Technically, embedded structures require the use of finite elements or finite difference methods to establish kinematic interaction. However, there are good approximations available based on one-dimensional wave propagation theory. The reader is referred to Refs. 52 and 60 for more details.

Step 2 - Evaluation of soil stiffness and damping:

The rigid foundation makes it possible to decribe foundation stiffness in terms of 6 DDOF, or less if symmetry is present. In most cases, the foundation will have one or more axes of symmetry so that less than 6 DDOF is sufficient. For the case of a circular foundation, the force-displacement relationship for horizontal and rocking motions can be written as [60]

$$\begin{Bmatrix} F \\ M \end{Bmatrix} = \begin{bmatrix} K_{xx} & K_{x\theta} \\ K_{\theta x} & K_{\theta\theta} \end{bmatrix} \begin{Bmatrix} u \\ \theta \end{Bmatrix} \tag{5.4}$$

where: F = the horizontal force at the base of the containment;

M = the rocking moment at the base of the containment;

u and θ = the horizontal and rotational displacements, respectively.

In the stiffness matrix, the elements K_{xx}, $K_{\theta\theta}$ and $K_{\theta x}$ are soil stiffness "functions" which depend on the frequency of excitation Ω of the forces or moments. These stiffness functions are complex functions since the forces and resulting displacements are out of phase with each other. Stiffness functions are directly affected by:

1) foundation rigidity

2) foundation shape

3) embedment

4) nature of surrounding subgrade material.

In this method, the foundation is assumed rigid; flexible foundations require the direct method or general substructure technique. The last three effects must, however, be incorporated into the stiffness functions. Stiffness functions can be evaluated by a numerical technique (e.g., finite elements) or by available closed form solutions. The closed form solutions are usually referred to as continuum solutions or "impedance" functions. The general form of a stiffness or impedance function is [52,60]:

$$K^{\circ}(k+ia_{o}c)(1+2i\beta)$$

where: K° = static stiffness of soil

β = material damping (fraction of critical damping)

$i = \sqrt{-1}$

a_{o} = dimensionless quantity reflecting excitation frequency, foundation shape and subgrade properties

k and c = frequency dependent coefficients normalized with respect to K°.

In this expression, $ia_{o}c$ is interpreted as relating to the radiation damping and $2i\beta$ to the material damping of the soil.

A finite element evaluation of the stiffness functions can be found for surface or embedded foundations that are circular (axisymmetric modeling) or narrow rectangular footings (plane-strain modeling). Practical computational constraints rule out modeling arbitrary shapes.

Generally, therefore, the actual shape must be modeled in some "equiva-
lent" circular or narrow rectangular form. The finite element model used
to evaluate stiffness functions represents the soil in the same manner as
the direct method and includes only the containment foundation, modeled
as rigid and massless. Finite element solutions can consider subgrade
characteristics, such as layering, at the same time that embedment
effects are being accounted for.

In brief, stiffness functions are determined from a finite element
model by dynamically exciting it with a steady state harmonic unit force
or unit displacement having a frequency Ω. The results (displacements or
forces) will also have the same frequency Ω but, in general, will be out
of phase with the input. A number of different values of Ω will need to
be evaluated. These data may be used to numerically represent the com-
plex stiffness functions of the stiffness matrix.

A closed form evaluation of the stiffness functions can be found
when conditions at the site are congruent with the assumptions used in
the established closed form solutions. These solutions will hereafter be
referred to as "impedance" functions. Impedance functions express the
three-dimensional stiffness and damping (i.e., radiation damping)
experienced when a rigid, massless disk or plate resting on the surface
of a half-space representation of the soil is subjected to harmonic
excitation (Fig. 5.8). These functions are complex valued and dependent
on the frequency of excitation.

Representing the soil as a half-space means that the soil region is
assumed to be a semi-infinite continuum. As a general rule, half-space

solutions do not apply if a rigid boundary, such as a soil-rock inter-face, is encountered within a distance from the foundation base of twice the diameter of the foundation base. In this case, finite element dis-cretizations of the soil are generally employed.

The half-space assumes the soil to be an elastic [81] or viscoelas-tic [117] material. There are impedance functions available for homogen-eous half-spaces [52] and also for layered half-spaces [59,69,70]. Impedance functions are unique for each type of soil profile described above. In addition, impedance functions for layered half-spaces are very frequency dependent and should not be approximated by frequency indepen-dent expressions as is often done for homogeneous half-spaces [24,100].

Impedance functions are available for circular, rectangular, and narrow rectangular shapes. Embedment effects can also be approximated by theoretical and experimental modifications to the half-space solutions [24,52,60].

In summary, for ideal situations of a rigid foundation with little or no embedment on a homogeneous half-space, impedance functions may be directly used as stiffness functions. As embedment and layering become significant, approximate correction factors and/or alternate half-space theories must be used. Alternatively, the elements of the stiffness matrix can be evaluated using numerical methods. In some instances this may be the only applicable method.

Step 3 - Determination of dynamic response:

At this point, the parameters of the model shown in Fig. 5.6 have been quantified and its dynamic response remains to be found. The spring

bases of the model (e.g., Fig. 5.6) are subjected to the motions found in Step 1. The subgrade springs and radiation damping are found in Step 2. Soil material damping of the order of 10 percent critical or less should also be added to the radiation damping [122]. The dynamic response is found by Eq. 4.2 of Sec. 4.4, shown again here as

$$[M]\{\ddot{X}(t)\} + [C]\{\dot{X}(t)\} + [K]\{X(t)\} = -[M]\ddot{u}_g(t)\{1\} \qquad (4.2)$$

where: $\{X\}^T = [P_s, P_b]$ a set of physical coordinates relative to the input motion at the spring bases [52].

$\{P_s\}$ = Set of physical coordinates of the superstructure (i.e., containment) relative to the input motion.

$\{P_b\}$ = Set of rigid body physical coordinates of the total structure (i.e., containment and foundation base) relative to the input motion.

$\ddot{u}_g(t)$ = Input ground motions from Step 1.

$\{1\}$ = Appropriate unit vector with ones corresponding to excited mass degrees of freedom.

$[M]$ = Partitioned mass matrix of containment and foundation.

$[C]$ = Partitioned damping matrix of containment and soil damping.

$[K]$ = Partitioned stiffness matrix of containment and soil stiffness.

The reader is specifically referred to Appendix B of Ref. 52 for an excellent discussion and general three-dimensional formulation of the above.

Immediate complications occur when one attempts to solve Eq. 4.2, including SSI effects, by standard methods such as modal or time integration analysis. The first complication is that the foundation stiffness functions are frequency dependent. Therefore, the equations of motion should be solved in the frequency domain by the Fast Fourier Transformation method [71] or by the Foss method [36]. However, it has been shown that if a homogeneous half-space exists then constant parameter (frequency independent) foundation impedances are sufficient to simulate the SSI [100]. With this modification, the equations of motion can be solved by direct, step-by-step numerical integration, or by the two methods mentioned above. The constant parameter approximation should not be made if there is significant layering at the site, in which case the stiffness functions are highly frequency dependent [24]. In general, solution in the frequency domain is required if a homogeneous half-space does not approximately exist.

The second complication arises if the analyst attempts to solve the equations of motion by the normal mode method. It is supposed here that frequency independent foundation impedances are used and that damping matrix of the SSI system is assembled. Now, it will be found that the assembled damping matrix [C] for the SSI system is not diagonalized under the same transformation that diagonalizes both the mass and stiffness matrices. However, even though classical normal modes do not exist, it has been found that a normal mode approximation is adequate provided that proper values of modal damping are used [83,99,100]. That is, weighted values of modal damping are calculated and used in the uncoupled

equations of motion. It should be remembered that the frequency independence of the foundation stiffness functions must be a valid assumption before the approximate modal analysis method can be used.

5.1.2.2.3. General substructuring   The general substructuring approach is included separately here because the composite system is analyzed as separate subsystems and therefore the analysis may be thought of as a multistep process. However, it should be realized that all of Sec. 5.1.2.2 could technically be considered as varations of the substructuring approach.

For the SSI problem, the composite system is analyzed in two stages, each dealing with one of the two substructures, namely, the containment building and surrounding soil. The results of the two separate analyses are then synthesized or coupled together to yield the final solution. As a result, the procedure also generally depends on the principle of super-position. Therefore, it is necessary to approximate soil nonlinearities by using strain-compatible equivalent soil properties. Also, debonding of the containment building from the soil interface is not considered (this is also true in half-space theories).

There are various formulations available by which the two subsystems are separately analyzed and then coupled together [26,61,87]. Basically, these solution algorithms differ as to whether the equations of motion are solved in the time or frequency domain [111]. However, in common, they all derive from enforcing displacement compatibility and force equilibrium at the interface of the two subsystems.

Substructuring techniques are particularly useful because they incorporate advantages found in both lumped spring and finite element modeling methods. For this reason, substructuring techniques are also referred to as hybrid approaches. A substructure method described in Ref. 26 allows the analyst to model the soil with finite elements or, when appropriate, to use available continuum solutions for the soil region. Substructuring methods are usually generalized to handle flexible foundations and then can be simplified for rigid foundation idealizations.

As noted earlier, three-dimensional behavior, specifically translational and torsional coupling, cannot be readily done in the direct approach. It can be done with the lumped spring model provided accurate foundation springs and spring base motions can be found. However, the substructure techniques offer an attractive alternative. With substructuring it is possible to synthesize a three-dimensional containment model with a plane-strain finite element model of the soil [61]. Thus, the problems of embedment and layering are accounted for and three-dimensional response in the superstructure is represented.

This points out a potential error that has the appearance of substructuring. Sometimes a relatively simple model of a structure is placed on a foundation that rests on a plane-strain or axisymmetric finite element model of the soil. The motions are then found at the base of the structure and later applied to a more detailed three-dimensional model of the structure. Now, in general, the motion of the foundation in the coupled SSI system should be suppressed at frequencies corresponding

to the mode frequencies of the simple model on a fixed base. However, almost inevitably, the detailed model will have slightly different resonance characteristics than the simple model used in the computation of base motions. Therefore, large amplifications may erroneously be computed in the detailed model [111].

Substructuring can also make use of modal analysis methods. Referred to as the modal synthesis method, this technique is useful because it provides a rational basis for formulating the nonproportional damping matrix based on the modal damping of the individual subsystems (Sec. 4.3.4). The subsystems are composed of single materials (e.g., steel, concrete, and soil) which have fairly well agreed upon values of modal damping. The model synthesis procedure consists of extracting modes from each subsystem and then doing a coupled analysis using the model synthesis technique [87] with the extracted modes and modal damping ratios. The procedure results in a nonproportional damping matrix for the composite structure and the equations of motion can be solved by direct integration or by uncoupling them by the use of complex eigenvectors.

However, extracting the necessary modes for the soil substructure is, computationally, an inefficient process. In order to get enough soil modes to analyze the higher frequencies of the ground motion, Ref. 1 reported the need for 60 modes while Ref. 52 states that it is not unusual to include more than 150 modes. Therefore, when the soil is modeled with finite elements, a solution in the frequency domain may be preferred over the modal analysis method. However, the existence of the modes is often of great benefit. With respect to substructuring

techniques, the representation of the containment building by its predominate modes reduces the number of simultaneous equations and consequently the problem size [26,61].

In summary, substructing retains the full power of the direct method while allowing for potential simplifications that are found in the lumped spring method. Further, the multistep aspect of the substructing technique allows for computational savings over the direct method.

5.2. Pressure

Elastic analysis of steel containments for LOCA and SRV gas pressure will generally involve a dynamic analysis for short-term pressures and a static analysis for long-term pressures. A static analysis of pressure loading is adequate when the rise time t_r of the pressure to its peak is large compared to the predominate vibration mode periods T_n of the containment shell, i.e., $t_r \gg T_n$ [11]. This may be the case in PWR dry containments in which t_r is on the order of 10 seconds (Sec. 3.2.1.2.1). Most other containment types experience an initial pressure transient that causes significant dynamic behavior in the shell. In this case, the short-term pressure response often controls the design of the containment shell, assuming that the safety-related plant features fulfill their function. Without safety systems operating, the consequences of a LOCA can exceed design basis conditions for the steel containment. As a result, gas pressure loads, among others, would rise relatively slowly to intensities beyond the containment elastic design capacity.

Such a condition, referred to as overpressure, requires a nonlinear analysis to quantify stress-strain states in the containment shell.

5.2.1. Short-term pressure

Significant transient dynamic pressure loading of the containment shell occurs when the gas pressures associated with LOCA or SRV actuation occur in relatively small containment volumes as discussed in Secs. 3.2.1.1 and 3.2.1.2.2. These pressures can be nonaxisymmetric, varying in both the circumferential and meridional directions. In any case, the time-dependent problem is three-dimensional and the analytical or numerical methods used must, therefore, account for this. In practice, numerical methods such as finite element are used. If the time-dependent pressures rise symmetrically in the containment, then theoretically only a n=0 circumferential displacement shape is excited. The number of axial waves m depends on the nature of the meridional variation of the symmetric pressure. If the time-dependent pressures also vary circumferentially, then they are referred to as nonaxisymmetric and will also excite n=1,2,3...i circumferential displacements.

The manner in which pressure time-histories are input into a discretized model of the containment will depend on the type of discretization used. Beam element models with the pressure resolved into components and then applied at the nodes have been shown to be inadequate [31]. Three-dimensional models built from two-dimensional plate and shell elements (Fig. 5.9) have been used [28,64]. In models of this type, DDOF are assigned to the nodes considering their anticipated dynamic response. In general, nodes directly subjected to dynamic pressure load are assigned

DDOF in the direction of the load; other DDOF are evenly distributed to the horizontal and vertical diretions. The pressure-time history applied to the nodes will either be based on the contributory area for the node or by the "consistent" force method, analogous to that used for lumping mass (Sec. 4.3.2) [7,29].

Probably the most common approach is to construct a three-dimensional model with one-dimensional axisymmetric finite elements (Fig. 4.3). This model is described in Sec. 4.2 and is generally the most cost-effective model for overall analyses. When this model is used for dynamic loading, the circumferential presure distribution at each time step is decomposed into a sufficient number of Fourier harmonics (Fig. 3.13) and then the solutions for each harmonic are generated and combined. A Fourier representation of the circumferential distribution is applied to each nodal circle. This allows the meridional variation of pressure intensity to be varied also.

The response of the discrete model to the pressure-time history is found using Eq. 4.1 where $F(t)$ is the pressure-time history at the appropriate nodes. The dynamic analysis is generally performed in the time domain by a modal analysis (Sec. 4.4.1). The uncoupled equations of motion (Eq. 4.6) are solved by numerical integration in the time domain, e.g., Eq. 4.14 or Sec. 4.4.2. The resulting acceleration-time histories at the various DDOF can be used to generate response spectra for attached equipment. The displacement-time histories are used to compute a set of design basis equivalent static loads or stress levels to be used in

various load combinations. Equation 4.11 yields these node forces, the maximums of which can be found in the time domain.

5.2.2. Long-term pressure

Elastic analysis of long-term internal pressure is one of the simpler loadings to analyze. The peak pressure postulated for the facility is applied as a static, uniform internal pressure on the containment. If the geometry of the containment is relatively simple and clean, then closed form solutions found in Refs. 6 and 82 could feasibly be used to assess stresses and strains. However, in the usual cause, stiffeners and complex geometries make it more convenient to perform a static analysis run using the containment model that is available for other analyses.

5.2.3. Overpressure

Analysis of long-term overpressure also considers static, uniform internal pressure applied on the containment. However, the emphasis for this analysis is not on the stress-strain state of the containment but rather on the peak pressure value that causes integrity failure of the containment. Such an analysis must include nonlinear behavior and antic-ipate the ultimate mode of failure. References 108 and 109 study this problem and present the analysis in terms of probability of failure con-cepts. Overpressure analysis is done to quantify ultimate containment capacity in the event of a severe LCOA and does not currently represent a design basis analysis.

5.3. Hydrodynamics

When the water in the suppression pool of BWR containments is set in motion, it produces time varying pressures acting on the pool boundaries in excess of the hydrostatic pressure. Hydrodynamic pressures on the containment may be caused by LOCA, SRV actuation or seismic excitation of the pool water. A distinction and complication of the dynamic liquid pressure problem over the dynamic gas pressure problem (Sec. 5.2) is that part of the liquid mass acts as if it is attached to the flexible steel shell, thus increasing the inertial forces [18,62]. In addition, as the containment vibrates, it produces another pressure field in the pool that is proportional to the radial displacements of the containment. The above phenomenon, referred to as fluid-structure interaction (FSI), occurs in flexible structures and has been shown to be significant in steel containments [62].

The hydrodynamic problem requires a three-dimensional discretized model as described in Sec. 5.2.1 for dynamic gas pressure analyses. Usually the model will be built using axisymmetric shell and solid finite elements (Fig. 5.10). In addition, the analyst must make provisions for the model and analysis to adequately reflect the effective added mass of the pool water and the total dynamic pressure loading (i.e., incident plus FSI pressure). If the bottom of the pool is also the foundation of the containment, then it may be necessary to include the effects of soil-structure interaction. For example, a LOCA or SRV actuation in Mark II or III containments may cause structural vibrations that display the

effects of soil-structure interaction [54,101]. The significance of these effects may be negligible depending on the foundation and soil characteristics [54]. A model with two-dimensional axisymmetric finite element representation of the soil is shown in Fig. 5.10. Lumped spring modeling (e.g., a Winkler foundation) have also been used [28,57,101]. It should be noted that the soil-structure interaction discussed here is due to internal loading. In principle, it is the same as seismically induced soil-structure interaction, however, the methods of modeling are not necessarily the same [28].

The dynamic analysis methods of Sec. 4.4 are applicable to the solution of this problem. However, there are two techniques by which the peculiarities of hydrodynamic pressure loading on the flexible containment shell are handled. The first to be described is the simpler method, known as the "add-mass" method, in which some portion of the pool water is lumped to the DDOF of the containment shell. The second method includes the pool water as discrete elements coupled with the containment model discretization.

5.3.1. Add-mass method

The accuracy of this method depends greatly on assigning correct values of the hydrodynamic mass assumed to vibrate together with the steel shell. Unrealistic results can also occur if pressure loading is not correctly defined. When the pool is seismically excited there is no explicit forcing function to be defined, rather the internal forces associated with correct added-mass stress the containment.

Since this method reduces the problem to an equivalent structural problem with added mass at the structural wet boundary, the LOCA or SRV actuation source pressures in the pool must be converted to forcing functions to be applied at the DDOF of the wet boundary of the structural model (Fig. 5.11(a)). The magnitude and spatial distribution of these forcing functions are obtained by empirical rules based on experiments as discussed in Refs. 8,9,18,54 and 72. Nonaxisymmetric loading conditions are handled using a full or partial Fourier series expansion of the load (Fig. 5.12)[63].

When a test pressure trace is obtained at a pool boundary that is flexible, the influence of FSI is already reflected in the pressure trace [54]. Therefore, if the measured pressures are in turn applied to the respective DDOF of a model of the same structure, the dynamic analysis should be performed excluding the pool water. However, current practice includes the effect of FSI in the dynamic response analysis to account for uncertainties in the load definition and differences in structures [54]. This approach has resulted in very conservative results which have been questioned and challenged [8,9,18,54]. Technically, the load definitions provided should be in the form of wall load-time histories which would exist on the structure if it were rigid, i.e., incident pressures [34].

There are a number of ways in which the hydrodynamic water mass can be assumed to act with the containment shell. When test pressure traces of simulated LOCA or SRV actuation are considered, a lower bound could be considered to occur when no water is included in the analysis model. Of

course, this would not be applicable to a water pool that is seismically excited. In this case, the inertial effect of the hydrodynamic mass must be included.

An approximate method to include the water is to consider that the water within half of the pool width participates in the vibration of the steel shell at the pool surface and assume no water participation at the bottom of the pool where the shell is rigidly anchored into the foundation [54]. The variation of the water mass between the top and bottom of the pool is then assumed to vary either linearly or parabolically. A technically more precise method is to lump the added mass consistently, based on assumed displacement shapes of the shell [7,18]. Good results have also been reported in Refs. 8 and 9 wherein the problem is solved in the frequency domain. In this case, the hydrodynamic (added) mass is made frequency dependent. In effect, the participation of the water mass will depend on the frequency content of the loading. The frequency domain solution is also considered advantageous for hydrodynamic containment analysis because, once the problem is formulated, it is more economical to analyze many loading cases in the frequency domain than in the time domain. Many loading cases need to be considered because of the various LOCA or SRV actuation sequences possible and because of the uncertainties in the magnitude and frequency content of the loading.

5.3.2. Water discretization method

In this method, the water is included in the model as discrete elements. For example, if an axisymmetric model is used then the water is modeled with two-dimensional axisymmetric finite elements like those used

to model the containment foundation and supporting soil. The properties
of the element are chosen to make their stress-strain law analogous to
the acoustic equations of a compressible fluid [34]. The containment
shell and pool are treated as a coupled mathematical model.

LOCA and SRV actuation source pressures are applied at the appli-
cable location in the pool (Fig. 5.11(b)). For an axisymmetric
structural model with non-axisymmetric loading, the Fourier series
expansion of the load is again used. The response to each harmonic is
obtained and the solution obtained by summation.

More details on this method can be found in Ref. 18. While complete
discretization has the potential of more correctly solving the hydrody-
namic problem and, therefore, removing some of the unnecessary conserva-
tism of the add-mass method, the expense and understanding required for
correct results limits its practical application.

5.4. Thermal Stress

There are three major sources of energy which can potentially be
released in the steel containment. These are discussed in Sec. 3 and
are: stored energy inventory of reactor and primary system water; decay
heat energy; and hydrogen generation and burn energy. This released
energy, basically stored in the form of saturated steam, transfers energy
to the steel containment shell upon contact (Sec. 3.2.2.1). The steel
heats up and induces a state of stress as described in Sec. 3.2.2.2.
Generally, thermal stresses are considered to be self-limiting and are

not emphasized [23]. However, it is matter of fact that they do exist
and therefore must be quantified.

As pointed out in Sec. 3.2.2.1, it would be possible to analyze the
overall containment using a finite element computer program which ac-
counts for the variation of the heat transfer coefficient h. Such an
analysis could be made to account for material nonlinearities and output
the resulting stress-strain condition of the containment also. However,
such sophistication may not be appropriate considering the uncertainty of
the actual temperature in the containment after an internal event and the
low emphasis placed on such an analysis in the first place.

Adequate results may be obtained by considering the thermal stress
states and their origins that were described in Sec. 3.2.2.2 and then
judiciously developing appropriate thermal loading conditions to be com-
bined with the other coincident loads. That is, a few different thermal
load conditions can be calculated and then applied as a quasi-steady
state to the critical responses found for other loads. Thermal load
cases should be assigned an appropriate time frame in which they can be
concurrently combined with the other time dependent load cases (e.g.,
pressure or hydrodynamic).

Noting that a gradient can initially be formed in the steel shell,
as discussed in Sec. 3.2.2.3 and exemplified in Figs. 3.15 and 3.16;
potential gradient effects can be included in a thermal load case to be
combined with initial peak dynamic responses that are occurring at
roughly the same time. Since the steel shell has a fast time response to

heat, the gradient effects will have subsided considerably after about a minute (Fig. 3.15 and 3.16).

A practical method by which thermal gradient load cases can be converted to an overall stress state in the containment is to divide the containment shell into a number of sections at different points along the meridional direction of the shell and dome [43]. The section analysis is a local analysis, in effect, with appropriate boundary conditions assumed. A procedure is to assume that the section is subject to rotational restraint only and that thermal gradients cause changes in the moments in the containment shell. The overall stress state of the containment can be found by enforcing compatibility of rotational displacements between the segments as described in Ref. 6. The gradient through the thickness of a section under transient conditions is usually nonlinear. The ASME Code suggests replacing this with an approximate linear variation and considering the difference between the linear and nonlinear distribution as a local stress subject to its appropriate service levels [4,NE-3213.13]. Interaction diagrams reflecting the effects of thermal gradients on the shell moment capacity can be useful tools for evaluating the influence of thermal effects.

Regardless of the heat transfer coefficient h, after about a minute the containment shell will approach a steady state, taking on the temperature of the high energy atmosphere in the containment (Fig. 3.17). Thermal stresses at gross and local discontinuities can be estimated by assuming that the entire containment is heated to the peak atmosphere temperature in the containment. If the containment is relatively clean

and its geometry simple, then Refs. 6 and 98 can be used to calculate stresses; otherwise, computer methods may be appropriate.

The methods suggested here to analyze thermal stress are analytically rigorous. However, the thermal loading (i.e., temperature distributions) of the containment shell reflects more approximation than normally done for the other loadings. This also generally simplifies the solution process. Since thermal stresses tend to be self-limiting and, consequently, not likely to govern containment design [23,43], less refinement of the time-space variations may be permissible. The ASME Code [4,NE-3221] allows higher allowable stresses for loading combinations which include self-limiting loads. The suppositions used to develop the thermal load cases should reflect the time frame but it may not be necessary to explicitly express them as a function of time.

5.5. Impulse and Impact

This section applies to the analysis of loads that are of a <u>local</u> dynamic nature on the steel containment shell. Such loads include those discussed in Secs. 3.2.4 and 3.2.5. Generally, analyses of these loads allow for the steel to strain into the inelastic range. Inelastic straining in the steel shell membrane due to local dynamic loads is governed by Appendix F of the ASME Code. The ASME Code defines local dynamic loads as Category D Loads which includes loads such as jet impingement, pipe whip, and pipe reaction loads [4,NE-3113.4]. Because of the potential inelastic and dynamic response of the structure to local pulse and impact loads, it becomes appropriate to consider: the dynamic

properties of structural materials (i.e., effects of increasing strain rate); characterization of material nonlinearity; and allowance for the effects of geometric nonlinearity. These last two effects reflect the failure to satisfy the criteria defined in Sec. 4.1.1 for linear analysis and its principle of superposition.

5.5.1. Impulse

Impulsive loads include: compartment pressurization due to LOCA; various phases of hydrodynamic loading due to SRV and LOCA discharge; hydrogen detonation blast pressures; and jet impingement and the resulting support reactions that result from a broken pipe. The first two examples are global type loads under which the containment shell is typically required to remain elastic. The dynamic analysis of the impulse loads associated with them are treated in Secs. 5.2 and 5.3. The last two examples are local type loads for which dynamic analysis techniques are introduced in this section.

Dynamic analysis techniques of this section differ from those previously discussed primarily because of the localized and inelastic response characteristics encountered. The type of pulse loads (Sec. 3.2.4) being discussed are often very localized compared to the overall size of the containment. A possible exception is hydrogen detonation. Because of the local nature of the pulse, it is often possible to analyze a reduced model that represents a segment or region of the containment. Boundary conditions for the reduced model are based on actual conditions and anticipated behavior of the containment at the location where the reduced model was removed. For example, the boundary conditions of a

modeled segment removed from the containment could conceivably be ideal-
ized by imposing axial restraint and neglecting rotational restraint.
Applicable boundary loadings can be obtained from a previous overall
analysis of other concurrent loads on the containment. Refs. 82 and 98
can be used as aids in determining the extent of the model required.
That is, the model must be large enough so that effect of the disturbance
can be adequately characterized.

The response of the containment shell to the local pulse can be
found using computer analysis techniques or simplified methods. It may
be the case that these analyses are conducted to verify the integrity of
the containment design rather than to actually design its shell thick-
ness. With this in mind, the inelastic capacity of the shell is often
considered in accordance with the ASME Code (e.g., Category D service
limits) and the acceptance of the NRC.

5.5.1.1. Simplified methods   This method reduces the continuous
mass of a containment shell segment to an equivalent one degree of free-
dom (DOF) system [11]. To be successful it is important that the pulse
results in predominant structure response in a single deformation mode.
As a single DOF system, it is possible to use available closed form
solutions or numerical techniques to obtain solutions. Particularly, if
the impulse load-time history can be idealized by some simple mathe-
matical shape, parametric curves of Ref. 11 can be directly used for
elastic or inelastic analyses.

The parametric curves of Ref. 11 for inelastic analysis yield the
maximum response of elastoplastic one DOF systems. The structure

nonlinearity is idealized by a bilinear resistance function, i.e., linear up to a limit load and constant thereafter. This resistance function can also be used in numerical techniques. In this way, the ductility of the containment shell in the plastic range can be used to absorb energy of the impulse load.

Before the usual solution techniques can be applied, it is first necessary to idealize the shell model in terms of an equivalent one DOF system. That is, it is necessary to evaluate equivalent parameters for the equation of motion [11]:

$$M_e \ddot{d}(t) + K_e d(t) = F_e(t) \qquad (5.5)$$

where:

M_e = equivalent mass

K_e = equivalent stiffness

$F_e(t)$ = equivalent load.

Thus, the continuous shell mass is idealized as a concentrated mass. The equivalent system should be chosen so that the deflection of the concentrated mass is the same as that for some significant point. For example, the centroid of impulse load distribution on the shell (i.e., probable location of maximum shell displacement) may be appropriate. From Eq. 5.5, the maximum deflection of the concentrated mass can be found and then the stresses in the real structure can be calculated.

The parameters, M_e, K_e and $F_e(t)$, are evaluated on the basis of an assumed displaced shape ϕ of the actual containment shell. The validity of the displacement-time response found by the equivalent system

depends upon how well ϕ matches the actual shell displacement and the fact that ϕ is the predominant response of the containment shell. This shape ϕ is typically taken as the result of a static application of the impulse load distribution. In this respect, finite element/difference codes are of great use in identifying ϕ. They are also useful in verifying that the extent of shell segment mode is adequate. In general, ϕ is used to evaluate the equivalent parameters by energy or work equivalent expressions.

When the system goes into the plastic range, the equation of motion is

$$M_e \ddot{d}(t) + R_{me} = F_e(t) \qquad (5.6)$$

where:

R_{me} = equivalent limit load of the shell

and R_m is the actual limit load found by finite element analysis or calculated by considering the internal membrane and bending energy present when plastic mechanisms form with respect to the assumed displaced shape. If the natural period is five or more times the pulse duration, then energy principles can be used to show that [11]

$$R_{m \text{ req'd}} = \frac{i\omega}{\sqrt{2\mu-1}} \qquad (5.7)$$

where:

i = impulse = $\int f(t)dt$

ω = $T/2\pi$

μ = ductility ratio = allowable plastic strain/material yield strain.

It must be cautioned that as the shell progresses through the different stress ranges, i.e., elastic, elastic-plastic and plastic, the assumed shape ϕ is different for each stage. A complete solution requires that each stage be treated separately. Because of the difficulty in establishing ϕ this method can appear less desirable than using a finite element model and doing a direct time integration. And, in fact, the tendency now is toward doing a complete dynamic time-history analysis. However, this is expensive and must be repeated for various pulse-time histories or containment geometeries encountered, whereas, within parametric ranges of impulses and containment geometries, equations determined herein can be used again and again. An example of the implementation of this method can be found in Ref. 109.

5.5.1.2. Computer analysis   In computer analysis methods, the shell model is discretized and the solution is found by finite difference or finite element procedures. In either case, the dynamic response is obtained by solving the system of equations of motion which, including nonlinearities, may be expressed as:

$$[M]\{\ddot{D}(t)\} + [C(\dot{D}(t))] + [K(D(t))] = \{F(t)\} \qquad (5.8)$$

Since nonlinearities are generally considered, the solution is typically solved by direct time integration (Sec. 4.4.2) wherein the stiffness and damping matrices must be continually updated. Material nonlinearity occurs when stresses (or strains) exceed elastic limits. Therefore, a stress-strain curve of the steel must be defined that extends into the inelastic range. Frequently, the stress-strain curve is represented by a

bilinear curve as was used in the previous section for the resistance function.

Geometric nonlinearity occurs when deformations become large compared to the dimensions of the structural members. As a result, the bending stiffness is effectively reduced due to the interaction of the membrane force. Therefore, the establishment of equilibrium requires that shell geometry be updated at each time step.

Selection of a proper time step for the direct time integration is necessary for accurate solutions. The time step must be small enough to insure stability of the integration scheme and accurately characterize the shell response. Analysis of short duration loads are particularly sensitive to the time step size because a large number of higher modes can be excited (Sec. 4.4.2).

As mentioned in the previous section, computer analysis techniques can also be of great use in performing accurate simplified analyses. Structural analysis computer codes used for dynamic analyses that include material and geometric nonlinearities are expensive to employ. However, these codes (and less sophisticated codes) can be economically used for static, linear analyses to verify model adequacy (e.g., extent); identify displacement shapes ϕ; predict limit loads; and determine the location and onset of nonlinear behavior.

5.5.2. Impact

Analysis methods introduced in this section are for local impact loads caused by plant generated missiles striking the inside of the containment. Roughly, impact loads can be thought of as very large and

quickly applied impulse loads. However, the problem is further compli-
cated because of the structural interaction of the missile and contain-
ment and the severe local deformations that may occur. Also, the pres-
ence of stress wave propagation and corresponding high number of modes
that can be excited becomes more pronounced.

The type of impact loads considered here are similar to the impulse
loads previously discussed in that local failure is the primary concern.
This is not to imply that overall instability of the containment is not
to be checked. However, in most cases, the characteristics of plant-
generated missiles (Sec. 3.2.5) are such that local failure will govern
the analysis [13]. Therefore, discussion will center on the impact
effects in the vicinity of missile contact and potential missile
perforation.

Current practice for checking the containment shell against missile
perforation is to use empirical formulae. These formulae are typically
for hard missiles (i.e., deformation of the missile is negligible rela-
tive to that of the target) and can be found in Refs. 13 and 92. Com-
puter analysis for missile performation is not practical, particularly
considering the low probability of the impact event.

The vicinity or region around the point of impact should be analyzed
to predict resulting stresses and deformation in the shell. This is
particularly important from the standpoint of containment stability. To
predict the local response of the shell, a reduced model of a segment or
region of the containment can be used as was discussed for impulse loads.
If the impact event can be expressed by a force-time history, then the

analysis can proceed using the methods described for impulse loads; including the effects of material and geometric nonlinearities. Again, if a numerical method in the time domain is chosen, extremely small time steps must be used to account for stress wave propagation and the corresponding high number of modes excited.

In lieu of using an approximate force-time history for the analysis, a computer analysis can be conducted based on the energy imparted to the shell. As the missile strikes the target a stress wave propagates radially from the impact point. An appropriate velocity field is assumed within the bounds of the stress wave in the shell at the time the missile and target separate [13,92]. This velocity field is then used as initial conditions for a computer analysis for nonlinear response.
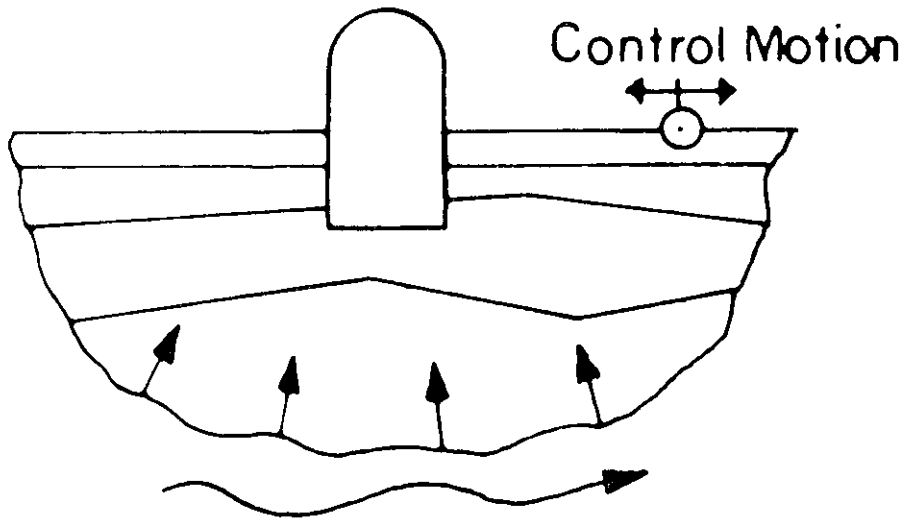
Fig. 5.1a. Schematic of complete analysis of
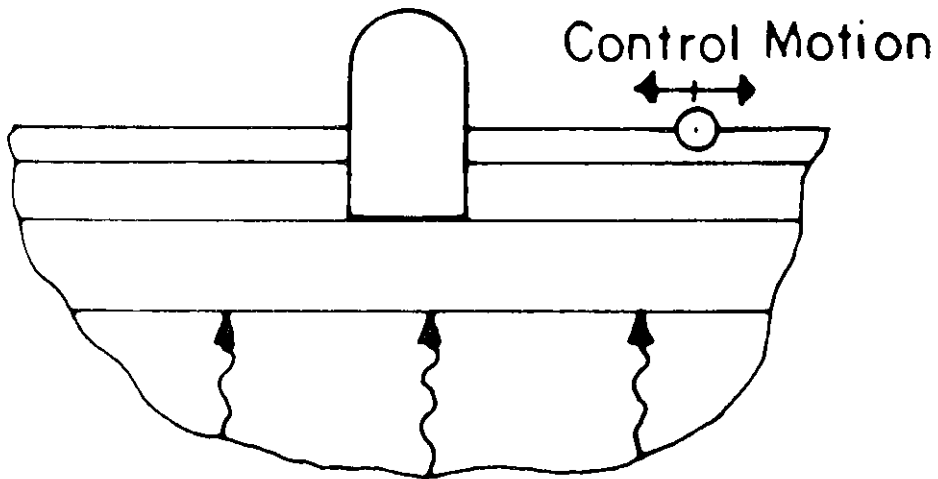soil-structure interaction [84]

Fig. 5.1b. Schematic of idealized complete analysis
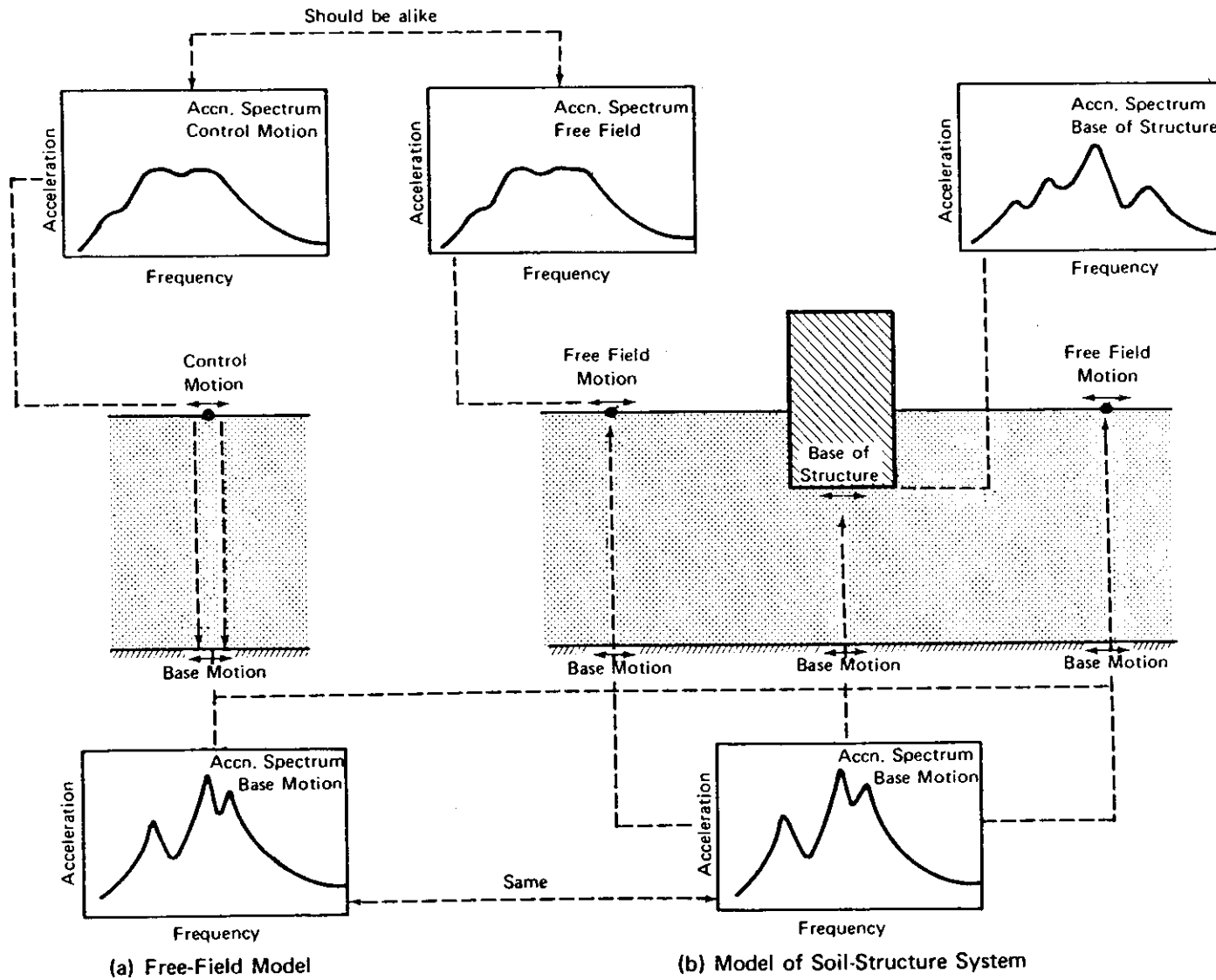of soil-structure interaction [84]

Fig. 5.2.   Schematic representation of soil-structure interaction analysis using finite elements [52]

a. Axisymmetric model (3-D)   b. Plane-strain model (2-D)
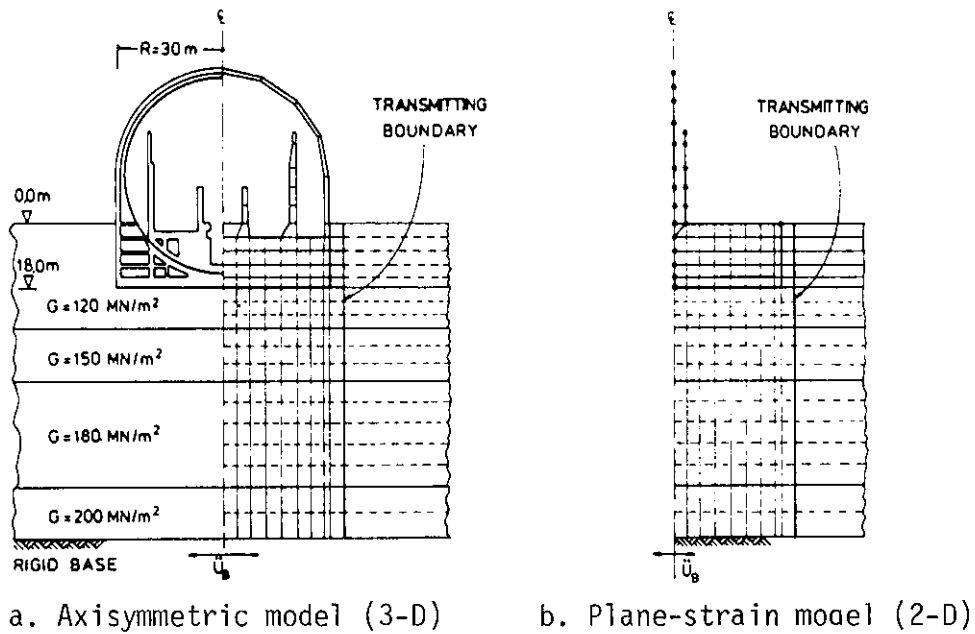
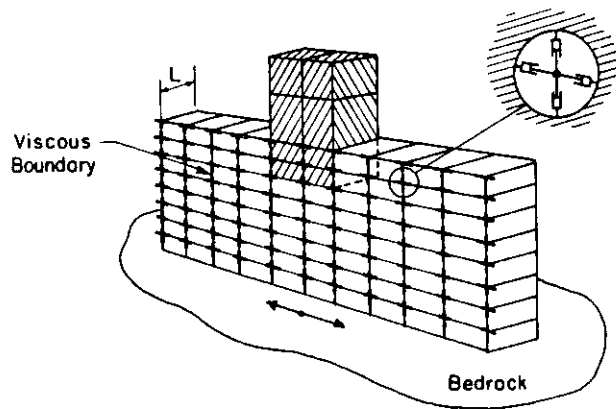Fig. 5.3. Finite Element Models [118]

Fig. 5.4. Schematic of a plane-strain model
           modified with viscous dampers to
           emulate three-dimensional soil
           behavior [84]
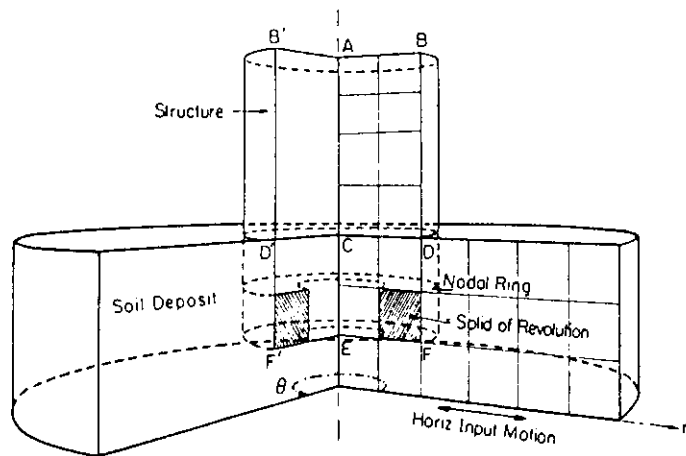
Fig. 5.5. Schematic view of an axisymmetric model [84]
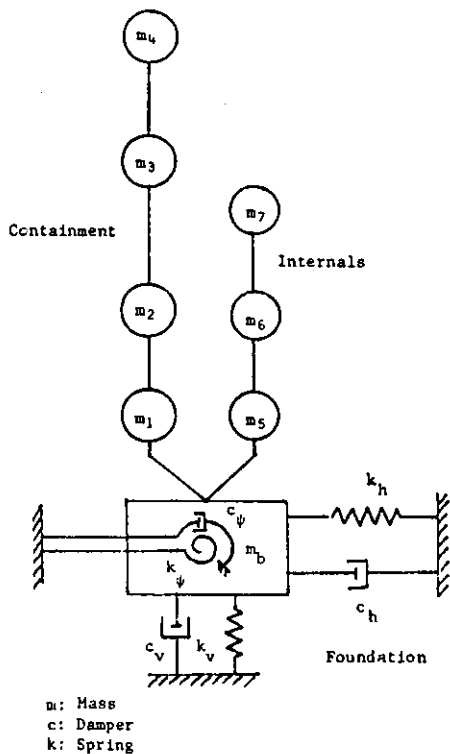
Fig. 5.6. Lumped spring model for structure-foundation system [56]

$$K = \begin{Bmatrix} k_{xx} & k_{x\phi} \\ k_{\phi x} & k_{\phi\phi} \end{Bmatrix}$$

$\ddot{\phi}_I$

y_I

M
F

$\ddot{\phi}_I$

$\ddot{y}_I$

$\ddot{Y}_G$

$\ddot{Y}_G$

TOTAL SOLUTION   =   (1)   +   (2)   +   (3)
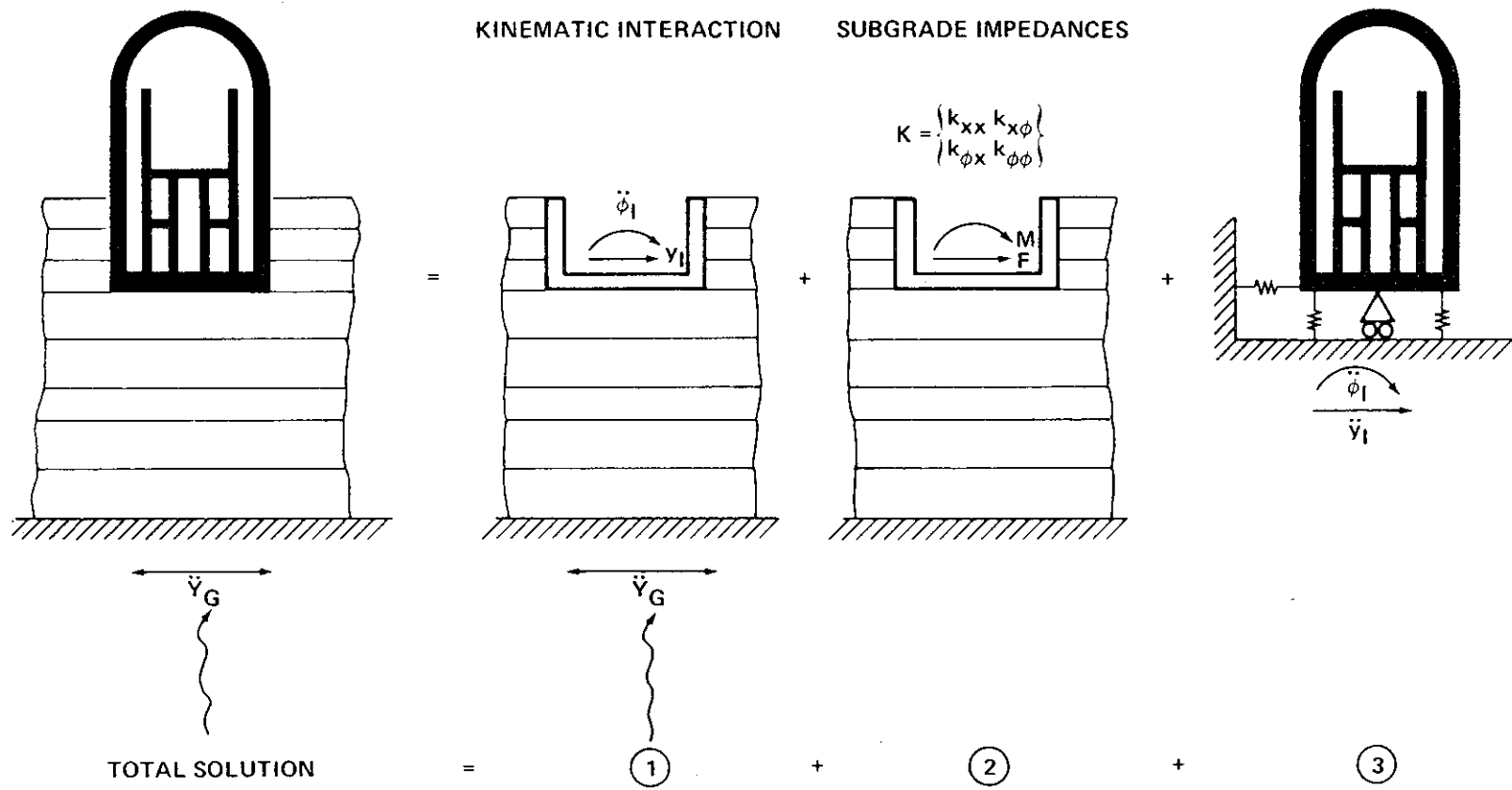
Fig. 5.7. The 3-step solution of the soil-structure interaction problem [60]
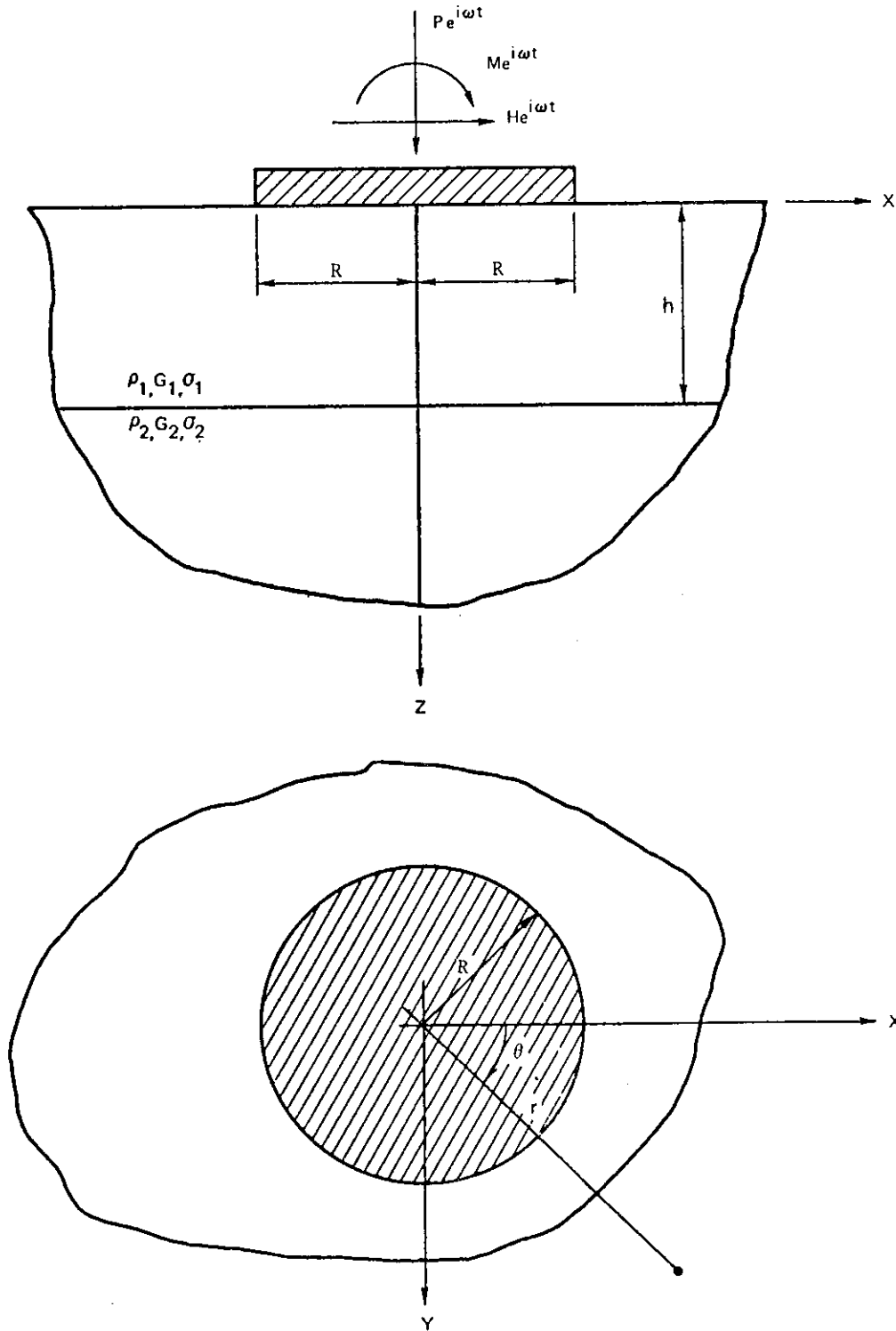
Fig. 5.8. Typical mathematical model used for closed form evaluation of supporting soil stiffness and damping [52]
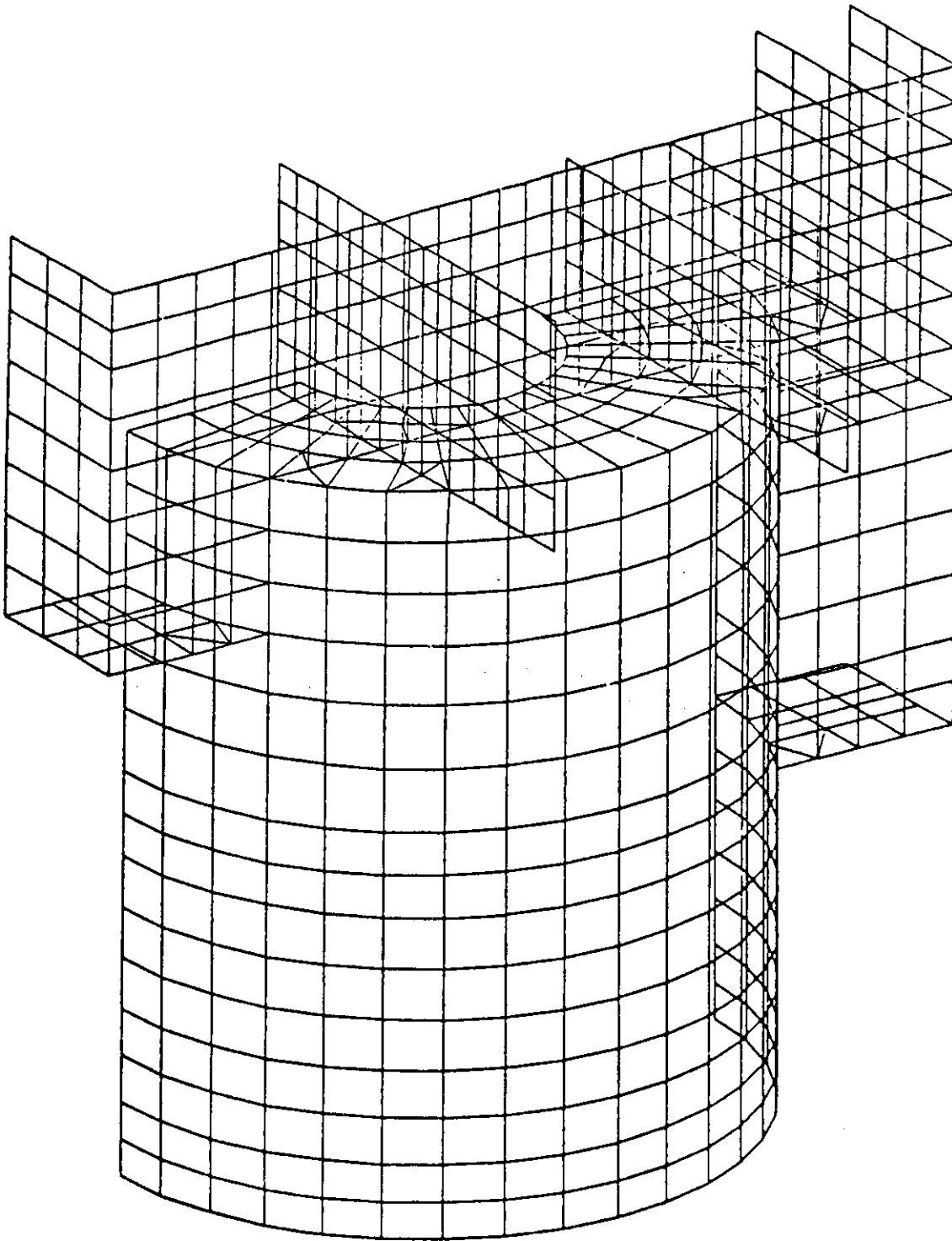
Fig. 5.9. Finite element model of drywell in Mark III containment [64]
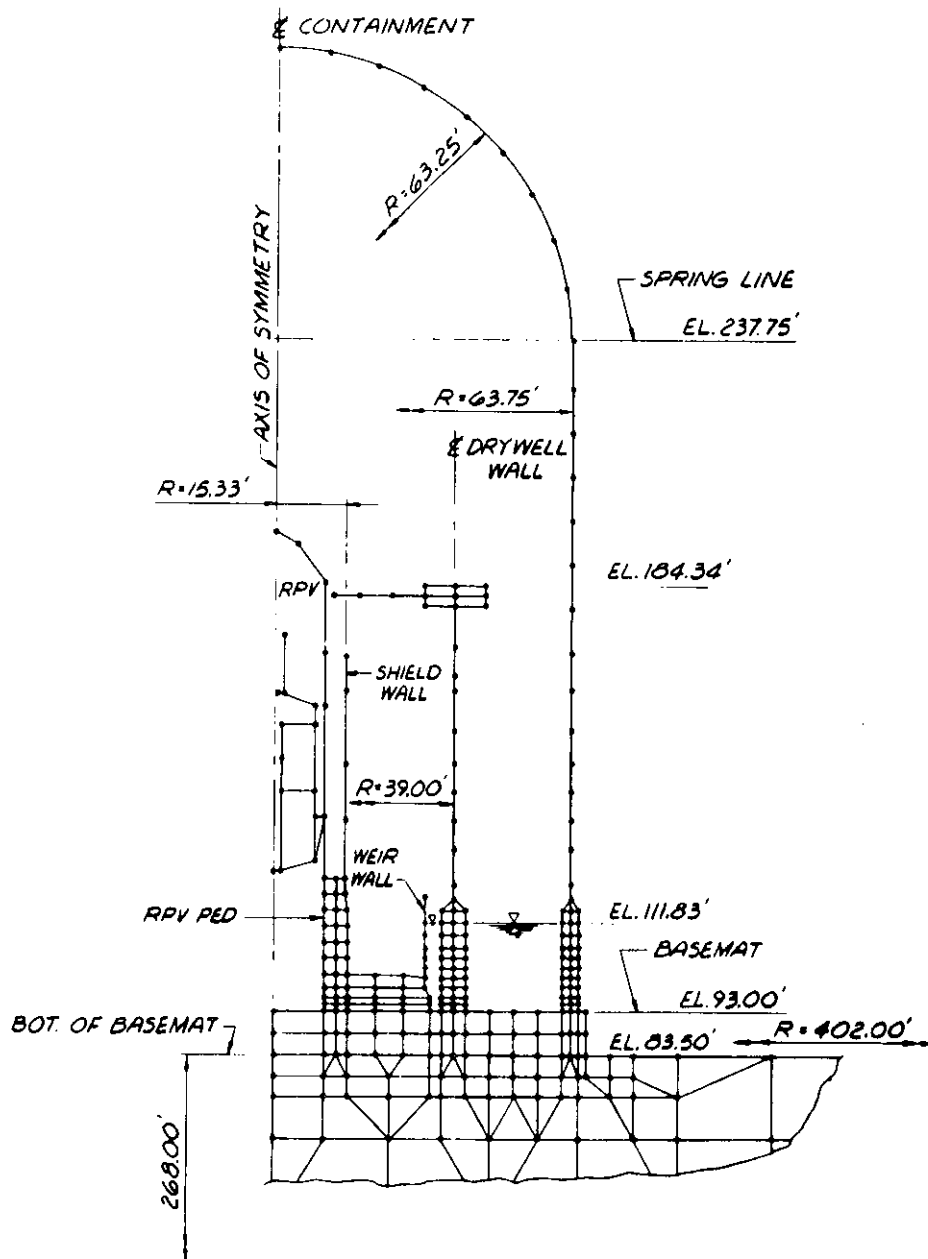
Fig. 5.10. Containment and foundational soil modeled with one- and two-dimensional axisymmetric finite elements [63]
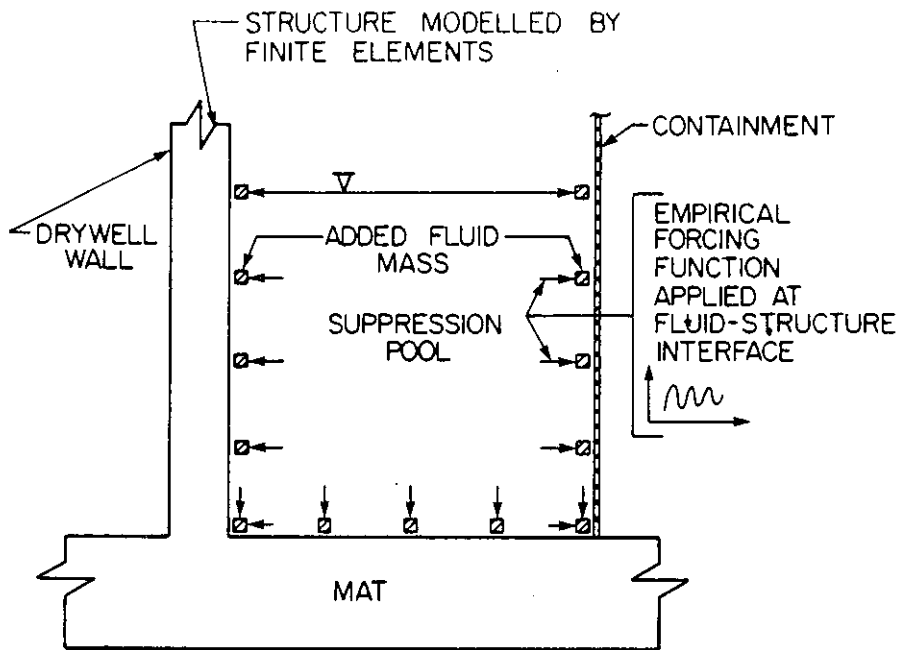
Fig. 5.11a. Schematic description of add-mass model [18]
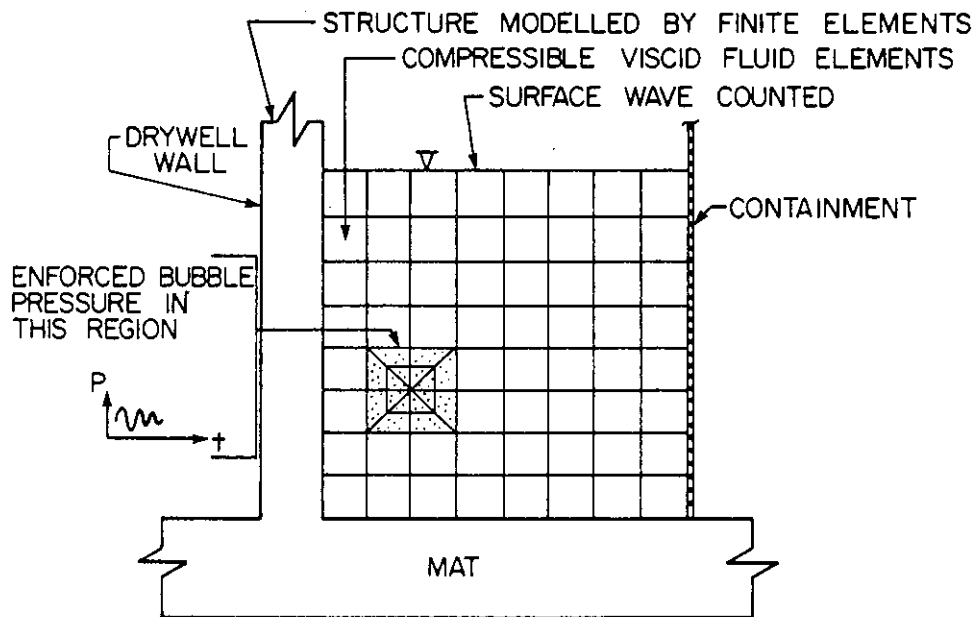
Fig. 5.11b. Schematic description of discretized
suppression pool model [18]
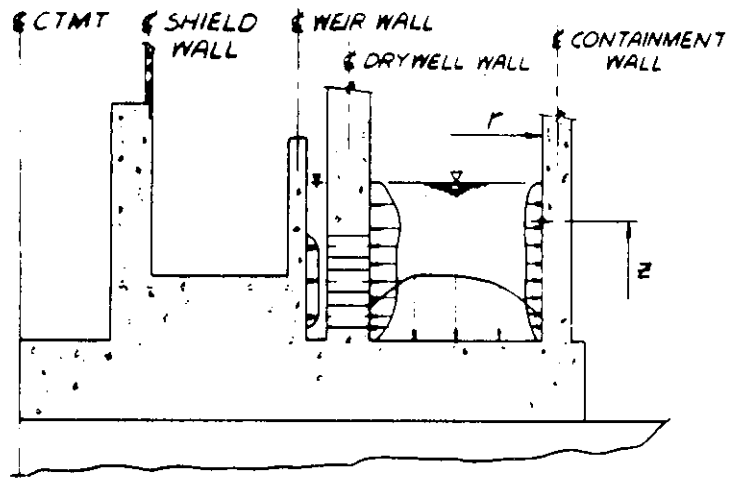
SECTION
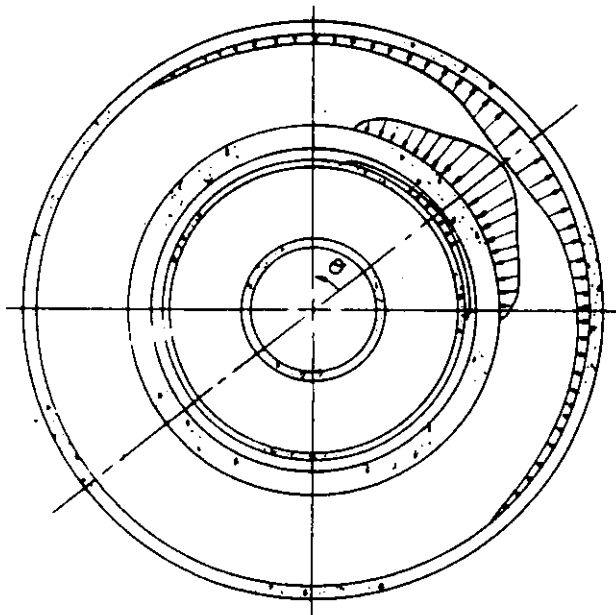
PLAN

Fig. 5.12. Typical hydrodynamic pressure distribution at a given
moment in a Mark III suppression pool as a result of
a single safety relief valve actuation [63]

6. ANALYSIS ASSESSMENT

In Secs. 4 and 5 methods were discussed by which the loads of Sec. 3 can be transformed into stress-strain states in the steel containment. The effect (or response) from an applied load creates a condition that must be resisted by the steel containment. As pointed out in Sec. 2, the stresses due to the load are in fact random variables Q. Likewise, the capacity (or total resistance) of the steel containment is some distribution of random variables R. If accurate distributions of Q and R are known, it is possible to determine the probability of failure p_f and then decide if this represents an acceptable design. One should note that the term failure used above does not necessarily imply collapse or other catastrophic events. Rather, it expresses a limit state defined in terms such as gross deformation at which loss of intended function occurs.

Presently, the distributions of Q and R are not sufficiently well-defined to allow probabistic design of steel containments. Current practice is to design steel containments using deterministic criteria. That is, only the nominal values of load and resistance are used. The philosophy of the ASME Code is to place limits on stress which the unfactored load responses must not exceed. These stress limits represent some fraction of the expected resistance (or stress capacity) of the structure.

6.1. Load Combinations

Probability concepts also apply to the formulation of load combinations. A load combination is a set of loads (e.g., pressure, dead load,

etc.) that are considered to act concurrently on the structure. In

reality, each type of load (Sec. 3) has a corresponding probability of

occurrence varying from greater than zero to one. However, because of

the difficulty in determining these occurrence probabilities, it is cur-

rent practice to consider "worst case" events at the nuclear facility as

a basis to determine what loads need to be combined. As a result, low

probability loads, such as severe LOCA and SSE, are typically required to

be combined to assure a conservative design [105,114].

The ASME Code [4] does not specify which loads should be combined.

However, NRC-approved guidance is provided in USNRC Standard Review Plan,

Sec. 3.8.2 [114] and USNRC Regulatory Guide 1.57 [105]. These documents

describe and/or list various load combinations to be considered. The

load combinations therein are based on postulated situations such as:

    1)   OBE occurring during normal operations;

    2)   OBE occurring during LOCA;

    3)   OBE occurring during plant recovery after LOCA;

    4)   SSE occurring during LOCA.

where: OBE is an operating basis earthquake; SSE is a safe shutdown

earthquake; and LOCA is a loss-of-coolant accident as was explained in

Sec. 3. Clearly, these situations represent severe to extreme cases on

which to base load combinations.

From the example situations shown above, it can also be noted that

the probability of occurrence for each load combination can be signifi-

cantly different. This is also recognized in the ASME Code as was dis-

cussed in Sec. 2.2. It may be recalled that stress limits vary in

accordance with the Load Category (i.e., Service Levels A thru D) assigned to a particular load combination. This assignment is based on descriptive definitions provided in the ASME Service Levels [4, NE-3113]. The ASME Code together with Refs. 105 and 114, thus imply a design format that is expressed as

$$S \geqslant Q_1 + Q_2 + Q_3 + \ldots$$

where the Q's are the expected responses (stresses in this case) of loads in the given load combination, and S is the appropriate allowable stress limit as denoted and governed in the ASME Code [4, NE-3221]. The value of S is some fraction less than the expected resistance R of the containment shell.

Table 6.1 shows various load combinations that are essentially in agreement with Refs. 105 and 114. This table is not exhaustive, however. For example, hydrodynamic loads (Sec. 3.2.3) caused by SRV actuation and LOCA in BWR plants are not included in Table 6.1. Also, hydrostatic loads generated by post-LOCA flooding of the containment, if any, are not included. Since, in general, the load combinations of Table 6.1 apply to all steel containments, the examples mentioned above are sometimes referred to as system specific loads. System specific loads must also be included in the load combinations considered appropriate to their anticipated occurrence. SRV actuation, for example, could conceivably occur at any time except during a LOCA when the BWR is depressurizing.

At this point the question of what loads need to be combined has been addressed. It has also been pointed out that the probability of

occurrence for a given load combination is accounted for in the allowable design stresses. Another important question that must be dealt with is: "How should individual load responses be combined, particularly dynamic responses?"

It will be recalled that the loads of a given load combination are considered to act concurrently. If the containment behaves linear elastically, the principle of superposition applies and each type of load can be analyzed separately. The results of each analysis are stored and later recalled and combined with other loads defined for a given load combination. On the other hand, if an inelastic analysis is done on the overall containment to assess, for example, buckling capacity; then it becomes necessary to simultaneously apply all loads (with proper time phasing) identified in the load combination considered most demanding on the containment buckling capacity. Inelastic analysis is the exception rather than the rule and so discussion will assume elastic analyses as was done in Secs. 4 and 5.

If static loads are being combined, then their response values are simply added to one another. In some instances, loads will depend on time only in terms of a broad interval of time and may be combined in the load combination as if they are static. The responses to dynamic loads cannot be combined in this straightforward manner.

Combining dynamic responses is complicated by the uncertainty in selecting a proper time phasing between the various load types and by the uncertainty in the time history of the individual loads. To conservatively account for these uncertainties, current practice uses the so-

called absolute summation (ABS) method of simply adding the absolute value of the peak structural responses due to the individual dynamic loads. This method can lead to overly conservative designs. An alternate approach is to use the square-root-of-the-sum-of-the-squares (SRSS) of the peak responses due to the individual dynamic loads as an estimate of the combined response (Sec. 4.4.1) [27]. This method is applicable because the dynamic responses of the individual loads (e.g., SSE, transient pressure, hydrodynamic pressure, etc.) are esssentially independent, random phenomena.

6.2. Stress Intensity Limit

Postulated conditions of loading form the basis of the various load combinations subjected to the steel containment. Linear elastic analysis of each type of load provides corresponding states of stress in the containment. The peak stress states from the respective loads in a given load combination are then combined to produce an overall state of stress. If necesary, the time variation of the stress state for a given load combination may need to be considered also. Whether time dependence is important or not, a given load combination yields at least one overall state of stress that must be assessed to make sure that allowable design stresses are not exceeded.

In this section, it will be assumed that the structure is stable. This means that the allowable design stresses defined in the ASME Code, NE-3221, are directly applicable as a basis for investigating the integrity of the containment material. If the containment shell becomes

unstable (Sec. 6.3), it may be necessary to reduce the defined design stresses until an acceptable factor of safety against buckling is achieved.

Allowable stresses in the ASME Code are based on the maximum-shearing-stress theory of failure. The maximum shear stress at a point is equal to one-half the difference between the algebraically largest and the algebraically smallest of the three principal stresses at a point in the containment shell. Related to this, the ASME Code (and subsequent discussion) uses the more specific term "stress intensity" to describe and assess the state of stress in the containment shell.

The stress intensity caused by the applied loads is defined as the difference between the algebraically largest principal stress and the algebraically smallest principal stress at a given point. This is equal to twice the maximum shear stress. In effect, "stress intensity" is a convenient measure of the equivalent intensity of combined stress in lieu of usual parameters of measure dealt with in engineering mechanics. The allowable stress intensities S (usually subscripted) are some fraction of twice the material shearing elastic limit.

For a given load case, stress intensities are computed for many stations on the containment and categorized for comparisons with specified allowable stress intensities. The following definitions are used in the ASME Code to identify components of stress in the containment:

- Primary stress P - normal or shear stress; not self-limiting. Examples of this are general membrane stress P_m in the continuous region of a pressurized shell and bending stresses P_b in central region of a flat head due to pressure.

- Secondary stress Q - normal or shear stress; self-limiting. Examples of Q are bending stress at a gross structural discontinuity and general thermal stresses.

- Local primary membrane stress P_L - membrane stress associated with a primary or discontinuity effect; has some characteristics of a secondary stress.

- Peak stress F - usually a highly localized stress of interest as a possible source of a <u>fatigue</u> crack or a brittle fracture. Examples of F are thermal shock and stress concentrations (i.e., notch effect).

The definitions above are used as a basis to form "stress categories" that describe the various states of stress at different stations on the containment. The categories are:

- General primary membrane stress intensity P_m;
- Local membrane stress intensity P_L;
- Primary general or local membrane plus primary bending stress intensity $P_L + P_b$;
- Primary plus secondary stress intensity $P_L + P_b + Q$;
- Peak stress intensity $P_L + P_b + Q + F$.

Different allowables are established for each stress category. As discussed in Sec. 6.1, allowable stress intensity also varies with respect

to the probability of occurrence of the load combination being investigated. Table 6.2, adapted from Ref. 114 and slightly modified, illustrates the above for the various Load Categories and stress categories.

From studying Table 6.2 it is evident that, for a given load combination, the analyst must consider each stress category against its respective allowable stress intensity. For instance, suppose a station at the crown of a spherically dished (torispherical) containment domes is being investigated for a Load Category B load combination. According to the ASME Code [4, Fig. NE-3221-2], $P_m \leqslant S_{mc}$ and $P_L + P_b \leqslant 1.5 \ S_{mc}$ where S_{mc} is the allowable stress intensity found in Table I-10.0, Appendix I of the ASME Code. Therefore, in this case the components of stress (membrane and bending) should be given individualized attention. However, it will also often be the case that the detailed stress analysis will give combinations of stress components (i.e., P_L, Q, etc.) that directly make up a stress category and whose individual components require no separate study.

When substantial operating loads, associated with plant start-up, operation and shut-down, are specified, the containment must be checked for its ability to withstand fatigue loading. The transient peaks caused by pressure, temperature and pipe reactions due to the above contribute to the peak stress intensity category $P_L + P_b + Q + F$. The rules used to check $P_L + P_b + Q + F$ for potential fatigue problems are provided in Par. NE-3221.5 of the ASME Code, titled Analysis for Cyclic Operation. In most cases, the cyclic analysis of plant operation can be handled simply by showing compliance with the rules in NE-3221.5(d).

There are cyclical loads, however, that are considered to be operating basis loads but are of such intensity that NE-3221.5(d) may not be satisfied. Specifically, the dynamic containment responses to SRV actuation and OBE are two prominent examples of this. In this case the procedures of NE-3221.5(e) must be followed. This involves the computation of usage factors for different load cycles (e.g., an OBE would constitute one load cycle) and comparing the summation (over the life of the component) of these usage factors with an allowable of 1.0.

A load cycle of any dynamic load will result in numerous stress cycles. As noted in Sec. 6.1, the ABS method or the SRSS method are often used to predict the maximum response of a load combination that contains dynamic loads. However, as explained above, it is also necessary to study the potential number of stress cycles in the load combination as a source of fatigue failure. The alternating stress intensity S_{alt} is determined in accordance with NE-3216 and used in conjunction with NE-3221.5 criteria and the design fatigue strength curves of Figs. I-9.0 found in Appendix I of the ASME Code. In addition, thermal stress ratcheting, defined in NE-3221.6, represents a cyclic load that must also be checked.

An exception to fatigue analysis is granted to load combinations in Load Categories C and D. These load combinations constitute extremely severe conditions and do not represent load cycles for which the nuclear facility will continue operating. Related to this, secondary stresses Q do not need to be evaluated for Categories C and D (NE-3221.4).

The ASME Code allows for inelastic containment capacity in such cases as: local and gross discontinuities, thermal stress ratchet, and loads of a local dynamic nature (Load Category D). Allowable stress limits for primary plus secondary stress intensity and thermal stress ratchet can be relaxed if plastic analysis is used (NE-3228). Inelastic capacity of the containment can also be considered for Category D local dynamic loads such as: jet impingement, pipe wipe, and pipe reaction loads (NE-3113.4). Appendix F of the ASME Code is referenced for specific rules. The rules and stress intensity limits differ depending on whether or not the loaded area is integral and continuous.

6.3. Shell Stability

The analysis methods of Secs. 4 and 5 were almost exclusively for containments assumed to behave linearly elastic. When this is true, the deformations are proportional to the applied loads and the displacements or the internal forces caused by a set of effects can be found by super-position. However, when internal forces in the containment shell are relatively high, this way may not be true. Two important effects may arise that invalidate linear analyses: 1) stresses exceed elastic limits and the material behaves nonlinearly (material nonlinearity), and 2) deformations become large compared with the dimensions of the structural members (geometric nonlinearly).

A _loaded_ structure is said to be stable if, after subjecting it to a very small disturbance, it will return to its original position upon removal of the disturbance. With respect to stability it is possible for

some of the structure material to enter the inelastic range and still maintain a stable structure. The loss of stability is more closely associated with relatively large deformations (translations and/or rotations) which may or may not be inelastic, produced by compressive forces. When compressive forces in the containment shell are high, two virtually inseparable effects of geometric nonlinearity may occur: a change in the containment geometry arising from deformation of its shell components, and a change in the stiffness of the shell arising from amplified bending caused by membrane forces on the shell component. Geometric nonlinearity can precipitate containment instability while the containment material is still in the elastic range. For this reason, the ASME Code stress intensity limits of NE-3221 may be superseded by NE-3222 to provide adequate safety against buckling.

Instability precipitated by only geometric nonlinearity (and not material nonlinearity) is referred to as elastic buckling. Postbuckling behavior may eventually be accompanied by material nonlinearity. However, knowledge of the conditions present when elastic buckling is incipient are sufficient for design. Instability precipitated by geometric nonlinearity accompanied with material nonlinearity is referred to as inelastic buckling.

Many of the load cases prescribed for a containment will result in compressive stresses that must be examined for potential buckling. Buckling at the regional level (e.g., in and between stiffeners and around penetrations) and of the overall containment must be considered. The ASME Code, NE-3133, provides specific design rules for unstiffened or

ring stiffened cylindrical shells, spherical shells and formed heads under external pressure and unstiffened cylinders under axial compression. However, NE-3133 is generally too restrictive with respect to containment geometry and type of loading to be of much practical use beyond preliminary containment sizing. A more general evaluation of instability is provided for in NE-3222 of the ASME Code. The criterion of NE-3222 state that critical buckling stress can be determined by:

1) rigorous analysis which considers the effects of overall and local buckling, geometric imperfections, nonlinearities, large deformations and inertial forces;

2) classical linear analysis reduced by margins which reflect the difference between theoretical and actual load capacities;

3) tests of physical models.

This last method is generally not practical to realistically perform. Therefore, stress intensity limits with respect to buckling are usually found as some appropriate fraction of the critical buckling stress found by methods (1) or (2) above.

Before going into any discussion regarding methods (1) or (2), it is first necessary to understand some of the problems encountered in predicting the critical buckling load of structures. The buckling or instability of structural members is generally characterized by a disproportionate increase in displacement resulting from a small increase in compressive loads.

For columns and flat plates small-deflection theory predicts the buckling load very well and, in general, the theoretical buckling load is

used to establish allowable buckling loads [6,39]. The small-deflection

theory is modified for the effect of material nonlinearity for moderate

length columns and flat plates. Postbuckling behavior, which is of

minimal use from a design point of view, requires the inclusion of geo-

metric nonlinearity effects. The inclusion of inevitable geometric

imperfection (i.e., deviation from perfect shapes) in these members

causes geomertric nonlinear effects to be present from the moment the

load is applied to the member. However, the geometric imperfections

associated with fabrication and erection practices causes little discrep-

ancy from the buckling load based on small-deflection theory for columns

and flat plates.

The behavior described above is usually not true for steel contain-

ments. This is because the buckling load for some types of shells and

loadings can be much less than the load predicted by classical small-

deflection theory. This is particularly true for cylindrical and spher-

ical shells, of which containments are typically constructed.

When nonlinear elastic theory is applied to long, axially compressed

cylinders, the same "classical" buckling stress found by linear shell

theory is predicted and, in addition, the nonlinear equilibrium path

after buckling is predicted [6]. The point where the pre- and postbuck-

ling equilibrium paths intersect is often referred to as a "bifurcation"

point. Figure 6.1 shows characteristic postbuckling behavior of various

axially compressed elastic elements. From Fig 6.1, it can be observed

that the maximum load that cylindrical shells (and spherical shells) can

safely support is very sensitive to imperfection in the shell geometry.

The reason for this can be partially understood by examining the equilibrium paths of Fig. 6.1. Anywhere that the equilibrium path slopes upward, the compressed element is capable of carrying additional load, storing it in the form of internal strain energy. Horizontal or zero slope portions of the path indicate a neutral state in which the stability and the capability of the structure to carry additional load depend on the nature of the adjacent equilibrium path. Any downward sloping portion of the equilibrium path represents unstable behavior that can only occur if the displacement is a controlled variable with the load undergoing an appropriate decrease.

In real structures, the load is the controlled variable. As axial load is initially applied to cylinder test specimens, linear shell theory is essentially correct, accounting only for membrane forces. This is assuming, of course, that initial imperfections (e.g., curvature) in the test specimen are minimal. Figure 6.2 hypothetically illustrates the initial linear behavior by the OF segment of the load-displacement curve OL which is based on linear shell theory. In Fig. 6.2, the point D' may be thought of as the "classical" buckling load or as the linear theory bifurcation point. The solid line OABC represents the nonlinear load-displacement curve where rotations and some initial imperfections (since $P_A < D'$) are accounted for.

As the load is increased past P_B, the cylinder test specimens have been observed to jump from the unbuckled configuration to one of the nonlinear branches (e.g., branches FB or DE) without passing through the linear theory bifurcation point. These branch points, F and D, off the

equilibrium path are also referred to as bifurcation points. The buck-ling behavior of cylindrical shells (and others), as assumed in Fig. 6.2, prefers to bifurcate sometime after P_B, and before P_A, and move along a nonequilibrium path to some point on the nonlinear equilibrium path between B and C, viz., E [6]. The above behavior helps explain why shells buckle at 3 to 5 times less than the "classical" buckling load and why there is appreciable scatter observed in much recorded data.

Now, with respect to Figs. 6.1 through 6.3, it can be understood why the "classical" buckling load is rarely, if ever, attained. The basic reason is that the presence of initial imperfections precipitate premature buckling because they preclude the pure membrane state and provide a lower energy response path to the buckled state. Figure 6.3 represents load-displacement curves for imperfect cylinders found by nonlinear shell theory [6].

Real containments inevitably have geometric and material imperfec-tions (e.g., initial curvature and residual weld stresses, respectively). Very early on after the load is applied, these imperfections cause geo-metric nonlinearity effects to be present and equilibrium paths such as in Figs. 6.1 and 6.3 are plausible. Unlike columns and flat plates, these effects are significant on the compressive behavior of shell com-ponents of steel containments. In addition, the effects of material nonlinearity may also be very important, just as they potentially are for columns and flat plates.

At present, there are no generally accepted design purpose equations for compressive loading on imperfection sensitive shells. The nearest

thing to "equation" solutions for design-allowable buckling loads are obtained from "classical" equations modified by empirical factors. These empirical factors are typically obtained from graphs derived from experimental data. Reference 6 contains an excellent set of such graphs which represent a 90% nonexceedence probability. The above semi-empirical approach is method (2) of the ASME Code mentioned earlier.

A rigorous assessment of a containment against buckling, i.e., method (1) of the ASME Code, requires the use of computer programs. Subsequently, some considerations in the above two methods will be discussed. First, however, some general considerations regarding the determination of peak compression stresses from the load responses will be presented.

The load conditions which produce compressive stresses generally include external pressure, dead and live load, seismic, and nonaxisymmetric dynamic pressures or pulses. In addition, uniform internal pressure can result in compressive stresses in containments with other than spherical domes. Basically, almost all load combinations are potential sources of compressive stress.

The stations on the containment at which compressive stresses should be assessed depends, in general, on the source of distress in the shell and consequently on the anticipated mode of failure that would result. Some specific modes of failure that must be considered are [73]:

1) local buckling - buckling of the shell plate between stiffeners;

2) stringer buckling - buckling between circumferential rings of the shell plate and attached meridional stiffeners;

3) general instability - overall collapse of the containment.

In addition to the above, the presence of penetrations in the containment must be considered. Penetrations which are reinforced according to ASME Code replacement rules and which have an inside diameter that is small compared to the containment diameter have been shown by studies and experiments to not reduce the overall containment buckling strength [73]. Reference 73 further states that, for steel containments, properly reinforced penetrations that have an inside diameter not greater than 10 percent of the vessel diameter can be neglected in overall analysis. Typical practice, however, has often been to neglect the effect of all containment penetrations on overall containment response and capacity [25,67,103,121]. A local analysis on the large penetrations is then done to verify that their integrity matches or surpasses that of the unpenetrated shell.

Local and stringer buckling also require local analysis. The local analysis model must be provided with boundary conditions that deform the same as the typical containment shell. Boundary conditions may consist of defining the boundary node DOF (such as free or fixed) or may consist of boundary node forces or forced displacements that have been determined from previous overall analyses. Therefore, stations on the containment should be selected so that response data can be collected for subsequent local analyses.

Stations must also be selected to collect response data for assessing the overall stability of the containment. For example, critical buckling stresses may occur near the base of a cylindrical upright con-

tainment subjected to seismic load or in the dome under external pressure. The above only gives a small indication of the task. Realistically, the complex time-space variation of the loads requires numerous stations which are screened with a computer program to collect peak stresses.

Peak dynamic stresses in the shell are typically determined from a linear dynamic analysis. As such, they can be considered as quasi-static and applied to the shell as static loads.

The state of compressive stresses generated at the assessment stations is normally biaxial and not constant. They are biaxial because there are meridional and circumferential stresses acting together. They are not constant because the state of stress can vary in both the meriodional ad circumferential directions at any given point in time. In general, each station is screened for the maximum value of the meriodional compression, circumferential compression and in-plane shear stress. The maximum value of each of the above is in turn taken together with the other two concurrent stress components to form three sets of buckling stress components. From these three sets the containment is then checked for circumferential and meridional buckling at that particular station. With respect to meridional buckling, the peak meridional compressive stress can conservatively be assumed to act uniformly over the entire circumference [73,103]. When determining the three stress components, the meridional and circumferential components which are in tension may conservatively be set to zero when the critical circumferential and meridional sets, respectively, are being determined [73].

6.3.1. Semi-empirical buckling capacity determination

In this method, the classical linear bifurcation analysis is used as a basis for determining the buckling capacity of shell type structures. The bifurcation load is established analytically for a perfect shell model under the combined buckling effects of meridional membrane, circumferential membrane and in-plane shear stresses. The bifurcation loads for different combinations of buckling load components can be used to define an envelope of buckling capacities for the perfect shell model.

As previously explained, experiments have shown that for the types of shells and loading found in containments, the actual buckling load can be much less than that predicted by classical linear analysis. Empirical factors, usually referred to as "knock-down" factors, are used to reduce the classical value to a design purpose value that is compatible with experimental data. In this respect it is important that the knock-down factors used are based on experiments with similar shell parameters, boundary conditions and applied loads.

Often, the knock-down factors are not applied to the classical buckling envelope. A more convenient practice is to increase each load component of the combined buckling loads artificially by dividing each load component with its respective knock-down factor. The combined buckling loads are further increased by required factors of safety provided in Refs. 4, 73, 105, and 114. These increased load components represent a single load vector which is then compared against the classical buckling envelope for the particular shell segment being investigated.

This semi-empirical method is described in detail in ASME Code Case N-284 [73] wherein graphs of knock-down factors applicable to stiffened and unstiffened containments are provided. Case N-284 provides a practical set of rules for design of stiffened containments and for sizing of stiffeners.

When unusual geometries or loading conditions are encountered, there may not be any classical linear solutions available. In these instances, computer programs have been used to predict the linear bifurcation load. Careful judgment must be used in selecting proper knock-down factors in such cases. A more satisfactory solution may be found by rigorous analysis (Sec. 6.3.2).

6.3.2. Rigorous buckling capacity determination

As defined in the ASME Code, NE-3222.1, rigorous analysis of shell buckling should include the effects of: overall and local buckling, geometric imperfections, nonlinearities, large deformations, and inertial forces. The only practical way to include all of the above is to do a finite element or finite difference analysis of a discretized model of the containment. Typically, the containment is modeled as an axisymmetric structure discretized with axisymmetric ring segments (Sec. 4.2.1). The economic advantages of this model and the availability of well-proven programs such as BOSOR [16,17] for its analysis are currently considered to outweigh its limitations.

In a sense, when the above numerical methods are applied to a perfect shell model, the buckling capacity is rigorously determined. How-

ever, the solution must still be empirically corrected by knock-down
factors. As a result, this is a semi-empirical method.

When a structural analysis is performed it is usual practice to use
an idealized model that is perfect, with geometric and material imperfec-
tions neglected. Generally, this is found to be satisfactory in conven-
tional building design. However, compressive loads on real shell struc-
tures are very sensitive to imperfections and will cause geometric non-
linearity effects to become increasingly signficant as more load is
applied. As a result, it has been found necessary to include initial
imperfections in the analysis model in order to obtain results comparable
with experiments [6,39,103].

Of course, it is also necessary to use computer codes that will
include the effects of geometric nonlinearities. If the analysis is
being done to predict the buckling capacity of the structure, the load is
often increased in increments. For dynamic loads, the increments repre-
sent equivalent quasi-static loads found from a linear dynamic analysis.
For each increment, the effects of large deformations (i.e., geometric
nonlinearity) are usually accounted for by iteratively updating vessel
geometry coordinates and changes in shell stiffness until no appreciable
correction is obtained or deflections increase without bound.

In conjunction with the above, some of the containment material may
enter the inelastic range before buckling actually occurs. It is there-
fore desirable that the computer code should have provisions to include
the effects of material nonlinearities. If they are not included, the

results should be examined to be sure that the material did indeed remain elastic.

Failure should be defined for analyses conducted to predict buckling capacity. That is, it is of little use (for design) to continue computations along the equilibrium path after the containment behavior exceeds that acceptable for design. Therefore, the solution process may be stopped after a potential bifurcation branch is encountered (containment may still be elastic) or after excessive straining has occurred in the containment shell.

Supposing nonlinearities are correctly accounted for, the ability of the model to predict the correct mode of failure depends, basically, on the nature of the discretization. That is, the containment can only fail within the bounds defined by the discrete element displacement behavior. This implies that the discretization must be fine enough so that accurate numerical approximations are obtained [7,32,103].

The axisymmetric model will not be able to predict local buckling of the shell plate between vertical stiffeners. However, with fine enough mesh, this model can detect overall instability and stringer buckling. Stringer buckling is approximate in the sense that stringer stiffeners are often equivalently modeled by using orthotropic shell properties in the meridional direction (Sec. 4.2.1). A complete three-dimensional model using two-dimensional shell elements can potentially detect local, stringer, and overall buckling.
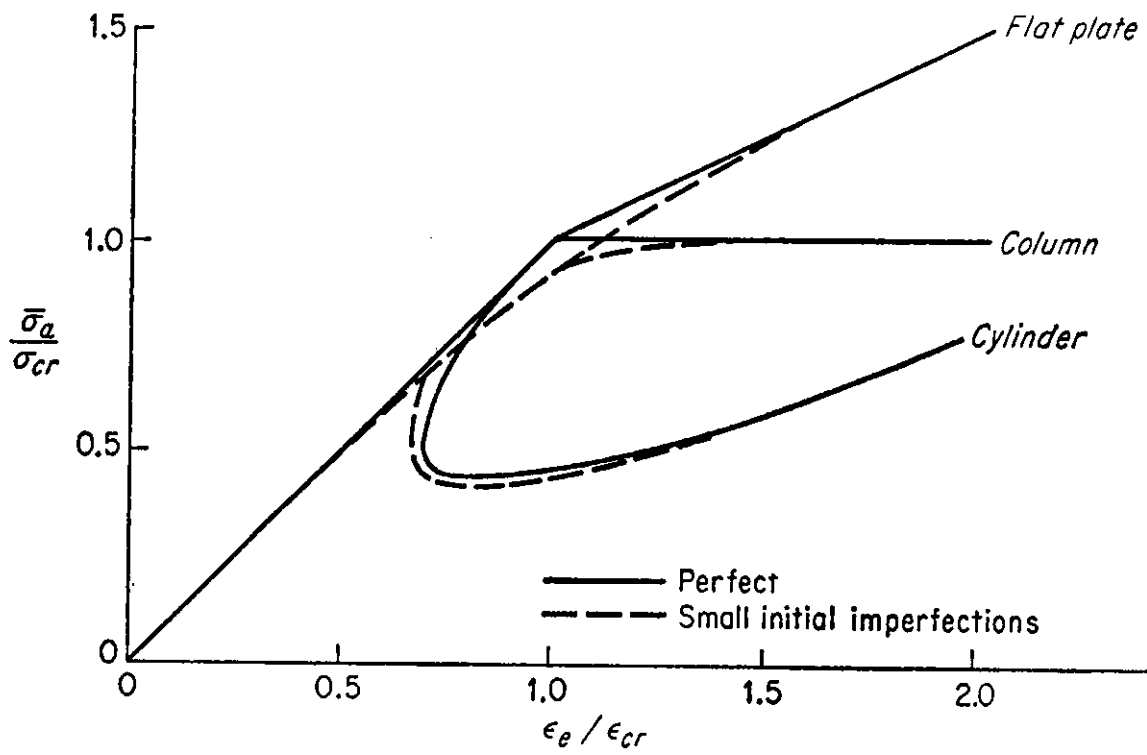
Fig. 6.1. Postbuckling behavior of axially
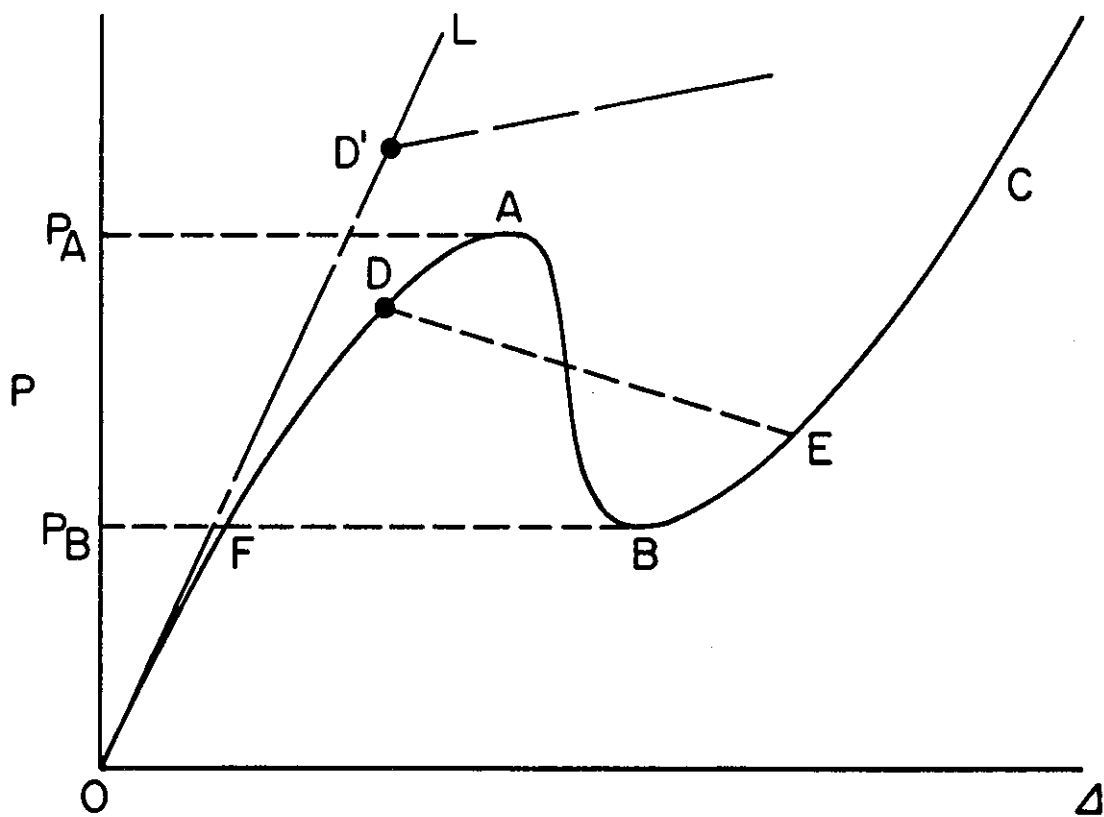compressed elastic elements [39]

Fig. 6.2.   Load-displacement curves illustrating linear
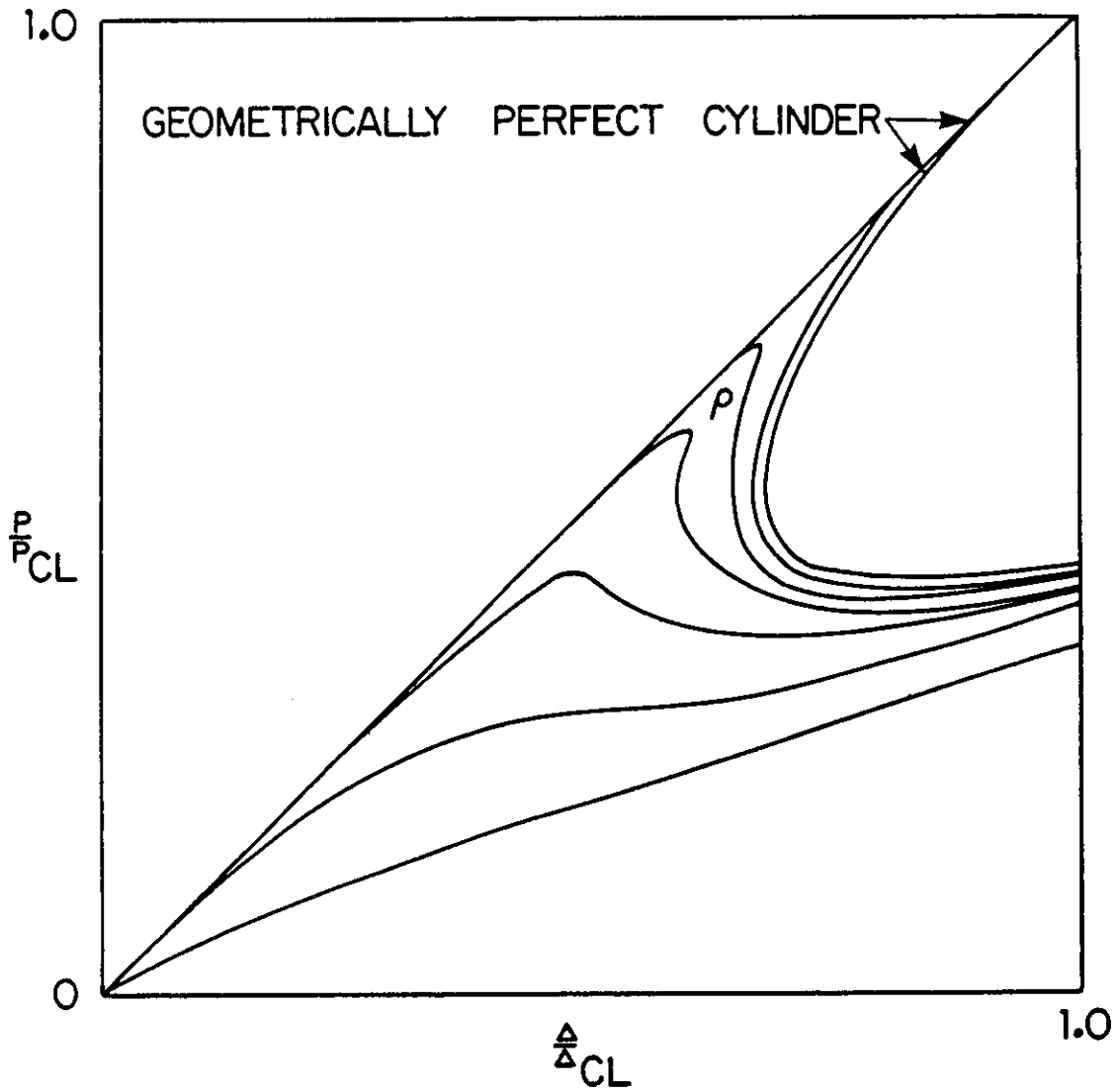   and nonlinear behavior of compressed shell [62]

Fig. 6.3. Load-displacement curves for imperfect cylinders [6]

Table 6.1. Load combinations for steel containments[a] [88]

No.	LOAD COMBINATION	Category	D	L	P_t	P_e	P_a	T_t	T_o	T_e	T_a	E	E'	R_o	R_e	R_a	Y_j	Y_r
(1)	Normal Operations	A	1.0	1.0	-	-	-	-	1.0	-	-	-	-	1.0	-	-	-	-
(2)	Abnormal/Normal Operation		1.0	1.0	-	-	1.0	-	-	-	1.0	-	-	1.0	-	1.0	-	-
(3)	Severe Environmental	B	1.0	1.0	-	-	-	-	1.0	-	-	1.0	-	1.0	-	-	-	-
(4)	Severe Environmental/External Pressure		1.0	1.0	-	1.0	-	-	-	1.0	-	1.0	-	-	1.0	-	-	-
(5)	Abnormal/Severe Environmental		1.0	1.0	-	-	1.0	-	-	-	1.0	1.0	-	-	-	1.0	-	-
(6)	Abnormal/Extreme Environmental	C	1.0	1.0	-	-	1.0	-	-	-	1.0	-	1.0	-	-	1.0	-	-
(7	Extreme Environmental/External Pressure		1.0	1.0	-	1.0	-	-	-	1.0	-	-	1.0	-	1.0	-	-	-
(8)	Abnormal Extreme Environmental/Jet Impingement	D	1.0	1.0	-	-	1.0	-	-	-	1.0	-	1.0	-	-	1.0	1.0	1.0
(9)	Test	E	1.0	1.0	1.0	-	-	1.0	-	-	-	-	-	-	-	-	-	-

[a] D = dead loads; L = live loads; P_t = test pressure; P_e = design external pressure; P_a = design basis accident pressure; T_t = test temperature; T_o = normal operation thermal loads; T_e = thermal loads consequent to event causing external pressure; T_a = thermal loads consequent to design basis accident; E = operating basis earthquake; E' = safe shutdown earthquake; R_o = normal operation pipe reactions; R_e = pipe reactions consequent to event causing external pressure; R_a = pipe reactions consequent to thermal conditions generated by design basis accident; Y_j = jet impingement; and Y_r = reaction of broken pipe during design basis accident.

Table 6.2. Stress limits for steel containments[a] [114]

Load Category		Primary Stresses				Peak Stresses	Buckling
		Gen. Mem. P_m	Local Memb. P_L	Bend.+Local Memb. P_B+P_L			
A & B		S_{mc}	$1.5S_{mc}$	$1.5S_{mc}$	$3S_{ml}$	Consider for Fatigue Analysis	Allow. given by NE-3222.1
C	Not integral and continuous	S_{mc}	$1.5S_{mc}$	$1.5S_{mc}$	N/A	N/A	
							120% of Allow. given by NE-3222.1
	Integral and continuous	The Greater of $1.2S_{mc}$ or S_y	The Greater of $1.8S_{mc}$ or S_y	The Greater of $1.8S_{mc}$ or S_y	N/A	N/A	
D	Not integral and continuous	The Greater of $1.2S_{mc}$ or S_y	The Greater of $1.8S_{mc}$ or S_y	The Greater of $1.8S_{mc}$ or S_y	N/A	N/A	
							150% of Allow. given by NE-3222.1
	Integral and continuous	S_f[b]	$1.5S_f$[b]	$1.5S_f$[b]	N/A	N/A	

[a] S_{mc} = Stress intensity limits listed in Tables I-10.0 of ASME Code Appendix I;
S_{ml} = Stress intensity limits listed in Tables I-1.0 of ASME Code Appendix I;
S_y = Yield strength listed in Tables I-2.0 of ASME Code Appendix I;
S_f = 85% of the general primary membrane allowable permitted in Appendix F of ASME Code.

[b] Applies to elastic analysis.

7. SUMMARY

Steel containment design requires the expertise of many engineering specializations and frequently presents problems that demand the most advanced of the available engineering tools. This study was conducted to provide a perspective on the above and to provide a guide to literature where detailed treatment of specific analysis problems can be found.

The containment response from an applied load creates a condition that must be resisted by the steel containment. The stresses or strains created by the loads are actually random variables Q. Likewise, the resistance capacity of the steel containment is some distribution of random variables R. If the distributions of Q and R are known, a probability of failure can be calculated for the steel containment and the risk associated with nuclear power plant facilities can be quantified.

Presently, the distributions of Q and R are not sufficiently well defined to allow probabilistic design of steel containments. However, the circumstances in the foregoing paragraph are reflected in the ASME Code. The philosophy of the ASME Code is to place limits on stress which the unfactored load responses must not exceed. The limit that is selected as the allowable stress reflects the recognition of load and resistance variability.

Nuclear containments differ from conventional structures in that severe plant mishaps and/or severe natural phenomena form the basis of design and the normal operating loads are dwarfed in comparison. Containment loads can be classified as either normal operation loads, inter-

nal events, or external events. In general, this classification reflects the source of the load and the internal and external events represent the design basis loads. The sources and characteristics of the loads were described, illustrating the orders of magnitude and time-space variations involved.

Because of the complexity of the design basis loads and containment geometries, closed form solutions have limited application to containment design. As a result, the containment shell is typically represented by a discretized mathematical model whose response to design loads is found by numerical techniques, e.g., finite element or finite difference. The model is usually assumed to behave linear-elastically so that deformations are proportional to the applied loads and the displacements or the internal forces caused by a set of effects can be found by superposition. Currently, the most practical and popular containment models are constructed with one-dimensional axisymmetric elements. The main limitation of this model is that all structural characteristics of the actual containment are modeled as rotationally symmetric about a vertical axis in the containment center.

One-dimensional beam finite elements can be used to model the containment shell under some circumstances. Specifically, the adequacy of the beam model has been verified for upright, cylindrical shells subjected to horizontal base excitation.

The dynamic response of the above two containment models can be found in the time or frequency domain. For example, time domain solutions can be found by modal analysis and/or time integration while fre-

quency domain solutions can be found by the Fast Fourier Transform method. The selection of a solution procedure will depend on the characteristics of the problem, cost-effectiveness considerations, and availability and user familiarity of the solution algorithms. Design basis loads are typically dynamic and include: seismic, fluid pressures, thermal stress and localized impulse and impact loads.

Seismic response should include the reciprocal influence of the supporting soil unless the containment is founded on rock or rock-like material. Solutions inluding the soil-structure interaction can be found by:

1) Time or frequency domain solutions of a discretization of the combined soil and structure model.

2) Generally, frequency domain solutions of the separated soil and containment models as substructures.

A popular special case of (2), which occurs when the foundation is rigid, is the lumped spring method in which the soil stiffness and damping are frequency dependent.

Dynamic gas pressures are usually solved in the time domain by modal analysis and/or time integration. Dynamic liquid pressure (in BWRs) can also be solved in the time domain but may be best handled in the frequency domain. The suppression pool water must be included in the containment model.

Thermal stresses reach their highest levels during a loss-of-coolant accident (LOCA). Critical containment regions and points in time after a LOCA can be assessed and appropriate thermal stress fields evaluated for

subsequent combination with other stresses. Local containment integrity must be checked for impulsive, local loads. A model of a portion of the containment shell is often adequate.

Current practice, as defined in the ASME Code and USNRC guides, is to conservatively assume that internal and external load events occur concurrently. The peak or critical states of these load combinations are determined by adding the absolute values of response peaks due to the individual loads or by using the square-root-of-the-sum-of-the-squares of the response peaks due to the individual loads. The unfactored peak stress states are compared with allowable service limits in the ASME Code. The magnitude of these allowable service limits depends on the type, origin and location of the containment stress.

Buckling is a potential failure mode for thin, steel containment shells. There are two methods available to estimate buckling capacity. The first is a semi-empirical method where classical buckling values are lowered by empirical knock-down factors. The second method is a computer solution of a discretized model which inludes initial imperfections and nonlinear behavior.

8. BIBLIOGRAPHY

1. Agrawal, P. K., S. L. Chu and H. H . Shah. "Comparative Study of Soil Spring and Finite Element Models for Seismic Soil-Structure Interaction Analysis of Nuclear Power Plants." Pages 63-82 in ASCE Specialty Conference on Structural Design of Nuclear Plant Facilities. Vol. 2. New York:ASCE, 1974.

2. Albersebaer, J. K. and K. Wiedner. "Containment Structure for Trojan Nuclear Plant." Journal of the Power Division, ASCE, 97, No. PO2 (March 1971), 351-366.

3. Allred, J. F., R. O. Barnett and F. D. Stidham. "Sequoyah Ice Condenser Containment Structure." Journal of the Power Division, ASCE, 99, No. PO2 (May 1973), 19-40.

4. ASME Boiler and Pressure Vessel Code, Section III, Division 1, Subsection NE. New York:American Society of Mechanical Engineers, 1980.

5. Ang, A. H-S. and N. M. Newmark. "A Probabilistic Seismic Safety Assessment of the Diablo Canyon Nuclear Power Plant." Report to the U.S. Nuclear Regulatory Commission from N. M. Newmark Consulting Services, Urbana, Illinois, November 1977.

6. Baker, E. H., A. P. Capelli, L. Kovalevsky, F. L. Rish and R. M. Verette. "Shell Analysis Manual." NASA CR-912. Springfield, Virginia:National Technical Information Service, 1968.

7. Bathe, K-J. Finite Element Procedures in Engineering Analysis. Englewood Cliffs, New Jersey:Prentice-Hall, Inc., 1982.

8. Bedrosian, B. and M. Ettouney. "Response of a BWR Mark II Containment Structure to Chugging Loads." Paper J/7 in 5th Int. Conf. on Struct. Mech. in Reactor Technol. Amsterdam, Netherlands:North-Holland Publishing Co., 1979.

9. Bedrosian, B., J. Brennan, P. K. Kask and M. Ettouney. "Response of a BWR Mark II Containment Structure to SRV Loads." Paper J/16 in 6th Int. Conf. on Struct. Mech. in Reactor Technol. Amsterdam, Netherlands:North-Holland Publishing Co., 1981.

10. Bedrosian, B., A. A. Shah and J. Walters. "Behavior of Water Jet from the Dowcomer Vent During Post Water Clearing Phase of a LOCA in a BWR Mark II Containment." Paper J2/3 in 6th Int. Conf. on Struct. Mech. in Reactor Technol. Amsterdam, Netherlands:North-Holland Publishing Co., 1981.

11. Biggs, J. M. Introduction to Structural Dynamics. New York:McGraw-Hill, Inc., 1964.

12. Broman, R. "Structural Evaluation of Nuclear Facilities for Pipe Rupture." Pages 151-171 in ASCE Specialty Conference on Structural Design of Nuclear Plant Facilities. Vol. 1. New York:ASCE, 1974.

13. Broman, R., C. V. Subramanian and T. J. Vinsion. "Design of Containment for Impulse and Impact Loads." Pages 84-96 in Proceedings of the Specialty Conference on Code Requirements for Nuclear Containments. Chicago, Illinois:ASCE, 1975.

14. Brosche, D. and G. Mansfeld. "Calculation of Transient Long Term Pressure and Temperature Behavior in a Containment after a Loss-of-Coolant Accident." Paper J1/3 in 2nd Int. Conf. on Struct. Mech. in Reactor Technol. Amsterdam, Netherlands:North-Holland Publishing Co., 1973.

15. Brosche, D. and G. Mansfeld. "Vent Clearing Transients, Load Maxima of Responses and Pressure Difference in a Pressure Suppression System during the Short Term Behavior." Paper J1/4 in 2nd Int. Cont. on Struct. Mech. Reactor Technol. Amsterdam, Netherlands: North-Holland Publishing Co., 1973.

16. Bushnell, D. "Stress, Stability and Vibration of Complex Branched Shells of Revolution." Computers and Structures, 4 (1974), 399-435.

17. Bushnell, D. "BOSOR5-Program for Buckling of Elastic-Plastic Complex Shells of Revolution including Large Deflections and Creep." Computers and Structures, 6 (1976), 221-239.

18. Chang, H. S., T. Wang, I. H . Chou and E. Odar. "Effect of Fluid-Structure Interaction Methodologies on the Responses due to Hydrodynamic Loads." Pages 109-118 in Advances in Containment Design and Analysis. New York:ASME, 1982.

19. Chang, P. S. and M. M. Moussa. "Mark II Containment Vessel/Annulus Concrete Design." Paper J2/11 in 6th Int. Conf. on Struct. Mech. in Reactor Technol. Amsterdam, Netherlands:North-Holland Publishing Co., 1981.

20. Chao, R. N. P. "The Consideration of a Loss of Coolant Accident Load in the Design of Sub-containments of Containment Internal Structures." Paper J1/2 in 2nd Int. Conf. on Struct. Mech. in Reactor Technol. Amsterdam, Netherlands:North-Holland Publishing Co., 1973.

21. Chauvin, G. A. "Containments for Nuclear Plants." Paper GEC-P93. Chicago, Ill.:Sargent and Lundy, Inc., 1971.

22. Chen, C. "Seismic Resistant Analysis of Heavy Equipment of PWR Plants." Paper K6/4 in 2nd Int. Conf. on Struct. Mech. in Reactor Technol. Amsterdam, Netherlands:North Holland Publishing Co., 1973.

23. Chen, T. H. and G. F. Davenport. "A Unified Approach for Interior Concrete Design." Paper J3/8 in 4th Int. Conf. on Struct. Mech. in Reactor Technol. Amsterdam, Netherlands:North-Holland Publishing Co., 1977.

24. Chen, W. W. H., M. Challerjee and S. M. Day. "Seismic Response Analysis for a Deeply Embedded Nuclear Power Plant." Paper K7/6 in 5th Int. Conf. on Struct. Mech. in Reactor Technol. Amsterdam, Netherlands:North-Holland Publishing Co., 1979.

25. Chicago Bridge and Iron Company. "Comments on NUREG CR-0793-Buckling Criteria and Application of Criteria to Design of Steel Containment Shells." Available upon request from USNRC, Washington, D.C., 1979.

26. Chopra, A. K. and J. A. Guttierrez. "Earthquake Analysis of Structures Including Soil-Structure Interaction by a Substructure Method." Paper K2/8 in 4th Int. Conf. on Struct. Mech. in Reactor Technol. Amsterdam, Netherlands:North-Holland Publishing Co., 1977.

27. Chou, C. K. "Load Combination Research Program at the Lawrence Livermore National Laboratory." Paper J1/12 in 6th Int. Conf. on Struct. Mech. in Reactor Technol. Amsterdam, Netherlands:North-Holland Publishing Co., 1981.

28. Chu, K. D., H. J. Kuo and T. T. Huang. "Structural Dynamic Analysis of BWR Mark II Plant Under SRV Blowdown Oscilation." Paper J6/6 in 4th Int. Conf. on Struct. Mech. in Reactor Technol. Amsterdam, Netherlands:North-Holland Publishing Co., 1977.

29. Clough, R. W. and J. Penzien. Dynamics of Structures. New York: McGraw-Hill, Inc., 1975.

30. Dalal, J. S. H. B. Seed and D.-L. Wu. "Site-dependent Seismic Response Spectra for Soft Sites." Journal of the Power Division, ASCE, 103, No. P01 (July 1977), 15-25.

31. Denton, D. R., C. T. Shen and C. K. Webster. "Development of Response Spectra for a Thin Shell Structure." Pages 571-590 in ASCE Specialty Conference on Structural Design of Nuclear Plant Facilities. Vol. 2. New York:ASCE, 1974.

32. Desai, C. S. and J. F. Abel. Introduction to the Finite Element Method. New York:Van Nostrand Reinhold Co., 1972.

33. Eckert, E. R. G. and R. M. Drake, Jr. Heat and Mass Transfer. 2nd ed. New York:McGraw-Hill, Inc., 1959.

34. Edwards, N. W. "Practical Application of Current Fluid/Structure Interaction Technology to the Design and Analysis of BWR Containment Vessels." Paper B8/7 in 5th Int. Conf. on Struct. Mech. in Reactor Technol. Amsterdam, Netherlands:North-Holland Publishing Co., 1979.

35. Eringen, A. C., A. K. Gaghdi and C. C. Thiel. "State of Stress in a Circular Cylindrical Shell with a Circular Hole." Welding Research Council Bulletin No. 102, 1955.

36. Foss, K. A. "Coordinates Which Uncouple the Equations of Motion of Damped Linear Systems." Journal of Applied Mathematics, 25 (1958), 361-364.

37. Gallagher, R. H. Finite Element Analysis Fundamentals. Englewood Cliffs, New Jersey:Prentice-Hall, Inc., 1975.

38. Gebhart, B. Heat Transfer. New York:McGraw-Hill, Inc., 1961.

39. Gerard, G. Introduction to Structural Stability Theory. New York: McGraw-Hill, Inc., 1962.

40. Godfred, D. A. and D. Q. LeMouss. "Analytical Techniques used in the Design of Steel Containments-Part I." Pages 53-63 in Proceedings of the Specialty Conference on Code Requirements for Nuclear Containments. Chicago, Illinois:ASCE, 1975.

41. Godfrey, A., A. S. Madan and W. A. Loeb. "Spherical Containment System has many Advantages." Nuclear Engineering International, 22 (December 1977), 44, 47-48.

42. Gröber, H., S. Erk and U. Grigull. Fundamentals of Heat Transfer 3rd ed. New York:McGraw-Hill, Inc., 1961.

43. Gurbuz, O. and T. D. Kohli. "Design of Nuclear Containments for Thermal Effects." Paper J4/2 in 4th Int. Conf. on Struct. Mech. in Reactor Technol. Amsterdam, Netherlands:North-Holland Publishing Co., 1977.

44. Guzman, R. A. and P. C. Jennings. "Design Spectra for Nuclear Power Plants." Journal of the Power Division, ASCE, 102, No. PO2 (November 1976), 165-178.

45. Hadjian A. H. "Earthquake Forces on Equipment in Nuclear Power Plants." Journal of the Power Division, ASCE, 97, No. PO3 (July 1971), 649-665.

46. Hadjian, A. H. "Discussion of Interaction of Soil and Power Plants in Earthquakes." Journal of the Power Division, ASCE, 99, No. PO2 (November 1973), 431-434.

47. Hadjian, A. H. and T. S. Atatik. "Discrete Modeling of Symmetric Box-Type Structures." Pages 1151-1164 in Proceedings of the International Symposium on Earthquake Structural Engineering. Vol. 2. Rolla, Missouri:University of Missouri, 1976.

48. Hadjian, A. H., G. E. Howard and C. B. Smith. "A Comparison of Experimental and Theoretical Investigations of Embedment Effects on Seismic Response." Paper K2/5 in 4th Int. Conf. on Struct. Mech. in Reactor Technol. Amsterdam, Netherlands:North-Holland Publishing Co., 1977.

49. Haga, P. B. and J. D. Stevenson. "PWR Containment Structures Design Experience." Journal of the Power Division, ASCE, 96, No. PO1 (January 1970), 145-155.

50. Hart, G. C. Uncertainty Analysis, Loads and Safety in Structural Engineering. Englewood Cliffs, New Jersey:Prentice-Hall, Inc., 1982.

51. Hibbeler, S. H. Engineering Mechanics:Dynamics. New York:Macmillan Publishing Co., Inc., 1978.

52. Idriss, I. M., R. P. Kennedy, P. K. Agrawal, et al. Analyses for Soil-Structure Interaction Effects for Nuclear Power Plants. New York:ASCE, 1979.

53. Iredale, A. J. and N. P. Grimm. "Ice Condenser Reactor System Containment." Nuclear Engineering International, 16 (October 1971), 864-868.

54. Jan, C. M. "Dynamic Effects on Structures and Equipment due to Safety Relief Valve Discharge Loads." Nuclear Engineering and Design, 59 (1980), 171-183.

55. Johnson, J. J. and R. P. Kennedy. "Earthquake Response of Nuclear Power Facilities." Journal of the Power Division, ASCE, 105, No. EY1 (January 1979), 15-32.

56. Johnson, T. E. "Design of Containments for Seismic Loads." Pages 75-83 in Proceedings of the Specialty Conference on Code Requirements for Nuclear Containments. Chicago, Illinois:ASCE, 1975.

57. Kadar, I. "Computer Methods used in the Complex Structural Analysis of a Drywell Structure." Paper J6/3 in 4th Int. Conf. on Struct. Mech. in Reactor Technol. Amsterdam, Netherlands:North-Holland Publishing Co., 1977.

58. Kalins, A. "Static, Free Vibration, and Stability Analysis of Thin, Elastic Shells of Revolution." Technical Report AFFDL-TR-68-144. Air Force Flight Dynamic Lab, Wright-Patterson Air Force Base, Ohio, 1969.

59. Kausel, E., J. M. Roesset and G. Waas. "Dynamic Analysis of Footings on Layered Media." Journal of the Engineering Mechanics Division, ASCE, 101, No. EM5 (October 1975), 679-693.

60. Kausel, E., R. V. Whitman, E. Elsabee and J. P. Morray. "Dynamic Analysis of Embedded Structures." Paper K2/6 in 4th Int. Conf. on Struct. Mech. in Reactor Technol. Amsterdam, Netherlands:North-Holland Publishing Co., 1977.

61. Khanna, J. K., A. V. Setlur nd D. V. Pathak. "Nonlinear Seismic Soil-Structure Interaction Analysis of Nuclear Power Plant Structures." Paper K2/5 in 4th Int. Conf. on Struct. Mech. in Reactor Technol. Amsterdam, Netherlands:North-Holland Publishing Co., 1977.

62. Krieg, R., B. Göller and G. Hailfinger. "Admissible Blowdown Loading for Spherical Containments with Pressure Suppression System." Paper J2/4 in 6th Int. Conf. on Struct. Mech. in Reactor Technol. Amsterdam, Netherlands:North-Holland Publishing Co., 1981.

63. Larkin, P. A., R. E. Stoner, R. L. Beck and T. F. Huang. "Mathematical Modeling of a Mark III/BWR-6 Containment for LOCA and SRV Analysis." Paper J2/9 in 5th Int. Conf. on Struct. Mech. in Reactor Technol. Amsterdam, Netherlands:North-Holland Publishing Co., 1979.

64. Lee, H. W. and T. H. Chen. "Analysis of G.E. Mark III Containment System Drywell Structure." Paper J6/2 in 4th Int. Conf. on Struct. Mech. in Reactor Technol. Amsterdam, Netherlands:North-Holland Publishing Co., 1977.

65. Lin, C. W. "Seismic Response of Nuclear Reactor Containment Vessels." Nuclear Engineering Design, 9 (1969), 234-238.

66. Lin, C. W. "On the Simultaneous Application of the Vertical and Horizontal Response Spectra in the Seismic Analysis." Nuclear Engineering Design, 24 (1973), 232-238.

67. Lin, Y. J. and A. H. Hadjian. "Discrete Modeling of Containment Structures." Pages 899-912 in Proceedings of the International Symposium on Earthquake Engineering. Vol. 2. Rolla, Missouri: University of Missouri, 1976.

68. Lin, Y. J. and A. H. Hadjian. "The Effect of Rotatory Inertia on the Dynamic Response of Cantilever Structures." Paper K3/13 in 4th Int. Conf. on Struct. Mech. in Reactor Technol. Amsterdam, Netherlands:North-Holland Publishing Co., 1977.

69. Luco, J. E. "Impedance Functions for a Rigid Foundation on a Layered Medium." Nuclear Engineering and Design, 31 (January 1974), 204-217.

70. Luco, J. E. "Vibrations of a Rigid Disc on a Layered Viscoelastic Medium." Nuclear Engineering and Design, 36 (January 1976), 325-340.

71. Lui, S. C. and L. W. Fagel. "Earthquake Interaction by Fast Fourier Transform." Journal of the Engineering Mechanics Division, ASCE, 197, No. EM4 (August 1971), 1223-1237.

72. "Mark II Containment Dynamic Forcing Function - Information Report." Report No. NEDO-21061. Schenectady, N.Y.:General Eletric Co.; Chicago, Ill.:Sargent and Lundy, Inc.

73. "Metal Containment Shell Buckling Design Methods." ASME Code Case N-284. Cases of ASME Boiler and Pressure Vessel Code. New York: ASME, 1980.

74. Morozov, E. M. and Ya. B. Fridman. "Thermal Stresses and their Calculation." In Strength and Deformation in Nonuniform Temperature Fields. Ed. Ya. B. Fridman. New York:Consultants Bureau Enterprises, Inc., 1964, pp. 17-61.

75. Namatame, K., Y. Kukita, I. Takeshita and M. Shib. "Multivent Full-Scale Test on Mark II Pressure Suppression System." Paper J2/9 in 6th Int. Conf. on Struct. Mech. in Reactor Technol. Amsterdam, Netherlands:North-Holland Publishing Co., 1981.

76. Newmark, N. M., J. A. Blume and K. K. Kapur. "Seismic Design Spectra for Nuclear Power Plants." Journal of the Power Division, ASCE, 99, No. PO2 (November 1973), 287-303.

77. Olivieri, M., A. Saulle, S. Porcile and L. Bertoncello. "Experimental and Analytical Investigations on Caorso BWR Mark II Containment Dynamics Response Following Safety Relief Valve Discharge." Paper J2/1 in 6th Int. Conf. on Struct. Mech. in Reactor Technol. Amsterdam, Netherlands:North-Holland Publishing Co., 1981.

78. Pahl, J. P. "Modal Response of Containment Structures." In Seismic Design for Nuclear Power Plants. Ed. R. J. Hansen. Cambridge, Mass.:The M.I.T. Press, 1970, pp. 344-400.

79. Pajuhesh, J. and A. H. Hadjian. "Dynamic Interaction of Components, Structure, and Foundation of Nuclear Power Facilities." Paper K3/9 in 4th Int. Conf. on Struct. Mech. in Reactor Technol. Amsterdam, Netherlands:North-Holland Publishing Co., 1977.

80. Popper, S. H. "Beaver Valley Containment Structure." Journal of the Power Division, ASCE, 99, No. P01 (May 1973), 51-67.

81. Richart, F. E., J. R. Hall and R. D. Woods. Vibration of Soils and Foundations. Englewood Cliffs, New Jersey:Prentice-Hall, Inc., 1971.

82. Roark, R. J. and W. C. Young. Formulas for Stress and Strain. 5th ed. New York:McGraw-Hill, Inc., 1975.

83. Roesset, J. M., R. V. Whitman and R. Dobry. "Modal Analysis for Structures with Foundation Interaction." Journal of the Structural Division, ASCE, 99, No. ST3 (March 1973), 399-416.

84. Seed, H. B. and J. Lysmer. "Soil-Structure Interaction Analysis by Finite Element Methods, State-of-the-Art." Paper K2/1 in 4th Int. Conf. on Struct. Mech. in Reactor Technol. Amsterdam, Netherlands: North-Holland Publishing Co., 1977.

85. Seed, H. B., C. Ugas and L. Lysmer. "Site Dependent Spectra for Earthquake Resistant Design." Bulletin of the Seismological Society of America, 66 (February 1976) 221-244.

86. Sharpe, R. L. "Systems Aspects of Seismic Design for Nuclear Plants." Journal of the Power Division, ASCE, 99, No. P01 (May 1973), 175-192.

87. Singh, A. K. "Dynamic Analysis using Modal Synthesis." Journal of the Power Division, ASCE, 104, No. P02 (April 1978), 131-140.

88. Skundric, L. I. "Metal Containments: Nature of Loads and Behavior Limits." Paper J5/6 in 4th Int. Conf. on Struct. Mech. in Reactor Technol. Amsterdam, Netherlands:North-Holland Publishing Co., 1977.

89. Snyder, M. O., D. E. Shaw and J. R. Hall. "Structure-Soil-Structure Interaction of Nuclear Structures." Paper K2/9 in 3rd Int. Conf. on Struct. Mechanics in Reactor Technol. Amsterdam, Netherlands: North-Holland Publishing Co., 1975.

90. Stevenson, J. D. "Design Load Combinations and Behavior Limits." Pages 39-40 in Proceedings of the Specialty Conference on Code Requirements for Nuclear Containments. Chicago, Illinois:ASCE, 1975.

91. Stevenson, J. D., A. Bingaman, R. Broman, et al. (Eds.). *Structural Analysis and Design of Nuclear Plant Facilities.* Draft for trial use and comments. New York:ASCE, 1976.

92. Stevenson, J. D., A. Bingaman, R. Broman, et al. (Eds.). *Structural Analysis and Design of Nuclear Plant Facilities.* New York:ASCE, 1980.

93. Tagart, S. W. "Evaluation of Load Combination Equations for ASME Section III, Division 1 Components." Paper J1/2 in *5th Int. Conf. on Struct. Mech. in Reactor Technol.* Amsterdam, Netherlands: North-Holland Publishing Co., 1979.

94. 10 CFR Part 50. *General Design Criteria for Nuclear Power Plants.* 1982.

95. 10 CFR Part 100. *Reactor Site Criteria.* 1982.

96. Timoshenko, S. P. and J. M. Gere. *Theory of Elastic Stability.* 2nd ed. New York:McGraw-Hill, Inc., 1961.

97. Timoshenko, S. P. and J. N. Goodier. *Theory of Elasticity.* 3rd ed. New York:McGraw-Hill, Inc., 1970.

98. Timoshenko, S. P. and S. Woinowsky-Krieger. *Theory of Plates and Shells.* 2nd ed. New York:McGraw-Hill, Inc., 1959.

99. Tsai, N. C. "Modal Damping for Soil-Structure Interaction." *Journal of the Engineering Mechanics Division, ASCE,* 100, No. EM2 (April 1974), 323-341.

100. Tsai, N. C., D. Niehoff, M. Swatta and A. H. Hadjian. "The use of Frequency-Independent Soil-Structure Interaction Parameters." *Nuclear Engineering and Design,* 31 (1973), 168-183.

101. Tseng, W. S. and N. C. Tsai. "Soil Structure Interaction for Transient Loads due to Safety Relief Valve Discharges." Paper J6/1 in *4th Int. Conf. on Struct. Mech. in Reactor Technol.* Amsterdam, Netherlands:North-Holland Publishing Co., 1977.

102. USNRC. *PRA Procedures Guide.* NUREG/CR-2300. Washington, D.C.:USNRC, 1981.

103. USNRC. *Probabilistic Seismic Resistance of Steel Containments.* NUREG-3127. Washington, D.C.:USNRC, 1982.

104. USNRC. *Reactor Safety Study- An Assessment of Accident Risks in U.S. Commercial Nuclear Power Plants.* WASH-1400 (NUREG 75/014). Washington, D.C.:USNRC, 1975.

105. USNRC. Regulatory Guide 1.57. "Design Limits and Load Combinations for Metal Primary Reactor Containment System Components." Washington, D.C.:USNRC, 1973.

106. USNRC. Regulatory Guide 1.60. "Design Response Spectra for Nuclear Power Plants." Washington, D.C.:USNRC, 1973.

107. USNRC. Regulatory Guide 1.61. "Damping Values for Seismic Design of Nuclear Power Plants." Washington, D.C.:USNRC, 1973.

108. USNRC. Reliability Analysis of Containment Strength. NUREG/CR-1891. Washington, D.C.:USNRC, 1982.

109. USNRC. Reliability Analysis of Steel Containment Strength. NUREG/CR-2442. Washington, D.C.:USNRC, 1982.

110. USNRC. Safety Evaluation Report - Tennessee Valley Authority Sequoyah Nuclear Plant, Units 1 and 2., NUREG-0011. Springfield, Virginia:National Technical Information Service, 1979.

111. USNRC. Soil Structure Interaction: The Status of Current Analysis Methods and Research - Seismic Safety Margins Research Program. NUREG/CR-1780. Springfield, Virginia:National Technical Information Service, 1981.

112. USNRC. Standard Review Plan. Seismic Input, section 3.7.1. NUREG-75/087. Washington, D.C.:USNRC, 1975.

113. USNRC. Standard Review Plan. Seismic System Analysis, section 3.7.2. NUREG-75/087. Washington, D.C.:USNRC, 1975.

114. USNRC. Standard Review Plan. Steel Containment, section 3.8.2. NUREG-75/087. Washington, D.C.:USNRC, 1975.

115. USNRC. A Technical Update on Pressure Suppression Type Containments in use in U.S. Light Water Reactor Nuclear Power Plants. NUREG-0474. Washington, D.C.:USNRC, 1978.

116. Valathur, M. and H. H. Shah. "Torsional Seismic Response of Symmetrical Structures." Journal of the Power Division, ASCE, 103, No. PO1 (July 1977), 65-75.

117. Veletsos, A. S. and B. Verbic. "Vibration of Viscoelastic Foundations." Earthquake Engineering and Structural Dynamics, 2, No. 1 (July-Sept. 1973), 86-102.

118. Waas, G. and W. Weber. "Soil Structure Interaction Analyses by Different Methods." Paper K6/1 in 5th Int. Conf. on Struct. Mech. in Reactor Technol. Amsterdam, Netherlands:North-Holland Publishing Co., 1979.

119. Wade, G. E. "Evolution and Current Status of the BWR Containment System." Nuclear Safety, 15, No. 2 (March-April 1974), 163-173.

120. Wahl, H. W. "Engineering Innovation for Davis-Besse Containment." Journal of the Power Division, ASCE, 99, No. PO1 (May 1973), 125-137.

121. Walser, A. "Analytical Techniques used in Design of Concrete Containments." Pages 72-74 in Proceedings of Specialty Conference on Code Requirements for Nuclear Containments. Chicago, Illinois: ASCE, 1975.

122. Whitman, R. V. and F. E. Richart "Design Procedures for Dynamically Loaded Foundation." Journal of the Soil Mechanics and Foundations Division, ASCE, 93, No. SM6 (November 1967), 169-193.

123. Wichman, K. R., A. G. Hopper and J. L. Mershon. "Local Stresses in Spherical and Cylindrical Shells due to External Loadings." Welding Research Council Bulletin No. 107, 1968.

124. Ybarrondo, L. J., C. W. Solbrig and H. S. Isbin. The "Calculated" Loss-of-Coolant Accident:A Review. Vol. 68, No. 7. New York: American Institute of Chemical Engineers, 1972.